# Identification of therapeutic targets in the Burkitt's lymphoma specific B cell antigen receptor signaling network

Dissertation

in partial fulfillment of the degree

"Doctor rerum naturalium"

of the Georg-August-University of Göttingen

within the doctoral program Molecular Biology of Cells

of the Georg-August University School of Science (GAUSS)

submitted by

**Vanessa Kruse**

born in Holzminden

Göttingen 2018

This thesis was conducted at the Institute of Cellular and Molecular Immunology at the Georg-August-University of Göttingen from March 2015 until August 2018 under the supervision of Dr. Michael Engelke and Prof. Dr. Jürgen Wienands.

**Thesis Committee**

Prof. Dr. Jürgen Wienands, Institute of Cellular and Molecular Immunology, University Medical Center, Göttingen

Prof. Dr. Dieter Kube, Department of Hematology and Oncology, University Medical Center, Göttingen

Prof. Dr. Lutz Walter, Department of Primate Genetics, German Primate Center, Göttingen

**Members of the Examination Board**

Referee: Prof. Dr. Jürgen Wienands, Institute of Cellular and Molecular Immunology, University Medical Center, Göttingen

2nd Referee: Prof. Dr. Dieter Kube, Department of Hematology and Oncology, University Medical Center, Göttingen

**Further members of the Examination Board**

Prof. Dr. Lutz Walter, Department of Primate Genetics, German Primate Center, Göttingen

Prof. Dr. Michael Thumm, Department of Cellular Biochemistry, University Medical Center, Göttingen

Prof. Dr. Matthias Dobbelstein, Institute of Molecular Oncology, University Medical Center, Göttingen

Prof. Dr. Steven Johnsen, Clinic for General, Visceral and Pediatric Surgery, University Medical Center, Göttingen

**Date of oral examination: October 15th, 2018**

## Affidavit

Herewith I declare that I prepared the doctoral thesis “Identification of therapeutic targets in the Burkitt’s lymphoma specific B cell antigen receptor signaling network” on my own and with no other sources and aids than quoted.

Göttingen, August 31st, 2018

Vanessa Kruse

## Acknowledgements

I would like to take this opportunity and thank everyone who supported me throughout the course of my PhD project.

First, I would like to express my gratitude to Prof. Dr. Jürgen Wienands for giving me the opportunity to join his department to discover the exciting world of B cells. Thank you for your advice and helpful discussions. I sincerely thank the members of my thesis committee Prof. Dr. Dieter Kube und Prof. Dr. Lutz Walter for their guidance, helpful advice and constructive criticism in the committee meetings.

Michael, thank you for your superb supervision. I am very thankful for your patience and support and advice especially in the last few months. Thank you for critically proof-reading this thesis and also encouraging me to focus more on positive than negative results.

Ines, thank you for your invaluable technical assistance, for always offering a helping hand and your positive attitude, brightening up the days in the lab. Many thanks also to Gabriele Sonntag for helping with technical questions and Anika Schindler and Ingrid Teuteberg for excellent administrative management.

I also want to thank all former and present members of the department for the great time through the years. Special thanks to Caren, Stela, Michael, Kai, Matthias, Jens, Christoffer, Kathrin, Arshiya, Kanika, Niklas, Christina, Julius and Kristin. Thank you for inspiring conversations and fun coffee breaks in the lab as well as a lot of fun activities outside the lab including barbecues, visits to the Christmas market, Flammkuchen ad absurdum, movie nights, visits to the theater and several sport events. Special thanks to Caren and Stela. It was a pleasure sharing the office with you. Thank you both for your constant supply of encouragement and chocolate!

Furthermore, I want to thank Dr. Carmen Doebele and Dr. Thomas Oellerich for the great collaboration during the past years. Special thanks for the generation of shCD79A cell lines, for sharing data on survival relevant proteins and for the cooperation on mass-spectrometry analyses. In addition, I would like to thank Dr. Tobias Schmidt for the CRISPR plasmids and the Institute for Multiple Sclerosis Research, in particular Dr. Fred Lühder, for helping with cell sorting. Many thanks also to my talented lab rotation students, especially Johannes Liebig for contributing to the BIG2 story.

For financial support, I would like to thank the Deutsche Krebshilfe as well as the GGNB for the Bridging Fund Stipend financing the last three months of this thesis. Many thanks also to the GGNB office for always providing quick help and support on organizational issues.

I also want to thank my friends, who are always a source of laughter, joy and support, especially Nina and Hanan. Thanks to the both of you for proof-reading my thesis and sharing some of your expertise in scientific writing.

Last but not least, I want to thank my family for their love and unconditional support. I cannot thank you enough for your constant encouragement to pursue whatever I set my mind to. Thank you, Felix, for being at my side, inspiring me to always be curious and courageous.

## Abstract

Burkitt's lymphoma (BL) is an aggressive B cell neoplasm that is characterized by a chromosomal translocation, which brings the proto-oncogene *c-MYC* under the control of Immunoglobulin (Ig) enhancer elements leading to c-MYC overexpression. While high levels of c-MYC are important for the proliferation of BL cells, c-MYC overexpression leads to apoptosis in non-malignant cells. Studies have identified the pro-survival Phosphoinositide-3-kinase (PI3K)-AKT pathway to be continuously activated in BL cells and more recently it was shown that this pathway is activated by low levels of antigen-independent, tonic B cell antigen receptor (BCR) signals. During B cell development, continuous tonic BCR signaling is necessary for maturation and survival of B cells. Similar to its physiological function, tonic BCR signaling in BL contributes to survival of malignant BL cells. While we know that tonic BCR signals activate the PI3K-AKT pathway, the BCR-proximal molecular networks regulating tonic BCR signaling are less well defined. The goal of this thesis was therefore to characterize new BL-specific BCR effector proteins previously identified by phospho-proteomic approaches for their contribution to survival of BL cells with respect to tonic BCR signaling.

In this thesis, BL-specific effector proteins were selected based on previous reports stating their role for PI3K-AKT BCR signaling or based on a potential survival relevant role established in preliminary shRNA screens. CRISPR/Cas9 "knockout" BL cell lines for the adaptor proteins Nck1 and Nck2 as well as the guanine nucleotide exchange factor BIG2 and the inositol-5' phosphatase SHIP2 showed a decline in proliferation. For Nck1- and Nck2-deficient cells, the proliferative defect could be linked to a decrease in PI3K-AKT signaling mediated by tonic BCR signals, thus identifying Nck proteins as novel, proximal regulators of tonic BCR-dependent PI3K-AKT signaling. Moreover, I identified SHIP2 and BIG2 being relevant for BL survival as their absence increased apoptosis of BL cell lines, which, for BIG2, was accompanied by decreased c-MYC expression levels. Despite their survival relevant role, SHIP2 and BIG2 were identified as negative regulators of AKT signaling, thereby contrasting previous beliefs that survival of BL cells was mainly dependent on the PI3K-AKT pathway. BL-effectors analyzed here promoted signaling via the Mitogen-activated protein kinase (MAPK) c-Jun N-terminal kinase (JNK) pathway, indicating the relevance for this pathway for BL. Despite findings that JNK activation promotes apoptosis in other cell types, JNK was shown to have a unique pro-survival role in B cell malignancies. Here, I provide evidence that tonic BCR signals also involve JNK signaling and that the analyzed BL-effector proteins are regulators in this pro-survival pathway. Therefore, the identified effectors may not only be new therapeutic targets themselves but also revealed a novel, potentially druggable pathway dependent on tonic BCR signaling in BL.

# Table of Contents

## List of Figures

## List of Tables

## Abbreviations

Units and Prefixes are in conformity with the International system of Units (Système international d'unitès, SI).

| | |
|---|---|
| α | anti |
| ABC-DLBCL | Activated B cell like-DLBCL |
| AID | Activation-induced cytidine deaminase |
| AKAP | A-kinase anchoring protein |
| AMY-1 | Associate of MYC-1 |
| APC | Allophycocyanin |
| APS | Ammonium Persulfate |
| ARF | ADP-ribosylation factor |
| B-ALL | B cell acute lymphocytic leukemia |
| Bam32 | B cell adaptor protein of 32 kDa |
| BCAP | B cell adapter for PI3K |
| B-CLL | B cell chronic lymphocytic leukemia |
| BCR | B cell antigen receptor |
| BIG1 | Brefeldin A-inhibited guanine nucleotide-exchange factor 1 |
| BIG2 | Brefeldin A-inhibited guanine nucleotide-exchange factor 2 |
| BL | Burkitt's lymphoma |
| BLAST | Basic Local Alignment Search Tool |
| bp | Base pairs |
| BSA | Bovine serum albumin |
| Btk | Burton's tyrosine kinase |
| CBL | Casitas-B-lineage lymphoma |
| CD | Cluster of differentiation |
| cDNA | Complementary DNA |
| CIN85 | Cbl-interacting protein of 85 kDa |
| CIP | Calf-intestine phosphatase |
| Cit | Citrine |
| CMV | Cytomegalovirus |
| CRAC | Calcium release activated channe |
| CRISPR | Clustered Regularly Interspaced Short Palindromic Repeats |
| CRISPRi | CRISPR interference |
| DAG | Diacylglycerol |
| $ddH_2O$ | Double-destilled water |
| DLBCL | Diffuse large B cell lymphoma |
| DMEM | Dulbecco's Modified Eagle Medium |
| DMSO | Dimethyl sulfoxide |
| DNA | Deoxyribonucleic acid |
| dNTP | Deoxynucleotide |
| Dox | Doxycyline |

| | |
|---|---|
| DSB | Double strand break |
| EBNA-2 | Epstein-Barr virus nuclear antigen 2 |
| EBV | Epstein-Barr virus |
| ECL | Enhanced chemiluminescence |
| env | Envelope, gene encoding glycoprotein 160 |
| ER | Endoplasmic reticulum |
| ERK | Extracellular signal-regulated kinase |
| ERM | Ezrin/radixin/moesin |
| $F(ab')_2$ | Bivalent antigen-binding fragment |
| FACS | Fluorescence activated cell sorting |
| Fc | Fragment crystallizable |
| FCS | Fetal Calf Serum |
| FOXO | forkhead transcription factor |
| gag | Gene encoding p55 (core protein) |
| GC | Germinal Center |
| GCB-DLBCL | Germinal center B cell like - DLBCL |
| GEF | Guanine nucleotide exchange factor |
| GFP | Green fluorescent protein |
| Grb2 | Growth factor receptor-bound protein 2 |
| GSK3β | Glycogen synthase kinase 3β |
| HRPO | Horseradish peroxidase |
| Ig | Immunoglobulin |
| Indel | Insertion/deletion |
| $IP_3$ | Inositol-1,4,5-trisphosphate |
| IP3R1-3 | $IP_3$ receptors |
| IPTG | Isopropyl-β-D-thiogalacto-pyranoside |
| ITAM | Immunoreceptor-tyrosine-based activation motifs |
| ITIM | Immunoreceptor tyrosine-based inhibitory motif |
| JIP1 | JNK-interacting protein 1 |
| JNK | c-Jun N-terminal kinase |
| LB | Lysogeny broth |
| LC-MS | Liquid chromatography MS |
| LEF | Lymphoid enhancer binding factor |
| LIC | Ligation-independent cloning |
| LMP | Latent membrane protein |
| MALT | Mucosa-associated lymphoid tissue |
| MAP2K7 | Mitogen-Activated Protein Kinase Kinase 7 |
| MAP3K2 | Mitogen-activated protein kinase kinase kinase 2 |
| MAPK | Mitogen-activated protein kinase |
| MCL | Mantle Cell lymphoma |
| MMLV | Moloney murine leukemia virus |
| MS | Mass-spectrometry |
| mTOR | Mammalian target of rapamycin |
| Nck | Non-catalytic region of tyrosine kinase |
| NFAT | Nuclear factor of activated T cells |

| | |
|---|---|
| NFκB | Nuclear factor of kappa light polypeptide gene enhancer in B cells |
| NHEJ | Nonhomologous end joining |
| NIK | Nck-interacting kinase |
| NP40 | Nonidet P40 |
| OD | Optical density |
| PAGE | Polyacrylamide gel electrophoresis |
| PAM | Protospacer adjacent motif |
| PBS | Phosphate-buffered saline |
| PCR | Polymerase chain reaction |
| PDK1 | 3'-phosphoinositide dependent kinase 1 |
| PH | Pleckstrin-homology |
| PI | Propidium iodide |
| $PI(3,4)P_2$ | Phosphatidylinositol (3,4)-bisphosphate |
| $PI(3,4,5)P_3$ | phosphatidyl-inositol-3,4,5-trisphosphate |
| $PI(4,5)P_2$ | phosphatidyl-inositol-4,5-bisphosphate |
| PI3K | Phosphoinositide-3-kinase |
| PKA | cAMP-dependent Protein kinase A |
| PKC | Protein kinase C |
| PlatE | Platinum-E |
| PLCɣ2 | Phospholipase C ɣ2 |
| PMS | Phenazine methosulfate |
| pol | Retroviral DNA polymerase |
| PTEN | 3'-phosphatase and Tensin homolog |
| PTK | Protein tyrosine kinase |
| PTP | Protein tyrosine phosphatase |
| Ras | Rat sarcoma |
| rcf | Relative centrifugal force |
| RFP | Red fluorescent protein |
| RNA | Ribonucleic acid |
| RNAi | RNA interference |
| RPMI | Roswell Park Memorial Institute |
| RT | Room temperature |
| SD | Standard deviation |
| SDS | Sodium dodecyl sulfate |
| SFK | Src-family kinases |
| sgRNA | Single guide RNA |
| SH2 | Src Homology 2 |
| SH3 | Src Homology 3 |
| SHIP1 | SH2-containing inositol 5-phosphatase 1 |
| SHIP2 | SH2-containing inositol 5-phosphatase 2 |
| SHP1 | Src homology region 2 domain-containing phosphatase-1 |
| SHP2 | Src homology region 2 domain-containing phosphatase-2 |
| shRNA | Short hairpin RNA |
| SILAC | Stable isotope labeling with amino acids in cell culture |
| siRNA | Small interfering RNA |

| | |
|---|---|
| SLP65 | SH2-domain containing leucocyte adapter protein of 65 kDa |
| SMZL | Splenic marginal zone lymphoma |
| ssDNA | Single strand DNA |
| Syk | Spleen tyrosine kinase |
| TALE | transcription activator-like effector |
| TAPP | tandem PH-containing protein |
| TCF | T cell factor |
| TCR | T cell receptor |
| TEMED | N,N,N',N'-tetramethylethylene-diamine |
| UV | Ultraviolet |
| VSV-G | Vesicular stomatitis virus glycoprotein |
| wt | Wild-type |
| X-gal | 5-bromo-4-chloro-3-indolyl-beta-D-galacto-pyranoside |
| XTT | 2,3-Bis-(2-methoxy-4-nitro-5-sulfophenyl)-2H-tetrazolium-5-carboxanilide salt |

**Deoxyribonucleotides**

| | |
|---|---|
| G | deoxyguanosine monophosphate |
| A | deoxyadenosine monophosphate |
| T | deoxythymidine monophosphate |
| C | deoxycytidine monophosphate |

**Single-letter Amino Acid Code**

| | |
|---|---|
| A | Alanine |
| C | Cysteine |
| D | Aspartic Acid |
| E | Glutamic-Acid |
| F | Phenylalanine |
| G | Glycine |
| H | Histidine |
| I | Isoleucine |
| K | Lysine |
| L | Leucine |
| M | Methionine |
| N | Asparagine |
| P | Proline |
| Q | Glutamine |
| R | Arginine |
| S | Serine |
| T | Threonine |
| V | Valine |
| W | Tryptophan |
| Y | Tyrosine |

# 1 Introduction

## 1.1 Burkitt's lymphoma - why we still need improved therapeutic approaches

Burkitt's lymphoma (BL) is a rare but highly aggressive form of mature B cell neoplasm arising from a sub-population of B lymphocytes, which are an integral part of our immune system that defends us against a broad range of pathogens. BL is one of the fastest growing human tumors, with a doubling time of only 24 - 48 h (Molyneux et al. 2012; Klein et al. 1968) and was first described as a jaw tumor in children by Dr. Denis Burkitt in 1958 while working in malarial areas in Africa (Burkitt 1958). Even today, BL is most prevalent in children living in malarial regions of equatorial Africa who are also frequently infected with Epstein-Barr virus (EBV) (Schmitz et al. 2012). This type of BL is labeled as endemic BL. Outside of continental Africa, cases of BL can be separated into sporadic or immunodeficiency-associated BL. For these forms of BL, EBV infection is less common. 15% of patients with sporadic and 40-50% of patients with immunodeficiency-associated BL are infected with EBV (Spender & Inman 2014). It is not yet entirely clear, how EBV infection contributes to BL pathogenesis. However, EBV has been shown to provide signals for transformation and survival of B cells that can induce malignant transformations through the expression of viral proteins such as Epstein-Barr virus nuclear antigen 2 (EBNA-2), EBV latent membrane proteins (LMP)-2A and LMP-1 (reviewed by Spender & Inman 2014).

Due to its high rate of proliferation, BL is generally treated with a combinatorial therapy of different genotoxic agents and rituximab, a chimeric monoclonal antibody targeting the B cell marker CD20 (Fowler & Davis 2013; Jacobson & LaCasce 2014; Jabbour & Kantarjian 2016). In countries with a high median household income, chances of successful treatment can be considered excellent as the cure rate of the sporadic form of BL is roughly 90% (reviewed by Klumb 2012). Although this regimen is successful in most cases, short- and long-term toxicities of high-dose chemotherapy limits the application for older patients and those suffering from endemic BL (Staudt 2012). Especially for patients in less developed countries, the necessary supportive care for high-dose chemotherapy regimens is often not available and lower-dose therapies must be given to avoid treatment-related mortality (Klumb 2012). In addition, prognosis of refractory or relapsed patients is very poor and highlights the need of novel therapeutic approaches (Jacobson & LaCasce 2014). While the available therapeutic agents interfere with the proliferation of BL cells, they are rather unspecific as they do not exclusively target BL cells. Although the genetic background in BL has been known for some time, the scientific community has just recently begun to understand the molecular signaling

networks driving high rates of proliferation and survival which are characteristic for BL cells. To explain why especially BL cells proliferate so aggressively, we need to shed some light on their cellular origin.

## 1.2 B cell neoplasms arise at different stages of B cell development

While the existence of antibody-producing cells was already proposed by Paul Ehrlich in 1897, it was not until 1965 that B cells were described as a distinct lymphoid cell lineage (Cooper et al. 1965). B cells are named after the bursa of Fabricius, a hindgut lymphoid organ in birds that was identified as the site of antibody production in chicken (Glick, Chang, & Jaap, 1956; reviewed in Cooper, 2015). In mammals, B cells develop in the bone marrow, where they irreversibly rearrange immunoglobulin (Ig) gene segments, in a process termed V(D)J recombination (Hozumi & Tonegawa 1976) (Figure 1). This re-arrangement occurs randomly, only one locus is re-arranged at a time at different stages of B cell development and allelic exclusion ensures that each B cell expresses only one receptor specificity. In the first step, B cells only rearrange the Ig heavy chain, which can pair with a surrogate light chain to form the pre-B cell antigen receptor (BCR), which promotes high levels of proliferation. During this process, chromosomal translocations and mutations can also lead to B cell acute lymphocytic leukemia (B-ALL) (Iacobucci et al. 2012). In the next developmental stage, B cells rearrange their Ig light chains and the pre-BCR is replaced by a functional BCR composed of a heavy and a light chain. Theoretically, V(D)J recombination could thereby result in a diversity of at least $10^{12}$ distinct B cell antigen receptors enabling the immune system to fend off a plethora of antigens (Alberts et al. 2002). While this random process increases the B cell repertoire, it can also generate B cells that react to ubiquitous self-antigens and thus could induce auto immune reactions. These auto-reactive B cells are removed from the B cell repertoire during B cell development by different processes selecting for self-tolerance (Pelanda & Torres 2012).

Immature B cells then leave the bone marrow to become mature naïve B cells in the spleen. Mature B cells can give rise to indolent non-mutated B cell chronic lymphocytic leukemia (B-CLL) or mantle cell lymphoma (MCL) (Seifert et al. 2012). Naïve B cells circulate via the bloodstream and enter secondary lymphoid tissues such as lymph nodes and spleen. Thereby, they increase the probability to bind to their respective antigen, which can either be soluble or provided in a cell-bound manner e.g. by macrophages (Unanue 1984). Upon binding of most antigens, naïve B cells require a secondary co-stimulatory signal of an activated helper T cell to become fully activated. Activation leads to proliferation and differentiation into either antibody-secreting plasma cells or memory B cells.

Additionally, activation can induce a germinal center (GC) reaction in secondary lymphoid organs. In the dark zone of the GC, B cells proliferate rapidly and undergo immunoglobulin somatic hypermutation of Ig genes to increase antigen affinity. B cells then migrate into the light zone of the GC, where the newly arranged Igs are selected for their antigen affinity with the help of follicular dendritic cells and T helper cells (Basso & Dalla-Favera 2015). Notably, positively selected light zone cells can re-enter the dark zone for further rounds of cell division and somatic hypermutation to potentially further improve antigen affinity. Besides somatic hypermutation, Ig genes are remodeled by class-switch recombination in the light zone of GC to produce different isotype classes (De Silva & Klein 2015). Class-switching depends on the support of helper T cells and functionally optimizes the antibody since each Ig class has particular functions and a unique distribution. While in naïve B cells, alternative splicing leads to expression of IgM or IgD, GC B cells can rearrange this DNA locus and to eventually produce IgG, IgA, or IgE isotypes with different effector functions.

Somatic hypermutation and class switch recombination are regulated by Activation-induced cytidine deaminase (AID). AID induces DNA mutations and double strand breaks which are susceptible to error-prone repair thereby increasing antibody diversity. However, AID activation must be tightly regulated to avoid chromosomal translocations and development of B cell malignancies (Pettersen et al. 2015). Therefore, it not surprising that GC B cells are the origin of different B cell lymphomas including Follicular lymphoma, Diffuse large B cell lymphoma (DLBCL) and BL, which together account for ~80% of mature B cell neoplasms (Basso & Dalla-Favera 2015). While gene expression profiling reveled BL cells to derive from rapidly proliferating dark zone GC B cells, the germinal center B cell like (GCB)-DLBCL and follicular lymphoma cells resemble light zone B cells and Activated B cell like (ABC)-DLBCL is derived from GC cells arrested in early stages of plasma cell differentiation (Victora et al. 2012; Dave et al. 2006; Alizadeh et al. 2000; Basso & Dalla-Favera 2015).

In addition, GC-derived plasma cells can give rise to multiple myeloma while GC-derived memory B cells are discussed to be the origin of a mutated form of B-CLL (Seifert et al. 2012; Röllig et al. 2015). Moreover, marginal zone B cells are mature B cells resident in the marginal zone of the spleen, which are also believed to be generated through a GC reaction in humans (Weill et al. 2009; Dunn-Walters et al. 1995). They can give rise to splenic marginal zone lymphoma and mucosa-associated lymphoid tissue (MALT) lymphoma (Baliakas et al. 2015; Isaacson & Spencer 1987).

Considering the diversity of B cell neoplasms arising from different developmental stages, it is not surprising that the drivers for abnormal proliferation are characteristic for each subtype, which have been nicely reviewed by others (Rickert 2013; Vaqué et al. 2014). Despite these differences - with

the exception of multiple myeloma - B cell malignancies discussed here retain their BCR expression after their neoplastic transformation indicating that they remain dependent on BCR signaling for survival and proliferation (Küppers 2005; Buchner & Müschen 2014).

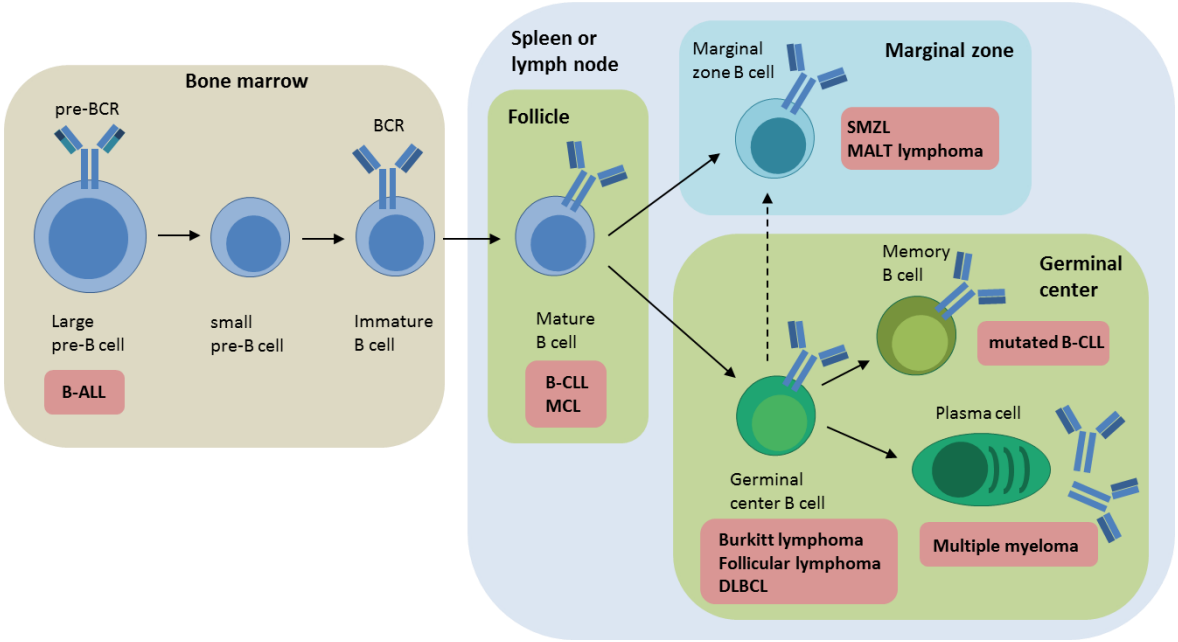


**Figure 1: B cell neoplasms arise at different stages of B cell development.**
In the bone marrow, B cell acute lymphocytic leukemia (B-ALL) arises from large pre-B cells expressing a pre-BCR with a surrogate light chain. Small pre-B cells undergo light chain re-arrangement and the complete BCR is expressed in immature B cells. Immature B cells leave the bone marrow and become mature naïve B cells in the periphery. They are the cellular origin of B cell chronic lymphocytic leukemia (B-CLL) and Mantle cell lymphoma (MCL). Burkitt's lymphoma (BL), Follicular lymphoma or Diffuse large B cell lymphoma (DLBCL) originate from germinal center (GC) B cells. GC B cells can either differentiate into memory B cells or antibody-secreting plasma cells. Memory B cells are the cellular origin of a mutated subtype of B-CLL while plasma cells can give rise to multiple myeloma. In humans, marginal zone B cells are also reported to have undergone GC reaction and can give rise to splenic marginal zone lymphoma (SMZL) and mucosa-associated lymphoid tissue (MALT) lymphoma. Adapted from Rickert, 2013.

## 1.3 Signaling via the B cell antigen receptor

### 1.3.1 The B cell antigen receptor (BCR)

The B cell antigen receptor (BCR) contains a transmembrane version of Ig, which consists of two identical heavy and two identical light chains, forming a Y-shaped molecule. The two heavy chains are connected to each other by a disulfide bond in addition to disulfide bonds connecting heavy and light chains. The heavy chains are encoded by $V_H$, $D_H$, $J_H$ and $C_H$ gene segments, whereas the light chains are encoded by $V_L$, $J_L$, and $C_L$ either of the κ or λ subtype.

To form a functional BCR, the membrane Ig is non-covalently associated to CD79A (Igα) and CD79B (Igβ). CD79A and CD79B are invariant protein chains which are connected by disulfide bonds to form a heterodimer (Reth et al. 1991). The CD79A-CD79B heterodimer is required for both surface expression of the Ig as well as signal transduction via their immunoreceptor-tyrosine-based activation motifs (ITAMs) in their cytoplasmic tails. ITAMs share a consensus sequence of **Y**XX(L/I)$X_{6-8}$ **Y**XX(L/I) (where X denotes any amino acid) (Reth 1989) and are also found in signaling chains associated to T cell or natural-killer cell receptors as well as in certain Fc receptors (Humphrey et al. 2005). In B cells, stimulation of the BCR and activation of protein tyrosine kinases triggers ITAM tyrosine (Y) phosphorylation thus initiating a cascade of several signaling pathways.

### 1.3.2 BCR signaling upon stimulation

It is still under debate how the BCR in resting cells is organized and how the dynamics of the cytoskeleton interfere with this process. The first model, known as the confirmation-induced oligomerization model or cross-linking model, proposes that BCR monomers are dispersed in the membrane in a closed, inactive confirmation in resting B cells. Upon cross-linking with a multivalent antigen or monovalent antigen presented by antigen-presenting cells, a conformational change in the Ig allows oligomerization and formation of BCR microclusters in lipid rafts and opens cytoplasmic domains for signaling (Treanor 2012; Treanor et al. 2010; Pierce & Liu 2010). Reth and colleagues previously proposed a different model named dissociation activation model based on findings of large macromolecular complexes of IgM and IgD in resting cells (Schamel & Reth, 2000; Yang & Reth, 2010a). Their model proposes that BCRs are organized in auto-inhibitory oligomers in resting B cells. Binding of a polyvalent antigen to the receptor triggers BCR oligomer dissociation, which exposes the cytoplasmic domains of CD79A and CD79B for subsequent signal transduction in defined areas (Treanor, 2012; Yang & Reth, 2010b).

While there is still an ongoing debate about BCR dynamics in resting B cells, early events of BCR-dependent signaling have been characterized in-depth in recent years and are generally agreed upon. The engagement of the BCR with its cognate antigen leads to phosphorylation of ITAMs in the CD79A-CD79B heterodimer and a non-ITAM tyrosine residue in CD79A by Src-family kinases (SFK) such as Lyn, Fyn and spleen tyrosine kinase (Syk) (Pao et al., 1998; Schmitz et al., 1996) (Figure 2). The phosphorylated ITAMs serve as docking sites for tandemly arranged Src homology 2 (SH2) domains of Syk (Fütterer et al. 1998) thereby compromising autoinhibition and leading to full activation of Syk (Engelke et al., 2007; Rolli et al., 2002). Once activated, Syk can additionally phosphorylate other ITAMs of neighboring BCRs thereby amplifying BCR signaling (Rolli et al. 2002).

Besides Syk, the SH2-domain containing leucocyte adapter protein of 65 kDa (SLP65, also known as BLNK or BASH) is recruited to the phosphorylated non-ITAM tyrosine residue (pY204) in CD79A and is subsequently phosphorylated by Syk at various tyrosine residues (Engels et al. 2001). Tyrosine phosphorylated SLP65 then recruits Burton's tyrosine kinase (Btk) and phospholipase C (PLC) ɣ2 into a multiprotein complex known as the $Ca^{2+}$ initiation complex (Engelke et al., 2007; Hashimoto et al., 1999). In context of this complex, Btk is activated and subsequently phosphorylates and thereby activates PLCɣ2. The complex localizes at the plasma membrane with the help of Pleckstrin homology (PH) domains of Btk and PLCɣ2 binding to phosphatidyl-inositol-3,4,5-trisphosphate [$PI(3,4,5)P_3$] (Salim et al. 1996; Falasca et al. 1998), while membrane recruitment of SLP65 requires the constitutive interaction with CBL-interacting protein of 85 kDa (CIN85) (Oellerich et al. 2011). At the plasma membrane, activated PLCɣ2 hydrolyzes its substrate phosphatidyl-inositol-4,5-bisphosphate [$PI(4,5)P_2$] to produce the second messengers inositol-1,4,5-trisphosphate ($IP_3$) and membrane-resident diacylglycerol (DAG).

The second messenger $IP_3$ induces $Ca^{2+}$ mobilization from the endoplasmic reticulum (ER) and the extracellular space. $IP_3$ serves as a ligand for $IP_3$ receptors (IP3R1-3) being $Ca^{2+}$ channels in the in the ER, which open upon binding of $IP_3$ and release $Ca^{2+}$ stored in the ER into the cytosol (Taylor & Tovey, 2010). The fast decrease of $Ca^{2+}$ in the ER is sensed by transmembrane proteins of the ER, named stromal interaction molecules (STIMs) that upon binding of $Ca^{2+}$ can activate Calcium release activated channels (CRACs) in the plasma membrane (Baba & Kurosaki 2015; Kar et al. 2012). Activation of CRACs leads to sustained influx of extracellular $Ca^{2+}$ into the cytosol (reviewed by Engelke et al. 2007; Oh-hora & Rao, 2009). One target of sustained $Ca^{2+}$ flux in B cells is the transcription factor nuclear factor of activated T cells (NFAT). In the cytosol, phosphorylated NFAT is inactive and activation requires the dephosphorylation by the phosphatase Calcineurin, which is activated by the $Ca^{2+}$ sensor Calmodulin (Klee et al. 1979). De-phosphorylated NFAT can then rapidly translocate into the nucleus and activate its target genes. NFAT regulates cell cycle progression in naïve B cells via Cyclin E and was shown to be involved in efficient plasma cell differentiation (Engelke et al. 2007).

Among other pathways, membrane-bound DAG regulates activation of the transcription factor NFκB (nuclear factor of kappa light polypeptide gene enhancer in B cells) via recruitment of the serine/threonine protein kinase C (PKC)β. $Ca^{2+}$ binding fully activates PKCβ, which subsequently activates the IκBα kinase complex and releases NFκB from its negative regulator IκB. When released, NFκB translocates into the nucleus and induces transcription of its target genes. NFκB signaling plays an important role in innate and adaptive immune responses by regulating genes involved in

proliferation, survival, and differentiation (Hayden et al. 2006; Oeckinghaus & Ghosh 2009).

Additionally, Mitogen-activated protein kinases (MAPKs) are activated following BCR stimulation. While BCR-induced activation of the MAPK extracellular signal-regulated kinase (ERK) in chicken and mouse B cells requires the DAG-dependent recruitment of Ras guanyl nucleotide-releasing proteins (GRPs), in human B cells, ERK is primarily activated by the adaptor function of SLP65 (Oh-hora et al. 2003; Coughlin et al. 2005). SLP65 binds the adaptor Growth factor receptor-bound protein 2 (Grb2), thereby mediating the recruitment of Sos, a guanine nucleotide exchange factor (GEF) (Wienands et al. 1998; Aronheim et al. 1994). Sos in turn activates the small G-protein Ras thereby initiating ERK activation (Aronheim et al. 1994). Moreover, SLP65 is also central protein in the activation of MAPK c-Jun N-terminal kinase (JNK). SLP65 is associated with the small GEF Vav, which activates Rho-family GTPases like Rac1. (Brezski & Monroe 2007; Wienands et al. 1998). In addition, SLP65 recruits PLCɣ2, and activation of both PLCɣ2 and Rac1 is necessary for subsequent JNK activation (Ishiai et al. 1999). Moreover, DAG-mediated activation of PKCβ promotes signaling pathways leading to MAPK p38 activation (Hashimoto et al. 1998). MAPK signaling induces activation of many transcription factors, which are involved in lymphocyte proliferation, survival and differentiation (Khiem et al. 2008; Yasuda et al. 2011; Kyriakis & Avruch 2001).

Besides the formation of the $Ca^{2+}$ complex and activation of its downstream effectors, BCR engagement and activation of the co-receptor CD19 also initiates the recruitment of Phosphoinositide-3-kinase (PI3K) to the plasma membrane. Protein tyrosine kinases Syk, Fyn, and Btk phosphorylate CD19 and the B cell adapter for PI3K (BCAP), which provides binding sites for the p85 subunit of PI3K (Okada et al. 2000). In addition, the adapter protein Nck can bind to the phosphorylated non-ITAM tyrosine residue (pY204) in CD79A and recruit BCAP, serving as a direct link between BCR activation and PI3K signaling (Castello et al. 2013). Upon recruitment and activation, PI3K phosphorylates $PI(4,5)P_2$ to $PI(3,4,5)P_3$, which mediates the translocation of the AKT kinase (also referred to as PKB) and the 3'-phosphoinositide dependent kinase (PDK)1 to the plasma membrane (Vanhaesebroeck & Alessi 2000). AKT is phosphorylated at T308 by PDK1 in the activation loop and at S473 in the carboxylterminal hydrophobic motif by a complex of rictor and mammalian target of rapamycin (mTOR) to become fully activated (Sarbassov et al. 2005; Vanhaesebroeck & Alessi, 2000). Among the multitude of effectors functions, AKT promotes survival signaling through phosphorylation and inactivation of apoptosis-inducing targets such as pro-apoptotic BCL-2 related protein Bad, Caspase-9 and forkhead transcription factors (FOXOs) (Cardone et al. 1998; Downward 2004), while promoting cell cycle progression by inhibition of glycogen synthase kinase 3β (GSK3β)-mediated phosphorylation of Cyclin D (Diehl et al. 1998).

The 3'-phosphatase and Tensin homolog (PTEN) and the 5'-phospatases SHIP2 and SHIP2 are important negative regulators of the PI3K-AKT signaling pathway as they decrease the pool of $PI(3,4,5)P_3$ to $PI(4,5)P_2$ or $PI(3,4)P_2$, respectively (Leslie et al., 2012). However, $PI(3,4)P_2$ can also serve as a membrane anchor for both AKT and PDK1, even though PDK1 preferentially binds to $PI(3,4,5)P_3$ (Alessi et al., 1997; Manna et al., 2007; Xie, Erneux & Pirson, 2013).

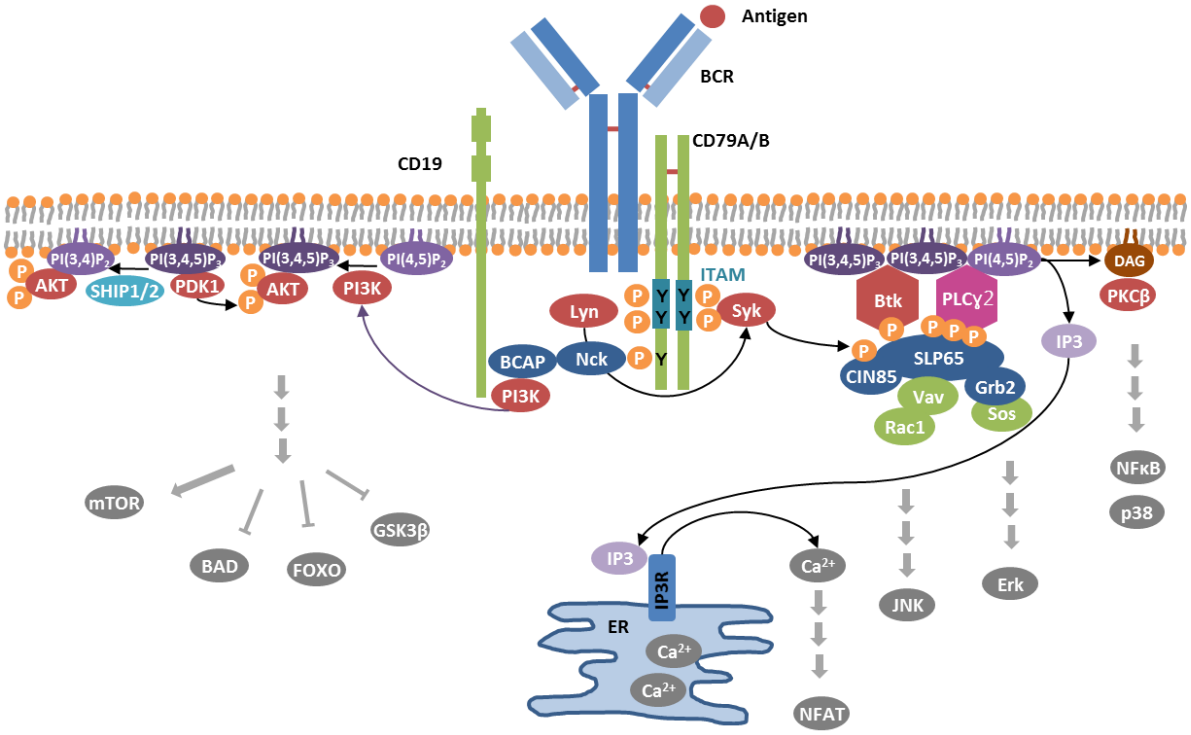


**Figure 2: Schematic depiction of B cell antigen receptor (BCR) signaling.**
Upon BCR engagement, activation of Src-family kinases such as Lyn and Syk phosphorylate ITAMs in CD79A and CD79B as well as one non-ITAM tyrosine (Y204) in CD79A. This leads to phosphorylation of SLP65 which recruits Btk and PLCγ2 for the formation of the $Ca^{2+}$ initiation complex. In the complex, PLCγ2 is phosphorylated by Btk and hydrolyzes $PI(4,5)P_2$ to the second messengers DAG and IP3. IP3 in turn induces $Ca^{2+}$ mobilization from the ER leading to subsequent NFAT activation. Membrane bound DAG mediates recruitment of PKCβ and activation of the NFκB and the p38 pathway. ERK signaling is triggered by Sos, while JNK signaling is mediated by activation of Rac1. Additionally, the PI3K pathway can be activated by recruitment of Nck to the phosphorylated non-ITAM in CD79A and subsequent binding to BCAP. BCAP is also phosphorylated upon CD19 activation and recruits PI3K, which phosphorylates $PI(4,5)P_2$ to $PI(3,4,5)P_3$. PDK1 and AKT are recruited to the plasma membrane by $PI(3,4,5)P_3$ leading to PDK1-dependent AKT phosphorylation and activation. Activation of the AKT pathway promotes survival and proliferation signaling, by increasing cell cycle and glucose metabolism and by inhibition of apoptosis. SHIP1 and SHIP2 decrease the pool of $PI(3,4,5)P_3$ by de-phosphorylation to $PI(3,4)P_2$, although $PI(3,4)P_2$ can also serve as a membrane anchor for PDK1 and AKT.

### 1.3.3 BCR signaling in B cell malignancies

*Activation of BCR signaling by foreign or self-antigens*

Indolent B cell neoplasms such as splenic marginal zone lymphomas, B-CLL and MALT lymphomas are characterized by their recognition of foreign or self-antigens that induce aberrant BCR signaling (Craig et al. 2010; Rossi & Gaidano 2010). A subset of these lymphomas expresses near-identical, stereotyped BCRs, leading to the suggestion that they were selected for with a restricted repertoire of antigen epitopes (Henry Dunand & Wilson 2015). In B-CLL, one of the most frequent B cell malignancies in the United States (Morton et al. 2006), stereotyped monoclonal antibodies can for example react to self-antigens derived from apoptotic cells, which correlates with poor prognosis (Chu et al. 2010). Stereotyped BCRs can also signal autonomous and thereby independent of external antigens. The heavy chain complementary determining region of these stereotyped BCRs can bind to an internal epitope of neighboring BCRs on the same cell, thus constantly activating BCR signaling (Minden et al. 2012).

*Constitutive BCR activation by somatic mutations in BCR signaling components*

In most aggressive B cell lymphomas, such as DLBCL, mutations in BCR effector molecules initiate a chronic, constitutive activation of the BCR signaling cascade. In the case of ABC-DLBCL, proximal BCR signaling proteins such as CD79A and CD79B are mutated in ~20% of cases thereby preventing BCR endocytosis and inhibiting the negative regulation of Src-family kinase Lyn (Davis et al., 2010). Additional mutations in *CARD11* and *MyD88* promote survival of cells by constitutive NF-kB activation, independent of BCR engagement (Lenz et al. 2008; Ngo et al. 2011). In B-ALL, mutations downstream the pre-BCR including the expression of the breakpoint cluster region-ABL1 fusion protein, impaired expression of SLP65 or Ras and SHP2 gain of function mutations contribute to ligand-independent survival signaling (reviewed by Rickert 2013). Despite their aggressive nature, BL cells do not harbor genetic mutations in proximal BCR-signaling effector proteins (Schmitz et al. 2012; Richter et al. 2012). The following chapter will therefore discuss the molecular characteristics contributing to their malignancy.

## 1.4 Molecular characteristics of Burkitt's lymphoma

On a molecular level, BL is characterized by a reciprocal chromosomal translocation of the *c-MYC* proto-oncogene and one of three immunoglobulin genes. Upon translocation, c-MYC is brought under the control of transcriptionally active Ig enhancer elements either of the Ig heavy chain [t(8;14)] in 80% of cases (Hayday et al. 1984) or Ig κ [t(2;8)] or λ [t(8;22)] light chains, respectively, accounting for the remaining 20% (reviewed by Allday, 2009). As a result, c-MYC, which is normally repressed in dark zone B cells, is overexpressed in BL cells (Dominguez-Sola et al. 2012) while the normal c-MYC allele is silent in BL (ar-Rushdi et al. 1983). In a physiological context, c-MYC expression increases the cell mass prior to its division and subsequently promotes cell division by upregulation of cyclin D, E2F, and cyclin-dependent kinase 4, while repressing genes involved in cell cycle arrest (Spender & Inman 2014). To avoid uncontrolled cell growth, expression of c-MYC is tightly regulated. The c-MYC protein is degraded very rapidly with a half-life of only 20-30 min and if overexpressed triggers a stress-response leading to apoptosis (Spender & Inman 2014). However, BL cells depend on continuous c-MYC expression for survival and G1 cell cycle progression (Gomez-Curet et al., 2006; Marinkovic et al., 2004; Spender & Inman, 2012).

Thus, BL cells must have acquired additional properties to escape the apoptosis-inducing c-MYC regulation. High throughput RNA-sequencing data showed that besides mutations in *c-MYC* itself, the tumor-suppressor p53 (encoded by *TP53*), which is known to play a central role for c-MYC-induced apoptosis (reviewed in Allday, 2009), is frequently mutated in more than 30% of sporadic BL cases (Bhatia et al., 1992; Schmitz et al., 2012). Moreover, the transcription factor *TCF3* (E2A) or its negative regulator *ID3* are mutated in 70% of sporadic and immunodeficiency-related and in 40% of endemic BL cases (Schmitz et al. 2012; Love et al. 2012; Richter et al. 2012). E2A promotes G1-S cell-cycle progression by *CCND3* activation (encoding cyclin D3), which is frequently mutated in sporadic and HIV-associated BL (Schmitz et al. 2012). Additionally, E2A regulates expression of BCR signaling components by repressing mRNA and protein expression of the phosphatase SHP1, a negative regulator of BCR signaling while transactivating Ig heavy and light chain genes (Schmitz et al. 2012; Schmitz et al. 2014). Thereby, E2A activates the PI3K-AKT pathway, which drives proliferation and survival in B cells. In addition, also *PI3KR1*, encoding for the regulatory subunits p85α, p55α and p50α of the heterodimeric class 1 PI3K, is recurrently mutated in BL (Love et al. 2012) further highlighting the importance of this pathway for BL.

Besides the aforementioned mutations affecting this signaling pathway, PI3K signaling in BL is driven by tonic, antigen-independent low-level BCR signaling (Schmitz et al. 2012). Since tonic signaling via the BCR is considered to be a driving force for survival of BL cells, the next chapter will discuss tonic BCR signaling in more detail.

## 1.5 Tonic BCR signaling

BCR signaling is commonly associated with antigen-induced signaling, however, low levels of BCR signaling can also occur in the absence of the antigen, referred to as tonic BCR signaling. The direct molecular mechanism of tonic BCR signaling remains unclear, but the central role of Syk regulation by protein tyrosine phosphatases (PTPs) is well established in this context (Rolli et al. 2002; Monroe 2006; Wienands et al. 1996). Treating living cells with pervanadate/$H_2O_2$, an inhibitor of PTPs, suggests the existence of a pre-formed BCR transducer complex containing protein tyrosine kinases (PTKs) such as Syk and PTPs. BCR signaling could be activated by inhibition of PTPs and $H_2O_2$ even in the absence of BCR stimulation (Wienands et al. 1996). These findings are the cornerstone for a tonic signaling model that is based on stochastic phosphorylation and subsequent dephosphorylation of the BCR and its positive and negative co-receptors by PTKs and PTPs (Monroe 2006). In this model, the resting state of B cells is maintained as an equilibrium of stochastic triggering and termination of the signal by negative regulators (Figure 3). Stochastic interactions between the positive co-receptors such as CD45 and Src-family PTKs like Lyn result in single phosphorylation of the membrane proximal tyrosine in the ITAM in CD79A leading to subsequent partial Syk activation (Fütterer et al. 1998). However, PTKs also phosphorylate immunoreceptor tyrosine-based inhibitory motifs (ITIMs) in negative co-receptors like CD22. This leads to recruitment of PTPs such as SHP1, which de-phosphorylate the ITAMs, thus terminating tonic signaling (Cornall et al. 1998; Nitschke 2005). Additionally, Src-family PTKs phosphorylate Syk at Y317, thereby targeting it for Casitas-B-lineage lymphoma (CBL)-dependent ubiquitinylation and proteasomal degradation (Yankee et al., 1999). Beyond this model, also the interaction of the co-receptors CD45 and CD22 fine tunes tonic BCR signaling. CD45, by virtue of its extracellular domain, restrains CD22 inhibitory function to maintain tonic BCR signaling, presumably by restricting the pool of Src-family PTK Lyn to CD22 (Coughlin et al. 2015). Hence, tonic BCR signaling is believed to be a tightly regulated process of phosphorylation and de-phosphorylation of the BCR complex and its co-receptors thus resembling an equilibrium between low activation and negative regulation.

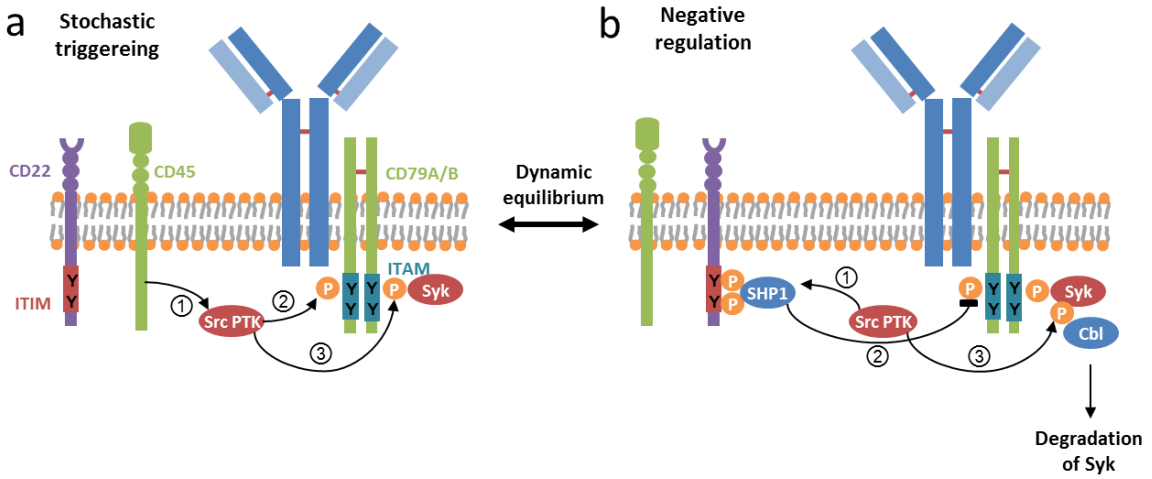


**Figure 3: Dynamic equilibrium model for tonic BCR signaling.**
The resting state of the non-aggregated BCR signaling complex is maintained as an equilibrium between stochastic triggering and negative regulation. (a) Stochastic triggering. ① Stochastic interactions between the positive co-receptor CD45 and Src-family kinases induces ② the phosphorylation of membrane-proximal ITAM tyrosine residues of CD79A and CD79B. ③ Syk is subsequently recruited and partially activated, leading to initiation the BCR signaling cascade as described in Figure 2. (b) Negative regulation. ① Src-family kinases phosphorylate ITIM motifs in negative co-receptors such as CD22. Phosphorylated ITIMs recruit protein tyrosine phosphatases like SHIP1 to the BCR complex and ② de-phosphorylate the ITAMs. ③ Src-family-kinases also mediate phosphorylation of Syk at Y317, thereby labeling it for CBL-dependent proteasomal degradation. Adapted from Monroe, 2006.

The importance of BCR expression and physiological tonic signaling for B cell survival is highlighted by several studies. These studies showed that the inducible knockdown of the BCR, ablation of CD79A or the selective excision of the CD79A ITAM leads to loss of mature B cells (Lam et al. 1997; Kraus et al. 2004). However, mature B cells without a BCR could be fully rescued from apoptosis by activating the pro-survival PI3K pathway, but not by NFκB signaling (Srinivasan et al. 2009). This indicates that tonic BCR signaling is promoting signaling via the PI3K pathway.

The concept that tonic BCR-induced PI3K signaling, beyond the MYC translocation, is the driving force in BL pathogenesis was first published by the group of Louis Staudt in 2012. They identified several genes involved in the PI3K pathway to be mutated in BL and could show that tonic BCR signaling via the PI3K pathway is essential for BL cell survival (Schmitz et al. 2012). The relevance of both c-MYC and PI3K activity for BL pathogenesis was also confirmed *in vivo*, leading to BL-like tumors in mice (Sander et al. 2012). Interestingly, although BL cells have acquired oncogenic pro-survival mutations, they still rely on BCR signals for their survival. This fact makes tonic BCR signaling a promising target for novel therapeutic approaches.

## 1.6 Aim of this study

Although the relevance of tonic BCR signaling via the PI3K pathway for BL cell survival is well established, the proximal cascade of the tonic BCR signaling network is not yet defined. Studies on Syk inhibition revealed that Syk is involved in tonic BCR signaling. Quantitative phospho-proteomics has furthermore identified multiple proteins within BL cell lines that are differentially phosphorylated upon Syk inhibition or CD79A knockdown (Corso et al. 2016). All of these findings indicate that also proteins upstream or independent of Syk are involved in proximal tonic BCR signaling. Based on the phospho-proteomics data combined with preliminary shRNA screens testing for a potential pro-survival role, I chose three BL-specific BCR effector proteins for detailed analysis of their role in BL-specific BCR signaling and addressed the following questions:

1. Are the BL-specific proteins identified by phospho-proteomics relevant BL cell proliferation and survival?
2. How do BL-specific BCR effectors regulate tonic signaling? Which pathways are affected that might contribute to BL cell proliferation and survival?

These aims were addressed by generating BL cell lines deficient for selected BCR effector proteins. Cells were functionally characterized by focusing on proliferation, apoptosis, and tonic BCR signaling.

# 2 Materials and Methods

## 2.1 Materials

### 2.1.1 Instruments

**Table 1: Instruments used in this study.**

| Name | Manufacturer |
|---|---|
| Agarose Gel Electrophoresis System | Peqlab |
| Amaxa Nucleofector™ | Lonza |
| Amnis ImageStream$^{®X}$ MarkII Imaging Flow Cytometer | Merck |
| Balance BP61 | Sartorius |
| Balance H95 | Sartorius |
| Cell Culture Incubator Hera Cell 150 $CO_2$ | Heraeus |
| Centrifuge Sorvall RC3B Plus | Sorvall |
| Chemi Lux Gel Imager | Intas Science Imaging |
| Countess Cell Counter | Invitrogen |
| Electrophoresis Power Supply EPS 301 | Amersham Biosciences |
| Electrophoresis System Hoefer SE600 | Amersham Biosciences |
| Flow Cytometer LSR II | Becton Dickinson |
| Freezer HeraFreeze | Heraeus |
| Freezer Platilab 340 | Angelantoni life science |
| GenePulser II Electroporation system | Bio-Rad Industires |
| Ice Machine | Ziegra |
| Incubation Shaker Unitron | Infors |
| Incubator Kelvitron T | Heraeus |
| Laminar Flow Cabinet HeraSafe | Heraeus |
| Light Microscope Teraval 31 | Zeiss |
| LSM 510 Meta | Zeiss |
| Magnetic stirrer M21/1 | Framo Gerätetechnik |
| Mastercycler Epgradient | Eppendorf |
| Microcentrifuge 5417R | Eppendorf |
| Microcentrifuge MiniSpin™ | Eppendorf |
| Microplate Reader Powerwave 340 | BioTEK |

| Name | Manufacturer |
|---|---|
| Mini Protean Tetra Cell | Bio-Rad Laboratories |
| Multifuge 3SR | Heraeus |
| NanoDrop 2000 | Thermo Scientific |
| Neubauer improved counting chamber | Laboroptik |
| pH-Meter inoLab® | WTW |
| Pipettes | Eppendorf |
| Rocking Shaker | Neolab |
| Rocking Shaker Duomax 1030 | Heidolph |
| Rotor SW41 Ti | Beckman |
| Semiphor Transphor Unit TE77 | Amersham Biosciences |
| Sprout Minizentrifuge | Biozym |
| Thermomixer Comfort | Eppendorf |
| ThermoMixer® C | Eppendorf |
| UV-Illuminator | Intas Systems |
| Vortex Genie 2 | Scientific Industries |
| Water Bath | Schütt Labortechnik |
| Water Purification System Milli-Q | Millipore, Sartorius |

### 2.1.2 Software and databases

**Table 2: Software.**

| Application | Software | Manufacturer |
|---|---|---|
| Citation Management Software | Mendeley | Elsevier |
| Flow cytometry data acquisition | FACSDiva | BD Bioscience |
| Flow cytometry data analysis | FlowJo 7.6.5 | Treestar |
| Illustration Software | BioRender | biorender.io |
| Image processing | ImageJ | W.Rasband, NIH |
| Sequence Data Analysis | Serial Cloner | Serial Basics |
| Sequence Data Analysis | Finch TV | Geospiza |
| Text processing, spreadsheets, illustrations | Microsoft Office | Microsoft |
| Western Blot Data Acquisition | Chemostar professional | Intas |

**Table 3: Databases.**

| Database | Application |
|---|---|
| http://crispr.mit.edu/ | CRISPR design |
| http://mfeprimer.igenetech.com/ | Primer quality control |
| http://multalin.toulouse.inra.fr/multalin/ | Sequence alignment |
| http://www.uniprot.org/ | General protein data |
| https://blast.ncbi.nlm.nih.gov/Blast.cgi | Sequence Alignment |
| https://thebiogrid.org/ | Protein-Protein Interactions |
| https://www.ensembl.org/index.html | Genomic and mRNA data |
| https://www.ncbi.nlm.nih.gov/ | Genomic and mRNA data |
| https://www.ncbi.nlm.nih.gov/tools/primer-blast/ | Primer design |
| https://www.proteinatlas.org/ | Protein expression data |

### 2.1.3 Consumables

**Table 4: Consumables used in this study.**

| Name | Manufacturer |
|---|---|
| 1.5 ml, 2 ml reaction tubes | Greiner bio-one |
| 10 ml syringes | BD Biosciences |
| 14 ml, 15 ml, 20 ml reaction tubes | Greiner bio-one |
| 2 ml, 5 ml, 10 ml, 25 ml serological pipettes | Greiner bio-one |
| 5 ml flow cytometry tubes | Sarstedt |
| 6-, 12-, 24-, 96-well suspension culture plates | Greiner bio-one |
| 60 mm, 100 mm, 145 mm cell culture plates | Greiner bio-one |
| Cryo tubes | Greiner bio-one |
| Electroporation cuvettes | Peqlab |
| Filter tips | Greiner bio-one |
| Nitrocellulose membrane Hybond ECL | Amersham Biosciences |
| Parafilm | American national can |
| PCR tubes 0.2 ml | Sarstedt |
| Pipette tips | Greiner bio-one |
| Sterile filter Filtropur, S 0.2, S 0.45 | Sarstedt |
| Whatman filter paper | GE Healthcare |
| Minisart® filter 0.45 | Sartorius |

### 2.1.4 Chemicals and reagents

All chemicals and solutions, which are only mentioned in the corresponding method section, were purchased from Carl Roth, Sigma or Merck, if not stated otherwise. Further reagents and solutions are specified in Table 5.

**Table 5: Chemicals and reagents.**

| Name | Manufacturer |
|---|---|
| 100x Bovine Serum albumin | NEB |
| Agarose | Peqlab |
| Bleomycin | Calbiochem |
| Bovine Serum albumin | Serva |
| Cytofix™ Fixation Buffer | Becton Dickinson |
| Deoxynucleoside triphosphate (dNTP) mix | NEB |
| DNA Ladder GeneRuler 1 kb | Fermentas |
| Fetal Calf Serum (FCS) | Biochrom |
| Fetal Calf serum (FCS), dialyzed | PAN biotech |
| Indo-1 AM | Life technologies |
| L-Arginine:HCL ($^{13}C_6$ $^{15}N_4$) | Cambridge Isotype Laboratories, Inc |
| L-Lysine:2HCL ($^{13}C_6$ $^{15}N_2$) | Cambridge Isotype Laboratories, Inc |
| NEBuffer 1, 2, 3, 4, Cutsmart | NEB |
| Pluronic F-127 | Life technologies |
| Prestained Protein Ladder PageRuler Plus | Thermo Scientific |
| Puromycin | InvivoGEN |
| RetroNectin® | Clonetech |
| T4-Ligase Buffer | NEB |
| Tans-IT X-239 | Mirus |
| Trypan blue solution (0.4%) | Thermo Scientific |

### 2.1.5 Buffers and solutions

**Table 6: Buffers and solutions.**

| Name | Composition |
|---|---|
| Antibody dilution solution | 1% BSA, 0.01% $NaN_3$, in TBS-T |
| Blocking solution | 5% BSA, 0.01% $NaN_3$, in TBS-T |
| Blotting buffer | 48 mM Tris, 39 mM glycine, 0.0375% SDS, 0.001% $NaN_3$, 20% MeOH, in $ddH_2O$ |
| DNA loading buffer (6x) | 60 mM EDTA (pH 8.0), 10 mM Tris/HCl (pH 7.6), 60% glycerol, 0.03% bromophenol blue, in $ddH_2O$ |
| ECL solution | 4 ml ECL solution A, 400 µl ECL solution B, 1.2 µl $H_2O_2$ (30%) |
| ECL solution SA | 100 mM Tris/HCl pH 8.6, 0.28 mM Luminol |
| ECL solution SB | 6.7 mM p-coumaric acid in 100% DMSO, stored in the dark |
| HeBS | 20 mM HEPES, 137 mM NaCl, 5 mM KCl, 0.7 mM $Na_2HPO_4$, 6 mM dextrose, in $ddH_2O$ |
| Krebs-Ringer buffer | 140 mM NaCl, 10 mM D-Glucose, 10 mM HEPES, 4 mM KCl, 1 mM $CaCl_2$, in $ddH_2O$ |
| Laemmli buffer (5x) | 150 mM Tris-HCl (pH 6.8), 15% SDS, 50% glycerol, 0.05% bromophenol blue, 0.5 M DTT, in $ddH_2O$ |
| NP-40 lysis buffer | 50 mM Tris/HCl (pH 7.5), 150 mM NaCl, add fresh: 5 mM NaF, 0.5% NP-40, 1mM sodium orthovanadate, 1:50 protease inhibitor cocktail, in $ddH_2O$ |
| PBS (1x) | 137 mM NaCl, 2.7 mM KCl, 4.3 mM $Na_2HPO_4x12H_2O$, 1.4 mM $KH_2PO_4$ (pH 6.6) |
| Pervanadate solution | 50 µl 50 mM PerVO4 and 15 µl 30% $H_2O_2$ were mixed and incubated for 5 min at RT. Then, 520 µl $H_2O$ was added and the solution was used 1:50. |
| Resolving gel buffer | 1.5 M Tris-HCl (pH 8.8), 14 mM SDS, in $ddH_2O$ |
| RIPA lysis buffer (modified) | 50 mM Tris/HCl (pH 7.5), 150 mM NaCl, 1 mM EDTA, 1% NP-40, 0.1% sodium deoxycholate, add fresh: 1:50 protease inhibitor cocktail, 5 mM β-glycerophosphate, 5 mM NaF, 1 mM sodium orthovanadate, 10 mM N-ethylmaleimide (prepare fresh every time), in $ddH_2O$ |
| SDS-PAGE buffer | 25 mM Tris, 192 mM glycine, 0.1% SDS, in $ddH_2O$ |

| | |
|---|---|
| Stacking gel buffer | 0.5 M Tris-HCl (pH 6.8), 14 mM SDS, in $ddH_2O$ |
| TAE (1x) | 40 mM Tris, 20 mM glacial acetic acid, 1 mM EDTA, in $ddH_2O$ |
| TAG lysis buffer | 10 mM Tris (pH 8.0), 50 mM KCl, 0.45% NP-40, 0.45% Tween 20, in $ddH_2O$ |
| TBS-T (1x) | 20 mM Tris, 137 mM NaCl (pH 7.6), 0.1% Tween 20, in $ddH_2O$ |
| Urea lysis buffer | 20 mM HEPES (pH 8.0), 9 M urea, 1 mM sodium orthovanadate, 2.5 mM sodium pyrophosphate, 1mM β-glycerophosphate |

### 2.1.6 Enzymes

**Table 7: Enzymes used in this study.**

| Enzyme | Manufacturer |
|---|---|
| Calf-intestine phosphatase (CIP) | NEB |
| PasI | Thermo Scientific |
| Phusion® DNA polymerase | NEB |
| Proteinase K | Macherey-Nagel |
| restriction endonucleases | NEB |
| T4 DNA ligase | NEB |
| T4 DNA polymerase | NEB |
| *Taq* DNA polymerase | NEB |
| *Taq* PCR Master Mix | Qiagen |

### 2.1.7 Oligonucleotides

**Table 8: Synthetic oligonucleotides used in this study.**

| Oligonucleotides | Sequence | Application |
|---|---|---|
| ARFGEF2_cDNA_fw | TCAAAACCCCAGTCCCCTGT | CRISPR clone analysis |
| ARFGEF2_cDNA_rev | TATCCACAACACACTGGGCATC | CRISPR clone analysis |
| ARFGEF2-1_fw | AGCGGAAAAGCATGGTCTGA | CRISPR activity test |
| ARFGEF2-1_rev | AGCCCAGGACTGTGTGACTA | CRISPR activity test |
| ARFGEF2-2_fw | GAAGGACCCAACTCATGCCA | CRISPR activity test |
| ARFGEF2-2_rev | CGTGAGTCCTGAATACGGGG | CRISPR activity test |
| EGFP-C1_fw | GTCCTGCTGGAGTTCGTG | Sequencing |
| NCK1_cl_fw_BglII | TAATAGATCTCATGGCAGAAGAAGTGGTGGTAGTA | Cloning |
| NCK1_cl_rev_NotI | TAATGCCGCCGCTCATGATAAATGCTTGACAAGATA | Cloning |
| NCK1_fw | GGATACCTTAGGCATTGGAAAAGTG | CRISPR activity test |

| Oligonucleotides | Sequence | Application |
|---|---|---|
| NCK1_mRNA_fw | AAGAGGACATGAAGGGGATTTCC | Expression analysis |
| NCK1_mRNA_rev | CAGTCACTTCTGGTCAGCAGTAT | Expression analysis |
| NCK1_rev | AGGTTATTGACGACTGCTGCTAA | CRISPR activity test |
| NCK2.1_seq_fw | GACCGCATCTACGACCTCAAC | CRISPR activity test |
| NCK2.1_seq_rev | CCGGTGTAGCTTATCTGTGGG | CRISPR activity test |
| NCK2_mRNA_fw | TAAAGCGTCAGGGAAGAACAAAC | Expression analysis |
| NCK2_mRNA_rev | GACCAAGCGACCTGAACATAAAG | Expression analysis |
| pLU6_rev | TGGATCTCTGCTGTCCCTGT | Sequencing |
| pMSCV-for | CCCTTGAACCTCCTCGTTCGACC | Sequencing |
| pMSCV-rev | GAGACGTGCTACTTCCATTTGTC | Sequencing |
| sgARFGEF2.1 | GGAAAGGACGAAACACCGGCAACGGGATAGCCGATGA CGTTTTAGAGCTAGAAATAGCAAGTTAAAATAAGG | CRISPR LIC assembly |
| sgARFGEF2.2 | GGAAAGGACGAAACACCGGTCCCATGAGCTGCGTTCC AGTTTTAGAGCTAGAAATAGCAAGTTAAAATAAGG | CRISPR LIC assembly |
| sgNCK2.1 | GGAAAGGACGAAACACCGCGAGAAGGGGGAGACCAT GGGTTTTAGAGCTAGAAATAGCAAGTTAAAATAAGG | CRISPR LIC assembly |
| SHIP2_mRNA_fw | GTACCACCGCGACCTGAG | CRISPR clone analysis |
| SHIP2_mRNA_rev | CCATTGGGAGCACTCTCAGCA | CRISPR clone analysis |
| universal reverse oligo | AACGGACTAGCCTTATTTTAACTTGCTATTTCTAGCTCTAA AAC | CRISPR LIC assembly |

### 2.1.8 Plasmids

**Table 9: CRISPR plasmids used for transient expression.**

| Vector | Source |
|---|---|
| pLU6-CMV-GFP | Dr. T. Schmidt |
| pLU6 sghNck1-CMV-GFP | Dr. T. Schmidt |
| pLU6-sghNck2.1-CMV-GFP | This thesis |
| pLU6-sghSHIP2-CMV-GFP | Dr. T. Schmidt |
| pLU6-sghARFGEF2.1-CMV-GFP | This thesis |
| pLU6 sghARFGEF2.2-CMV-GFP | This thesis |
| pRZ-CMV-mCherry-Cas9 | Dr. T. Schmidt |

**Table 10: Expression plasmids used in this study.**
Cit (Citrin-tag), puro (puromycin resistance), bleo (bleomycin resistance), *linearized using ScaI HF.

| Vector | cDNA | Source |
|---|---|---|
| LT3-GECIR | shCD79a-1 | Dr. C. Doebele, backbone Dr. J. Zuber |
| LT3-GECIR | shGL2 | Mohr et al. 2017, backbone Dr. J. Zuber |
| pApuro II | hARFGEF2* | Dr. M. Engelke |
| pcDNA3.1-HisC | hSHIP2 | Prof. C. Erneux |
| pcDNA3-HA | hNck1 | Addgene #45892 (Kebache et al. 2002) |
| pcDNA4-HisMax-C | hBIG2 | Prof. K. Nakayama |
| pCMV | ΔR8.91 | Dr. C. Doebele (Zufferey et al. 1997) |
| pCR2.1 | hNck1 | This thesis |
| pCR2.1 | hSHIP2 | This thesis |
| pCR2.1 | hARFGEF2 | This thesis |
| phCMV | VSV-G | Addgene #8454 (Stewart et al. 2003) |
| phCMV | GAL-V | Collins et al. 1996 |
| pMSCV-bleo-RFP | chNck2 | Dr. M. Engelke |
| pMSCV-puro | EGFP | Dr. M. Engelke |
| pMSCV-puroCit | hNck1 | This thesis |
| pMSCV-puroCit | hSHIP2 | Dr. M. Engelke |
| pMSCV-puroCit | chNck2 | Dr. M. Engelke |

### 2.1.9 Reaction Systems (Kits)

**Table 11: Ready-to-use kits used in this study.**

| Kit | Manufacturer |
|---|---|
| Amaxa®Cell Line Nucleofector® Kit L | Lonza |
| APC Annexin V Apoptosis Detection Kit with PI | Biolegends |
| Cell Proliferation Assay XTT, BC | Applichem |
| Nucleobond® XTRA Midi EF Plasmid Kit | Macherey-Nagel |
| Nucleospin® Gel and PCR Clean-up Kit | Macherey-Nagel |
| Nucleospin® Plasmid easy pure Kit | Macherey-Nagel |
| Nucleospin® RNA | Macherey-Nagel |
| One Taq® RT-PCR Kit | NEB |

| Kit | Manufacturer |
|---|---|
| ProtoScript® First Strand cDNA Synthesis Kit | NEB |
| TA™ cloning Kit with pCR™2.1 | Invitrogen |

### 2.1.10 Antibodies

**Table 12**: **Primary antibodies used for Western blot analysis.**
Antibodies were diluted in 1% BSA and 0.01% $NaN_3$ according to the manufacturer's instructions.

| Antibody | Isotype | Manufacturer |
|---|---|---|
| α-actin | IgG2b | CST |
| α-ARFGEF2 | rabbit | Abcam |
| α-BCAP (E-5) | mouse IgG1 | Santa Cruz |
| α-CD79a (EP3618) | rabbit | Abcam |
| α-c-MYC | mouse IgG1 | Biolegends |
| α-GFP | mouse IgG1 | Roche Diagnostics |
| α-Grb2 (3F2) | mouse IgG1 | Millipore |
| α-JNK | rabbit | CST |
| α-Nck (2) (8.8) | mouse IgG2b | Santa Cruz |
| α-Nck1 (15B9) | rabbit | CST |
| α-pAkt (S473) (D9E) | rabbit | CST |
| α-pan Akt (40D4) | mouse IgG1 | CST |
| α-pan Erk (Clone16) | mouse IgG2a | Becton Dickinson |
| α-pCD79a (Y182) | rabbit | CST |
| α-pErk (T202/Y204) | rabbit | CST |
| α-pFOXO1 (T24)/FOXO3 (T32) | rabbit | CST |
| α-pJNK (T183/Y185) (G9) | mouse IgG1 | CST |
| α-pp38 (T180/Y182) | mouse IgG1 | Becton Dickinson |
| α-pp85 (Y458)/p55 (Y199) | rabbit | CST |
| α-pPTEN (S380/T382/383) | rabbit | CST |
| α-pSyk (Y525/Y526) | rabbit | CST |
| α-SHIP1 | rabbit | CST |
| α-SHIP2 (C76A7) | rabbit | CST |

**Table 13: Secondary antibodies used for Western blot analysis.** Antibodies were diluted 1:10000 in TBS-T.

| Antibody | Isotype | Manufacturer |
|---|---|---|
| α-mouse IgG - HRPO | goat | Southern Biotech |
| α-mouse IgG1 - HRPO | goat | Southern Biotech |
| α-mouse IgG2a - HRPO | goat | Southern Biotech |
| α-mouse IgG2b - HRPO | goat | Southern Biotech |
| α-rabbit IgG - HRPO | goat | Southern Biotech |

**Table 14: Antibodies used for flow cytometry or stimulation.**

| Antibody | Fluorochrome | Isotype | Manufacturer |
|---|---|---|---|
| $F(ab')_2$ goat α-human IgG + IgM | n/a | goat | Dianova |
| α-human IgM | APC | mouse IgG1 | Southern Biotech |
| α-pJNK (T183/Y185) | Alexa Fluor® 647 | mouse IgG1 | Becton Dickinson |

### 2.1.11 Inhibitors

**Table 15: Inhibitors.**

| Inhibitor | Solvent | Manufacturer |
|---|---|---|
| AS1949490 (SHIP2 Inhibitor) | DMSO | Sigma |
| Wortmannin (PI3K inhibitor) | DMSO | Tocris |

### 2.1.12 Bacteria and bacteria medium

**Table 16: Bacterial strains used in this study.**

| Bacterial Strain | Manufacturer |
|---|---|
| One Shot TOP10F' chemically competent *E.coli* | Invitrogen |
| Electrocomp™ GeneHogs® *E.coli* | Invitrogen |

For amplification of plasmid DNA, *E.coli* were grown in lysogeny broth (LB) medium (10 g/l tryptone peptone, 5 g/l yeast extract, 5 g/l NaCl, pH 7). Before use, LB medium was autoclaved for 30 min at 121°C, 1.25 bar. For production of agar plates, 2% agar-agar was added to the LB medium. For selection, medium was supplemented with 100 µg/ml ampicillin or 50 µg/ml kanamycin.

### 2.1.13 Eukaryotic cell lines and cell culture media

**DG75 (DSMZ: ACC-83)**

Human Burkitt lymphoma cell line of the sporadic subtype derived from the pleural effusion from a 10-year old Caucasian boy with refractory, terminal Burkitt lymphoma in 1975 (Ben-Bassat et al. 1977). DG75 cells a have a t(8;14)(q24;q32) translocation and have no mutation in *TP53*, coding for p53 (Wiman et al. 1991). They express IgM paired with a κ light chain and are negative for EBV (Gabay et al. 1999).

**Daudi (DSMZ: ACC-78)**

Human Burkitt lymphoma cell line of the endemic subtype derived in a left orbital biopsy of a 16-year old African boy with Burkitt lymphoma (Klein et al. 1968). Cells express IgM paired with a κ light chain and are positive for EBV, but infection is classified as a latent infection without production of active viruses. Daudi cells have a nonsense mutation in *TP53*, a confirmed t(8;14)(q24;q32) translocation and an inactivating ID3 mutation (Kreck et al. 2013; Gaidano et al. 1991).

**BL60**

Human Burkitt lymphoma cell line of the endemic subtype derived in a maxillary biopsy from a north African 4-year old girl (Bornkamm et al. 1984). Cells express IgM, are positive for EBV and have a (8;22) chromosomal translocation and a mutation in *TP53* (Gaidano et al. 1991).

**HEK293T/17 (ATTC: CRL-11268)**

In this study, HEK239T/17 cells were used for generation of lentiviral particles. They are derived from the HEK293T cell line, established from a primary embryonal kidney and transformed with adenovirus type 5 (Russell et al. 1977). HEK293T/17 cells constitutively express a temperature sensitive simian virus large T antigen and clone 17 was chosen for high transfection levels (Pensiero et al. 1999).

**Platinum-E (PlatE)**

In this study, PlatE cells were used for generation of retroviral particles. Plat-E is a HEK293T-derived packaging cell line stably transfected with the moloney murine leukemia virus (MMLV) packaging genes *gag*, *pol* and *env* (Morita et al. 2000). The Plat E system is an ecotropic packaging system but retroviral particles can be pseudotyped by co-transfecting the envelope glycoprotein of vesicular stomatitis virus (VSV-G) for infection human cell lines.

**Table 17: Knock-out cell lines generated in this study.**

| Parental cell line | Genetic background |
|---|---|
| DG75 | *Nck1*$^{-/-}$<br>*Nck2*$^{-/-}$<br>*Nck1-2*$^{-/-}$ |
| Daudi | *SHIP2*$^{-/-}$<br>*BIG2*$^{-/-}$ |
| BL60 | *SHIP2*$^{-/-}$ |

**Table 18: Media for eukaryotic cell lines.**

| Medium | Company | Cell type | Supplements |
|---|---|---|---|
| DMEM | Merck Millipore | PlatE<br>HEK293T/17 | 10% FCS<br>1% Penicillin/Streptomycin<br>1 mM L-glutamine |
| RPMI 1640 | Merck Millipore | DG75, Daudi, BL60 | 10% FCS<br>(1% FCS for apoptosis assays)<br>(5% FCS for XTT proliferation assays)<br>(20% FCS for stressed cells to recover)<br>1% Penicillin/Streptomycin<br>1 mM L-glutamine<br>50 µM β-mercaptoethanol |
| SILAC RPMI 1640 | Thermo Scientific | | 10% dialyzed FCS<br>0.115 mM L-arginine ($^{13}C_6$ $^{15}N_4$)<br>0.27 mM L-lysine ($^{13}C_6$ $^{15}N_2$)<br>1 mM L-glutamine<br>0.2 g/l L-proline |

## 2.2 Methods

### 2.2.1 Molecular Biology

If not stated otherwise standard molecular biology methods were performed as recommended by the manufacturer's protocol or as described in "Molecular Cloning: A Laboratory Manual" (Sambrook & Russell 2001).

#### 2.2.1.1 Isolation of genomic DNA

To isolate genomic DNA of human B cell lines, $1x10^6$ cells were washed once with PBS and subsequently lysed in 200 µl TAG lysis buffer containing 1 µl proteinase K (20 mg/ml, Macherey-Nagel) for at 56°C for 3 h followed by heat-inactivation at 95°C for 15 min. Samples were either directly used for polymerase chain reaction (PCR) or stored at 4°C until further use.

#### 2.2.1.2 Generation of cDNA

*Isolation of mRNA*

For isolation of mRNA the NucleoSpin® RNA reaction kit (Macherey-Nagel) was used. Concentration of mRNA was measured by the NanoDrop 2000 (Thermo Scientific). mRNA was either directly used for reverse transcription into cDNA or stored at -80° C.

*Reverse transcription of mRNA*

Reverse transcription of mRNA into cDNA was performed using the ProtoScript® First Strand cDNA Synthesis Kit or the One Taq® RT-PCR Kit (NEB). cDNA was directly used for PCR or stored at -20°C.

#### 2.2.1.3 Polymerase chain reaction (PCR)

Polymerase chain reaction is used to rapidly amplify specific DNA sequences in *vitro* (Mullis et al. 1986). Here, PCR was used to generate DNA sequences harboring specific restriction sites for cloning purposes or for analytical purposes to amplify potential sites of double-strand breaks induced by CRISPR/Cas9 gene editing.
Phusion® DNA polymerase (NEB) was used to amplify DNA for cloning purposes, since it harbors a proof-reading activity. The reaction set up is depicted in Table 19.

**Table 19: Composition of the PCR reaction mix for cloning.**

| Reagent | Volume [ul] | Final concentration |
|---|---|---|
| 5x Phusion HF buffer | 10 | 1x |
| dNTPs (10 mM, NEB) | 1 | 200 µM |
| Forward primer (10 µM) | 2.5 | 0.5 µM |
| Reverse primer (10 µM) | 2.5 | 0.5 µM |
| Template | 1 | 50-200 ng/µl |
| Phusion polymerase (2000 U/ml, NEB) | 0.5 | 1 U/reaction |
| $ddH_2O$ | to final volume of 50 µl | |

To study potential sites modified by CRISPR/Cas9 gene editing, the *Taq* PCR master mix (Qiagen) was used due to its easy reaction set up. As the master mix already contains the *Taq* polymerase, the adequate buffer and dNTPS, only the template with its corresponding primers and $ddH_2O$ needed to be added (Table 20). The standard PCR programs for both Phusion and *Taq* polymerase are depicted in Table 21. The annealing temperature was adjusted 3-5°C below the lowest primer melting temperature ($Tm_{primer}$).

**Table 20: Composition of the PCR reaction mix for analytical purposes.**

| Reagent | Volume [ul] | Final concentration |
|---|---|---|
| 2x *Taq* PCR master mix | 5 | 1x |
| Forward primer (100 µM) | 0.1 | 1 µM |
| Reverse primer (100 µM) | 0.1 | 1 µM |
| Template | 1 | 50-200 ng/µl |
| $ddH_2O$ | to final volume of 10 µl | |

**Table 21: Standard PCR programs.**

| | Step | PCR with Phusion® polymerase | PCR with *Taq* polmerase |
|---|---|---|---|
| | Initial denaturation | 98°C, 30 s | 94°C, 2 min |
| 35x | Denaturation | 98°C, 10 s | 94°C, 20 s |
| | Annealing | x°C*, 30 s | x°C *, 30 s |
| | Extension | 68°C, 30 s/kb | 72°C, 60 s/kb |
| | Final Extension | 68°C, 2-fold extension time | 72°C, 2-fold extension time |
| | Stop | 10°C, ∞ | 10°C, ∞ |

* Annealing temperature = $Tm_{primer}$-3-5°C

Primers were designed by using the web-based Primer-BLAST program (NCBI). Common guidelines were considered for primer design (Primer guidelines, Howard Judelson, 10.06, p. 1) which include a Tm between 55°C and 65°C, which usually corresponds to a base composition 50-60% (G+C) and a primer length of 17-28 bp, if possible. To avoid mispriming, low specific binding at the 3' end was considered as well as lack of secondary priming sites in the template. Dimerization and hairpin formation capability was kept to a minimum. To this end, primers were additionally checked for formation of secondary structures using the web-based program MFEprimer-3.0. Primers were ordered and synthesized by eurofins MWG.

#### 2.2.1.4 Enzymatic digest of DNA

Site-directed enzymatic digest of plasmid DNA or PCR products was either used to obtain DNA fragments containing the desired sequence for molecular cloning or to screen for alterations in the genomic DNA induced by CRISPR/Cas9 genome editing. DNA was incubated with the respective restriction enzyme(s) (NEB or Thermo Scientific) according to the manufacturer's recommendations for 1-2 h. Samples were subjected to agarose gel electrophoresis followed by gel extraction of the desired DNA fragments if necessary.

#### 2.2.1.5 Agarose gel electrophoresis

PCR products or plasmid DNA were separated using agarose gel electrophoresis. 1-2% (w/v) agarose was melted in Tris-acetate-EDTA (TAE) buffer, cooled down to ~50°C before ethidium bromide (Roth) was added to a concentration of 0.5 µg/ml. Agarose gels were casted and samples were mixed with 6x DNA loading buffer (NEB) before loading. Gels were run at 220mA and 100V for 30-45 min and visualized using UV light.

#### 2.2.1.6 Purification of DNA from agarose gels or PCR reactions

Extraction of DNA was performed using the NucleoSpin® Gel and PCR Clean-Up system (Macherey-Nagel). DNA samples were eluted in 15-30 µl of 5mM Tris-HCl (pH 8.5) and were either directly used or stored at -20°C.

#### 2.2.1.7 Ligation of DNA fragments

After enzymatic digest and purification, DNA inserts and vector backbones were ligated using T4 DNA ligase (NEB). In case only one restriction enzyme was used, the vector backbone was additionally treated with calf intestine phosphatase for 1h at 37°C. Calf intestine phosphatase removes the 5' and 3' phosphate groups from DNA thereby preventing vector self-ligation. Ligation reactions were either incubated for 1h at RT or overnight at 16°C before proceeding with transformation of bacteria.

#### 2.2.1.8 Transformation of chemically competent bacteria

To amplify bacterial plasmid DNA, *E.coli* TOP10F' and GeneHog (50 µl) were transformed using a pre-existing plasmid (1-2 µl) or ligation reaction (5-10 µl). After 30 min incubation on ice, heat-shock was performed at 42°C for 45 s followed by an incubation on ice for 5 min. For recovery, 200 µl pre-warmed antibiotic-free LB medium was added and samples were incubated on a shaker at 37°C for 30 min. Bacteria were plated on agar-plates containing the appropriate antibiotic and cultured overnight at 37°C. For transformations of *E.coli* TOP10F' using the pCR2.1 plasmid, blue-white screening was performed by equally distributing 50 µl X-gal (5-bromo-4-chloro-3-indolyl-beta-D-galacto-pyranoside, 50 mg/ml in DMF) and 50 µl IPTG (isopropyl-β-D-thiogalacto-pyranoside, 0.1M) on agar plates prior to plating bacteria.

#### 2.2.1.9 Preparation of plasmid DNA

*Mini Preparation*

To isolate plasmid DNA from bacteria, 4 ml of LB medium containing the appropriate antibiotic (100µg/ml ampicillin or 50µg/ml kanamycin) were inoculated with a single *E.coli* colony and incubated overnight with constant agitation at 37°C. Plasmid DNA was isolated using the NucleoSpin® Plasmid Easy Pure kit.

*Midi Preparation*

To obtain higher yields of bacterial plasmid DNA, 4 ml LB medium containing an *E.coli* colony was prepared as described above and incubated for 8 h with constant agitation at 37°C. This pre-culture was then used to inoculate 200 ml of LB medium with the same antibiotic. Bacteria cells were grown overnight with constant agitation at 37°C. Isolation of bacterial plasmid DNA was performed using the NucleoBond® Xtra Midi EF Plasmid kit. DNA was eluted in 100-200 µl nuclease free $H_20$.

### 2.2.1.10 Sequencing of DNA

Validation of plasmids and PCR products was performed by the company Microsynth Seqlab (Sequence Laboratories, Göttingen). Samples were prepared mixing 1.2 µg of DNA, 0.3 µl of primer (100 pmol/µl) and dd$H_2O$ to a final volume of 12 µl.

### 2.2.1.11 CRISPR/Cas9 genome editing

To generate stable "knockout" cell lines, the Clustered Regularly Interspaced Palindromic Repeats (CRISPR)/Cas9-based genome editing was used. The CRISPR/Cas system was originally discovered as a microbial adaptive immune response in bacteria and archaea which utilizes RNA-guides nucleases to cleave foreign genetic elements such as plasmids and viruses (Ran et al. 2013; Deveau et al. 2010; Garneau et al. 2010; Horvath & Barrangou 2010; Bhaya et al. 2011). The CRISPR/Cas9 technique uses a single-guide RNA (sgRNA) that binds to a target DNA through Watson-Crick base pairing to guide the Cas9 nuclease to the target site (Figure 4). The Cas9 nuclease (derived from *Streptococcus pyrogenes*) recognizes the protospacer adjacent motif (PAM, 5'NGG) sequence and induces a double strand break (DSB) between the 17$^{th}$ and 18$^{th}$ base in the target sequence (3 bp 5' of the PAM) (Jinek et al. 2012). DSB are re-ligated by the cell's DNA repair machinery via nonhomologous end joining (NHEJ) which in many cases induces errors in the form of insertion/deletion (indel) mutations. As indel mutations in exons often lead to frameshift and premature stop codons, the CRISPR/Cas9 technique is especially suitable to induce gene knockouts (Ran et al. 2013).

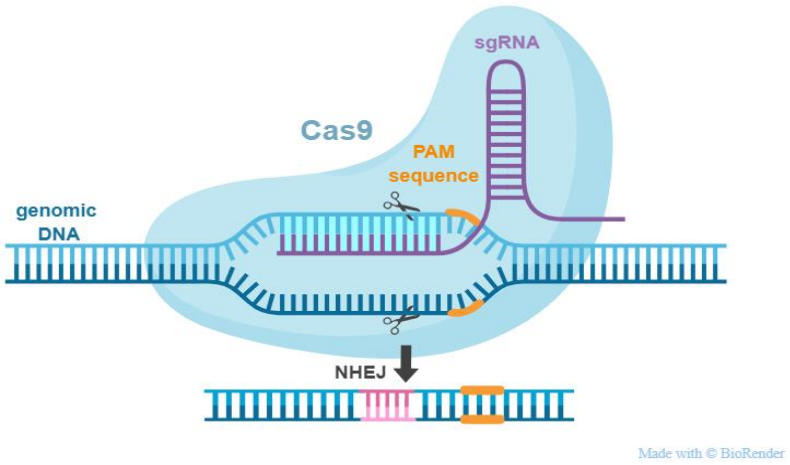


**Figure 4: Schematic depiction of CRISPR/Cas9 gene editing.**
The Cas9 nuclease is targeted to genomic DNA by an sgRNA, which consist of a 20-nucleotide guide sequence and a scaffold, forming a hairpin structure (violet). The guide aligns with the target DNA upstream of the PAM (5'NGG motif; orange). Cas9 induces a DSB ~ 3 bp upstream of the PAM sequence. The endogenous and error-prone DNA repair machinery of the cell rejoins and repairs the DNA ends via nonhomologous end joining (NHEJ; pink), leading to indel mutations (modified from Ran et al. 2013).

*Ligation-independent cloning assembly for sgRNA expression*

Ligation-independent cloning (LIC) assembly was used to generate vectors expressing an sgRNA for CRISPR/Cas9-genome editing from synthesized ssDNA. The sgRNA sequence was selected using the CRISPR Design software (http://crispr.mit.edu/) based on a high sore for specificity and a restriction site to evaluate the activity of editing. The ssDNA was ordered from MWG and used for LIC assembly with pLU6-sgRNA-CMV-GFP as described previously (Schmidt et al. 2015).

*CRISPR/Cas9 activity Test*

Following electroporation (see section 2.2.3.4), a batch of sorted cells were expanded and genomic DNA was isolated as described in section 2.2.1.1. to test for the activity of the CRISPR constructs. Therefore, the loci spanning the sgRNA sequence were amplified by PCR and an enzymatic digest with the appropriate enzyme was performed according to the manufacturer's instructions. Samples were analyzed by agarose gel electrophoresis. Active CRISPR/Cas9 constructs alter the genomic DNA leading to absence of the restriction site and hence to incomplete digest with the respective restriction enzyme.

*Screening of CRISPR/Cas9 clones*

In order to obtain single cell clones, sorted cells were seeded in 96-well plates at a concentration of 0.6 cells per well in 20% FCS culture medium. Cells were expanded and analyzed either using the CRISPR/Cas9 activity test (see section) or analyzed for the deficiency of the respective protein by Western Blot analysis (2.2.2.4). Single cell clones lacking the protein of interest were subjected to sequence analysis. Therefore, primers spanning the genomic loci were used to amplify either genomic DNA or cDNA via PCR. PCR products were cloned into pCR2.1 to distinguish individual sequences. Cells were considered to be deficient for the respective protein, if both alleles showed an alteration, leading to a premature stop codon.

## 2.2.2 Biochemistry

### 2.2.2.1 Stimulation of B cells

To analyze BCR stimulation events, cells were harvested and washed once with PBS and counted. They were then starved in serum-free RPMI at 37°C for 20 min at 650 rpm to reduce the stimulatory effects of FCS. After starvation, cells were either stimulated with 5-10 µg/ml $F(ab')_2$ goat α-human IgG/IgM for indicated times or left unstimulated. For analysis of phosphorylation events after SHIP2 inhibition, cells were incubated with 5 µM AS1949490 for 30 min during starvation. To identify

general protein phosphorylation, cells were starved and incubated for 10 min with the phosphatase inhibitor pervanadate (1:50). After stimulation, cells were quickly moved to ice and then pelleted at 4°C. The supernatant was removed and cells were subjected to cellular lysis (refer to 2.2.2.2).

### 2.2.2.2 Preparation of cleared cellular lysates

For preparation of cleared cellular lysates (CCLs), cells were lysed in 15-20 µl of 0.5% NP40 lysis buffer per $1x10^6$ cells. Samples were incubated on ice for at least 25 min. If higher cell numbers cells were used, lysis was performed at 4°C under mild agitation. After cell lysis, nuclei and cell debris were pelleted by centrifugation (16000 rcf, 4°C for 30 min) and the supernatant was collected and mixed with 0.25 volumes of 5x Laemmli buffer. Samples were then boiled at 95°C for 5 min and stored at -20°C until further use.

### 2.2.2.3 SDS polyacrylamide gel electrophoresis

To separate proteins from CCL samples, discontinuous SDS polyacrylamide gel electrophoresis (PAGE) was performed. It allows separation of proteins according to their size and is based on a protocol originally described by Weber & Osborn in 1969. The discontinuous gel system consists of a stacking gel (5% acrylamide) to concentrate the proteins before they are separated in the resolving gel (10% acrylamide) (Table 22).

**Table 22: Composition of Resolving and Stacking gel.** *TEMED and APS were added just before pouring.

| Reagent | Resolving Gel | Stacking Gel |
|---|---|---|
| Resolving gel Buffer | 375 mM Tris/HCl (pH 8.8), in $ddH_2O$ | |
| Stacking gel Buffer | | 125 mM Tris/HCl (pH 6.8) in $ddH_2O$ |
| Acrylamide/bis-Acrylamide | 10 % | 5 % |
| SDS | 0.1% | 0.1% |
| TEMED* | 0.1% | 0.1% |
| 10 % APS* | 10% | 10% |
| $ddH_2O$ | add to final volume | add to final volume |

Gels were casted in between two glass plates starting with adding the mix for the resolving gel. Isopropanol was used to flatten the surface of the gel and to prevent oxygen diffusion into the gel. After polymerization, the isopropanol layer was discarded and the mix of the stacking gel was added. A comb was placed on top to form sample wells. Once the stacking gel polymerized, gels were ready for gel electrophoresis using the Mini-PROTEAN system (Bio Rad). Samples were boiled for 5 min at 95°C prior to loading and were run alongside Page Ruler Prestained protein Ladder (Thermo Scientific) to determine the molecular weight of proteins. Gels were run using SDS running buffer at a current of 10 mA/gel. After the samples reached the resolving gel, the current was increased to 20 mA/gel. Once the dye front migrated to the bottom of the gels, gels were subjected to immunoblotting.

#### 2.2.2.4 Western Blot analysis

For detection of proteins separated by SDS PAGE, proteins were transferred to a nitrocellulose membrane by using semi-dry western blot (Towbin et al. 1989). The gel, nitrocellulose membrane and two pieces of Whatman paper were equilibrated in 1x blotting buffer. The gel and nitrocellulose membrane were then placed between the Whatman papers to facilitate the transfer of negatively charged proteins onto the membrane. Air bubbles were removed by rolling the stack with a pipette. The transfer was performed at 16V, 240 mA for 70 min.

After successful transfer, the membrane was incubated with 5% bovine serum albumin (BSA) in TBS-T + 0.1% $NaN_3$ for 1 h at 4°C or at least 30 min at RT at constant agitation. Primary antibodies were diluted according to the manufacturer's instructions in 1% BSA in TBS-T + 0.01% $NaN_3$. Incubation with the primary antibody was performed at 4°C overnight at constant agitation. After washing the membrane 3-4 x with TBS-T for 10-15 min, the secondary HRPO-conjugated antibody was added at a dilution of 1: 10,000 in TBS-T and incubated for 1 h at RT. The membrane was then washed again 3-4 x with TBS-T for 10-15 min. The proteins were visualized using an enhanced chemoluminescence (ECL) solution. In presence of $H_2O_2$, the HRPO catalyzes the oxidation of luminol resulting in emission of light. The emitted chemoluminescence was detected by the ChemiLux Gel Imager (Intas). In case the membrane was to be incubated with another primary antibody, the HRPO was inactivated by incubation of 1% $NaN_3$ in TBS-T for 1 h, followed by washing 3-4 x with TBS-T for 10-15 min before adding the antibody.

### 2.2.3 Cell Biology

#### 2.2.3.1 Cell culture and maintenance

All cell culture work was carried out under aseptic conditions using a laminar-flow clean bench. Cells were cultured in the appropriate cell culture media (see 2.1.13) at 37°C and 5% $CO_2$ in a humidified incubator. For maintenance, DG75 and BL60 were passaged every other day 1:10. Daudi cells were usually passaged daily 1:3-1:4. For passaging of adherent Plat-E cells, cells were detached by adding 0.05% trypsin-EDTA (Thermo Fisher Scientific) and plated 1:5-1:10 every other day. Cells were counted using a Neubauer improved counting chamber by mixing the cell suspension with an equal volume of 0.4% trypan blue solution to distinguish between living and dead cells. If not indicated otherwise, all centrifugation steps were carried out at 300 rcf for 4 min at RT.

#### 2.2.3.2 Storage and revitalization of cells

For long term storage of cells, cells were resuspended in freezing medium (10% DMSO in FCS) at a density of approximately $5x10^6$ cells per ml. Cryotubes were stored at -80°C in a polystyrene box before being transferred to -150°C for long-term storage. Frozen cell stocks were thawed in a 37°C water bath and quickly transferred into pre-warmed medium. Subsequently, cells were centrifuged and resuspended in fresh culture medium.

#### 2.2.3.3 SILAC labeling of human B cell lines

To identify changes in the phospho-proteome of "knockout" cells, cells were labeled for quantitative mass spectrometry in SILAC RPMI-1640 medium devoid of arginine and lysine containing either "heavy" amino acids 0.115 mM L-arginine ($^{13}C_6$,$^{15}N_4$) (+10) and 0.27 mM L-lysine ($^{13}C_6$,$^{15}N_2$) (+8) or "light" non-labeled amino acids (Sigma). Additionally, the medium was supplemented with 10-20% dialyzed FCS, Penicillin/Streptomycin, 1 mM L-glutamine and 0.2 g/l L-proline. Expansion of cells for 7-13 days in their respective medium ensured complete incorporation of amino acids. Cells were harvested at 300 rcf, RT, for 4 min, washed 1-2x in PBS and $1x10^7$ cells were lysed in Urea Buffer at RT for phospho-tyrosine enriched analysis. For global phospho-proteome analysis, $5x10^6$-$1x10^7$ cells were lysed in modified RIPA buffer at 4°C on ice for 30 min. To ensure lysis of nuclei, all samples were passed through a 20G needle 5-10 times before freezing them at -80°C until further processing. Samples were sent for mass spectrometry analysis to the DKTK Proteomics Core Facility, University Hospital Frankfurt. There, samples were separated by size by SDS-PAGE and processed for quantitative mass spectrometry analysis as described in Corso et al. 2016.

#### 2.2.3.4 Electroporation of human B cells lines

For transient transfection of cells, $1x10^7$ cells were washed twice with cold PBS, resuspended in 700 µl serum-free RPMI-1640 and transferred to an electroporation cuvette. Subsequently, 12.5 µg pLU6-sgRNA-CMV-GFP and 20 µg pRZ-CMV-mCherry-Cas9 plasmid were added and the suspension was incubated on ice for 30 min. Electroporation was performed using a GenePulser II (BioRad) with a capacitance extender at 260 V and 960 µF. Cells were incubated on ice for additional 15 min before seeding them in 10 ml pre-warmed medium.

#### 2.2.3.5 Amaxa® Nucleofection

Daudi BIG2-deficient cells were nucleofected using the Amaxa®Cell Line Nucleofector® Kit L. For nucleofection, $2x10^6$ subconfluently cultured cells were harvested by centrifugation and the supernatant was carefully aspirated. Cells were mixed with 82 µl Nucleofector solution, 18 µl Supplement and 2 µg of plasmid DNA and transferred into a certified cuvette which was placed into the NucleofectorTM II device (Amaxa/Lonza). Cells were transfected by running the program A-020 twice, before transferring them into 1 ml pre-warmed 20% FCS medium for regeneration.

#### 2.2.3.6 Retroviral transduction of human B cell lines

*Transfection of Plat-E cells*

To generate virus particles for retroviral transduction of human B cell lines, the packaging cell line Plat-E was transfected with the respective plasmid DNA. To this end, Plat-E cells were grown on 6 cm dishes at 70-80% confluency. For transfection, 1.8 µg plasmid DNA, 7 µl Trans-IT transfecting reagent and 0.8 µg pCMV-VSV-G were mixed in 300 µl serum-free RPMI-1640 and incubated for 30 min at RT. Meanwhile, Plat-E cell medium was replaced by 3 ml pre-warmed fresh target cell medium and DNA was added dropwise to the Plat-E cells. After 24 h, 1 ml fresh medium was added to enhance virus-production.

*Infection of target cells*

On the second day after transfection, the supernatant containing retroviral particles was harvested and centrifuged to pellet residual Plat-E cells. The clarified supernatant was carefully aspirated and mixed with $1.5x10^6$ target cells and 2 ml fresh medium. In addition, polybrene was added to a final concentration of 3 µg/ml to improve the efficiency of the infection. The next day, the medium was changed to remove the polybrene. Selection started the day after using either 1 µg/ml puromycin

(InvivoGen) for BL60 and Daudi or 3 µg/ml for DG75 cells for 3 days. In case bleomycin (Calbiochem) was used for selection, 50 µg/ml were applied for 2 days to select DG75 cells.

*Concentration of retroviral particles and spinfection*

To improve infection efficiency of Daudi and BL60 cells, the virus-containing supernatant was clarified using a Minisart® filter with 0.45 µm pore size (Sartorius). Additionally, the supernatant was concentrated by centrifugation in 2x2 ml reaction tubes per sample at 4°C 20000 rcf for 90 min. Per tube, 1.25 ml of the supernatant was discarded and the remaining 2x750 µl were then used for spinfection. The spinfection protocol used here was originally described for transduction of primary B cells (see PhD thesis Dr. L. König). To this end, $1x10^6$ target cells were mixed with 1.5 ml concentrated virus-containing supernatant and polybrene (3 µg/ml) in a 50 ml Falcon® tube and were spun at 1200 rcf for 3.5 h at 33°C. Cells were then transferred into fresh 20% FCS medium to recover. Selection with puromycin started 2 days after the infection.

### 2.2.3.7 Lentiviral transduction of human BL cell lines

The lentiviral transduction of human B cell lymphoma cell lines was performed in collaboration with Dr. C. Doebele, Department of Medicine II, Hematology & Oncology, University Hospital Frankfurt.

*Calcium Phosphate Transfection*

For production of lentiviral particles, HEK293T/17 cells were plated the day before the transfection at a density of $0.5x10^6$ cells per ml medium without antibiotics. At the day of the transfection, 14.5 µg pCMV-dR8.91, 15.2 µg LT3-GECIR and 6 µg phCMV-GALV were mixed with 150 µl 2.5 M $CaCl_2$ and 1350 µl sterile water. The mixture was added dropwise under constant vortexing to a tube containing 1.5 ml HeBS and incubated at RT for 30 min. For transfection, 1 ml of the reaction mixture was added to the HEK293T/17 cells. After 4 h, the medium was replaced with 20 ml fresh medium.

*Viral Transduction using RetroNectin® reagent*

At day 4 after the transfection, cells were transduced with lentiviral particles using RetroNectin® reagent (Clonetech) to promote co-localization of virus and target cells to enhance transduction efficiency. To this end, a 24-well plate was coated with 20 µg/ml RetroNectin® at RT for 1 h. After aspiration of the reagent, the plate was incubated with 2% BSA in PBS solution for 30 min before washing twice with HBSS/Hepes. Per well, 1.5 ml of virus supernatant was added and the plate was centrifuged at 32°C at 1500 rcf for 30 min to facilitate binding of the virus particles with the RetroNectin® reagent. The virus supernatant was aspirated and approximately $0.5x10^6$ target cells

were mixed with remaining virus supernatant and 10 µg/ml polybrene. The plate was centrifuged at 500 rcf for 5 min and incubated overnight at 37°C. The next day, cells were transferred to a new virus-coated plate before adding 600 µl fresh medium on the following day.

#### 2.2.3.8 Proliferation assay

To determine the growth rate of cells, the Cell Proliferation Assay XTT (Applichem) was used. The assay is based on the 2,3-Bis-(2-methoxy-4-nitro-5-sulfophenyl)-2H-tetrazolium-5-carboxanilide salt (XTT), a yellow tetrazolium salt, which is reduced by succinate dehydrogenase system of the mitochondrial respiratory chain to formazan, an orange colored water-soluble dye (Scudiero et al. 1988). As only living cells have an intact mitochondrial membrane and therefore active dehydrogenase, the intensity of the dye is proportional to the number of metabolically active cells. Phenazine methosulfate (PMS) also needs to be added, which serves as an intermediate electron acceptor.

XTT assays were performed in 96-well plates. Cells were plated at a density of 6000 cells per 100 µl 5% FCS medium per well. If applicable, AS1949490 and DMSO were added to a final concentration of 5 µM. 3-4 wells containing only medium were used for blank absorbance readings. The XTT reagent solution and the activation solution were defrosted immediately prior to use, were mixed and added to the cells according to the manufacturer's instructions. Plates were incubated at 37°C, 5% $CO_2$ for 4 h before being measured with an ELISA reader (Powerwave 340, BioTek) at 450 nm for specific absorbance and 630 nm for reference absorbance.

#### 2.2.3.9 Flow cytometry

*Analysis of expression levels by flow cytometry*

For detection of cell surface proteins or fluorescent-labeled proteins, $1x10^6$ cells were harvested, washed twice with PBS and, if applicable, were stained with the respective fluorescent-labeled antibody in 100 µl PBS according to the manufacturer's recommendations. Cells were incubated on ice for 20-30 min, then washed 2x with cold PBS and resuspended in 300 µl PBS for flow cytometric measurement.

*Intracellular flow cytometry of phosphorylated proteins*

For the detection of phosphorylated proteins by intracellular flow cytometry, $1x10^6$ subconfluently cultured cells per sample were harvested, washed with PBS and reconstituted in 100 µl RPMI only for serum starvation for 20 min at 37°C at 650 rpm. If applicable, cells were stimulated for 10 min

using 10 µg/ml F(ab')$_2$ goat α-human IgG/IgM. To stop the reaction, an equal volume of Cytofix™ Fixation Buffer (BD) was added and samples were incubated at 37°C for 10 min for fixation (final concentration 2% PFA). Following, samples were centrifuged at 500 rcf for 6 min, the supernatant was discarded and cells were permeabilized using 400 µl 0.2% Triton-X100 in PBS at RT for 5 min. Following centrifugation, cells were reconstituted in 300 µl 100 mM glycine in PBS and incubated for another 10 min at RT under mild agitation. Cells were spun again and reconstituted in 100 µl 1% BSA in PBS and stained with Alexa Fluor® 647 Mouse α-JNK (pT183/pY185) (BD) according to the manufacturer's recommendations for 30-60 min in the dark at RT under mild agitation. After staining, samples were filled up with 400 µl 1% BSA in PBS for washing. Cells were reconstituted in 200-400 µl PBS and filtered through Falcon® tubes with cell strainer snap cap (BD) for flow cytometric measurement.

*$Ca^{2+}$ mobilization assay*

Mobilization of $Ca^{2+}$ from the ER into the cytoplasm is a key event following BCR stimulation. Intracellular $Ca^{2+}$ concentration can be measured by using Indo-1-AM, a cell-permeable, ratiometric, UV-light excitable $Ca^{2+}$ indicator. Upon $Ca^{2+}$ binding, emission of Indo-1-AM shifts from 475 nm (blue) to 400 nm (violet). For $Ca^{2+}$ mobilization assays, cells were grown to a density of 0.5-0.75x$10^6$ cells per ml to avoid pre-activation. Per sample, 1x$10^6$ cells were harvested, reconstituted in 700 µl pre-warmed 5% FCS Medium and transferred into light-opaque microcentrifuge tubes. Cells were loaded with 1 µM Indo-1-AM and pluronic F-127 to a final concentration of 0.015% and incubated at 30°C for 25 min under mild agitation. To each sample, 800 µl of pre-warmed 10% FCS medium was added and samples were incubated for another 10 min at 37°C. Cells were washed 1x with Krebs-Ringer buffer containing 1 mM $CaCl_2$ at 300 rcf for 4 min before finally reconstituting them in 300 µl Krebs-Ringer buffer containing 1 mM $CaCl_2$. To minimize pre-activation of cells, cells were rested at 25-30°C for 20-30 min before the measurement. $Ca^{2+}$ flux was measured 25 s before stimulation to establish a baseline of resting cells and up to 5 min after the stimulation of the BCR. Cells were stimulated by using 5-10 µg/ml F(ab')$_2$ goat α-human IgG/IgM.

*Apoptosis assay*

Apoptosis assays were performed to assess the amount of apoptotic and necrotic cells in different cell lines. For that purpose, the APC Annexin V Apoptosis Detection Kit with PI (Biolegends) was used. Annexin V is an intracellular protein that binds phosphatidylserine, which normally resides on the inner leaflet of the plasma membrane. During early apoptosis, the membrane symmetry is lost and phosphatidylserine is also found in the outer leaflet and therefore can be detected by fluorophore-labeled Annexin V. Propidium Iodide (PI) is a fluorescent dye that binds DNA. As early

apoptotic cells exclude the dye, it is used to distinguish early apoptotic from late apoptotic and necrotic cells (Vermes et al. 1995). For apoptosis assays, cells were plated 1-3 days before the measurement at a density of 0.25-0.5x$10^6$ cells per ml in either 1% FCS medium or RMPI only. On the day of analysis, 0.5-1x$10^6$ cells were harvested and washed 1x with cold Staining buffer (2% FCS in PBS + 0.1% $NaN_3$). For staining, cells were reconstituted in 100 µl Annexin-V Binding buffer and Annexin V and PI and were incubated at RT for 20 min in the dark according to the manufacturer's instructions. Subsequently, 400 µl Annexin V Binding buffer was added and samples were subjected to flow cytometric measurement.

*Cell sorting by flow cytometry*

Fluorescent cell populations from a heterogenous cell population were separated by using flow cytometry-based cell sorting. Sorting of cells was either performed at the Institute for Multiple Sclerosis Research (IMSF) in Göttingen or at the Central Service Unit Cell Sorting at the University Medical Center in Göttingen.

# 3 Results

## 3.1 The role of Nck proteins in BL-specific BCR signaling

Our group has previously shown that the adaptor protein Nck activates the PI3K signaling pathway in a BCR-dependent manner in DT40 chicken B cells (Castello et al. 2013). By binding to the phosphorylated non-ITAM tyrosine residue Y204 in CD79A (Igα) Nck recruits BCAP and activates the PI3K pathway. In BL, tonic BCR signaling promotes survival and proliferation of malignant B cells via the PI3K pathway. Given the role of Nck as a link between BCR activation and PI3K signaling, I assessed a relevance for tonic BCR signaling. Compared to chicken, mice and humans have two Nck paralogs, Nck1 and Nck2. In a phospho-proteomic approach of screening BL cell lines Daudi and DG75, Nck1 was identified to be moderately phosphorylated at tyrosine 105 in tonic BCR signaling (Corso et al. 2016), whereas Nck2 was not identified. To gain more insight into the role of Nck proteins, I aimed to analyze if they are also relevant for BL-specific tonic BCR signaling and if so whether Nck isoforms have similar or diverging functions in this context. To this end, I used CRISPR/Cas9 gene editing to generate DG75 sub-cell lines deficient for Nck1, Nck2 or both.

### 3.1.1. Generation of a Nck1-deficient cell line

For targeting the *Nck1* gene locus, exon 3 was chosen as it is present in all 3 complete transcription variants of Nck1 deposited in the NCBI Nucleotide database (Figure 5 a). Possible guide sequences were picked by using the web-based “CRISPR Design” program (http://crispr.mit.edu/). The guide sequence was chosen to have minimal off-target activity and a restriction site for the PasI restriction enzyme at the site of the predicted double-strand break (DSB) induced by Cas9. In case of a successful site-directed modification by Cas9, the restriction site is no longer intact. The guide sequence was cloned into the pLU6-CMV-GFP backbone and together with pRZ-CMV-mCherry-Cas9 introduced into the cells using electroporation. After 48 h, cells were sorted for a $GFP^+$ $mCherry^+$ sub-population. The sorted cell batch was tested for the presence of gene editing by use of a PasI endonuclease recognition site 5’ of the PAM motif. Genomic PCR and subsequent PasI treatment revealed the sorted cell batch contained both, cells harboring mutations in *Nck1* (340 bp band) as well as the wt allele (260 bp band) (Figure 5 b). Following, cells were plated in 96-well plates for expansion of single cell clones. 48 single cell clones were analyzed by PCR and PasI digest, 9 of which showed a modified restriction site. 3 of these clones showed no expression of the protein using Western Blot analysis and 2 of those were confirmed for genomic DNA deletions by sanger sequencing (clone #11 and clone #25) (Figure 5 c).

Deletions in the genomic DNA led to premature stop codons, abrogating the translation of Nck1 as shown for clone #11 (Figure 5 d).

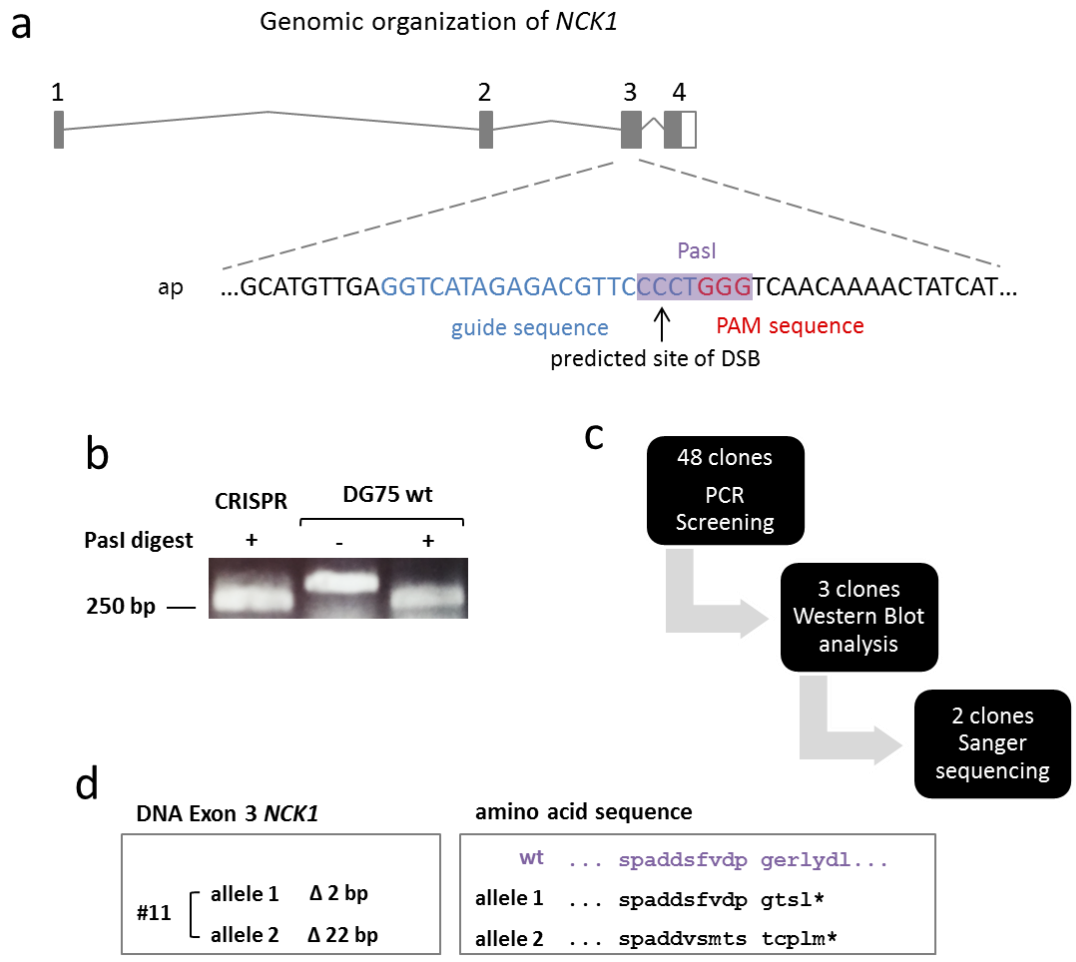


**Figure 5**: **Generation of a Nck1-deficient cell line using CRISPR/Cas9 gene editing.**
(a) Scheme of human *Nck1* gene locus with CRISPR targeting strategy. The chosen guide sequence (blue) targets exon 3. The PAM sequence (red) directs the Cas9 nuclease, which initiates a double strand break (DSB, indicated with an arrow). Predicted site of DSB is recognized by the PasI endonuclease (purple). (b) CRISPR activity test. Genomic DNA of exon 3 was amplified by PCR, treated with PasI and analyzed by gel electrophoresis. The size of DNA fragments is indicated on the left. (c) Overview of screening process for Nck1-deficient clones. (d) Analysis of clone #11 showed a deletion of 2 bp and 22 bp on the genomic DNA level leading to frameshift mutations and premature stop codons (*).

Cells were retrovirally transduced with pMSCV-puro-hNck1Cit (see 2.2.3.6) and were analyzed for expression of Citrine-tagged-Nck1 using flow cytometry (Figure 6 a) and Western Blot analysis (Figure 6 b) compared to non-transduced and DG75 wild-type (wt) cells. Western Blot analysis showed the correct apparent molecular weight of Citrine-tagged-Nck1. The faint residual signal of Nck as seen in the samples from Nck1 deficient cells might be due to an antibody's cross-reactivity with Nck2. Probing the blot with antibodies against the Nck1-interacting protein BCAP revealed an attenuated expression of BCAP in both clones with a more pronounced decrease in clone #25. Staining for IgM-BCR expression with APC-tagged a-human IgM antibody confirmed unaltered IgM surface expression levels in Nck1-deficient cells compared to their reconstituted sub-clones and DG75 wt cells (Figure 6 c).

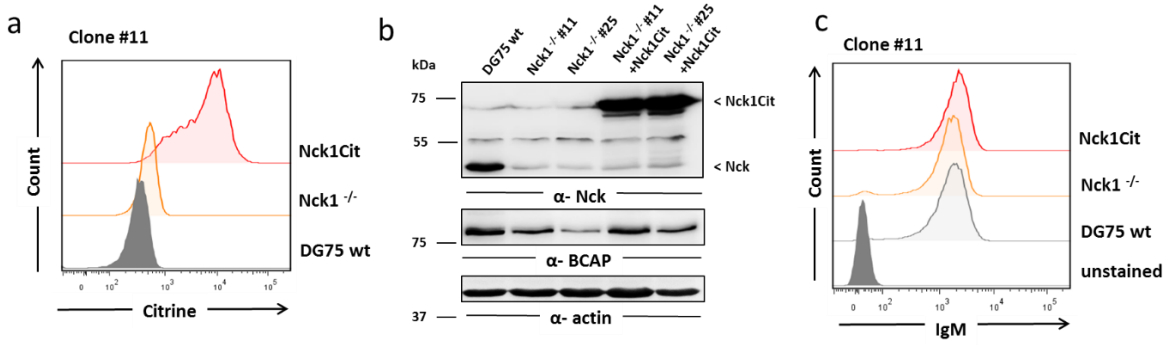


**Figure 6: Reconstitution of Nck1-deficient cells with Citrine-tagged Nck1.**
(a) Nck1-deficient (*Nck1*$^{-/-}$) cells were left untreated or transduced with constructs encoding a Citrine-tagged version of Nck1 (Nck1Cit) and were analyzed by flow cytometry. Wild-type (wt) DG75 cells served as control. (b) Western Blot analysis of lysates derived from DG75 wt, Nck1-deficient clones #11 and #25 and their reconstituted sub-clones. Blots were probed with α-Nck (upper panel), α-BCAP (second panel) and α-actin (lower panel) for loading control. Standard protein molecular masses are indicated in kDa. (c) Staining of DG75 wt, Nck1-deficient and Nck1Cit-expressing cells with APC-conjugated α-human IgM antibody for surface IgM expression. Samples were analyzed by flow cytometry. Unstained cells served as control.

### 3.1.2 Generation of Nck2 and Nck1-2-double deficient cell lines

Although according to phospho-proteome data Nck1 may be the prominent Nck family protein involved in BCR-signaling, Nck2 is also expressed in DG75 cells. Depending on cell type and signaling network, Nck1 and Nck2 have been described to exert both overlapping and protein-specific functions (Ngoenkam et al. 2014; Buvall et al. 2013; Chen et al. 1998)**.** Hence, I generated a Nck2-

deficient DG75 cell line in addition to a Nck1-2-double-deficient cell line on the background of the DG75 *Nck1*$^{-/-}$ cell line using CRISPR/Cas9 gene editing targeting *Nck2*. Guide RNA containing a StyI endonuclease restriction site 5' of the PAM motif was designed to target exon 4 in transcript variant 1 and 2 encoding for Nck2A, the only Nck variant comprising the full set of SH3 domains (Figure 7 a). Plasmids encoding the guide and Cas9 were introduced using electroporation, GFP$^{+}$ mCherry$^{+}$ cells were sorted and subjected to activity testing as described previously. Genomic DNA was amplified by PCR and treated with StyI (Figure 7 b). Agarose gel electrophoresis revealed the existence of edited alleles. After sub-cloning, 65 single clones from the Nck2 CRISPR batch and 39 single clones from the Nck1-2 CRISPR batch were analyzed and 4 potential clones per approach were picked for Sanger sequencing (Figure 7 c). Nck2-deficient clone #29 showed a 1 bp insertion and a 2 bp deletion in exon 4, thereby leading to a frameshift mutation resulting in a premature stop codon (Figure 7 d). Clone #29 is in the following referred to as Nck2-deficient DG75 cells (*Nck2*$^{-/-}$). For the Nck1-2 double deficient CRISPR approach, clone 13.1 was confirmed to have a 2 bp and a 26 bp deletion in exon 4, also leading to a frameshift mutation and premature stop codon (Figure 7 e). Following, clone #13.1 is referred to as Nck1-2-deficient DG75 cells (*Nck1-2*$^{-/-}$).

A BLAST search revealed that the Nck2 protein is highly conserved among species. The Nck2 protein from gallus gallus (chicken) shares 93% sequence identity with human Nck2A and resembles Nck2A in all functional domains including the peptide binding sites in the SH3 domains and the phosphotyrosine and hydrophobic binding pocket in the SH2 domain. Since a plasmid encoding for Nck2 from gallus gallus (chNck2) was readily available, *Nck2*$^{-/-}$ and *Nck1-2*$^{-/-}$ cells were reconstituted with a Citrine-tagged version of chNck2. For double expression of Nck1 and Nck2 in Nck-double deficient cells, cells were transduced with constructs encoding Citrine-tagged Nck1 and RFP-tagged chNck2. Cells were sorted for the expression of the respective fluorophore and were analyzed for protein expression using flow cytometry (Figure 8 a & b) and Western Blot analysis (Figure 8 c). Staining for IgM-BCR expression with APC-conjugated α-human IgM antibody confirmed unaltered IgM surface expression levels in Nck2-deficient (Figure 8 d) and Nck1-2-deficient (Figure 8 e) cells compared to their reconstituted sub-clones and wt DG75 cells.

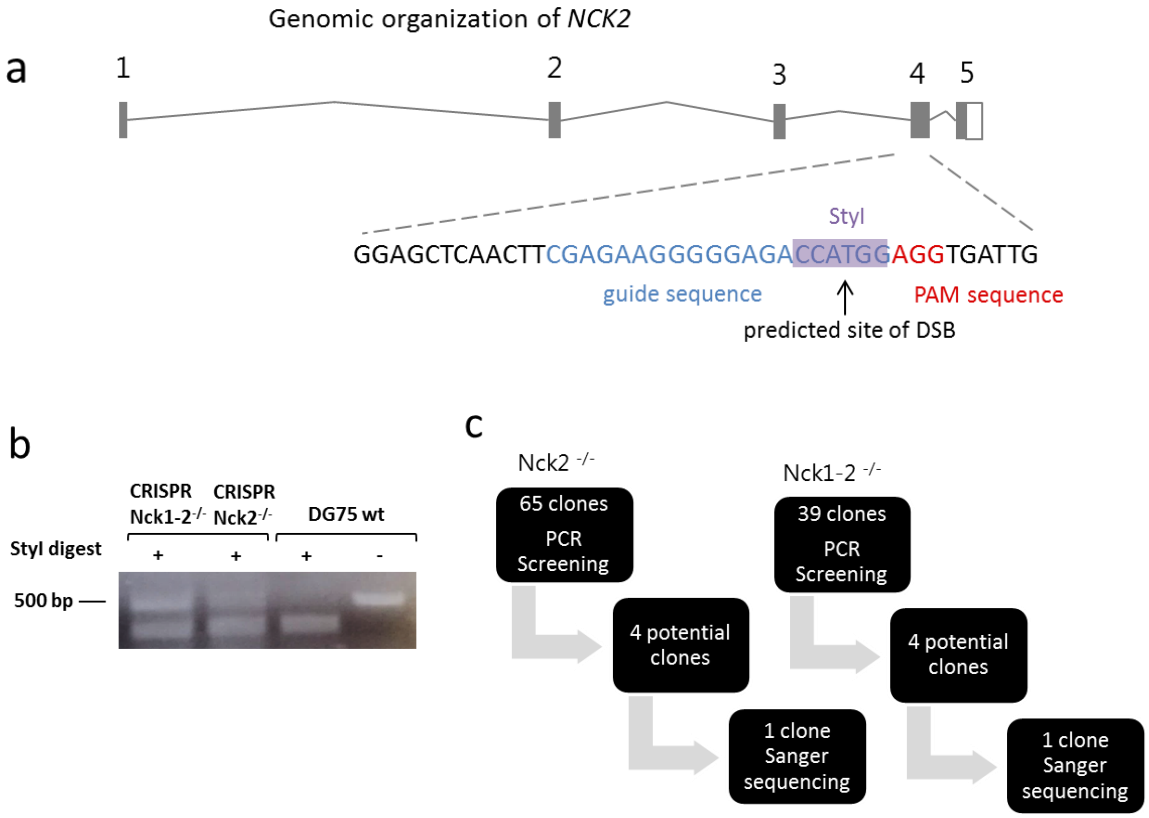


**Figure 7: Generation of Nck2- and Nck1-2-deficient cell lines using CRISPR/Cas9 gene editing.**
(a) Scheme of human *Nck2* gene locus with CRISPR targeting strategy. The chosen guide sequence (blue) targets exon 4. The PAM sequence (red) directs the Cas9 nuclease, which initiates a double strand break (DSB, indicated with an arrow). Predicted site of DSB is recognized by the StyI endonuclease (purple). (b) CRISPR activity test. Genomic DNA of exon 4 was amplified by PCR, treated with StyI and analyzed by agarose gel electrophoresis. The size of DNA fragments is indicated on the left. (c) Overview of screening process for Nck2- and Nck1-2-deficient clones. (d) Sequencing analysis of Nck2-deficient clone #29 showed a deletion of 2 bp and in insertion of 1 bp. (e) Nck1-2-deficient clone 13.1 displayed a deletion of 26 bp and 2 bp. In both clones, mutations led to frameshift mutations resulting in a premature stop codons (*).

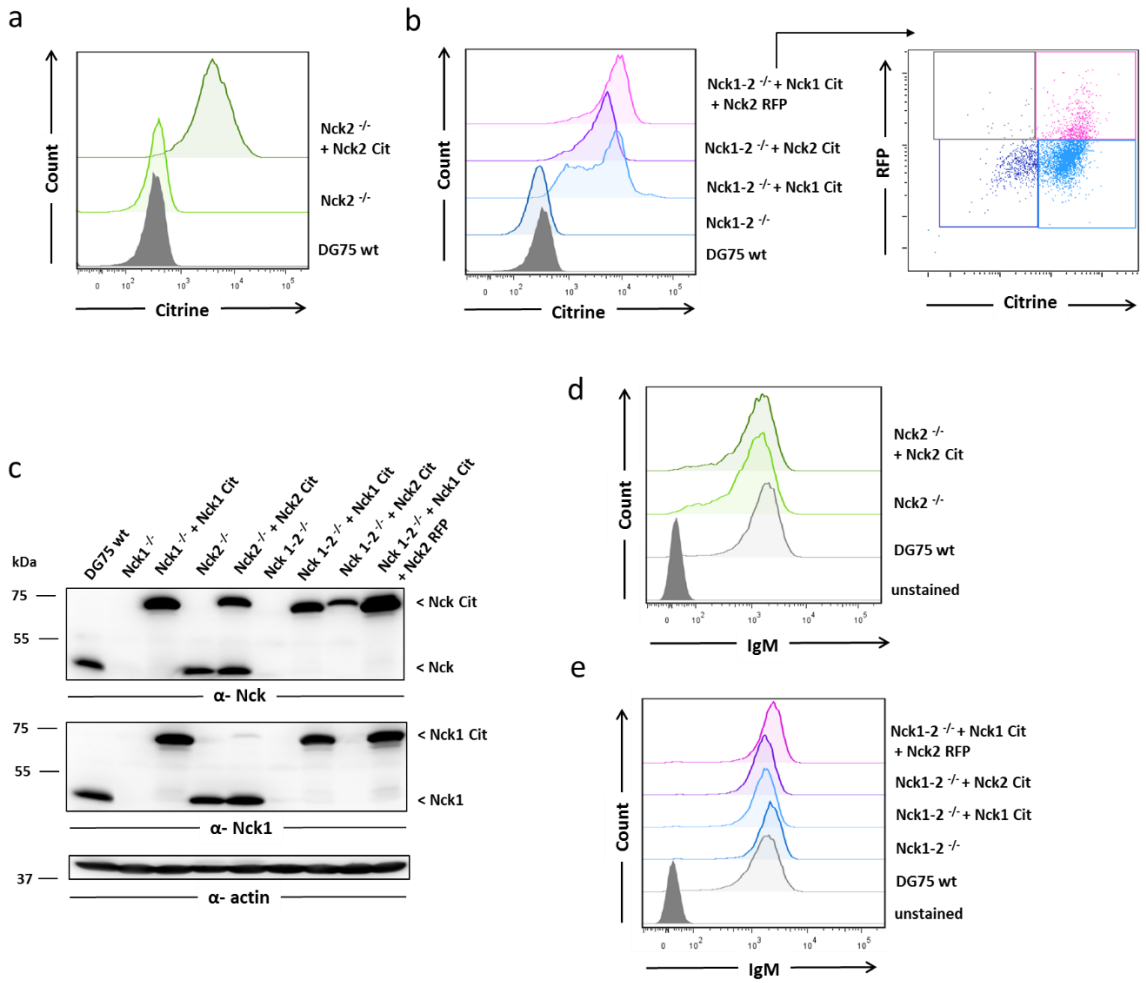


**Figure 8: Reconstitution of Nck2- and Nck1-2-deficient DG75 cells.**
(a) Nck2-deficient DG75 cells (*Nck2*$^{-/-}$) were left untreated or transduced with constructs encoding Citrine-tagged Nck2 and analyzed in comparison to DG75 wild-type (wt) cells for Citrine expression by flow cytometry. (b) Plasmids encoding fluorophore-tagged Nck1 and Nck2 were transduced into Nck1-2 deficient cells (*Nck1-2*$^{-/-}$) and cells were sorted to enrich for the positive cell population. Reconstituted cells were analyzed in comparison to Nck1-2-deficient and DG75 wt cells for Citrine expression (left panel) and double reconstituted cells additionally for Citrine/RFP expression (right panel) by flow cytometry. (c) Expression of ectopic fluorophore-tagged proteins was tested using Western Blot analysis by probing with α-Nck (upper panel) and α-Nck1 (second panel) antibodies. α-actin (lower panel) served as loading control. Standard protein molecular masses are expressed in kDa. Staining with APC-tagged α-human IgM antibody to test for surface IgM expression in (d) Nck2-deficient and (e) Nck1-2-deficient cells compared to reconstituted sub-clones and DG75 wt cells.

### 3.1.3 Nck1 positively regulates $Ca^{2+}$ mobilization in DG75 cells

Before examining tonic BCR signaling in the generated cell lines, I first aimed to verify whether Nck exerts functions in activated BCR signaling similar to those published earlier. In the DT40 chicken B cell line, loss of Nck decreased the $Ca^{2+}$ influx upon BCR activation (Castello et al. 2013). Because I found Nck1 to be the predominantly expressed Nck protein in human DG75 cells (data not shown), I first tested $Ca^{2+}$ mobilization in DG75-derived Nck1-deficient cells. For comparison, I included Nck1-

deficient cells reconstituted with Citrine-tagged Nck1 and DG75 wild-type cells. Cells were stained with Indo-1-AM and were analyzed for their ability to mobilize $Ca^{2+}$ by the ratio of a blue to violet shift in the emission spectrum of Indo-1-AM upon complex formation with free $Ca^{2+}$. After 25 s of baseline recording, cells were stimulated with 5 µg/ml $F(ab')_2$ α-IgM and $Ca^{2+}$ flux was recoded up to 5 min. $Ca^{2+}$ profiles of clone #11 and #25 were plotted against parental cells (wt) and Nck1-deficient cells reconstituted with Citrine-tagged Nck1 (Figure 9). Comparable to Nck-deficient DT40 cells, DG75 Nck1-deficient cells showed an attenuated response upon BCR stimulation. Reconstitution with the Citrine-tagged Nck1 variant was able to restore $Ca^{2+}$ mobilization partially in clone #11 (Figure 9 a) and entirely in clone #25 (Figure 9 b). For further experiments, clone #11 was chosen because of the reconstitution of BCR-induced $Ca^{2+}$ mobilization and because BCAP expression was more comparable to parental cells (Figure 6 b). Clone #11 is in the following referred to as Nck1-deficient DG75 cells (*Nck1*$^{-/-}$).

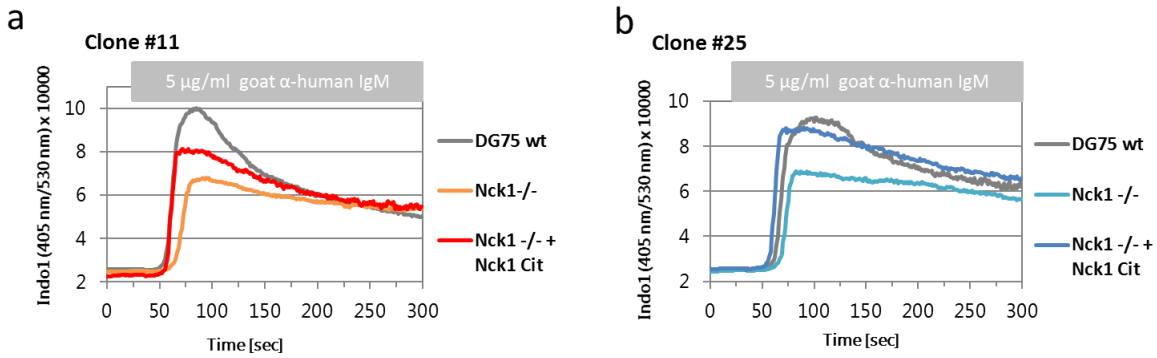


**Figure 9: Nck1 positively regulates $Ca^{2+}$ mobilization in human DG75 cells.**
Nck1-deficient (*Nck1*$^{-/-}$) DG75 cells of clone #11 (a, orange line) and clone #25 (b, light blue line), Citrine-tagged Nck1 reconstituted cells (*Nck1*$^{-/-}$ + Nck1Cit) (red and blue lines, respectively), and wt DG75 controls (grey lines), were loaded with the calcium-sensitive dye Indo-1-AM. A baseline was recorded for 25 s before cells were stimulated with 5 µg/ml $F(ab')_2$ α-IgM and $Ca^{2+}$ flux was monitored for up to 300 s. Plots are representative of three independent experiments.

To test whether the Nck1-mediated augmentation of $Ca^{2+}$ signals is caused by the PI3K-AKT pathway in human B cells similar to DT40 chicken B cells, I repeated the $Ca^{2+}$ mobilization assays using the PI3K inhibitor Wortmannin. As expected, Wortmannin was able to reduce the BCR-induced $Ca^{2+}$ response in DG75 wt (Figure 10 a) and in reconstituted cells (Figure 10 c). In contrast, *Nck1*$^{-/-}$ cells were only mildly affected by the inhibitor (Figure 10 b), indicating the decreased BCR-induced $Ca^{2+}$ mobilization in Nck-deficient cells is mainly caused by a reduced PI3K activity. In summary, these results indicate that Nck1 is relevant for BCR-induced PI3K activation also in human B cells.

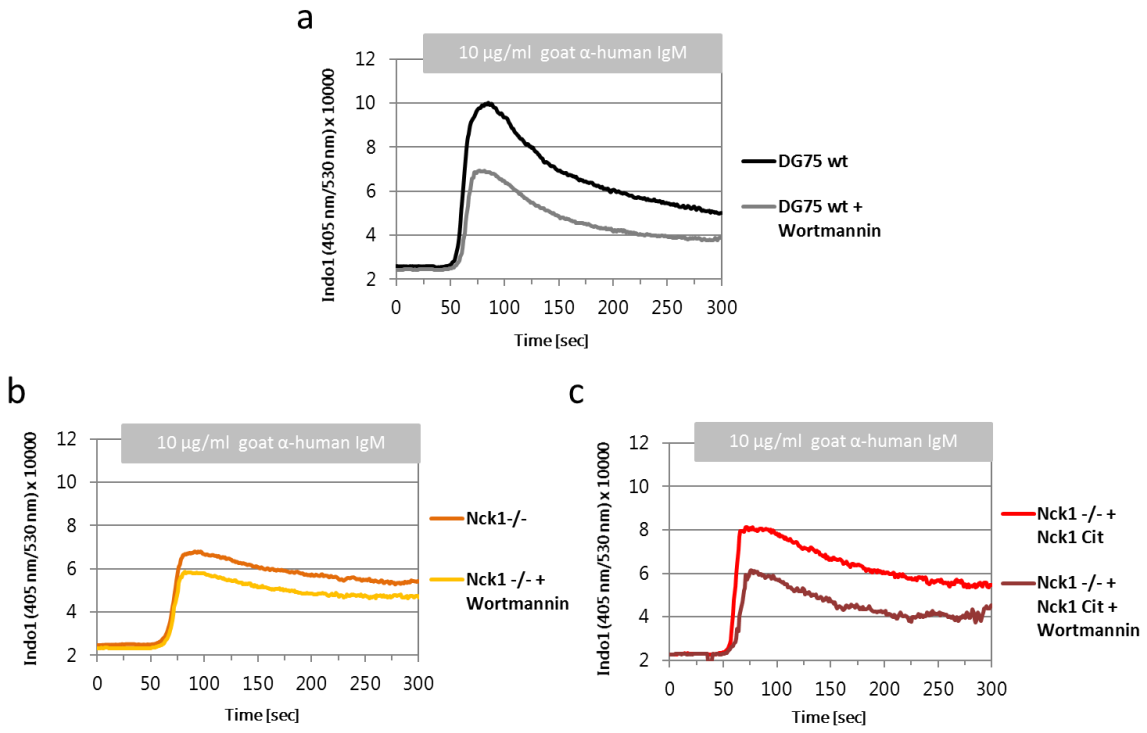


**Figure 10: $Ca^{2+}$ mobilization assays after treatment with PI3K inhibitor Wortmannin.**
(a) DG75 wild-type (wt), (b) Nck1-deficient (*Nck1*$^{-/-}$) DG75 and (c) Nck1-deficient DG75 cells reconstituted with Citrine-tagged Nck1 (Nck1Cit) cells were stained with the calcium-sensitive UV-light excitable dye Indo-1-AM. Cells were left untreated or were treated with 100 nM Wortmannin for 10 min before each measurement. After recording a 25 s baseline, cells were stimulated with 10 µg/ml $F(ab')_2$ α-IgM and $Ca^{2+}$ flux was monitored for up to 300 s. Plots are representative of two independent experiments.

### 3.1.4 Nck1 enhances JNK activity upon BCR activation

Having shown that Nck1 positively regulates $Ca^{2+}$ mobilization upon BCR activation, I aimed to analyze the impact of Nck1 in BCR-dependent signaling in more detail. To this end, I left the different DG75 cell lines described above untreated or stimulated them via the BCR for 3, 7 or 10 minutes. Following, cells were lysed and samples were subjected to Western Blot analysis. Blots were probed with phospho-specific antibodies against pivotal signaling proteins involved in both the PI3K (p85, AKT, FOXO1) and MAPK (ERK, pp38, JNK) signaling pathways.

While phosphorylation of the regulatory subunit of PI3K, p85, at Y458, appears to be constitutive and not BCR-inducible, AKT (S473) and its downstream target FOXO1 (T24) are phosphorylated with comparable intensity in all cell lines upon stimulation of the BCR (Figure 11 a). Interestingly, phosphorylation of FOXO1 in unstimulated cells was reduced in *Nck1*$^{-/-}$ cells in comparison to wt cells and reconstituted cells. Therefore, it is tempting to speculate that Nck1 might be also involved in tonic BCR signaling.

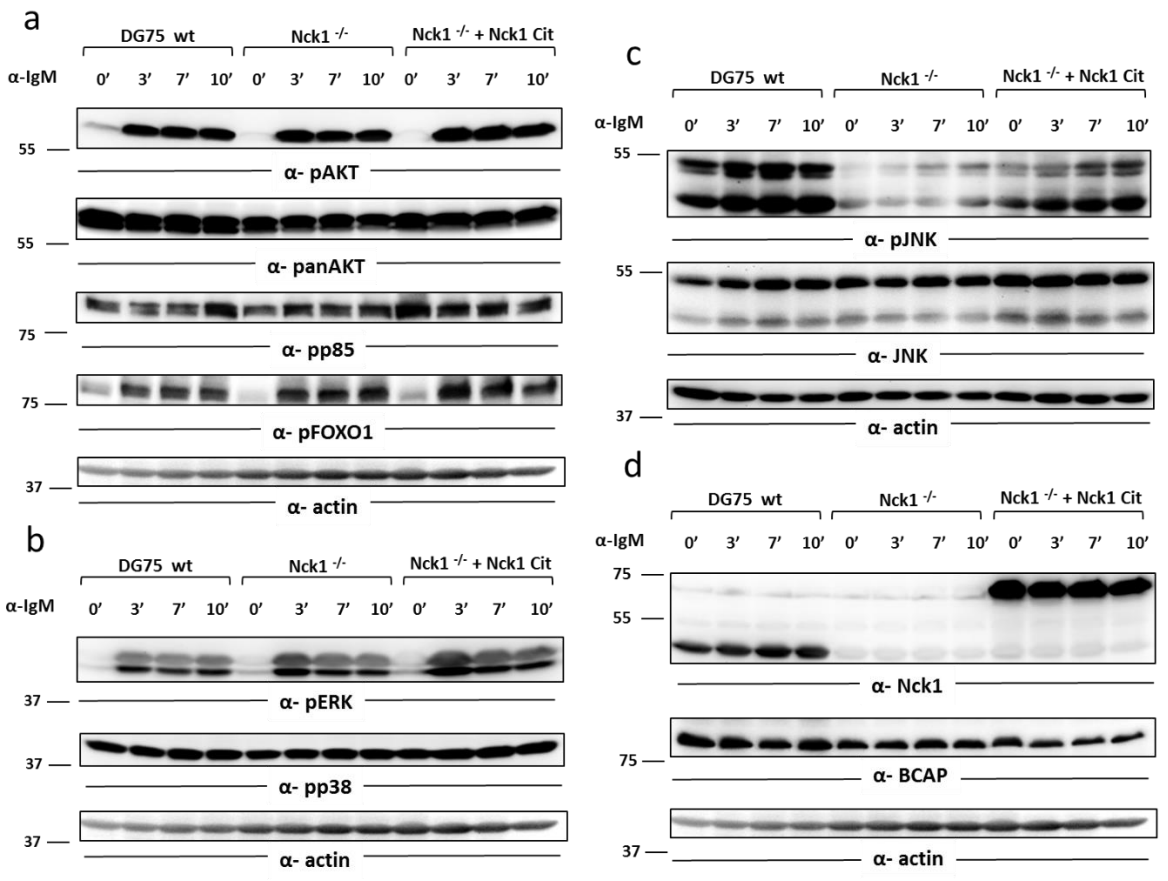


**Figure 11: Analysis of pivotal signaling proteins in Nck1-deficient DG75 cells downstream of BCR activation.** DG75 wild-type (wt), Nck1-deficient (*Nck1*$^{-/-}$) and their Citrine-tagged Nck1 reconstituted sub-clone (Nck1$^{-/-}$ + Nck1Cit) were stimulated with 10 µg/ml F(ab')$_2$ α-human IgM for 3,7, or 10 min or left unstimulated. Lysates were subjected to Western Blot analysis and analyzed for phosphorylation of key signaling proteins in the PI3K and MAPKs pathways. (a) Phosphorylation of effector proteins downstream of the PI3K pathway, AKT and FOXO1, was tested by using α-pAKT (S473) (upper panel), α-panAKT (second panel), α-pp85 (Y458) (third panel), α-pFOXO1 (T24) (fourth panel) and α-actin (lower panel) antibodies. (b) Phosphorylation of effector proteins downstream of the MAPKs pathways, ERK and p38 was tested by using α-pERK (T202/Y204) (upper panel), α-pp38 (T180/Y182) (second panel) and α-actin (lower panel). (c) Phosphorylation of the effector protein JNK downstream of the MAPK pathways was assessed by using α-pJNK (T183/Y185) (upper panel), α-JNK (second panel) and α-actin (lower panel). (d) Expression of Nck1 and its adaptor BCAP was tested by using antibodies against Nck1 (upper panel), BCAP (second panel) and actin (lower panel). Standard protein molecular masses are indicated in kDa.

Since MAPKs are important signaling hubs after BCR stimulation, I probed blots with antibodies detecting phosphorylated forms of central MAPKs ERK, p38 and JNK (Figure 11 b & c). The MAPK ERK is known to be phosphorylated after IgM BCR stimulation and ERK phosphorylation at T202 and Y204 was similar among cell lines (Figure 11 b). MAPK p38 was constitutively phosphorylated at T180 and Y182, indicating that it is not regulated upon BCR stimulation in DG75 cells. While phosphorylation of MAPK JNK (T183/Y185) was induced by BCR stimulation in all cells, the phosphorylation efficiency was markedly reduced in absence of Nck1 (Figure 11 c). Impaired JNK

phosphorylation could be rescued to some extent by expression of Citrine-tagged Nck1, thereby excluding clonal or off-target effects. Similar quantities of JNK, BCAP and Nck1 were confirmed by re-probing the membrane with α-JNK (Figure 11c, second panel), α-BCAP and α-Nck1 (Figure 11 d), respectively. In conclusion, while an impact of Nck1 on effectors of the PI3K pathway was not detectable, Nck1 was required for efficient BCR-induced activation of the JNK pathway.

### 3.1.5 Nck2 is dispensable for BCR-induced $Ca^{2+}$ mobilization in DG75 cells

To further test the impact of Nck proteins on activated BCR signaling in BL cell lines, I examined the role of Nck2 in the presence or absence of Nck1. Therefore, I analyzed Nck2-deficient and Nck1-2-deficient cells for their ability to mobilize $Ca^{2+}$ upon BCR stimulation. Cells described in 3.1.2 were stimulated via the BCR using 5 µg/ml F(ab')$_2$ α-human IgM. Nck2-deficient cells displayed no change in their $Ca^{2+}$ response compared to parental and Citrine-tagged Nck2 reconstituted cells (Figure 12 a). The response of Nck1-2-deficient cells was decreased upon BCR stimulation, in a similar manner like Nck1-deficient cells (Figure 12 b). Reconstitutions with Nck1, Nck2, and both proteins were only mildly effective. In summary, I concluded that Nck2 is dispensable for $Ca^{2+}$ mobilization upon BCR stimulation.

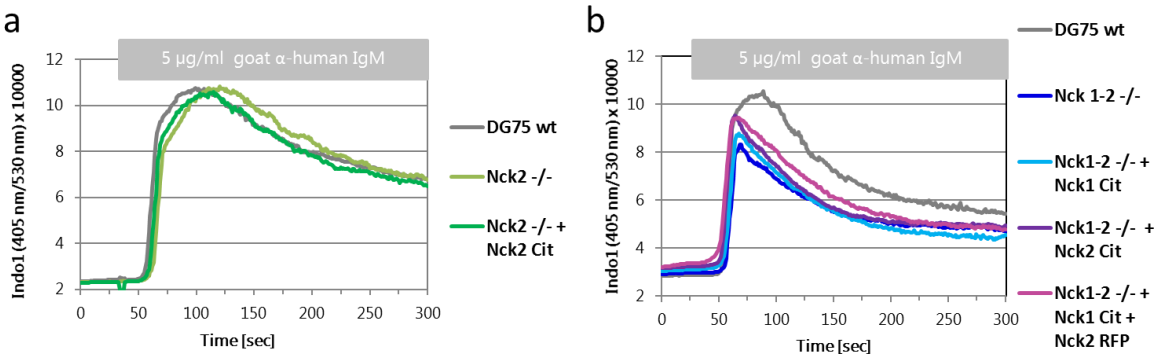


**Figure 12: Nck2 is dispensable for $Ca^{2+}$ mobilization in the presence of Nck1.**
Nck2-deficient (*Nck2*$^{-/-}$) (a, light green line) and Nck1-2-deficient (*Nck1-2*$^{-/-}$) cells (b, dark blue line) and their reconstituted sub-clones expressing Citrine-tagged Nck1 (Nck1Cit) (green line in (a) and light blue line in (b)), Citrine-tagged Nck2 (Nck2Cit) (purple line in (b)) or RFP-tagged Nck2 (Nck2RFP) in combination with Citrine-tagged Nck1 (pink line in (b)) and wt DG75 controls (grey lines) were loaded with the calcium-sensitive dye Indo-1-AM for flow cytometry analysis. After recording a 25 s baseline, cells were stimulated with 5 µg/ml F(ab')$_2$ α-human IgM and $Ca^{2+}$ flux was monitored for up to 300 s. Plots are representative of two independent experiments.

### 3.1.6. Functional analysis of Nck1 and Nck2 BL-specific BCR signaling

Based on the reported role of Nck for BCR-induced activation of the PI3K pathway and the Nck-functions in activated BCR signaling described above, I next assessed the impact of Nck proteins on BL-specific processes like proliferation, apoptosis, as well as tonic BCR signaling.

#### 3.1.6.1 Proliferation of Nck-deficient DG75 cells

To investigate BL survival, I performed XTT-based proliferation assays, which are commonly used to analyze the growth rate of cells (Scudiero et al. 1988). At d0, cells were plated at quadruplicates at a number of 6000 cells per well in 96-well plates under serum-limiting conditions in 5% FCS medium. I measured tests at d0 to establish a baseline level and at d2 and d4 to test for differences in cell proliferation.

Compared to parental cells, Nck1-deficient DG75 cells showed a reduced proliferation rate at d2 and d4, which, however, could not be enhanced by expression of Citrine-tagged Nck1 (Figure 13 a & b). For Nck2-deficient cells, the decrease was even more pronounced at d4, but the impaired proliferation could also not be rescued upon expression of Citrine-tagged Nck2 (Figure 13 c & d). Whereas for single Nck-deficient clones a significant reduction in proliferation became only apparent at d4, Nck1-2 double deficient clones showed an impaired cell growth already at d2 (Figure 13 e & f). Also in this experimental setup, the proliferative defect could not be reconstituted by re-expression of Nck1 and Nck2.

Although Nck-deficient cell lines displayed a profound reduction in proliferation compared to wt cells, the lack of functional reconstitution did not allow to draw conclusions because clonal effects could not be excluded. However, since this assay only measures metabolically active cells, possible differences in the number of cells undergoing apoptosis during the proliferation assay might obscure the overall results.

Due to the small sample size in this study ($n \leq 5$), descriptive statistics were used for sample analysis. The average is calculated as the mean and the standard deviation (SD), describing the spread of values in reference to the mean.

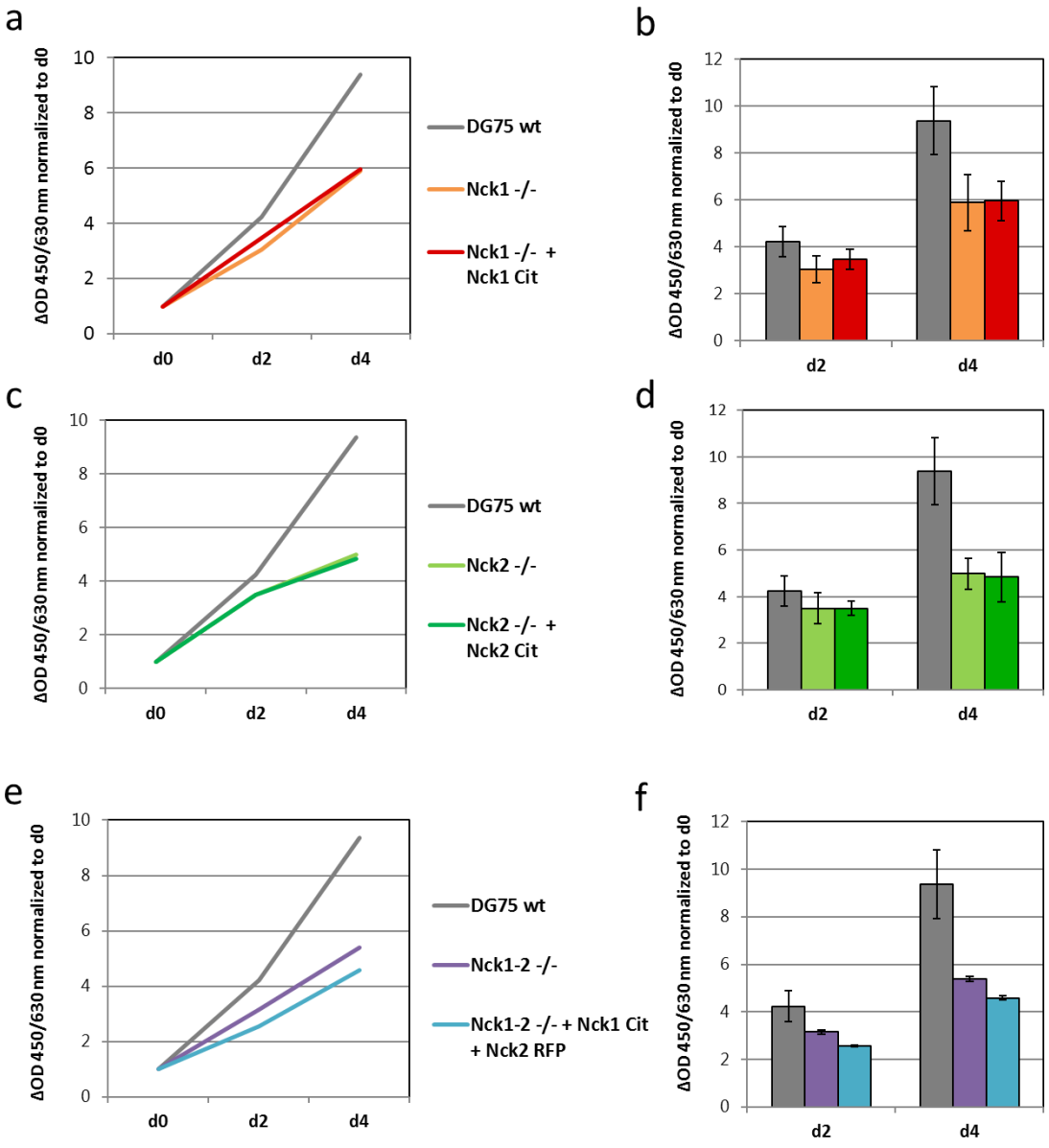


**Figure 13: Proliferation is decreased in Nck-deficient DG75 cells.**
For XTT-proliferation assays, single- and double-deficient Nck cells in comparison to their reconstituted sub-clones and DG75 wild-type (wt) were grown in 5% FCS medium and analyzed at d0, d2 and d4 for their growth rate. Mean ΔOD values of two independent experiments were normalized to d0 (a, c, e) and quantified for d2 and d4 + standard deviation (SD) (b, d, f). (a & b) Proliferation data of DG75 Nck1-deficient cells (*Nck1*$^{-/-}$, orange) and their Citrine-tagged Nck1 expressing sub-clone (*Nck1*$^{-/-}$ + Nck1Cit, red). DG75 wt cells (grey) served as control. (c & d) Proliferation of Nck2-deficient cells (*Nck2*$^{-/-}$, light green), their Citrine-tagged Nck2 expressing sub-clone (*Nck2*$^{-/-}$ + Nck2Cit, dark green) and DG75 wt cells (grey). (e & f) Proliferation of DG75 Nck1-2-deficient cells (*Nck1-2*$^{-/-}$, purple) and their Citrine-tagged Nck1 and RFP-tagged Nck2 expressing sub-clone (*Nck1-2*$^{-/-}$ + Nck1Cit + Nck2RFP, blue) in comparison to DG75 wt cells (grey).

### 3.1.6.2 Apoptosis rates are increased in absence of Nck1

To analyze the relevance of Nck proteins on apoptosis in BL cells, I grew 1x10$^6$ cells in 2-3 ml 1% FCS medium for three days. At d3, I used APC-tagged Annexin V to stain for apoptotic cells and additionally used propidium iodide (PI) to stain late apoptotic cells (Vermes et al., 1995). Samples were processed as described in section 2.2.3.9 and analyzed by flow cytometry. For analysis, I gated for live (AnnexinV$^-$/PI$^-$), early apoptotic (AnnexinV$^+$/PI$^-$) and late apoptotic (AnnexinV$^+$/PI$^+$) cells. The apoptosis assays of wt, Nck1-deficient, and reconstituted DG75 cells revealed an overall higher number of living cells in the absence and slightly increased number of apoptotic cells at d3 in the presence of Nck1 (Figure 14 a). In contrast, the apoptosis analysis of Nck2-deficient DG75 cells showed a reduction of living and an increase of apoptotic cells compared to wt and reconstituted cells (Figure 14 b). These data indicate that Nck2 but not Nck1 reduces the apoptosis rate of DG75 cells.

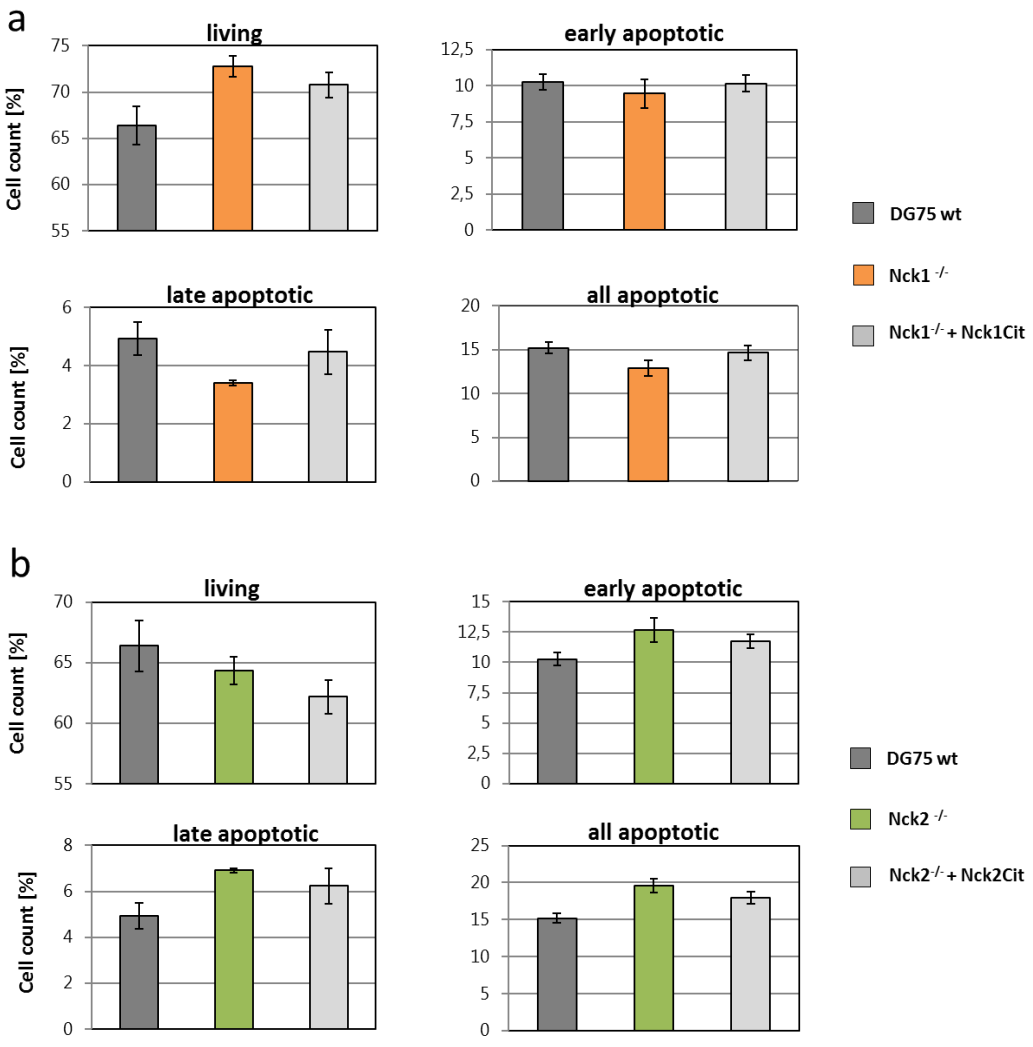


**Figure 14: Assay for apoptosis in Nck-single-deficient DG75 cells.** *For legend, see next page.*

**Figure 14 (*previous page*): Assay for apoptosis in Nck-single-deficient DG75 cells.**
After culturing single Nck-deficient cells, their reconstituted sub-clones and DG75 wild-type (wt) cells in 1% FCS medium for three days, cells were stained with APC-tagged Annexin V and PI to distinguish between living (left upper panel), early (right upper panel), late (left lower panel) and all apoptotic (right lower panel) cells by flow cytometry. (a) Apoptosis assay for Nck1-deficient cells (*Nck1*$^{-/-}$, orange) and their Citrine-Nck1 expressing sub-clone (*Nck1*$^{-/-}$ + Nck1Cit, light grey) in comparison to DG75 wt cells (dark grey). (b) Apoptosis assay for Nck2-deficient cells (*Nck2*$^{-/-}$, green), their Citrine-Nck2 expressing sub-clone (*Nck2*$^{-/-}$ + Nck2Cit, light grey) and DG75 wt cells (dark grey). Data represent means of four experiments, error bars show SD.

To further asses the differential impact of Nck proteins on apoptosis in BL cells, I analyzed Nck1-2 deficient cells and their reconstituted sub-clones in the same experimental set-up. Compared to wt DG75 cells, the proportion of living cells was markedly increased while the apoptosis rate decreased for all cells based on the Nck1-2-deficient clone, indicating a clonal effect (Figure 15). In support of the apoptosis data derived from the single-deficient DG75 cells described above, reconstitution of Nck1-2-deficient cells with only Nck2 did not alter the proportion of living or apoptotic cells compared to the parental clone whereas expression of Nck1 slightly reduced the proportion of living cells and augmented apoptosis rates. Collectively, despite the obstacles in apoptosis measurements due to clonal effects, these data further imply opposite functions of Nck isoforms in the induction of apoptosis.

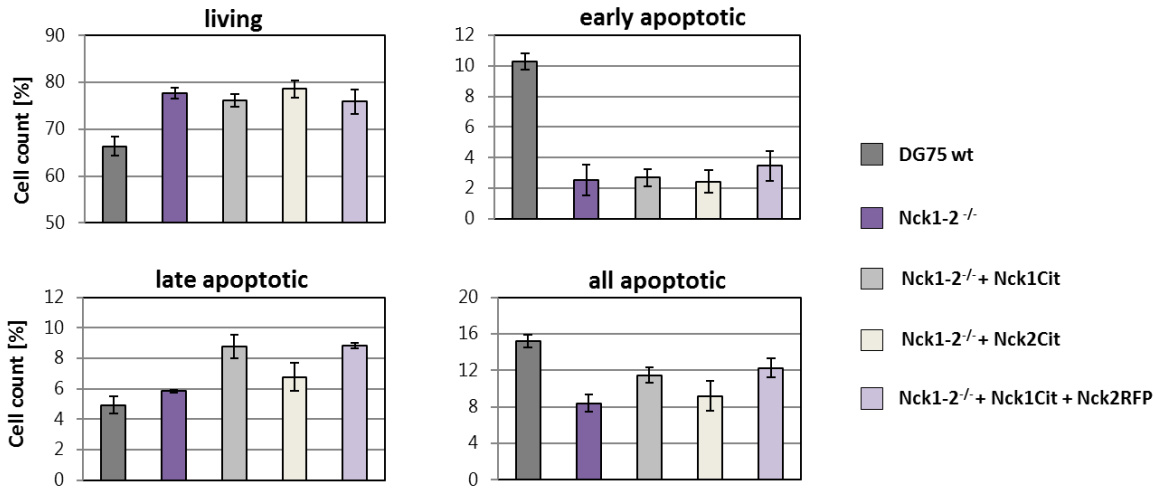


**Figure 15: Assay for apoptosis in Nck1-2-deficient DG75 cells.**
After culturing Nck1-2-deficient (*Nck1-2*$^{-/-}$, purple) DG75 cells, their sub-clones expressing Nck1Cit (light grey), Nck2Cit (beige) or Nck1Cit and Nck2RFP (lavender) and DG75 wt cells (dark grey) in 1% FCS medium for three days, cells were stained with APC-tagged Annexin V and PI to distinguish between living (left upper panel), early (right upper panel), late (left lower panel) and all apoptotic (right lower panel) cells by flow cytometry. Data represent means of four experiments, error bars show SD.

### 3.1.7 Role of Nck1 and Nck2 in tonic BCR signaling

The data described above indicate that Nck1 promotes a pro-apoptotic response in DG75 cells under serum-limiting conditions. At first sight, this observation contradicts its supposedly signaling promoting function via the survival and proliferation-promoting PI3K pathway. Therefore, I proposed that among its function in the PI3K pathway, Nck1 might also play a role in other signaling pathways which net result is induction of apoptosis. To test this hypothesis, I prepared lysates of unstimulated cells and subjected them to Western Blot analysis by probing with phospho-specific antibodies for proteins playing central roles in different signaling pathways.

#### 3.1.7.1 Nck1 and Nck2 augment the activation of the PI3K pathway in tonic BCR signaling

Considering that I identified an impact of Nck1 in the PI3K-AKT pathway upon BCR-induced $Ca^{2+}$ mobilization, I next aimed to analyze the role of Nck proteins in the context of tonic BCR signaling. Phosphorylation of the PI3K regulatory subunit p85 is an early event in activation of the PI3K pathway. Similar levels of p85 phosphorylation were identified in all cell lines although Nck2-deficient cells and their Nck2-reconstituted sub-clone showed a mildly enhanced signal for phosphorylation of p85 (Figure 16 a). Hence, the PI3K pathway is constitutively activated in DG75 cells. In Nck1-deficient cells, AKT phosphorylation was decreased but could not sufficiently be restored by re-expression of Citrine-tagged Nck1 (Figure 16 b). In Nck2-deficient cells overall AKT phosphorylation was also reduced compared to parental cells, although the decrease was less pronounced than in Nck1-deficient cells. Nck1-2 deficient cells displayed a medium reduction in AKT phosphorylation, which could not be enhanced by re-expression of Nck1 or Nck2 alone, but partially upon expression of both Nck isoforms.

In the PI3K pathway, FOXO1 is one of many targets to be phosphorylated by AKT. Phosphorylation of FOXO1 was reduced in Nck1-deficient cells and here, re-expression of Nck1 was able to restore the effect partially (Figure 16 c). A similar effect, however less pronounced, was detected in Nck2-deficient cells and could also be rescued by ectopic expression of Citrine-tagged Nck2. Although I could identify regulation of phosphorylation in the single Nck-deficient cell lines, phosphorylation of FOXO1 was not regulated in Nck1-2 deficient cells and their reconstituted sub-clones, thus indicating a clonal effect promoting constitutive FOXO1 phosphorylation. Notably, expression of BCAP, the pivotal Nck interaction partner for BCR-dependent PI3K signaling, was reduced in Nck1-deficient and Nck1-2-deficient cells and their sub-clones (Figure 16 d). Although clonal differences in BCAP expression thereby conceal which Nck isoform is primarily relevant, data suggest both Nck1 and Nck2 to augment signaling via the PI3K pathway also in tonic BCR signaling.

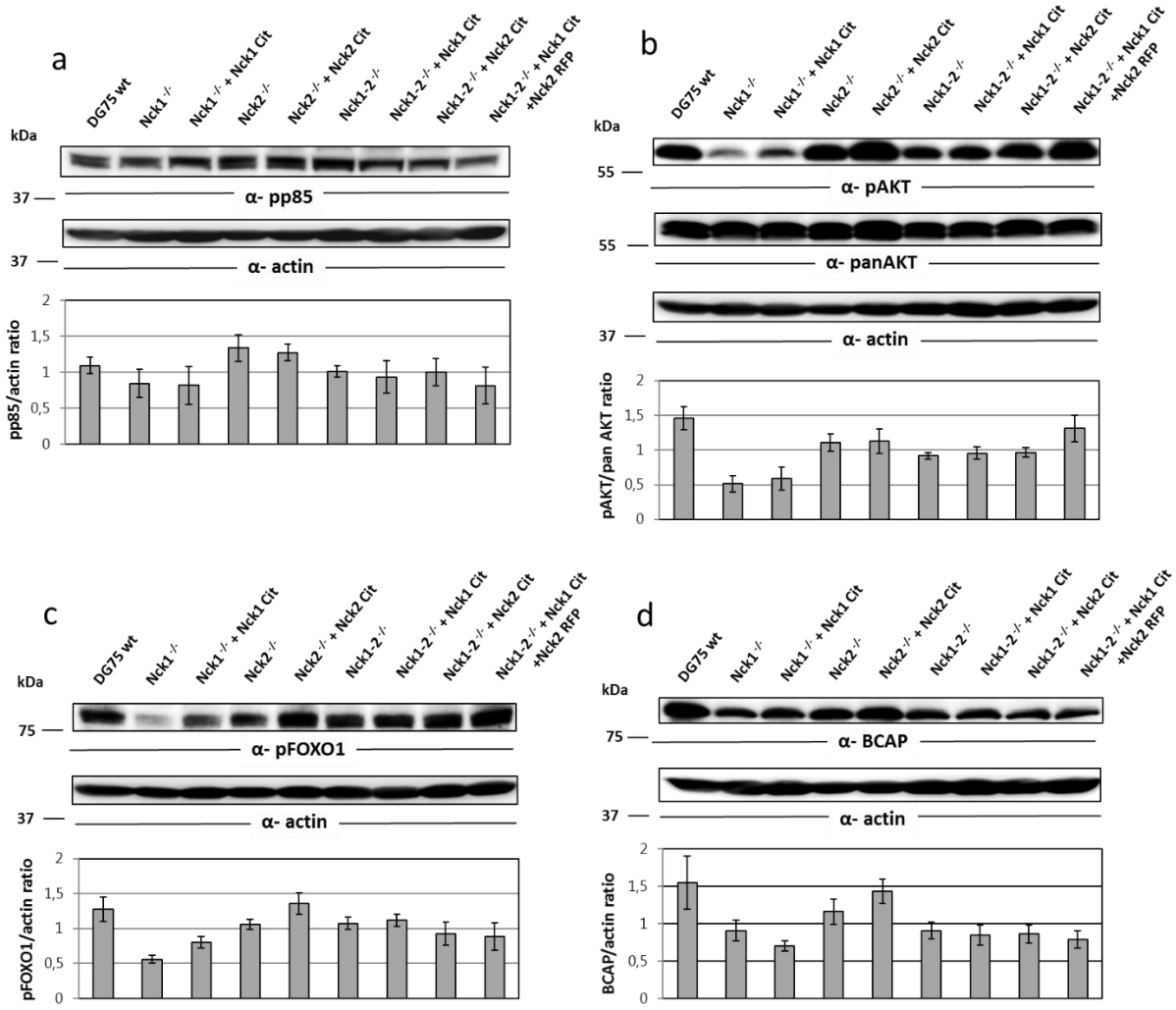


**Figure 16: Nck proteins augment PI3K pathway activation in tonic BCR signaling.**
Single (*Nck1*$^{-/-}$, *Nck2*$^{-/-}$) and double-deficient Nck (*Nck1-2*$^{-/-}$) DG75 cells in comparison to their reconstituted sub-clones (expressing Nck1Cit, Nck2Cit or Nck1Cit and Nck2RFP, respectively) and DG75 wild-type (wt) cells were lysed and subjected to Western Blot analysis. For each protein analyzed, exemplary immunoblots are shown in addition to ratios of signal intensities which were calculated and depicted as a bar diagram as the means + SD of three independent experiments. (a) Phosphorylation of PI3K subunit p85 was tested by using α-pp85 antibody (upper panel). Blots were re-probed with α-actin for loading control (second panel) and the ratios of signal intensities are depicted as a bar diagram (lower panel). (b) Immunoblots were decorated with α-pAKT (upper panel), α-panAKT (second panel) and α-actin (third panel). Ratios of α-pAKT to α-panAKT signal intensities are depicted as a bar diagram (lower panel). (c) Phosphorylation of the AKT downstream effector FOXO1 was determined using a-pFOXO1 antibody (upper panel) and membranes were re-probed with α-actin (second panel) for quantification of signal intensities which are depicted in a bar chart (lower panel). (d) Probing membranes with α-BCAP antibody to test for total levels of BCAP (upper panel) and α-actin (second panel). Ratio of signal intensities are depicted as a bar diagram (lower panel). Standard protein molecular masses are indicated in kDa.

### 3.1.7.2 Regulation of MAPK-pathway signaling upon Nck1 deletion

To complement the results obtained from PI3K pathway analysis, I additionally analyzed the main effectors involved in MAPK pathways downstream of BCR signaling namely ERK, JNK and p38. Since the ERK pathway can be activated by tonic BCR signals during B cell development (Rowland et al. 2010), I tested if ERK phosphorylation is also a relevant target of tonic BCR signaling in BL. By probing with phospho-specific α-ERK antibody, I could identify a basal level of ERK phosphorylation already in unstimulated cells (Figure 17 a). Nck2-deficient cells and their reconstituted sub-clone showed relatively comparable levels of ERK phosphorylation. In contrast, Nck1-deficient and Nck1-2 deficient cells and their sub-clones showed a strongly decreased level of basal ERK phosphorylation, which is probably caused by the clonality of cell lines. Since upon BCR stimulation, Nck1-deficient cells displayed no defect in ERK phosphorylation (Figure 11 b), the reduced basal phosphorylation levels of ERK seem to be negligible at least for activated BCR signaling.

Next, I tested for MAPK JNK phosphorylation and subsequent activation. Phosphorylation of JNK was decreased in Nck1- and Nck1-2 deficient cell lines (Figure 17 b). Re-expression of Nck1 could partially elevate the level of phosphorylation in Nck1-deficient cells, whereas in Nck1-2 deficient cells, only expression of both Nck isoform had a similar effect. Nck2-deficienct cells showed no relevant decrease, thereby indicating that JNK phosphorylation is mainly dependent on Nck1, however Nck1 could only reach full activation in the presence of Nck2.

Basal p38 phosphorylation levels were decreased in Nck1- and Nck1-2-deficient cells, which could be elevated by expression of Citrine-tagged Nck1, but not by Nck2 (Figure 17 c). p38 phosphorylation in Nck2-deficient cells remained unchanged. However, in Nck1-2 deficient cells, expression of both Nck isoforms increased p38 phosphorylation compared to expression of Nck1. In summary, JNK and p38 MAPK signaling pathways were mainly influenced by loss of Nck1 instead of Nck2, but Nck2 was supporting Nck1-dependent p38 and JNK activation in tonic BCR signaling.

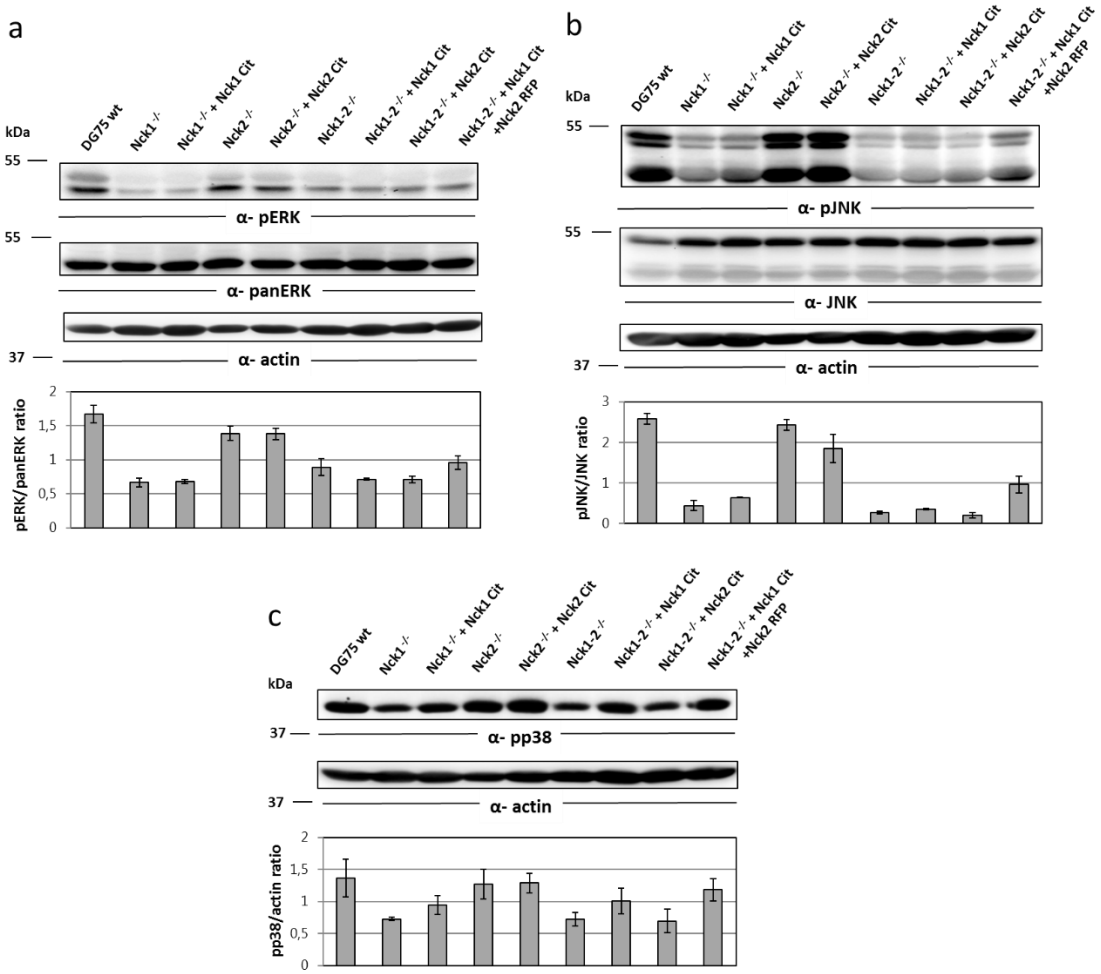


**Figure 17: Analysis of signaling via MAPK pathways in Nck-deficient DG75 cell lines.**
Single (*Nck1*$^{-/-}$, *Nck2*$^{-/-}$) and double-deficient Nck (*Nck1-2*$^{-/-}$) DG75 cells in comparison to their reconstituted sub-clones (expressing Nck1Cit, Nck2Cit or Nck1Cit and Nck2RFP, respectively) and DG75 wild-type (wt) cells were lysed and subjected to Western Blot analysis. Blots were decorated with phospho-specific antibodies for key MAPK effector proteins. For each protein analyzed, exemplary immunoblots are shown in addition to ratios of signal intensities which were calculated and depicted as a bar diagram as the means + SD of three (ERK, p38) and two (JNK) independent experiments. (a) Phosphorylation of ERK was tested by using α-pERK antibody (upper panel). Blots were re-probed with α-pan ERK (second panel) and α-actin for loading control (third panel). Ratios of α-pErk to α-panERK signal intensities are depicted as a bar diagram (lower panel). (b) Immunoblots were decorated with α-pJNK (upper panel), α-JNK (second panel) and α-actin (third panel). Ratios of α-pJNK to α-JNK signal intensities are depicted as a bar diagram (lower panel). (c) Phosphorylation of p38 was determined by using α-pp38 antibody (upper panel) and membranes were re-probed with α-actin (second panel) for quantification of signal intensities which are depicted in a bar diagram (lower panel). Standard protein molecular masses are indicated in kDa.

## 3.2 BIG2 is relevant for proliferation and survival of BL cell lines

The Brefeldin A-inhibited guanine nucleotide-exchange factor (BIG)2 was found to be phosphorylated in resting BL cell lines and phosphorylation was compromised upon knockdown of CD79A (Corso et al. 2016). Additionally, shRNA targeting BIG2 was toxic for BL cell lines DG75 and Daudi, while cell lines derived from other lymphoma subtypes such as GCB-DLBCL cell lines were not affected, suggesting a BL-specific role of BIG2. Moreover, BIG2 knockdown increased numbers of both early and late apoptotic cells compared to non-specific control shRNAs (Corso et al. 2016). Since these data indicate an important role of BIG2 for survival and proliferation of BL cells in an BCR-dependent manner, I aimed to identify the underlying signaling pathways affected by BIG2. To this end, I generated a BIG2-deficient cell line on the background of Daudi cells.

### 3.2.1 Generation of a BIG2-deficient cell line

For targeting BIG2, guide sequences for exon 8 and exon 10 of the *ARFGEF2* gene (encoding for BIG2) were chosen based on minimal off-target activity and restriction sites for AhdI and StyI, respectively (Figure 18 a). Guide sequences were cloned into pLU6-CMV-GFP backbone and together with pRZ-CMV-mCherry-Cas9 introduced into the cells by electroporation. Since the number of $mCherry^{+}GFP^{+}$ cells after sorting was low, cells were directly sub-cloned in 96-well plates. Following, clones were tested for CRISPR/Cas9 activity. To this end, genomic DNA spanning the predicted site of the DSB was amplified by PCR, treated with AhdI or StyI and analyzed using agarose gel electrophoresis (Figure 18 b). Out of 25 clones, only clone #24 showed a modified restriction site for exon 10 upon StyI digest, while no cell clone displayed an alteration in exon 8 upon AhdI digest (Figure 18 b & c). Western Blot analysis of cellular lysates derived from clone #24 confirmed the absence of BIG2 protein (Figure 18 d). Because sanger sequencing of genomic DNA was inconclusive, I isolated mRNA of clone #24 and synthesized cDNA to exclude intron sequences from the sequence analysis. On cDNA level, I could confirm an insertion of 162 bp as well as an indel mutation of 183 bp, leading to frameshift mutations and premature stop codons (Figure 18 e). Clone #24 is hereafter referred to as Daudi BIG2-deficient ($BIG2^{-/-}$) cells.

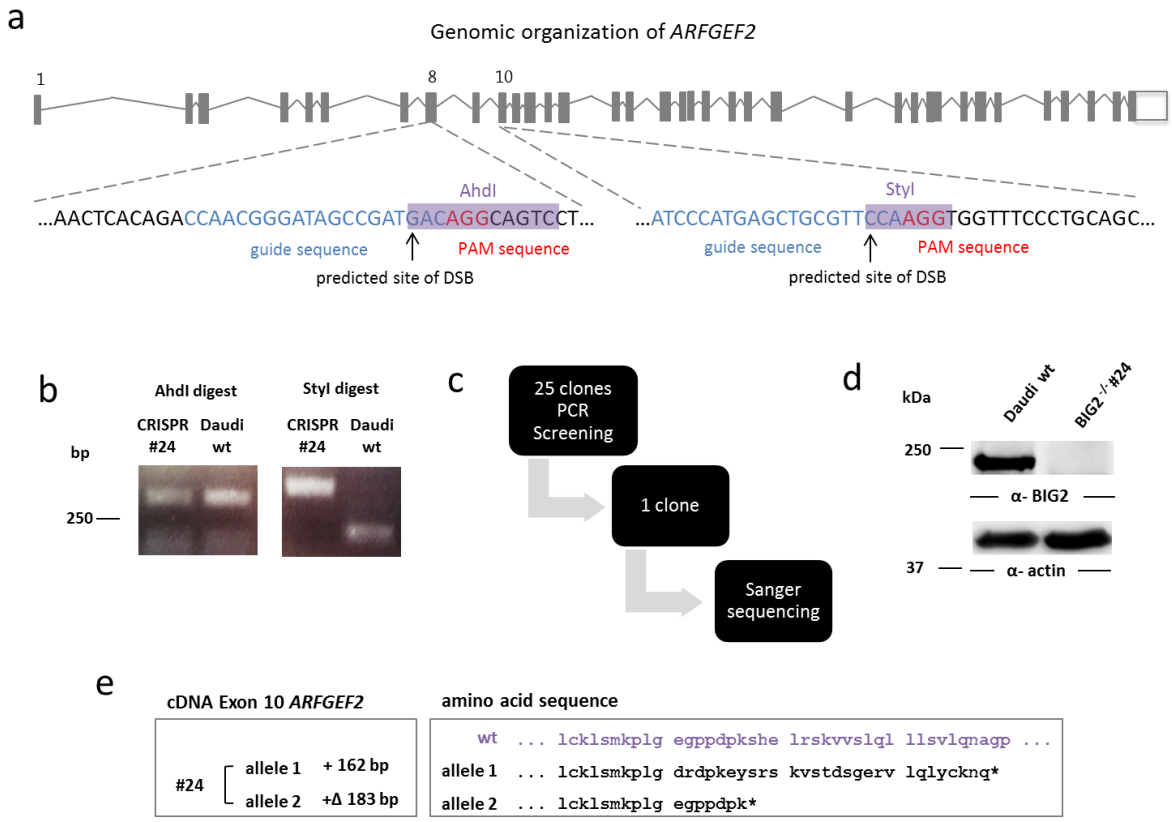


**Figure 18: Generation of BIG2-deficient Daudi cells.**
(a) Scheme of human *ARFGEF2* gene locus with CRISPR targeting strategy. The chosen guide sequences (blue) target exon 8 and 10. The PAM sequence (red) directs the Cas9 nuclease, which initiates a DSB (indicated with an arrow). Predicted sites of DSB are recognized by the AhdI or StyI endonucleases, respectively (purple). (b) CRISPR activity test. Genomic DNA of exon 8 and 10 was amplified by PCR, treated with AhdI or StyI and analyzed by gel electrophoresis. The size of DNA fragments is indicated on the left. (c) Screening process for Daudi BIG2 clones. (d) Western Blot analysis testing for BIG2 expression. Actin served as a loading control. Standard protein molecular masses are indicated in kDa. (e) cDNA analysis for clone #24 revealed an insertion (+) of 162 bp and an indel mutation (+Δ) of 183 bp, leading to frameshift mutations and which result in premature stop codons (*).

### 3.2.2 BIG2 is dispensable for $Ca^{2+}$ mobilization in Daudi cells

To test the role of BIG2 in activated BCR signaling, I reconstituted BIG2-deficient cells with a construct encoding a Citrine-tagged version of BIG2. After two rounds of sorting for Citrine-positive cells, successful reconstitution was confirmed by flow cytometry (Figure 19 a) and Western Blot analysis (Figure 19 b), respectively. Staining for IgM-BCR expression with APC-conjugated α-human IgM antibody confirmed unaltered IgM surface expression levels in BIG2-deficient cells compared to their reconstituted sub-clones and DG75 wt cells (Figure 19 c).

$Ca^{2+}$ mobilization assays revealed a higher pre-activation of BIG2-deficient cells and their sub-clones indicated by a higher baseline level (Figure 19 d). Upon BCR activation, BIG2-deficient cells showed a $Ca^{2+}$ profile comparable to Daudi wt cells. The response of both high and low expressing Citrine-tagged BIG2 cells was minimally decreased compared to BIG2-deficient cells. Since BCR expression levels were comparable and differences in the $Ca^{2+}$ response were minimal, I concluded that BIG2 is likely to be dispensable for $Ca^{2+}$ mobilization in Daudi cells.

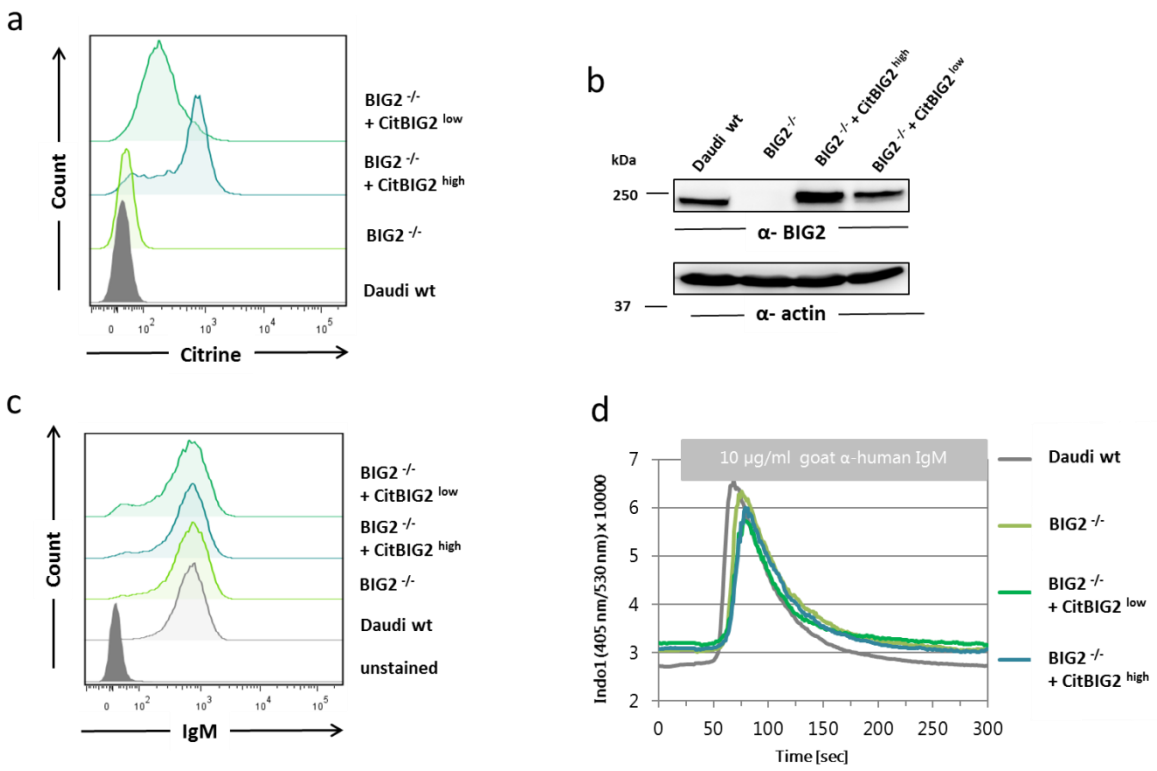


**Figure 19: Reconstitution, IgM expression and $Ca^{2+}$ mobilization of BIG2-deficient Daudi cells.**
(a) BIG2-deficient cells (*BIG2*$^{-/-}$, light green) were reconstituted with constructs encoding Citrine-tagged BIG2, sorted for high and low expression (*BIG2*$^{-/-}$ + CitBIG2$^{high}$ (cyan) and *BIG2*$^{-/-}$ + CitBIG2$^{low}$ (dark green)) and analyzed for Citrine expression by flow cytometry. Daudi wild-type (wt, grey) cells served as control. (b) Western Blot analysis with α-BIG2 antibody. Re-probing with α-actin was used as loading control. Standard protein molecular masses are indicated in kDa. (c) Cells were stained with APC-tagged α-human IgM antibody for analysis of surface IgM expression by flow cytometry in comparison to unstained cells (dark grey). Color code as seen in (a). (d) Cells were stained with $Ca^{2+}$ sensitive dye Indo-1-AM. Following a baseline recording for 25 s, cells were stimulated with 10 µg/ml $F(ab')_2$ α-human IgM and $Ca^{2+}$ flux was monitored for up to 5 min. Color code as seen in (a). Data represent results of three independent experiments.

### 3.2.3 BIG2-deficiency decreases proliferation and increases apoptosis in Daudi cells

Since shRNA experiments for BIG2 showed an effect on proliferation of BL cells (Corso et al. 2016), I aimed to confirm this effect in my cell line model as well. To this end, I performed XTT-based proliferation assays in 5% FCS medium as described previously. Proliferation assays were measured at d0 to establish a reference and at d3 and d4 to measure for the effect of BIG2 deficiency on proliferation. In accordance with the results obtained from the shRNA tests, BIG2-deficient cells displayed a growth defect, which was approximately half of the proliferation rate observed for Daudi wt cells (Figure 20). Reconstitution with a Citrine-tagged BIG2 variant did not increase proliferation of *BIG2*$^{-/-}$ cells, which is an indicator that BIG2-deficient cells might have acquired secondary pro-survival mutations.

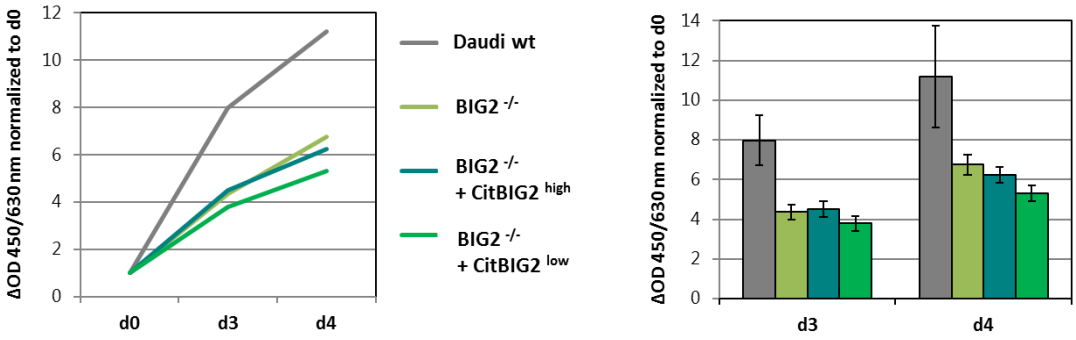


**Figure 20: XTT-based proliferation assays of BIG2-deficient cells**.
Daudi wild-type (wt, grey), BIG2-deficient (*BIG2*$^{-/-}$, light green) cells and their reconstituted sub-clones (*BIG2*$^{-/-}$ + CitBIG2$^{high}$ (cyan) and *BIG2*$^{-/-}$ + CitBIG2$^{low}$ (dark green)) were cultured in 5% FCS medium and their growth was monitored in an XTT-based proliferation assay at d3 and d4 after plating (d0). Mean ΔOD values of three independent experiments performed in duplicates were normalized to d0 and quantified for d2 and d4 + SD.

Besides affecting proliferation, shRNA targeting of BIG2 was also reported to enhance the number of apoptotic BL cells (Corso et al. 2016). To analyze the relevance of BIG2 on apoptosis in this BL cell line model, I grew cells for one day in RPMI 1640 medium without any supplements. Cells were then stained with APC-tagged Annexin V and PI as described previously and were measured by flow cytometry. BIG2-deficient Daudi cells showed a reduced number of living cells, while numbers of both early- and late apoptotic cells were increased (Figure 21). Similar results were observed for CitBIG2$^{high}$-expressing cells. However, CitBIG2$^{low}$-expressing were less prone to apoptosis. Therefore, although BIG2-deficient cells might have acquired pro-survival mutations, they could still benefit from BIG2 expression levels comparable to the endogenous situation (Figure 19 b).

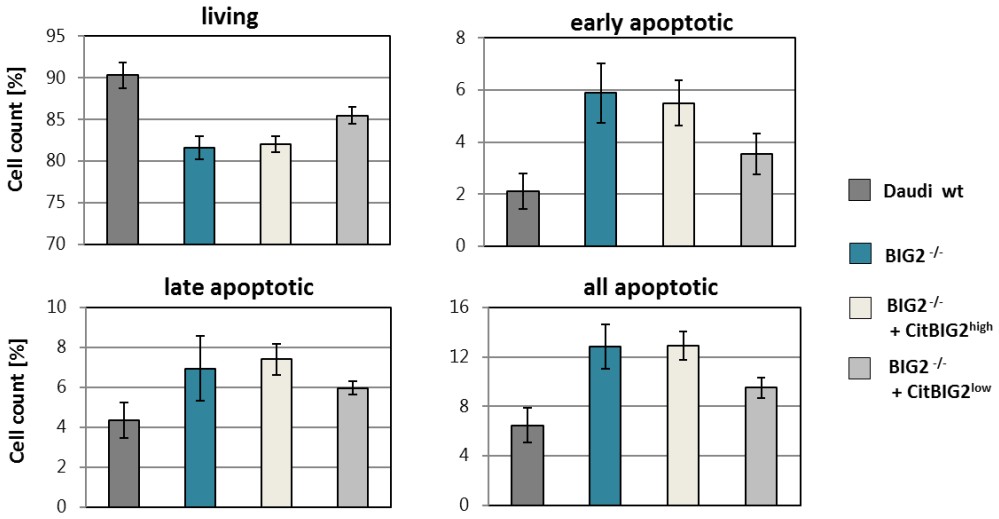


**Figure 21: BIG2-deficient Daudi cells are more prone to apoptosis.**
Daudi wild-type (wt, dark grey), BIG2-deficient (*BIG2*$^{-/-}$, cyan) cells and their reconstituted sub-clones (*BIG2*$^{-/-}$ + CitBIG2$^{high}$ (beige) and *BIG2*$^{-/-}$ + CitBIG2$^{low}$ (light grey)) were cultured in RPMI 1640 medium without supplements for one day before staining with APC-tagged Annexin V and PI for analysis of living (left upper panel), early apoptotic (right upper panel), late apoptotic (left lower panel) and all apoptotic (right lower panel) cells. Data are means of three independent experiments, one of which measured in duplicates. Error bars indicate SD.

### 3.2.4 Aberrant regulation of protein expression and downstream signaling pathways in BIG2-deficient Daudi cells

Following up on the proliferation and apoptosis assay, I aimed to identify which signaling pathways might be affected in BIG2-deficient cells. To this end, I prepared lysates of Daudi wt, BIG2-deficient and reconstituted cells to evaluate by Western Blot analysis. First, I tested for total protein levels of the adaptor protein Grb2, because its expression was described to be increased upon treatment of HeLa cells with small interfering RNA (siRNA) for BIG2 (Shen et al. 2012). In accordance with the results reported for HeLa cells, Grb2 levels were slightly enhanced in Daudi BIG2-deficient Daudi cells compared to wt and reconstituted cells (Figure 22 a).

In a different study also performed in HeLa cells, siRNA for BIG2 decreased mRNA levels of c-MYC (Li et al. 2016), which is overexpressed in BL. Protein expression of c-MYC was reduced in BIG2-deficient Daudi cells and could be restored with high levels of BIG2 almost to wt level, whereas lower levels of BIG2 were only partially able to restore c-MYC expression levels (Figure 22 b).

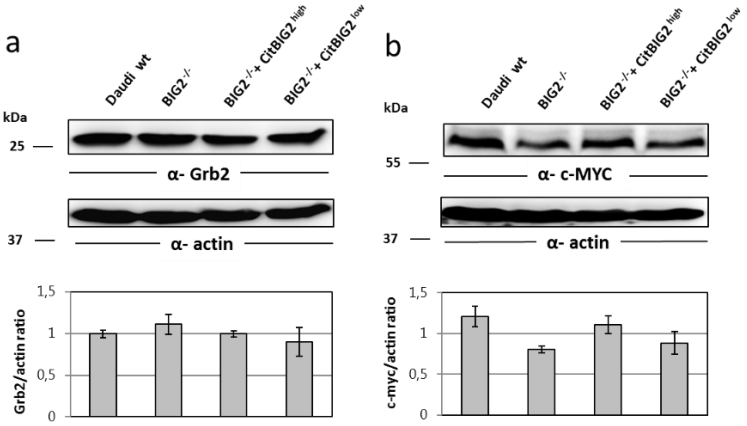


**Figure 22: BIG2 regulates expression of Grb2 and c-MYC.**
Lysates of unstimulated Daudi wild-type (wt), BIG2-deficient (*BIG2*$^{-/-}$) cells and their reconstituted sub-clones (*BIG2*$^{-/-}$ + CitBIG2$^{high}$ and *BIG2*$^{-/-}$ + CitBIG2$^{low}$) were evaluated by Western Blot analysis and probed for total expression of (a) Grb2 and (b) c-MYC. Blots were re-probed with α-actin for loading control. For each protein, exemplary immunoblots are shown (upper panels). Standard protein molecular masses are indicated in kDa. Ratios of signal intensities of α-Grb2 and α-c-MYC to that of α-actin were calculated and depicted as bar diagrams as the means + SD of three independent experiments (a and b, respectively, lower panels).

To analyze the role of BIG2 in tonic BCR signaling, I probed membranes with phospho-specific antibodies of key effector proteins in the PI3K-AKT pathway. For the regulatory PI3K subunit p85, phosphorylation was comparable among cell lines, although slightly decreased in BIG2-deficient cells (Figure 23 a). Downstream of p85 phosphorylation, phosphorylation of AKT (Figure 23 b) and its target FOXO1 (Figure 23 c) was increased in BIG2-deficient cells compared to both wt and reconstituted cells. Thus, BIG2 directly or indirectly attenuates AKT signaling.

Additionally, I analyzed activation of MAPK pathways by probing membranes with phospho-specific antibodies for MAPK key effector proteins ERK, JNK and p38. Basal phosphorylation of ERK was slightly decreased in BIG2-deficient cells compared to Daudi wt and reconstituted cells expressing low levels of Citrine-tagged BIG2 (Figure 24 a). Moreover, phosphorylation of JNK and p38 was slightly decreased in BIG2-deficient Daudi cells compared to wt cells and could be increased upon re-expression of high levels of BIG2 (Figure 24 b & c).

In conclusion, BIG2 was identified to influence c-MYC and Grb2 expression levels in BL cells as seen in HeLa cells. In addition, BIG2 attenuates AKT signaling while promoting JNK, ERK and p38 pathway signaling to varying degrees, indicating a possible dose-dependent effect of BIG2.

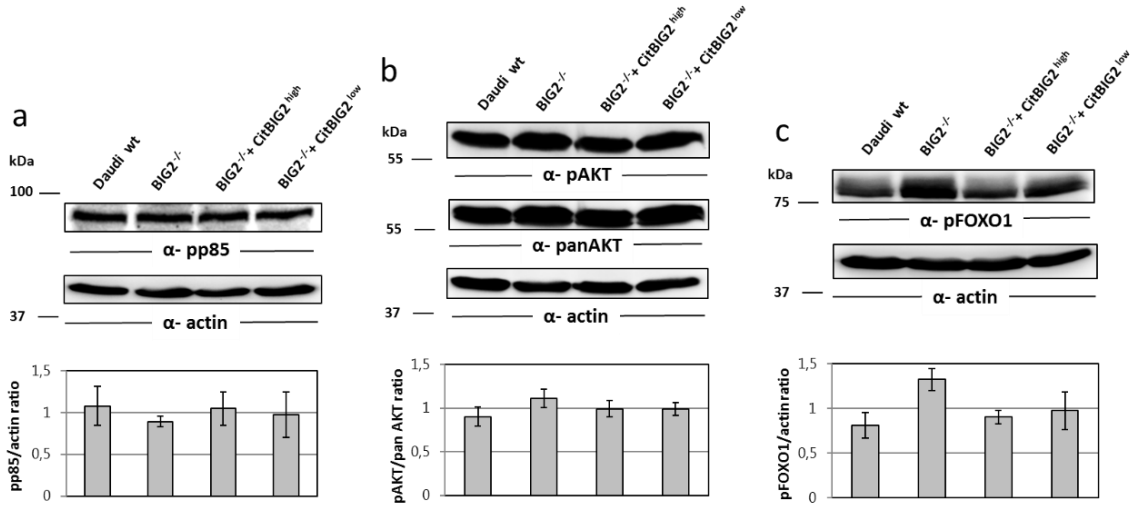


**Figure 23: BIG2 attenuates PI3K signaling in Daudi cells.**
Lysates of Daudi wild-type (wt), BIG2-deficient (*BIG2*$^{-/-}$) cells and their reconstituted sub-clones (*BIG2*$^{-/-}$ + CitBIG2$^{high}$ and *BIG2*$^{-/-}$ + CitBIG2$^{low}$) were subjected to Western Blot analysis and probed with phospho-specific antibodies detecting (a) p85 (b) AKT and (c) FOXO1. Re-probing with α-actin and α-panAKT served as loading control. For each protein, exemplary immunoblots are shown (upper panels). Standard protein molecular masses are indicated in kDa. Ratios of signal intensities of α-pp85 and α-pFOXO1 to that of α-actin (a and c, respectively, lower panels) and α-pAKT to that of α-panAKT (b, lower panel) were calculated and depicted in a bar diagram as the means + SD of three independent experiments.

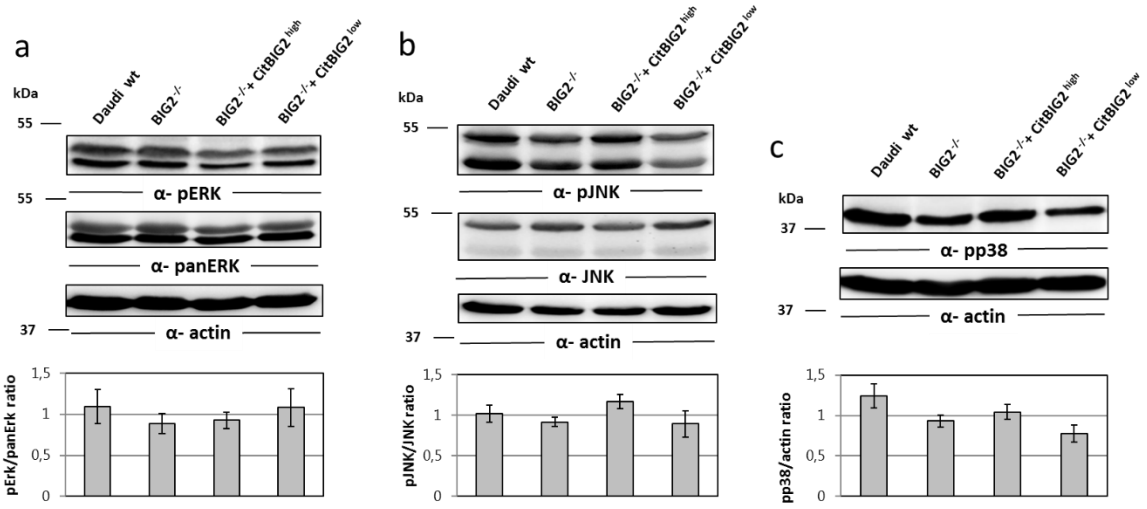


**Figure 24: BIG2 augments MAPK signaling in Daudi cells.**
Lysates of Daudi wild-type (wt), BIG2-deficient (*BIG2*$^{-/-}$) cells and their reconstituted sub-clones (*BIG2*$^{-/-}$ + CitBIG2$^{high}$ and *BIG2*$^{-/-}$ + CitBIG2$^{low}$) were subjected to Western Blot analysis and probed with phospho-specific antibodies for (a) ERK (b) JNK and (c) p38. Re-probing with α-actin served as loading control, total protein expression was determined using α-pan antibodies. For each protein, exemplary immunoblots are shown (upper panels). Standard protein molecular masses are indicated in kDa. Ratios of signal intensities of α-pERK and α-pJNK to that of their respective pan antibodies (a and b, respectively, lower panels) and α-pp38 to that of α-actin (c, lower panel) were calculated and depicted in a bar diagram as the means + SD of four (JNK & ERK) and three (p38) independent experiments.

## 3.3 The role of SHIP2 in BCR signaling

The 5'-inositol phosphatase SHIP2 is a negative regulator of PI3K signaling, since it decreases the pool of PI(3,4,5)$P_3$, which is a membrane anchor for PH-domain containing proteins, such as AKT (Frech et al. 1997). SHIP2 was found to be phosphorylated at S132 in tonic BCR signaling of DG75 cells and appears to be essential for BL cell survival according to shRNA-based drop out screening (unpublished results, Dr. Thomas Oellerich). Therefore, I aimed to identify the role of SHIP2 with respect to tonic BCR signaling in BL cell lines.

### 3.3.1 Generation of SHIP2-deficient cells

I used CRISPR/Cas9 gene editing to generate SHIP2-deficient cell lines on the background of BL60 and Daudi cells. The guide sequence was designed to target exon 1 in the *INPPL1* gene (coding for SHIP2 protein) (Figure 25 a). The pLU6-sghSHIP2-CMV-GFP plasmid encoding for the guide sequence was alongside the pRZ-CMV-mCherry-Cas9 plasmid introduced into the cells using electroporation. After 48 h, cells were sorted to enrich the $mCherry^+GFP^+$ subpopulation and subsequently sub-cloned. Following, I prepared lysates of the single clones and screened for the presence of the SHIP2 protein by Western Blot analysis. For BL60 cells, in 4 out of 42 clones, SHIP2 was not detected (Figure 25 b). Figure 25 c shows an exemplary Western blot analysis for lysates derived from clone #19 and BL60 wt cells. Sanger sequencing of cDNA confirmed clone #19 to have a 5 bp Indel mutation and an 83 bp deletion leading to frameshift mutations resulting in premature stop codons (Figure 25 d). In the following, clone #19 is referred to as SHIP2-deficient (*SHIP2*$^{-/-}$) BL60 cells.

For Daudi cells, in lysates of 3 out of 20 clones SHIP2 protein expression was not detected (Figure 25 e). 2 clones were analyzed by sanger sequencing of cDNA (Figure 25 f) confirming for clone #1 a 1 bp insertion and a 2 bp deletion, leading to frameshift mutations and subsequent premature stop codons (Figure 25 g). Clone #1 is hereafter referred to as SHIP2-deficient (*SHIP2*$^{-/-}$) Daudi cells. A reported SHIP2 splice variant lacking amino acids 1-242 due to alternative splicing was detected in lysates of both Daudi and BL60 wt but not in SHIP2-deficient cells (Figure 25 e and 26 b, respectively).

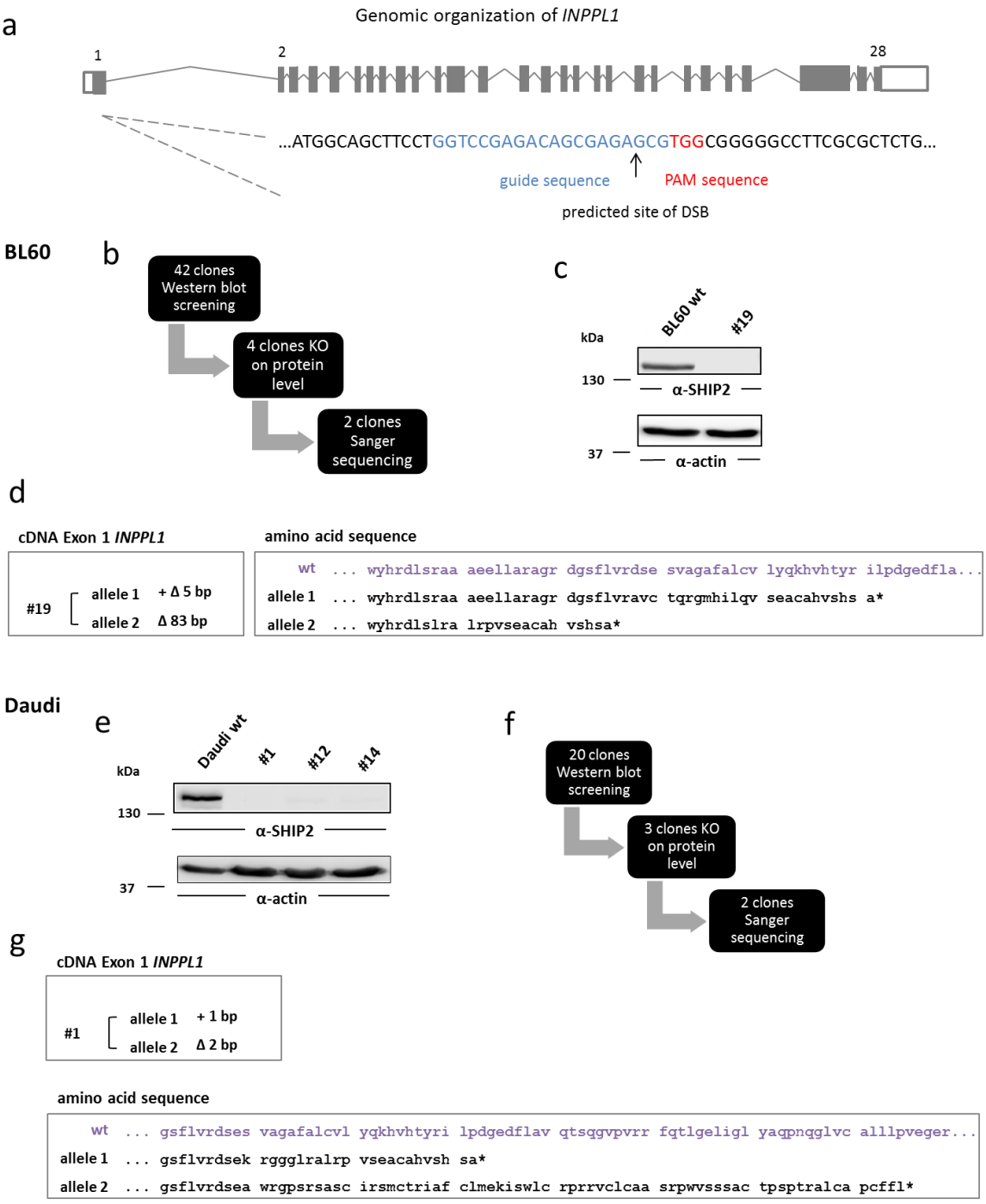


**Figure 25: Generation of SHIP2-deficient BL cell lines.**
(a) Overview of genomic organization of *INPPL1* gene (encoding SHIP2). Guide RNA sequence targeting exon 1 of *INPPL1*. Predicted site of DSB by Cas9 nuclease is depicted with an arrow. (b) Overview of screening for SHIP2-deficient clones in BL60 cells. (c) Exemplary Western Blot analysis of cellular lysates derived from BL60 wt and clone #19 detecting SHIP2 expression. Re-probing with α-actin served as loading control. Standard protein molecular masses are indicated in kDa. (d) cDNA sequence analysis of clone #19 verified genomic alterations in both alleles (5 bp indel mutation (+Δ) and 83 bp deletion (Δ)) leading to frameshift mutations resulting in premature stop codons (*). (e) Western Blot analysis showed absence of SHIP2 protein in Daudi derived clones #1, #12 and #14. Re-probing with α-actin served as loading control. Molecular weight of proteins is indicated in kDa. (f) Screening process to identify Daudi SHIP2-deficient clones. (g) Sequence analysis of Daudi SHIP2-deficient clone #1. Both alleles were targeted by Cas9, leading to a 1 bp insertion (+) and a 2 bp deletion (Δ). Mutations identified in the cDNA lead to frameshift and premature stop codons (*) upon translation.

To exclude CRISPR-induced off-target or clonal effects influencing further experiments, I retrovirally transduced BL60 and Daudi SHIP2-deficient clones with a Citrin-tagged SHIP2 (CitSHIP2)-encoding construct. After selection, the Citrine-expressing sub-populations were additionally enriched by cell sorting. The reconstituted BL60 cells were sorted for CitSHIP2$^{low}$- and CitSHIP2$^{high}$-expressing cells. Western Blot analysis of cellular lysates showed that CitSHIP2$^{low}$-expressing cells resembled expression of SHIP2 in BL60 wt cells (Figure 26 b). Analysis of Citrine expression by flow cytometry revealed CitSHIP2$^{low}$-expressing cells as a heterogeneous population of both Citrine$^{+}$ and Citrine$^{low}$ cells (Figure 26 a). For further characterization, I tested for surface IgM-BCR expression, since different expression levels could interfere with BCR signaling intensity. BL60 SHIP2-deficient cells and CitSHIP2$^{high}$-expressing cells displayed lower IgM expression levels compared to BL60 wt and CitSHIP2$^{low}$-expressing cells (Figure 26 c), which was observed in three independent experiments (Figure 26 d). Western Blot analysis of cellular lysates revealed an enhanced expression of SHIP1 in all cells derived from the SHIP2$^{-/-}$ clone characterizing it as clonal effect (Figure 26 e).

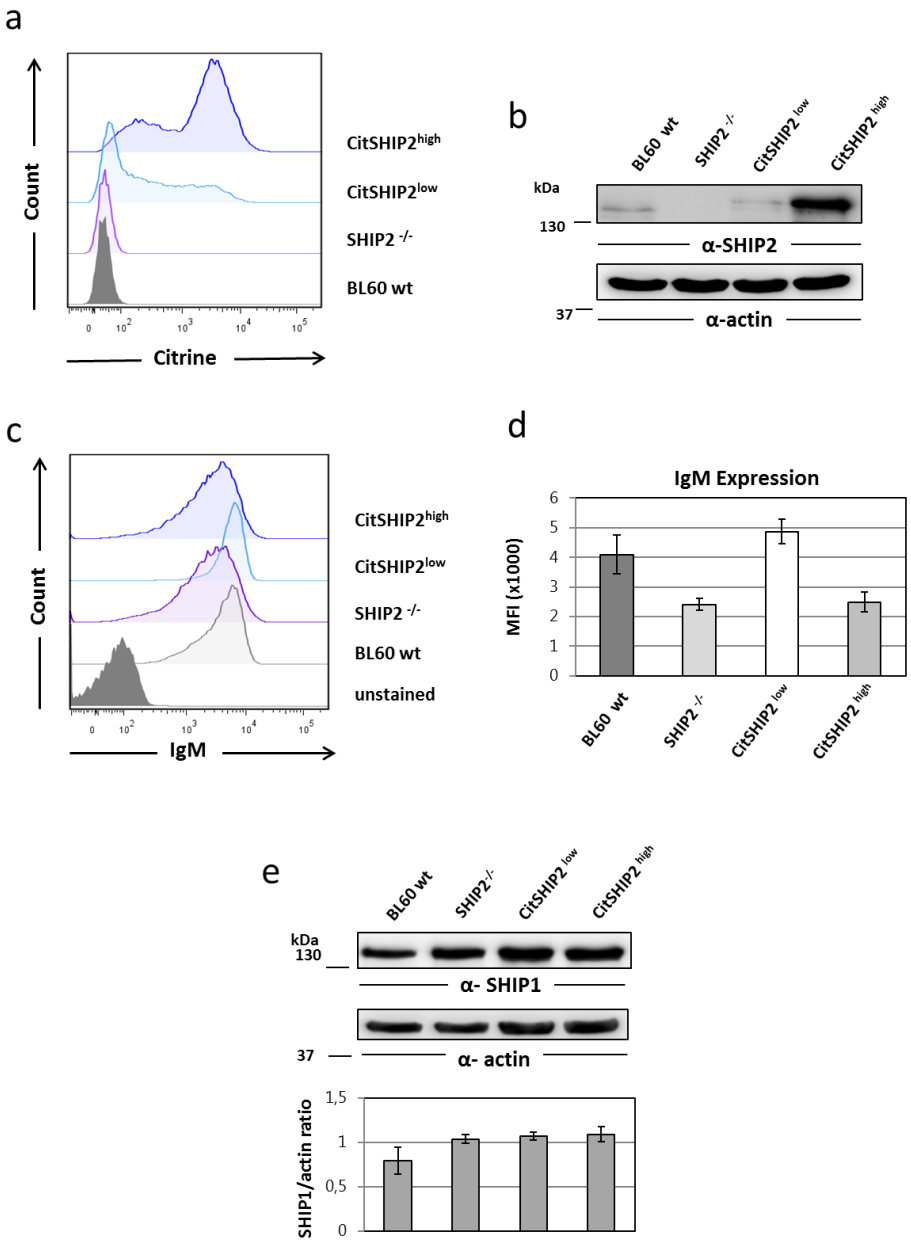


**Figure 26: Reconstitution of SHIP2-deficient BL60 cells, IgM and SHIP1 expression analysis.**
(a) SHIP2-deficient (*SHIP2*$^{-/-}$) BL60 cells were reconstituted with a Citrine-tagged SHIP2 encoding construct (CitSHIP2) and analyzed for Citrine expression by flow cytometry in comparison to BL60 wild-type (wt) cells. (b) Lysates of BL60 wt, SHIP2-deficient, CitSHIP2$^{low}$ and CitSHIP2$^{high}$ cells were prepared and subjected to Western Blot analysis. Blots were decorated with α-SHIP2 antibody. α-actin served as loading control. Standard protein molecular masses are indicated in kDa. (c) Staining for surface IgM using an APC-tagged α-human IgM antibody. Samples were analyzed by flow cytometry. Unstained BL60 wt cells (dark grey) served as control. (d) Quantification of IgM expression of three independent experiments. Error bars indicate SD. (e) Lysates of BL60 wt, SHIP2-deficient and reconstituted CitSHIP2$^{low}$ and CitSHIP2$^{high}$ cells were subjected to Western Blot analysis. Blots were decorated with α-SHIP1 antibody. α-actin served as loading control (upper panel). Standard protein molecular masses are indicated in kDa. Ratio of signal intensities for α-SHIP1 to α-actin were calculated and are depicted in a bar diagram as means + SD of three independent experiments (lower panel).

Additionally, Daudi SHIP2-deficient cells were reconstituted with Citrine-tagged SHIP2 (CitSHIP2)-encoding construct and cells were sorted for high (CitSHIP2$^{high}$), medium (CitSHIP2$^{med}$) and low levels (CitSHIP2$^{low}$) of CitSHIP2 (Figure 27 a). Western Blot analysis of cellular lysates verified different expression levels of CitSHIP2 (Figure 27 b) and showed that SHIP2 expression of CitSHIP2$^{low}$ cells was closest to that in Daudi wt cells. Flow cytometry analysis of surface IgM revealed, in contrast to BL60-derived cells, comparable BCR expression in Daudi-derived cell lines (Figure 27 c) which was verified in three independent experiments (Figure 27 d). Differences in SHIP1 expression were not identified (data not shown).

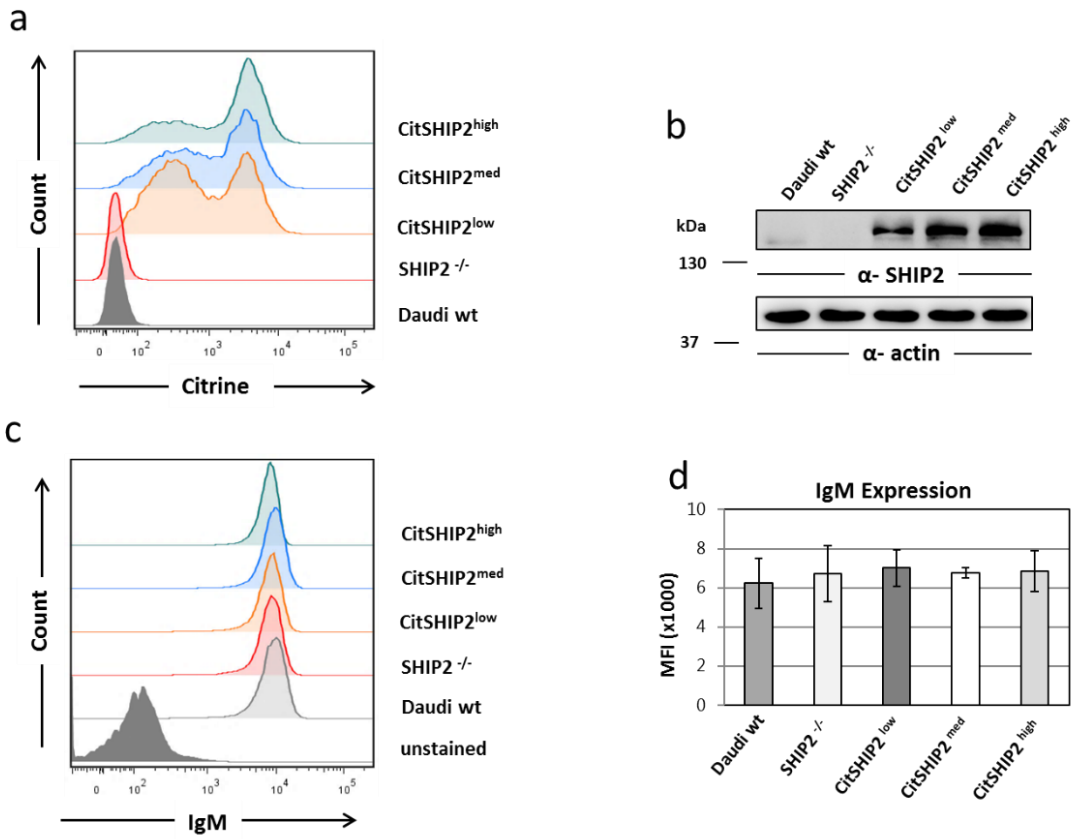


**Figure 27: Reconstitution of SHIP2-deficient Daudi cells and IgM BCR expression.**
(a) SHIP2-deficient (*SHIP2*$^{-/-}$) Daudi cells were reconstituted with a Citrine-tagged SHIP2 encoding construct (CitSHIP2), sorted for low, medium and high Citrine expression levels and analyzed for Citrine expression by flow cytometry in comparison to wild-type (wt, grey) Daudi cells. (b) Lysates of Daudi wt, SHIP2-deficient, CitHIP2$^{low}$, CitSHIP2$^{med}$ and CitSHIP2$^{high}$ cells were subjected to Western Blot analysis. Blots were probed with α-SHIP2 antibody. α-actin served as loading control. Standard protein molecular masses are indicated in kDa. (c) Surface staining for IgM using an APC-tagged α-human IgM antibody. Samples were analyzed by flow cytometry. Unstained wt BL60 cells (dark grey) served as control. (d) Quantification of IgM expression of three independent experiments. Data represent means + SD.

### 3.3.2 Negative role of SHIP2 in BCR-induced $Ca^{2+}$ mobilization

Before analyzing the role of SHIP2 in tonic BCR signaling, I tested its role in activated BCR signaling. To study BCR-induced mobilization of $Ca^{2+}$, I stained cells with the calcium-sensitive dye Indo-1-AM for flow cytometry. When activated via the BCR, Daudi SHIP2-deficient cells displayed an increased $Ca^{2+}$ response compared to Daudi wt cells, which could be fully reconstituted upon expression of the Citrine-tagged version of SHIP2 (Figure 28 a). Similar to Daudi SHIP2-deficient cells, BL60 SHIP2-deficient cells, despite having a weaker $Ca^{2+}$ signal than BL60 wt cells, showed an increased BCR-induced $Ca^{2+}$ response upon activation of the BCR when compared reconstituted cells (Figure 28 b). These data imply that SHIP2 has a similar negative regulatory function in the BCR-induced $Ca^{2+}$ mobilization that is reported for SHIP1 (Okada et al. 1998; Manno et al. 2016).

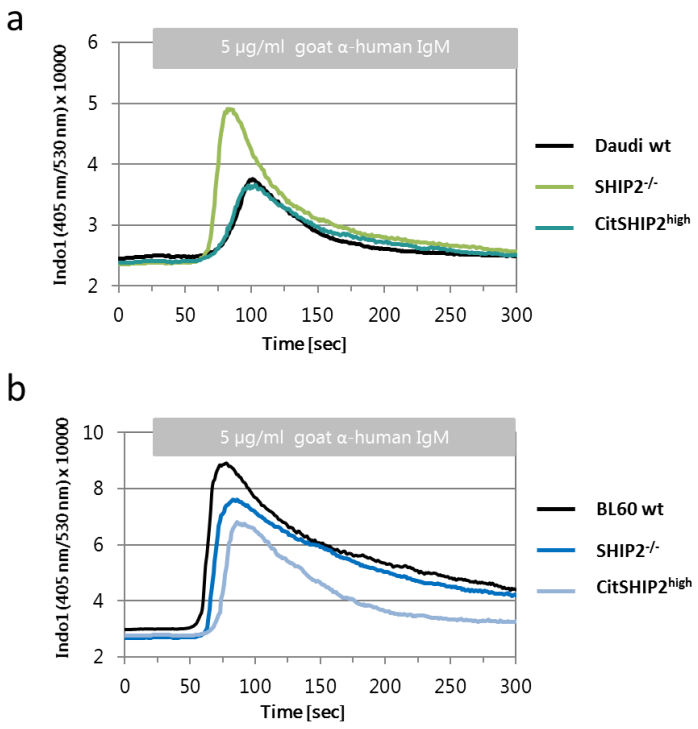


**Figure 28: $Ca^{2+}$ mobilization is increased in SHIP2-deficient BL cells.**
(a) Daudi wild-type (wt, black line), SHIP2-deficient (*SHIP2*$^{-/-}$, light green line) and reconstituted cells (CitSHIP2$^{high}$, dark green line) as well as (b) BL60 wt (black line), SHIP2-deficient (*SHIP2*$^{-/-}$, dark blue line) and reconstituted cells (CitSHIP2$^{high}$, light blue line) were loaded with the calcium-sensitive dye Indo-1-AM and analyzed by flow cytometry. A baseline was recorded for 25 s before the IgM BCR was stimulated with 5 µg/ml F(ab')$_2$ α-IgM and $Ca^{2+}$ flux monitored for up to 300 s. Displayed $Ca^{2+}$ mobilization assays represent three independent experiments with similar results.

### 3.3.2.1 SHIP2 negatively regulates downstream BCR signaling

Based on the identified impact of SHIP2 on BCR-induced $Ca^{2+}$ mobilization, I next aimed at investigating further pathways in the BCR signal transduction. This was done by Western Blot analysis of cellular lysates derived from Daudi cells, which were left either untreated or were stimulated via the BCR for 5 or 15 min. Daudi cells were used to avoid artefacts due to different BCR surface expression found in the generated BL60 cell lines.

To test for an early event in activated BCR signaling, I first analyzed the phosphorylation of Syk by using α-phospho-Syk and α-actin antibodies, respectively (Figure 29 a). Strong BCR-induced signals for phosphorylation of Syk were detected and found to be comparable among cell lines, indicating that SHIP2 does not affect Syk activation.

The activation of MAPKs is an important process downstream of BCR engagement. Hence, I tested for the BCR-induced activation of ERK by probing membranes with α-phospho ERK (α-pERK) antibody (Figure 29 b). Re-probing of the blot with α-pan ERK and α-actin antibodies, respectively, served as loading controls. Upon BCR stimulation, ERK was phosphorylated in all cell lines, however to the highest extent in Daudi wt cells. When compared to reconstituted cells, SHIP2-deficient cells appear to activate ERK more efficiently further indicating a negative regulatory role of SHIP2 in activated BCR-signaling.

Additionally, I tested for phosphorylation of the MAPKs p38 and JNK by Western Blot analysis of cellular lysates using respective phospho-specific and control antibodies. Daudi wt cells displayed an overall stronger phosphorylation of p38 compared to SHIP2-deficient cells, which was, however, constitutive and not BCR-inducible (Figure 29 c). When probing for phosphorylation of the MAPK JNK, I observed phosphorylation of JNK already in unstimulated cells, which was slightly increased upon BCR stimulation (Figure 29 d). SHIP2-deficient cells displayed a lower level of JNK phosphorylation in unstimulated cells as well as BCR-stimulated cells compared to wt and CitSHIP2$^{low}$-expressing cells implying a role of SHIP2 in the BCR-dependent JNK activation.

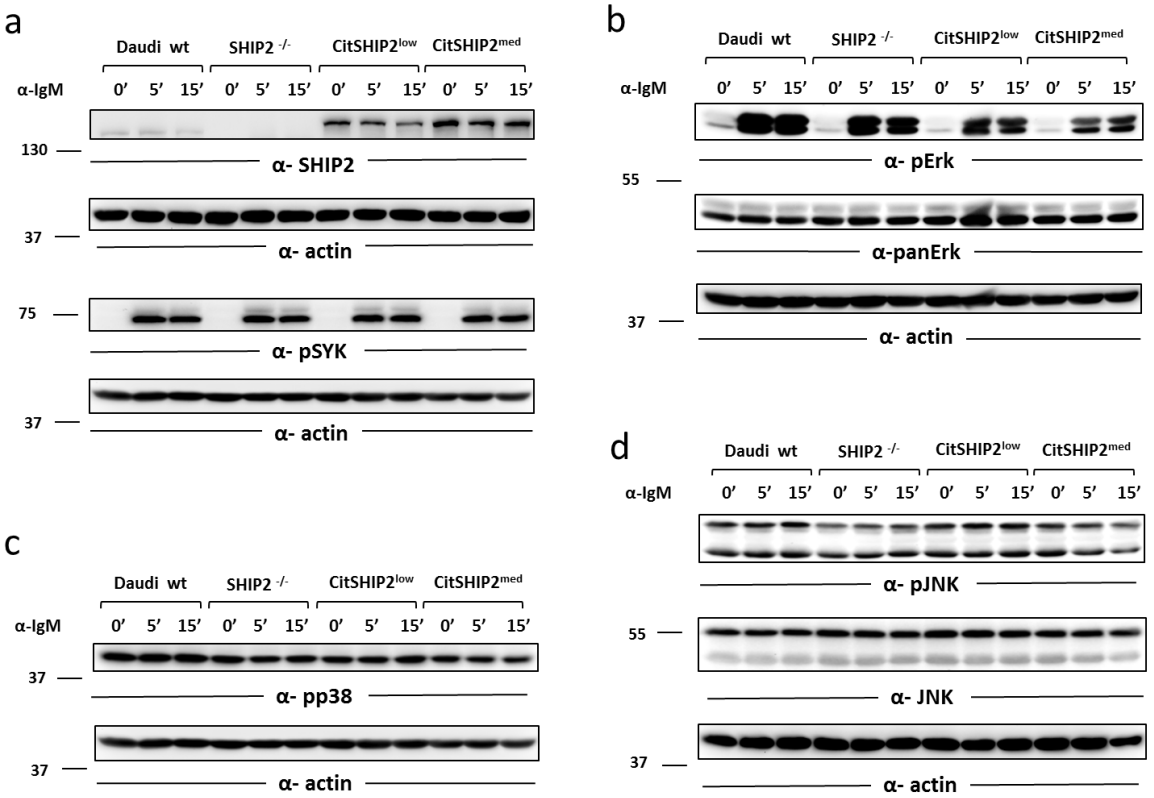


**Figure 29: Analysis of key MAPK signaling proteins activated upon BCR stimulation.**
SHIP2-deficient (*SHIP2*$^{-/-}$) Daudi cells were reconstituted and sorted for low and medium expression levels of CitSHIP2 (CitSHIP2$^{low}$ and CitSHIP2$^{med}$), were stimulated via the IgM-BCR using 10 µg/ml F(ab')$_2$ α-IgM for indicated time points or left unstimulated (0'). Daudi wild-type (wt) cells served as control. Lysates were prepared and subjected to Western Blot analysis. (a) Probing with α-SHIP2 (first panel) and α-actin (second panel) antibodies served as control. To analyze the impact of SHIP2 on BCR-induced activation, blots were probed with different phospho-specific antibodies detecting Syk (a, third panel), ERK (b, first panel), p38 (c, first panel) and JNK (d, first panel). For analysis of total protein expression, blots were re-probed with α-panERK (b, second panel) or α-JNK (d, second panel) or with α-actin for loading control (a-d, lower panels). Standard protein molecular masses are indicated in kDa. Blots represent data obtained in three independent experiments.

SHIP2 dephosphorylates PI(3,4,5)$P_3$ to PI(3,4)$P_2$ and thereby regulates the PI3K-AKT pathway in several cell types (Backers et al., 2003; C.-H. Fu et al., 2014; Taylor et al., 2000; Yang et al., 2014). Therefore, I tested for phosphorylation of key proteins involved in PI3K-AKT signaling. Since the regulatory subunit of PI3K, p85, is activated early in this pathway, I started by probing Western Blots prepared as described above with a phospho-specific α-p85 antibody (Figure 30 a). While all cell lines displayed a robust and similar phosphorylation of p85 already in resting cells, BCR engagement appears to cause a reduction in p85 phosphorylation. An impact of SHIP2 on this process remains unclear. In contrast to p85, phosphorylation of AKT is induced upon BCR stimulation (Figure 30 b). In Daudi wt and CitSHIP2-expressing cells, AKT phosphorylation decreased after 15 min of BCR stimulation but not in SHIP2-deficient cells. In line with these results, phosphorylation of FOXO1, a

downstream target of AKT, was also phosphorylated upon BCR activation and downregulated after 15 min of BCR stimulation in all but SHIP2-deficient cells (Figure 30 c). Taken together, these results demonstrate that SHIP2 negatively regulates the BCR-induced activation of AKT-dependent signaling events.

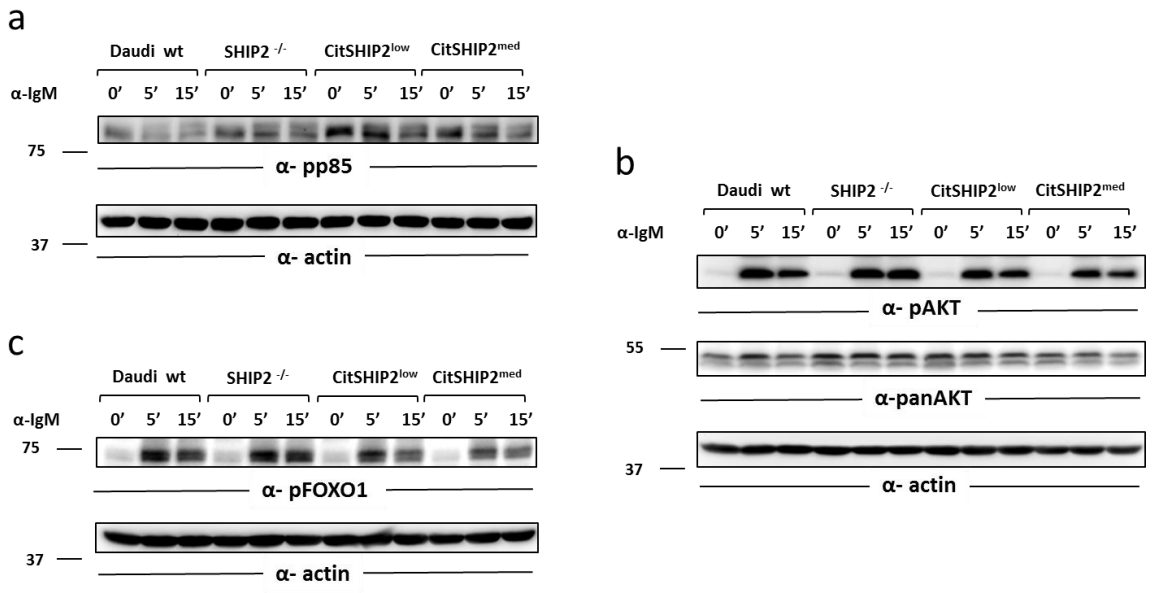


**Figure 30: Analysis of key PI3K signaling proteins activated upon BCR stimulation.**
SHIP2-deficient (*SHIP2*$^{-/-}$) Daudi cells were reconstituted and sorted for low and medium levels of CitSHIP2 (CitSHIP2$^{low}$ and CitSHIP2$^{med}$), were stimulated via the IgM-BCR using 10 µg/ml F(ab')$_2$ α-IgM for indicated time points or left unstimulated (0'). Daudi wild-type (wt) cells served as control. Lysates were prepared and subjected to Western Blot analysis. To analyze the impact of SHIP2 on BCR-induced activation, blots were probed with different phospho-specific antibodies for (a) p85 (first panel), (b) AKT (first panel) and (c) FOXO1 (first panel). For analysis of total protein expression, blots were re-probed with α-panAKT (b, second panel) or with α-actin for loading control (a-c, lower panels). Standard protein molecular masses are indicated in kDa. Blots represent data obtained in three independent experiments.

### 3.3.2.2 SHIP2 inhibition by small molecules mimics the loss of SHIP2 in BL cell lines

Another approach to decipher the role of SHIP2 in BL-dependent BCR signaling was the application of a selective small molecule SHIP2 inhibitor AS1949490 to complement my cell-based SHIP2-deficient model system. The inhibitor targets the phosphatase domain of SHIP2 and was reported to have a 30-fold affinity for SHIP2 over SHIP1 ($IC_{50}$ 0.62 µM for human SHIP2) (Suwa et al. 2009). Since Daudi SHIP2-deficient cells displayed a robust $Ca^{2+}$ phenotype upon BCR activation, I used $Ca^{2+}$ mobilization assays to titrate the effective concentration of the inhibitor. Prior to the measurement, cells were treated with the desired concentration of the inhibitor or DMSO for 30 min. At a

concentration of 5 µM AS1949490, the $Ca^{2+}$ response of Daudi wt (Figure 31 a) and CitSHIP2$^{high}$-expressing cells (Figure 31 b) resembled DMSO-treated Daudi SHIP2-deficient cells, while the BCR-induced $Ca^{2+}$ mobilization of SHIP2-deficient Daudi cells was only mildly affected upon treatment of AS1949490 compared to DMSO (Figure 31 c). To sum up, at a concentration of 5 µM, the SHIP2 inhibitor AS1949490 was able to mimic the impact of SHIP2 deficiency on the BCR-induced $Ca^{2+}$ mobilization and revealed only mild side effects.

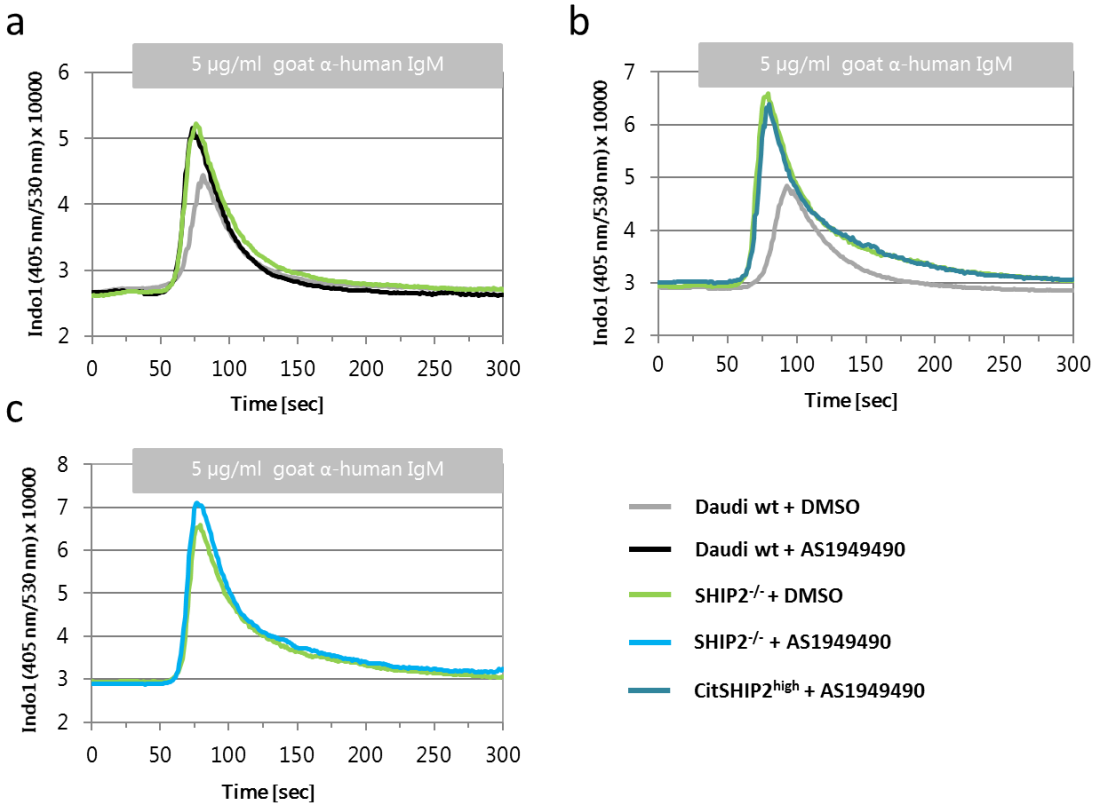


**Figure 31: Titration of SHIP2 inhibitor AS1949490 concentration in $Ca^{2+}$ mobilization assays.**
Daudi wild-type (wt), SHIP2-deficient (*SHIP2*$^{-/-}$) and reconstituted (CitSHIP2$^{high}$) cells were loaded with the calcium-sensitive dye Indo-1-AM. 30 min before the measurement, cells were incubated with DMSO or 5 µM AS1949490. Before BCR stimulation with 5 µg/ml F(ab')$_2$ α-human IgM, a baseline was recorded for 25 s and $Ca^{2+}$ flux was monitored for up to 300 s. (a) $Ca^{2+}$ flux of DMSO-treated (grey line) and AS1949490-treated (black line) Daudi wt cells compared to DMSO-treated SHIP2$^{-/-}$ cells (green line). (b) $Ca^{2+}$ flux of DMSO-treated Daudi wt (grey line) and *SHIP2*$^{-/-}$ cells (green line) compared to AS1949490-treated CitSHIP2$^{high}$ cells (cyan line). (c) $Ca^{2+}$ mobilization in Daudi *SHIP2*$^{-/-}$ cells treated with DMSO (green line) or AS1949490 (blue line). Plots are representative of three independent experiments.

### 3.3.3 SHIP2 influences proliferation and apoptosis in BL cells

Having two cell line systems and a potent SHIP2 inhibitor on hand, I aimed to analyze the relevance of SHIP2 for the survival of BL cell lines. To verify these observations, I performed XTT-based proliferation and apoptosis assays to decipher the influence of SHIP2 in the SHIP2-deficient cell line model systems.

#### 3.3.3.1 SHIP2 positively regulates proliferation

For proliferation assays, 6000 cells were seeded per well of a 96-well plate and their proliferation was indirectly monitored by their metabolic activity in an XTT-based proliferation assay. Proliferation assays were performed in 5% FCS medium as described previously. After three days, Daudi wt cells showed higher numbers of metabolically active cells compared to SHIP2-deficient cells (Figure 32 a). However, expression of CitSHIP2 could not sufficiently restore the numbers of living cells, although CitSHIP2$^{high}$-expressing cells showed a trend to partially restore the phenotype.

To circumvent possible clonal effects, I included treatment with the SHIP2 inhibitor AS1949490 and repeated the experiment. Treatment with DMSO was used as control. In all Daudi cell lines, proliferation of cells was decreased upon treatment with 5 µM AS1949490 after d2 and d4 of the analysis compared to DMSO treated cells (Figure 32 b). At this concentration, the inhibitor was also able to decrease the number of SHIP2-deficient cells, indicating that side effects of the inhibitor affect Daudi cell survival.

I used the same experimental set up to analyze proliferation of BL60 cell lines (Figure 32 c). Here, the inhibitor specifically decreased proliferation in cells expressing SHIP2, while SHIP2-deficient cells were only mildly affected compared to DMSO treated cells. In summary, both loss of SHIP2 or inhibition of its phosphatase activity decreased numbers of metabolically active BL cells but this effect could not be fully reconstituted.

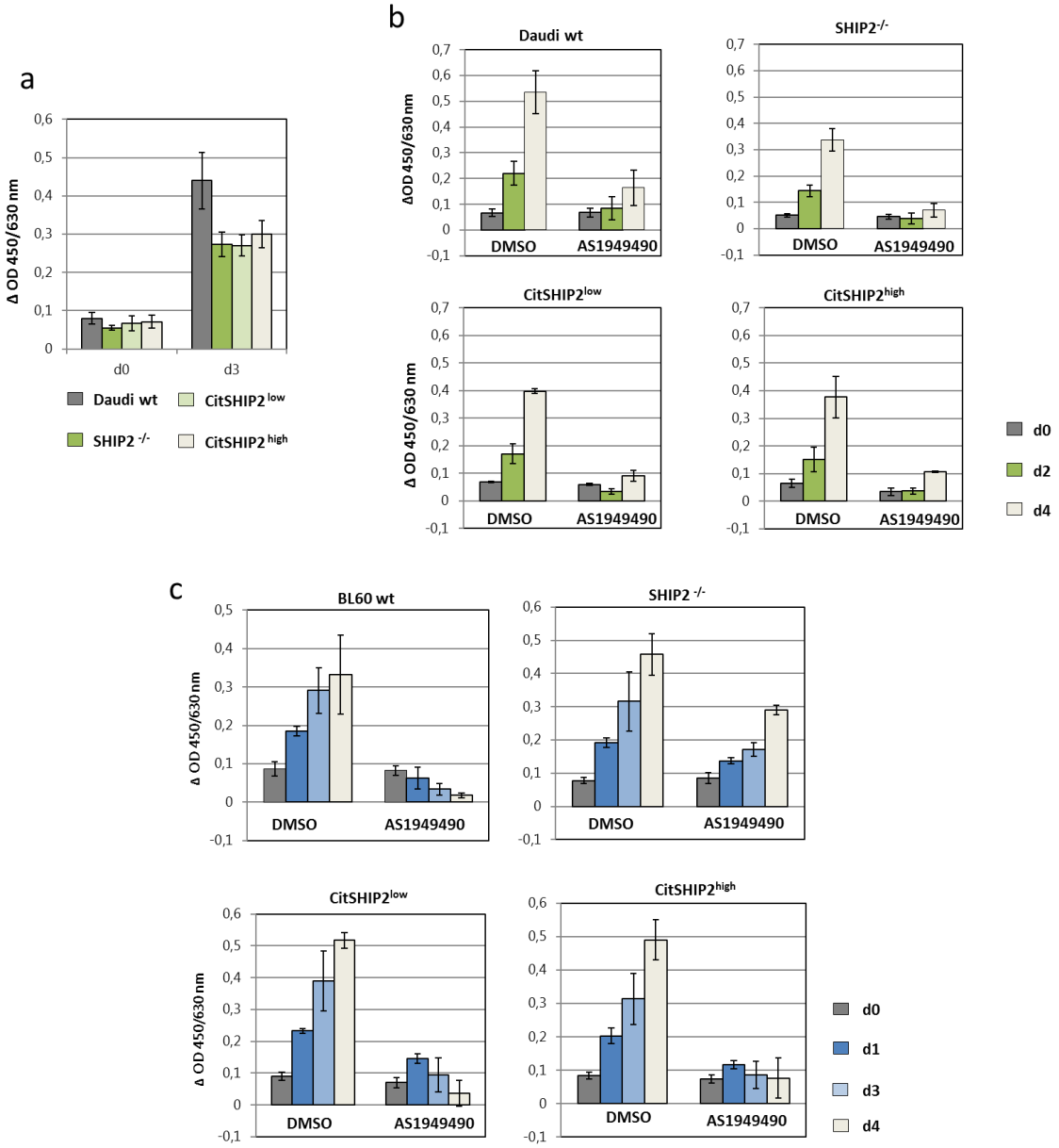


**Figure 32: Loss of SHIP2 and SHIP2 inhibition reduced proliferation in BL60 and Daudi cells.**
(a) Daudi wild-type (wt, grey), SHIP2-deficient (*SHIP2*$^{-/-}$, green) and reconstituted CitSHIP2$^{low}$ (light green) and CitSHIP2$^{high}$ cells (beige) were analyzed in XTT-proliferation assays at d0 and d3 in 5% FCS medium or (b) additionally treated with 5µM AS1949490 or DMSO and analyzed at d0 (grey), d2 (green) and d4 (beige). Data are means + SD of three independent experiments. (c) Proliferation of BL60 wt, SHIP2-deficient (*SHIP2*$^{-/-}$) and reconstituted CitSHIP2$^{low}$ and CitSHIP2$^{high}$ cells was analyzed in 5% FCS medium at d0 (grey), d1 (blue), d3 (light blue) and d4 (beige) upon treatment with 5 µM AS1949490 or DMSO. Data are means + SD of two (d2, d4) and four (d0, d3) independent experiments.

### 3.3.3.2 SHIP2 partially inhibits apoptosis

With respect to the proliferation assays, it remained unclear if SHIP2 directly influences cell proliferation or whether the observed effect is caused by increased cell death upon loss of SHIP2. To this end, I performed apoptosis assays by culturing cells in 1% FCS medium for three days and staining them at d3 with APC-tagged Annexin V and PI to distinguish live, early and late apoptotic cells by flow cytometry.

For Daudi SHIP2-deficient cells, the percentage of living cells was decreased by approximately 10% compared to Daudi wt and CitSHIP2-expressing cells (CitSHIP2$^{med}$ not shown), while the percentage of late apoptotic cells was increased (Figure 33 a). The effect of SHIP2 loss was even more pronounced in BL60 cells (Figure 33 b). In BL60 cells, SHIP2-deficiency decreased the percentage of living cells by approximately 20%, whereas percentages for both early and late apoptotic cells were significantly increased. CitSHIP2$^{low}$-expressing cells were able to fully functionally compensate for loss of SHIP2. In contrast, CitHIP2$^{high}$-expressing cells could only partially protect SHIP2-deficient cells from early apoptosis.

To analyze apoptosis induction in BL60 cells independent of different IgM BCR expression levels, I repeated the experiment by culturing BL60 wt and BL60 SHIP2-deficient cells with 5 µM AS1949490 or DMSO in 1% FCS medium and analyzed the cells at d2. In reference to the proliferation assays, I expected no induction of apoptosis in BL60 SHIP2-deficient cells upon inhibitor treatment. Indeed, while SHIP2-deficient cells were not affected by the inhibitor, the number of late apoptotic cells in BL60 wt cells increased approximately 20% upon treatment with 5 µM AS1949490 compared to DMSO control cells (Figure 33 c). In summary, SHIP2 is likely to partially protect BL cells from apoptosis.

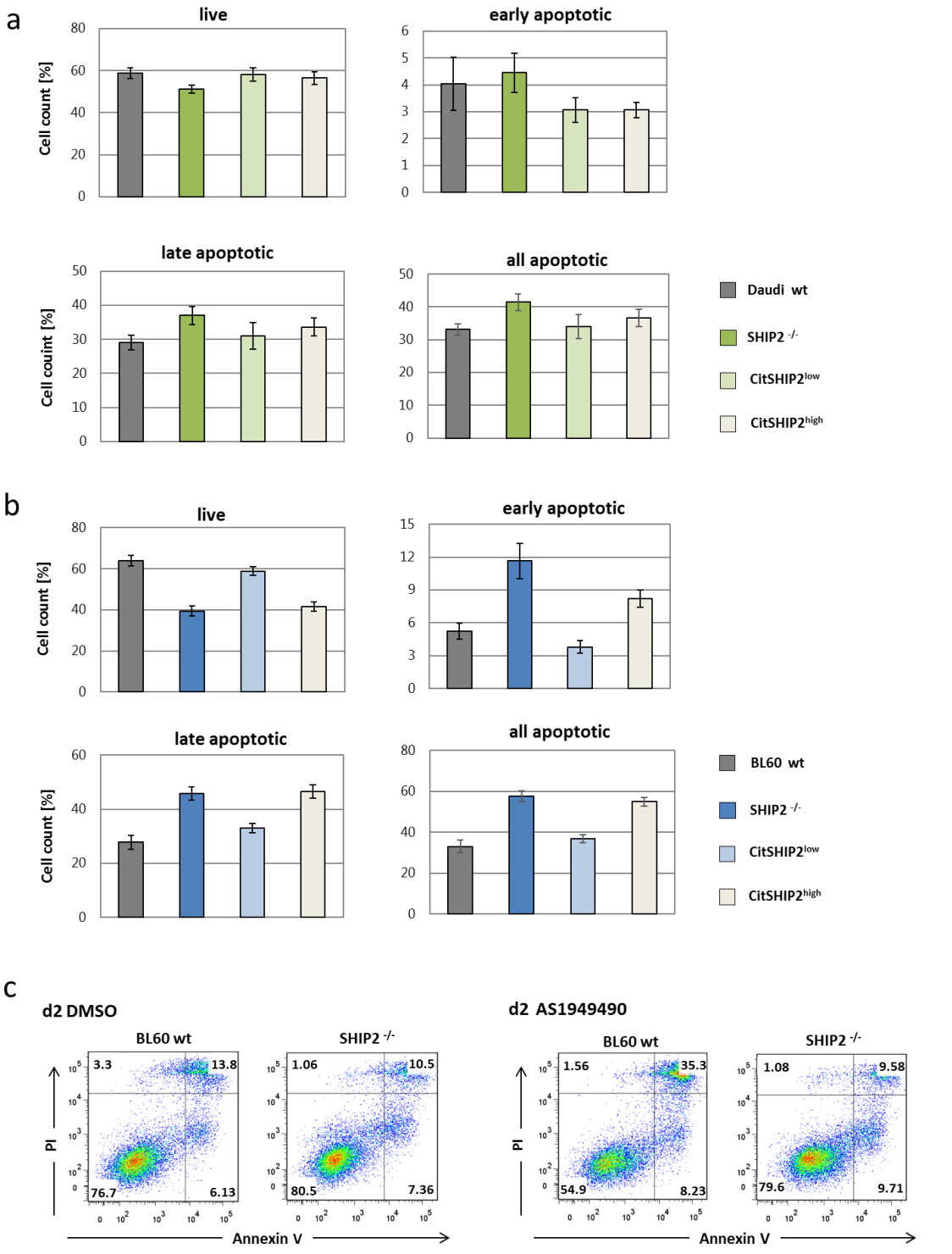


**Figure 33: Loss of SHIP2 induced apoptosis in BL cell lines.**
Daudi and BL60 parental (wt, grey), SHIP2-deficient (*SHIP2*$^{-/-}$, green or blue, respectively and reconstituted cells (CitSHIP2$^{low}$ (light green or light blue, respectively) & CitSHIP2$^{high}$ (beige)) were cultured in 1% FCS medium and analyzed by flow cytometry at d3 using APC-tagged Annexin V and PI. For analysis, cell populations were distinguished into live (Annexin V$^-$/PI$^-$), early apoptotic (Annexin V$^+$/PI$^-$), late apoptotic (Annexin V$^+$/PI$^+$) and all apoptotic (Annexin V$^+$) cells. (a) Analysis of apoptosis induction upon loss of SHIP2 in Daudi cells. (b) Apoptosis assay for SHIP2 deficiency in BL60 cells. Data represent means of five experiments (BL60) or represent means of four experiments performed in duplicates (Daudi). Error bars represent SD. (c) Representative apoptosis assay of BL60 wt and *SHIP2*$^{-/-}$ cells upon treatment with 5 µM AS1949490 or DMSO in 1% FCS medium for two days.

### 3.3.4 Analysis of tonic BCR signaling pathways in SHIP2-deficient cells

In the previous proliferation and apoptosis assays, I could show that both loss of SHIP2 or inhibition of its phosphatase activity led to apoptosis in BL cell lines. To elucidate the underlying signaling pathways, I aimed to decipher differences in phosphorylation events by analyzing the phospho-proteome of SHIP2-deficient compared to Daudi wt cells by quantitative mass-spectrometry (MS). To this end, I used the stable isotope labeling with amino acids in cell culture (SILAC) approach. For SILAC-labeling, SHIP2-deficient cells were grown in media containing normal (light) amino acids, while Daudi wt cells were cultured in media containing heavy isotope amino acids. If heavy isotope amino acids are incorporated during protein synthesis, the overall molecular mass of the protein increases. By mixing light and heavy labeled samples in a 1:1 ratio, this mass-shift can be used to distinguish the relative intensities of both the phosphorylated or un-phosphorylated peptide in the MS spectra (Zhang & Neubert 2009; Mann 2006). To ensure complete incorporation of labeled amino acids, cells were cultured at a similar density in light (K0/R0) or heavy (K8/R10) medium for 7 days before lysates were prepared. Samples were sent for MS analysis to the DKTK Proteomics Core Facility, University Hospital Frankfurt. There, samples were separated by size via SDS-PAGE and processed for liquid chromatography MS (LC-MS)/MS analysis as described in Corso et al. 2016.

In the scatter plot, log(2) converted relative abundance (H/L ratio) of differentially phosphorylated proteins was plotted against the -log(10) converted t-test p value (Figure 34). Phosphorylated proteins with a log(2) converted H/L ratio of >2 were considered to be specifically enriched in Daudi wt cells, while proteins with a log(2) H/L ratio of <-2 were considered to be enriched in SHIP2-deficient cells (Table 20). In Daudi wt cells, phosphorylation of transcription factors such as the TATA element modulatory factor (TMF1) and Transcription elongation factor A like 3 (TCEAL3) were enhanced. While not much is known about TCEAL3, TMF1 is described to mediate STAT3 degradation, thereby omitting its function as transcription activator (Perry et al. 2004). Also, increased phosphorylation of Nuclear nutoantigenic sperm protein (NASP) was detected. Knockdown of the testicular form of NASP, which is expressed in cancer cells, was previously shown to cause G1 phase arrest through ERK/MAPK pathway signaling (Fang et al. 2015).

Additionally, the Mitogen-activated protein kinase kinase kinase 2 (MAP3K2) was identified to be phosphorylated at S153. MAP3K2 regulates JNK and ERK5 signaling pathways by phosphorylation and subsequent activation of MAP2K7 and MAP2K5, respectively (Cheng, et al., 2000; Zhou et al., 1995).

**Table 23: Overview phospho-proteome analysis of Daudi wt and SHIP2-deficient cells.**
Daudi wt cells were cultured in heavy (K8/R10) SILAC medium while Daudi SHIP2-deficient cells (*SHIP2*$^{-/-}$) were grown in light SILAC medium (K0/R0). Cells were lysed and subjected for global phospho-proteome analysis by quantitative mass-spectrometry. Phosphorylation of proteins of with a log(2) H/L ratio >2 were considered to be enriched in Daudi wt cells, with a log(2) H/L ratio <-2 enriched in SHIP2-deficient cells.

| Protein | Gene | p-sites | Mean log2 H/L |
|---|---|---|---|
| **Transcriptional Regulators** | | | |
| TATA element modulatory factor | TMF1 | S344 | 5,16 |
| Transcription elongation factor A protein-like 3 | TCEAL3 | S121 | 2,97 |
| Transcription elongation factor A protein-like 3 | TCEAL3 | S65 | 2,33 |
| Leucine-rich repeat flightless-interacting protein 1 | LRRFIP1 | S714 | 2,25 |
| Serine/arginine repetitive matrix protein 2 | SRRM2 | T1043 | -2,61 |
| **Membrane proteins** | | | |
| CD44 antigen | CD44 | S330 | 3,32 |
| Solute carrier family 26 member 6 | SLC26A6 | S752 | 2,33 |
| Protein unc-79 homolog | UNC79 | S1479 | -3,38 |
| **Cell cycle & Proliferation** | | | |
| Nuclear autoantigenic sperm protein | NASP | S497 | 3,03 |
| Mitogen-activated protein kinase kinase kinase 2 | MAP3K2 | S153 | 2,31 |

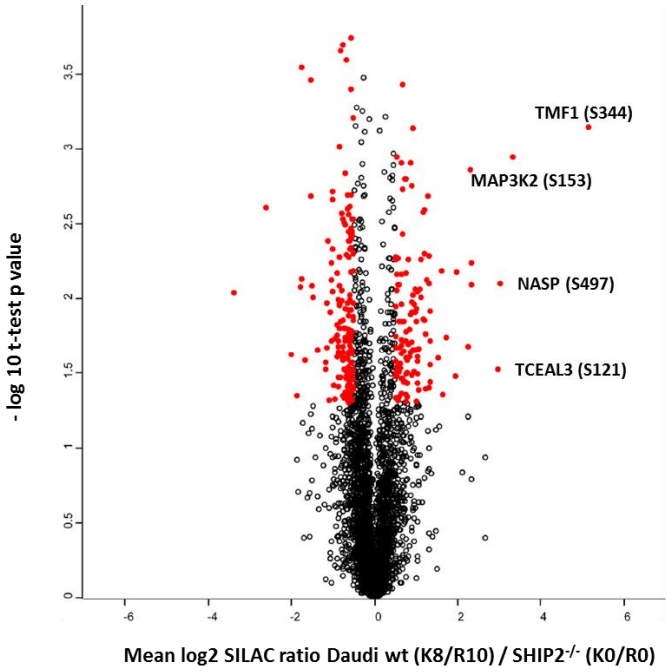


**Figure 34: Analysis of the phospho-proteome of Daudi wt and SHIP2-deficient cells.**
Daudi wt cells were cultured in heavy (K8/R10) SILAC medium while Daudi SHIP2-deficient cells (*SHIP2*$^{-/-}$) were grown in light SILAC medium (K0/R0). Cells were lysed and subjected for analysis of the global phospho-proteome by quantitative mass-spectrometry. For the scatter plot, the log(2) converted heavy (K8/R10)/light (K0/R0) ratio was plotted against the -log(10) converted t-test p value. Phosphorylation of proteins of with a log(2) H/L ratio >2 were considered to be enriched in Daudi wt cells.

Notably, this phospho-proteome analysis represents a single experiment and hence is somewhat preliminary. Further changes might be identified in additional analyses for which samples have been prepared but mass-spectrometry was not yet completed within the time frame of this thesis. Hence, I aimed at the biochemical analysis of tonic BCR signaling.

Based on my findings that SHIP2 regulates the PI3K pathway in activated BCR signaling, I assessed the role of SHIP2 in tonic activation of the PI3K pathway in the generated BL cell lines. I prepared cellular lysates of resting wt, SHIP2-deficient and CitSHIP2-expressing Daudi and BL60 cells, respectively, and compared different levels of phosphorylation by Western Blot analysis using phospho-specific antibodies.

I started by analyzing the phosphorylation of p85, the regulatory subunit of PI3K. In Daudi SHIP2-deficient cells, the tonic phosphorylation of p85 was decreased, which was partially reverted in CitSHIP2$^{low}$-expressing cells (Figure 35 a). In contrast, in BL60 SHIP2-deficient cells and CitSHIP2$^{high}$-expressing cells, phosphorylation of p85 was increased compared to parental and CitSHIP2$^{low}$-expressing cells (Figure 35 b).
Similar to SHIP2, the phosphatase PTEN can decrease the pool of PI(3,4,5)$P_3$ and is therefore described to negatively regulate PI3K signaling. I tested for phosphorylation of PTEN at S380/T382/383 which is described to lead to loss of its phosphatase activity and activation of the PI3K pathway (Patsoukis et al. 2013; Vazquez et al. 2000). While no changes in phosphorylation of PTEN were detected in Daudi-derived cellular lysates, BL60 SHIP2-deficient and CitSHIP2$^{high}$-expressing cells displayed a stronger phosphorylation compared to BL60 wt and CitSHIP2$^{low}$-expressing cells (Figure 35 c & d).

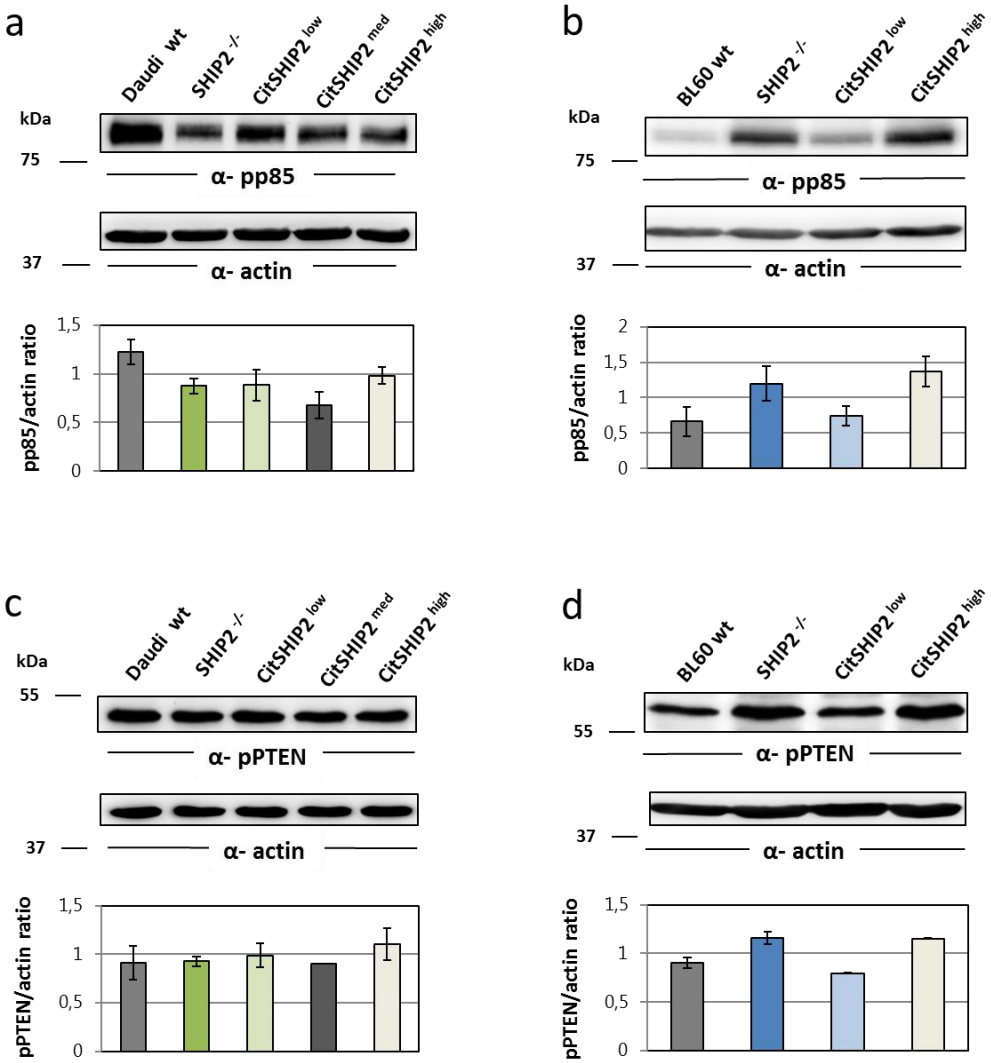


**Figure 35: Analysis of proximal tonic BCR signaling upon loss of SHIP2.**
Lysates of Daudi wild-type (wt, grey), SHIP2-deficient (*SHIP2*$^{-/-}$, green), CitSHIP2$^{low}$ (light green), CitSHIP2$^{med}$ (dark grey) and CitSHIP2$^{high}$ cells (beige) (a & c) as well as BL60 wt (grey), SHIP2-deficient (*SHIP2*$^{-/-}$, blue), CitSHIP2$^{low}$ (light blue) and CitSHIP2$^{high}$ cells (beige) (b & d) were prepared and evaluated by Western Blot analysis by probing with (a & b) phospho-specific α-p85 and (c & d) phospho-specific α-PTEN antibodies. Membranes were re-probed with α-actin for loading control. For each protein analyzed, exemplary immunoblots are shown (a-d, upper panels). Standard protein molecular masses are indicated in kDa. Ratios of signal intensities of α-pp85 and α-pPTEN to that of α-actin (a-d, lower panels) were calculated and depicted as bar diagrams as the means + SD of two (Daudi pPTEN) or three independent experiments (others).

Downstream of PI3K activation, AKT is phosphorylated at T308 and S473 to be fully activated. By probing blots with a phospho-specific-α-AKT (S473) antibody, samples of both SHIP2-deficient cell lines showed an increase in AKT phosphorylation, although to a different extent (Figure 36 a & b). The phosphorylation of AKT in BL60 SHIP2-deficient cells was almost doubled compared to BL60 wt and CitSHIP2$^{low}$-expressing cells. CitSHIP2$^{high}$-expressing cells could reduce AKT phosphorylation to some extent, although not to a comparable level as seen in BL60 and CitSHIP2$^{low}$-expressing cells. In contrast, in Daudi SHIP2-deficient cells, the increase in AKT phosphorylation was not as pronounced as seen in BL60 cells. However, with increasing expression levels of CitSHIP2, the effect could be fully restored, thereby suggesting a concentration-dependent effect of SHIP2. FOXO1 is phosphorylated at T24 by AKT, which retains FOXO1 in the cytoplasm. In line with AKT activation, phosphorylation of FOXO1 was increased in both Daudi and BL60 SHIP2-deficient cells (Figure 36 c & d). In BL60 cells, only the CitSHIP2$^{low}$-expressing but not CitSHIP2$^{high}$- expressing cells showed FOXO1 phosphorylation comparable to wt cells. In Daudi cells, loss of SHIP2 also led to increased FOXO1 phosphorylation, which could be restored by expression of CitSHIP2. In summary, SHIP2 is a negative regulator of the AKT signaling also in the context of tonic BCR signaling.

Since an increased AKT activity in absence of SHIP2 does not explain its role in apoptosis and given the fact that the phospho-proteome analysis implicated a role of SHIP2 in MAPK signaling in a tonic signaling state, I analyzed the tonic MAPK activity in the generated cell lines by Western Blot analysis as described above.

In SHIP2-deficient and CitSHIP2$^{high}$-reconstituted BL60 cells, MAPK ERK phosphorylation was elevated compared to BL60 wt and CitSHIP2$^{low}$-expressing cells (Figure 37 b). In SHIP2-deficient Daudi cells and their CitSHIP2-expressing sub-clones, a reduced phosphorylation of ERK was identified compared to Daudi wt cells, indicating a clonal effect (Figure 37 a). Similar to ERK, phosphorylation of the MAPK p38 was decreased in SHIP2-deficient Daudi cells and could not be restored by CitSHIP2 expression (Figure 37 c). In BL60 cells, levels of p38 phosphorylation remained similar among cell lines (Figure 37 d). Analysis for JNK-activation revealed that SHIP2-deficiency in Daudi and BL60 cells causes a marked reduction of JNK phosphorylation that was found to be restored in CitSHIP2$^{low}$-expressing cells (Figure 36 e & f), indicating a concentration dependent effect of SHIP2 in JNK phosphorylation.

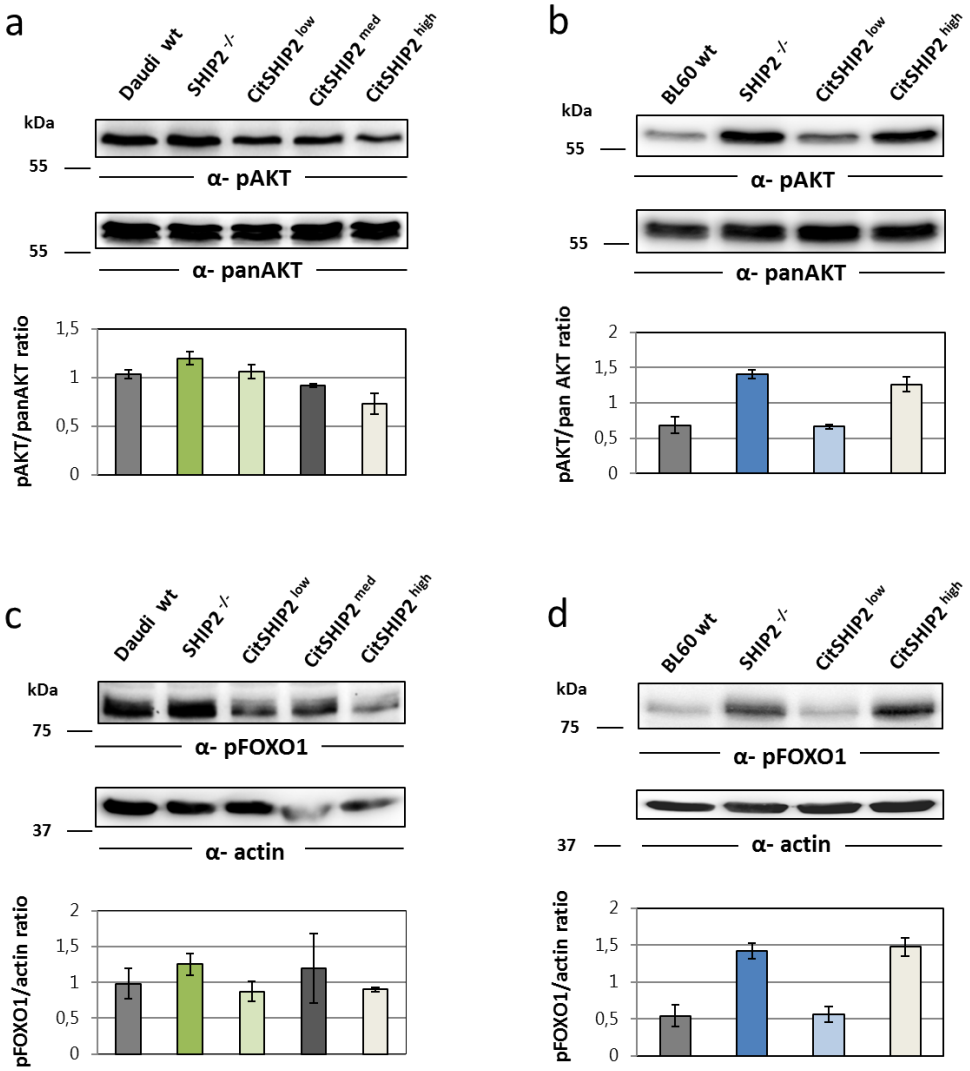


**Figure 36: Analysis of tonic AKT signaling upon loss of SHIP2.**
Lysates of Daudi wild-type (wt, grey), SHIP2-deficient (*SHIP2*$^{-/-}$, green), CitSHIP2$^{low}$ (light green), CitSHIP2$^{med}$ (dark grey) and CitSHIP2$^{high}$ cells (beige) (a & c) as well as BL60 wt (grey), SHIP2-deficient (*SHIP2*$^{-/-}$, blue), CitSHIP2$^{low}$ (light blue) and CitSHIP2$^{high}$ cells (beige) (b & d) were prepared and analyzed by Western Blot analysis by probing with (a & b) phospho-specific α-AKT and (c & d) phospho-specific α-FOXO1 antibodies. Membranes were re-probed with α-panAKT (a & b) and α-actin (c & d) for loading control. For each protein analyzed, exemplary immunoblots are shown (a-d, upper panels). Standard protein molecular masses are indicated in kDa. Ratios of signal intensities of α-pAKT and α-pFOXO1 to that of α-panAKT or α-actin, respectively (a-d, lower panels) were calculated and depicted in bar diagrams as the means + SD of three independent experiments.

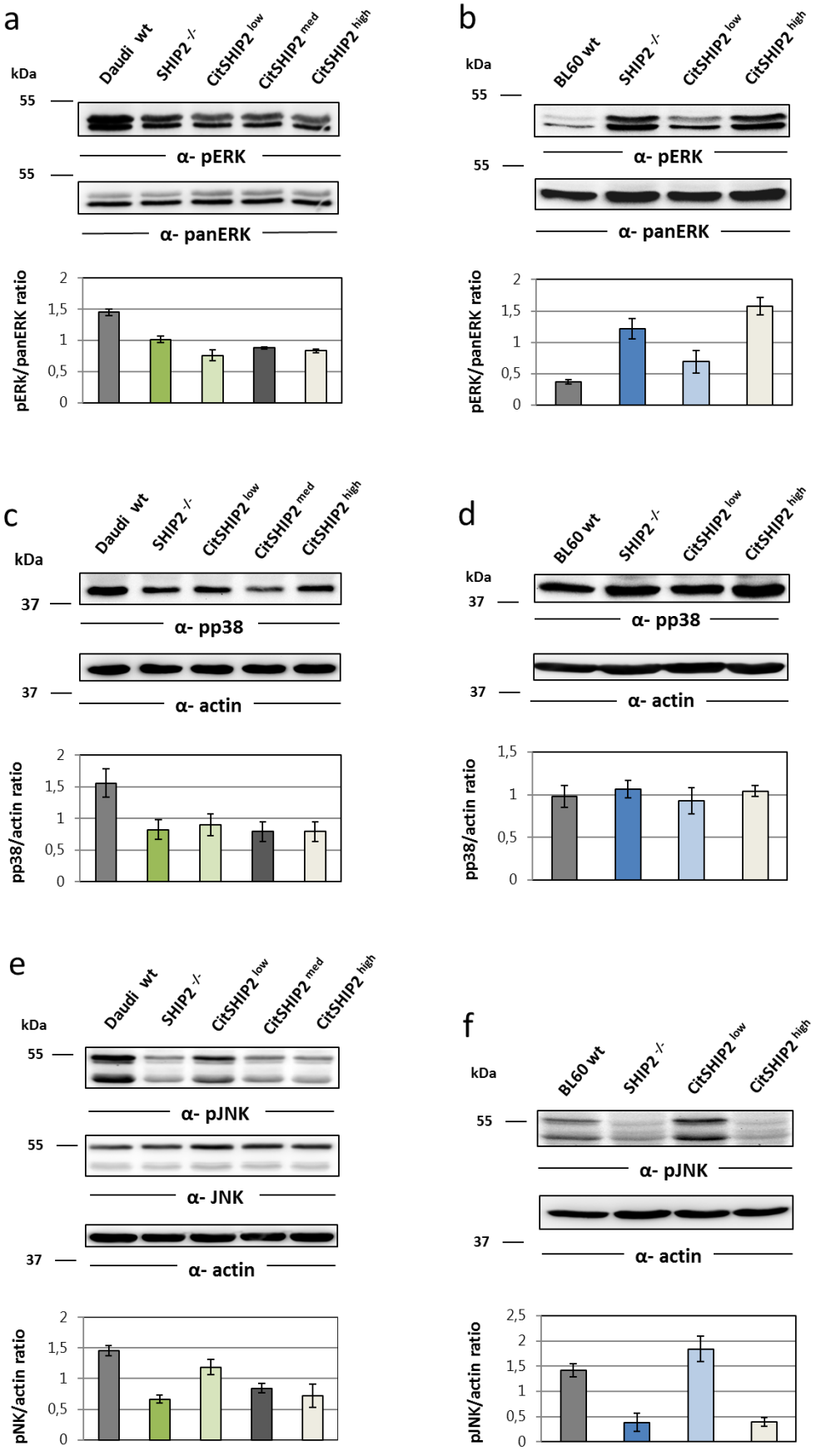


**Figure 37**: **Analysis of tonic MAPK signaling upon loss of SHIP2.** *For legend see next page*.

**Figure 37 (*previous page*): Analysis of tonic MAPK signaling upon loss of SHIP2.**
Lysates of Daudi wild-type (wt, grey), SHIP2-deficient (*SHIP2*$^{-/-}$, green), CitSHIP2$^{low}$ (light green), CitSHIP2$^{med}$ (dark grey) and CitSHIP2$^{high}$ cells (beige) (a & c) as well as BL60 wt (grey), SHIP2-deficient (*SHIP2*$^{-/-}$, blue), CitSHIP2$^{low}$ (light blue) and CitSHIP2$^{high}$ cells (beige) (b & d) were prepared and analyzed by Western Blot analysis by probing with (a & b) phospho-specific α-ERK, (c & d) phospho-specific α-p38 and (e & f) phospho-specific α-JNK antibodies. Membranes were re-probed with α-panERK (a & b), α-JNK (e) and α-actin (c, d, e & f) for loading control. For each protein analyzed, exemplary immunoblots are shown (a-f, upper panels). Standard protein molecular masses are indicated in kDa. Ratios of signal intensities of α-pERK, α-pp38 and α-pJNK to that of α-panERK (a&b) or α-actin (c, d, e & f), respectively, (a-f, lower panels) were calculated and depicted in bar diagrams as the means + SD of three independent experiments.

To confirm these results, I additionally performed intracellular staining using an α-phospho-JNK (T183/Y185) Alexa Fluor® 647 - tagged antibody. For this analysis, I mixed Daudi SHIP2-deficient cells with Daudi CitSHIP2$^{med}$-expressing and BL60 SHIP2-deficient with BL60 CitSHIP2$^{high}$-expressing cells. This allowed gating for a Citrine-negative population of SHIP2-deficient cells and a Citrine-positive population of reconstituted cells. Thereby, I could mitigate effects potentially caused by sample processing. For a positive control, I used BCR-stimulated BL60 wt cells. As shown in Figure 38 a, BCR-engagement led to a slight shift in the phospho-JNK signal. Analysis of JNK phosphorylation in the mixed Daudi sample revealed a mildly enhanced phosphorylation of JNK in the presence of CitSHIP2 compared to SHIP2-deficient cells (Figure 38 b, upper panel). This observation was confirmed by analyzing the mixed sample of BL60 SHIP2-deficient and CitSHIP2$^{high}$-expressing cells (Figure 38 b, lower panel). The observed shift of the signal in CitSHIP2-expressing cells was similar to that caused by BCR engagement described above. Hence, flow cytometric analysis confirmed a SHIP2-dependent activation of JNK in Daudi and BL60 cell lines. In summary, while the impact of SHIP2 on the tonic activation of ERK and p38 remains unclear, these data revealed a marked positive regulatory role of SHIP2 on the tonic activation of JNK in BL cell lines.

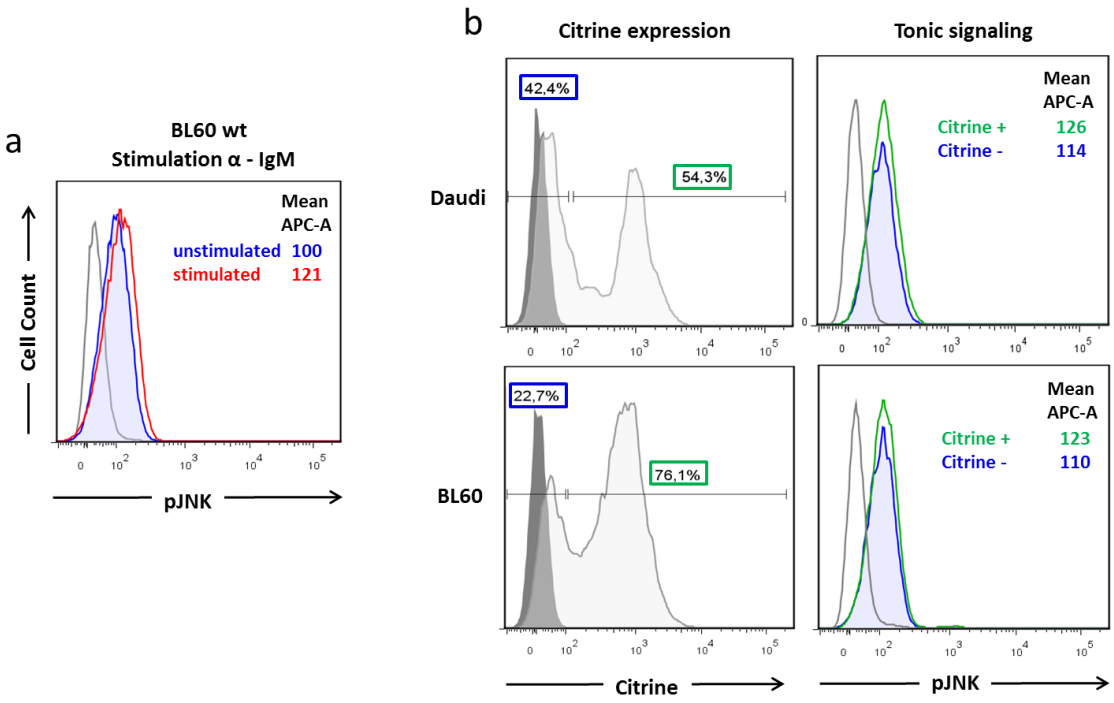


**Figure 38**: **Intracellular staining for JNK phosphorylation.**
For flow cytometric analysis of JNK phosphorylation, BL cell lines were fixed, permeabilized and stained with α-pJNK (T183/Y185) Alexa Fluor® 647 antibody. (a) BL60 wild-type (wt) cells were either stimulated with 10 µg/ml F(ab')$_2$ α-IgM (red) or left unstimulated (blue). Unstained cells (grey) served as control. SHIP2-deficient Daudi (blue, Citrine$^-$) and CitSHIP2$^{med}$ (green, Citrine$^+$) cells (b, upper panel) as well as SHIP2-deficient BL60 (blue, Citrine$^-$) and CitSHIP2$^{high}$ (green, Citrine$^+$) cells (b, lower panel) were mixed to be analyzed in the same sample. Plots show representative results of two independent experiments.

To further confirm these data, I included the SHIP2 inhibitor AS1949490 for the analysis of tonic signaling pathways. To this end, I treated Daudi wt, SHIP2-deficient and CitSHIP2$^{low}$-expressing cells with 5 µM SHIP2 inhibitor AS1949490 or DMSO for 30 min before cell lysis, subjected lysates to Western Blot analysis and probed blots with phospho-specific antibodies.

Phosphorylation of the PI3K subunit p85 was not changed upon inhibitor treatment in Daudi wt cells, while both for Daudi SHIP2-deficient and CitSHIP2$^{low}$-expressing cells phosphorylation of p85 was decreased after inhibitor treatment (Figure 39 a). By probing with phospho-specific PTEN antibody, I found a small increase in PTEN phosphorylation in all Daudi cell lines (Figure 39 b). Phosphorylation of PTEN is associated with activation of the PI3K pathway. Downstream of PI3K activation, AKT was increasingly phosphorylated upon SHIP2 inhibitor treatment in all Daudi cell lines (Figure 39 c), while FOXO1 phosphorylation was only positively affected in Daudi wt cells and in CitSHIP2$^{low}$-expressing cells (Figure 39 d). In summary, signaling via the PI3K-AKT pathway in Daudi cells was increased upon SHIP2 inhibitor treatment.

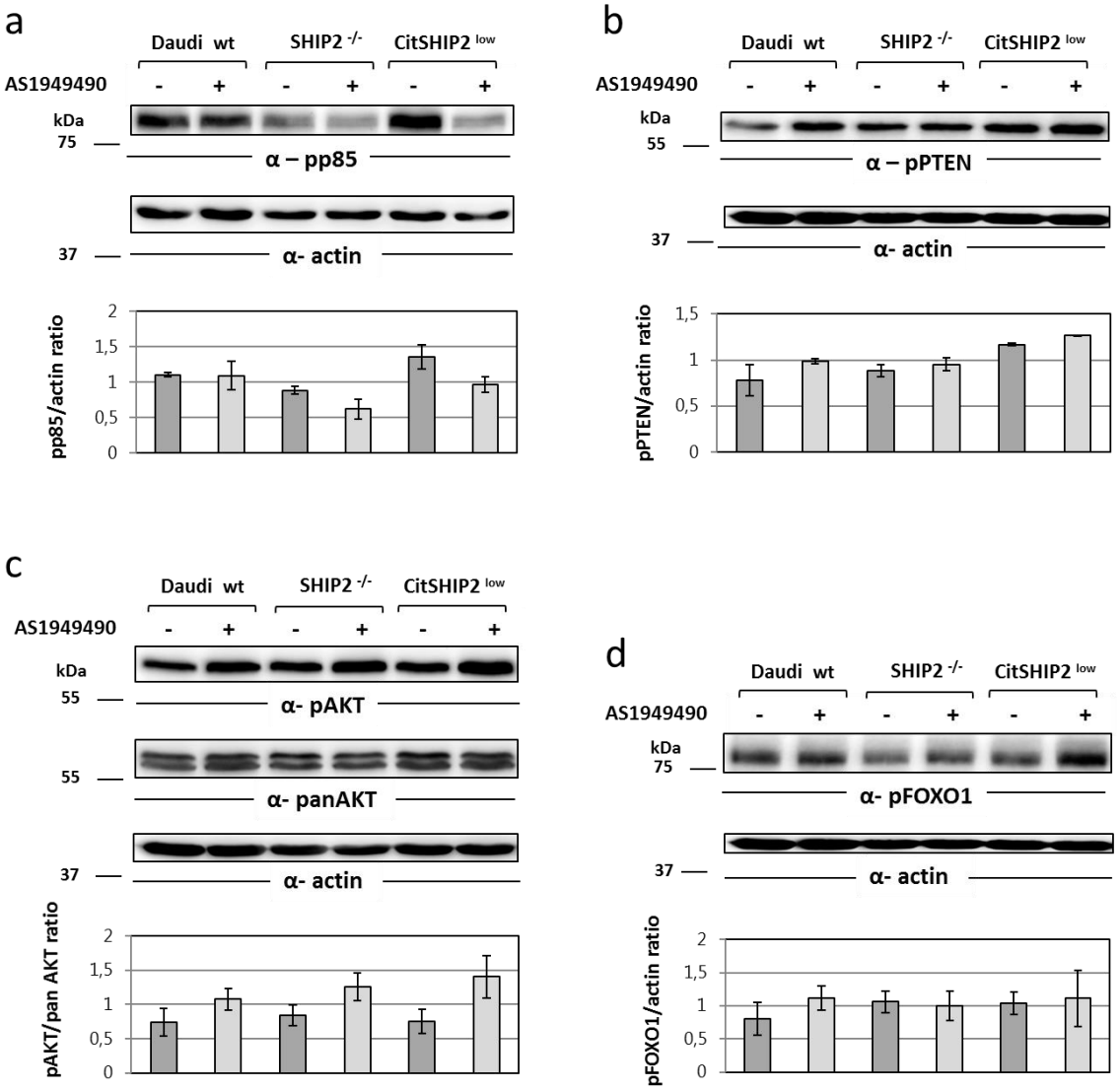


**Figure 39**: **SHIP2 inhibition affects PI3K signaling in Daudi cells.**
Daudi wild-type (wt), SHIP2-deficient (*SHIP2*$^{-/-}$) and CitSHIP2$^{low}$-expressing cells were treated with 5 µM AS1949490 (+, light grey) or DMSO (-, dark grey) for 30 min prior to cell lysis. Lysates were subjected to Western Blot analysis and blots were decorated with (a) phospho-specific α-p85, (b) phospho-specific α-PTEN, (c) phospho-specific α-AKT and (d) phospho-specific α-FOXO1 antibodies. Treatment with α-actin and α-panAKT antibodies was performed for loading control. For each protein analyzed, exemplary immunoblots are shown (a-d, upper panels). Standard protein molecular masses are indicated in kDa. Ratios of signal intensities of α-p85, α-pPTEN, α-pAKT and α-pFOXO1 to that of α-panAKT (c) or α-actin (a, b & d), respectively, (a-d) lower panels) were calculated and depicted as bar diagrams as the means + SD of two (pPTEN), four (pp85) or five (pAKT, pFOXO1) independent experiments.

To test whether the SHIP2 inhibitor could also mimic the effect of loss of SHIP2 concerning MAPK signaling, I probed Western Blots with phospho-specific α-ERK antibody. Although the effect was not as pronounced in Daudi wt cells, SHIP2-deficient and CitSHIP2$^{low}$-expressing cells showed an increase in ERK phosphorylation upon inhibitor treatment in comparison to DMSO treated cells (Figure 40 a). In contrast, phosphorylation of MAPK p38 was mildly reduced in all cell lines when

treated with the inhibitor (Figure 40 b). Also, phosphorylation of MAPK JNK was affected by SHIP2 inhibitor treatment. Upon SHIP2 inhibition, all Daudi cell lines showed a decrease in JNK phosphorylation, however, the effect was more prominent in Daudi wt and CitSHIP2$^{low}$-expressing cells (Figure 40 c). In summary, SHIP2 inhibitor AS1949490 was able to induce a downregulation of phosphorylation of MAPK p38 and JNK, whereas ERK phosphorylation was increased upon SHIP2 inhibitor treatment.

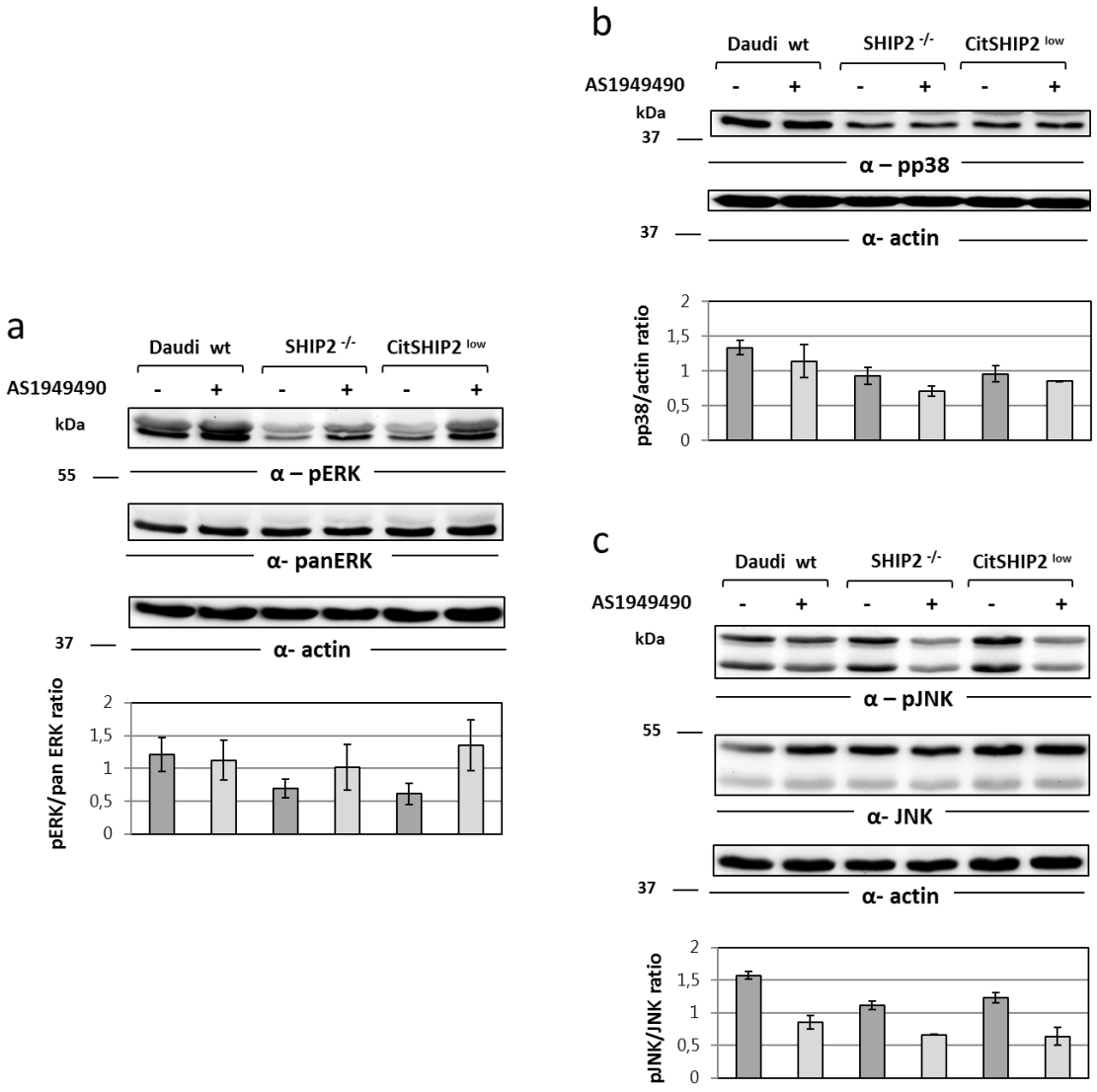


**Figure 40**: **SHIP2 inhibition affects MAPK signaling in Daudi cells.**
Daudi wild-type (wt), SHIP2-deficient (*SHIP2*$^{-/-}$) and CitSHIP2$^{low}$-expressing cells were treated with 5 µM AS1949490 (+, light grey) or DMSO (-, dark grey) for 30 min prior to cell lysis. Lysates were subjected to Western Blot analysis and blots were decorated with (a) phospho-specific α-ERK, (b) phospho-specific α-p38 and (c) phospho-specific α-JNK antibodies. Treatment with α-actin and α-panERK and α-JNK antibodies was performed for loading control. For each protein analyzed, exemplary immunoblots are shown (a-d, upper panels). Standard protein molecular masses are indicated in kDa. Ratios of signal intensities of α-pERK, α-pp38 and α-pJNK to that of α-panERK (a), α-actin (b) and α-JNK (c) respectively, (a-c) lower panels) were calculated and depicted as bar diagrams as the means + SD of two (pp38), three (pJNK) or five (pERK) independent experiments.

Next, I aimed to verify if the main effectors found to be differentially regulated upon SHIP2 inhibition in Daudi cells are also similarly regulated in BL60 cells. Therefore, I used BL60 wt, SHIP2-deficient, CitSHIP2$^{low}$- and CitSHIP2$^{high}$-expressing cells and prepared lysates as described above. Lysates were subjected to Western Blot analysis and blots were probed with phospho-specific antibodies against key effector proteins AKT, ERK and JNK. Similar to Daudi cells, AKT phosphorylation was increased in all BL60 cell lines upon SHIP2 inhibitor treatment (Figure 41 a), as well as ERK phosphorylation (Figure 41 b). However, JNK phosphorylation was not changed upon SHIP2 inhibitor treatment (Figure 41 c). In summary, while phosphorylation of AKT and ERK was similarly regulated in Daudi and BL60 cells, JNK phosphorylation in BL60 cells was not affected by the SHIP2 inhibitor in contrast to Daudi cells. This indicates that JNK signaling via SHIP2 might be differentially regulated in Daudi and BL60 cells. In BL60 cells, JNK phosphorylation is more likely dependent on the adaptor function rather than the phosphatase activity of SHIP2, which is more relevant for JNK phosphorylation in Daudi cells.

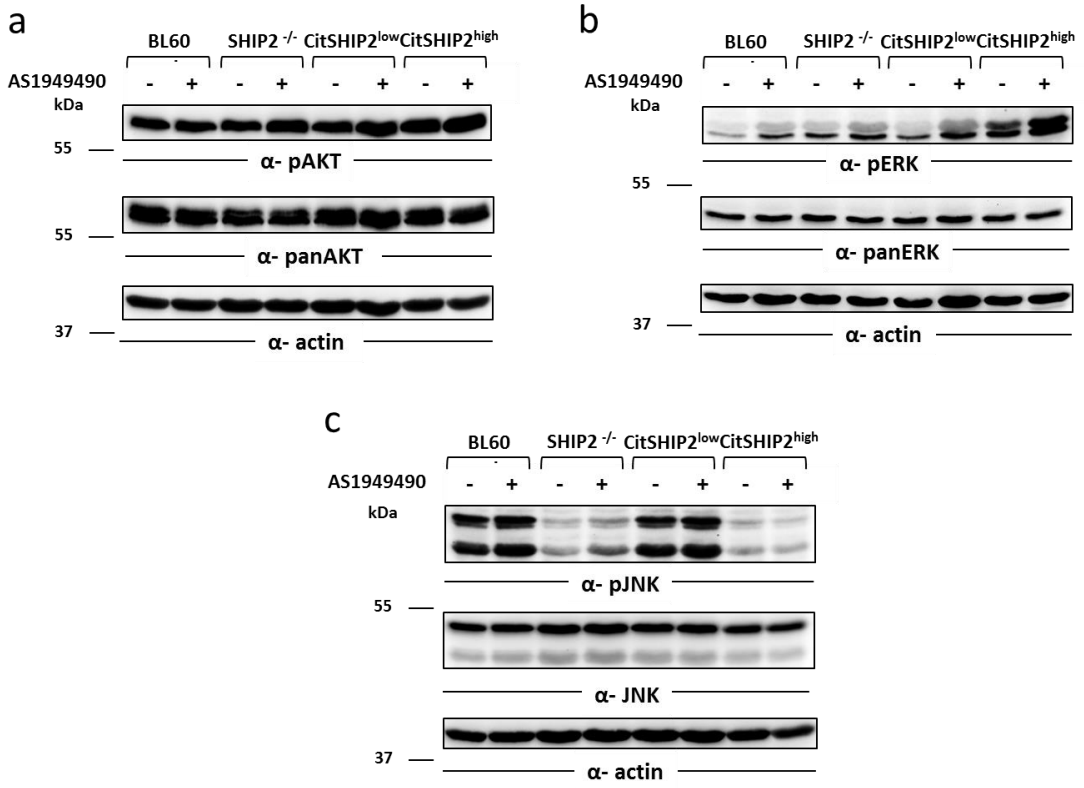


**Figure 41: SHIP2 inhibition affects signaling in BL60 cells.**
BL60 wild-type (wt), SHIP2-deficient (*SHIP2*$^{-/-}$), CitSHIP2$^{low}$- and CitSHIP2$^{high}$-expressing cells were treated with 5 µM AS1949490 (+) or DMSO (-) for 30 min prior to cell lysis. Cellular lysates were subjected to Western Blot analysis and blots were decorated with (a) phospho-specific α-AKT (b) phospho-specific α-ERK and (c) phospho-specific α-JNK antibodies (upper panels). Treatment with antibodies detecting total protein levels (second panels) and α-actin (lower panels) served as controls. Standard protein molecular masses are indicated in kDa. Blots are representative of two independent experiments.

### 3.3.5 BCR-induced JNK signaling in SHIP2-deficient BL60 cells

Because the JNK phenotype in BL60 SHIP2-deficient cells was so pronounced and not regulated by the SHIP2 inhibitor, I wanted to elucidate if the JNK signaling pathway in BL60 could still be regulated by other means. To this end, I stimulated BL60 wt, SHIP2-deficicient, CitSHIP2$^{low}$- and CitSHIP2$^{high}$-expressing cells with 5 µg/ml F(ab')$_2$ α-IgM for 10 min to check for BCR-dependent JNK activation. As controls, I treated cells with pervanadate for 10 min to inhibit protein tyrosine phosphatases or left cells untreated. After treatment, cells were lysed and evaluated by Western Blot analysis using phospho-specific antibodies.

As a control for induction of BCR signal transduction events, phosphorylation of Syk and ERK was analyzed and found to be phosphorylated in a BCR-inducible manner (Figure 42). While Syk was also phosphorylated in pervanadate-treated cells, phosphatase inhibition was apparently not sufficient to induce phosphorylation further downstream of BCR signal transduction. The different efficiency in Syk and ERK phosphorylation among the different cell lines correlates with the differences in BCR surface expression described in 3.3.1. In addition, BCR-engagement led to a slight increase of JNK phosphorylation in BL60 wt cells which was even less in SHIP2-deficient or CitSHIP2$^{high}$-expressing cells, indicating a more general defect of JNK activation in these cells.

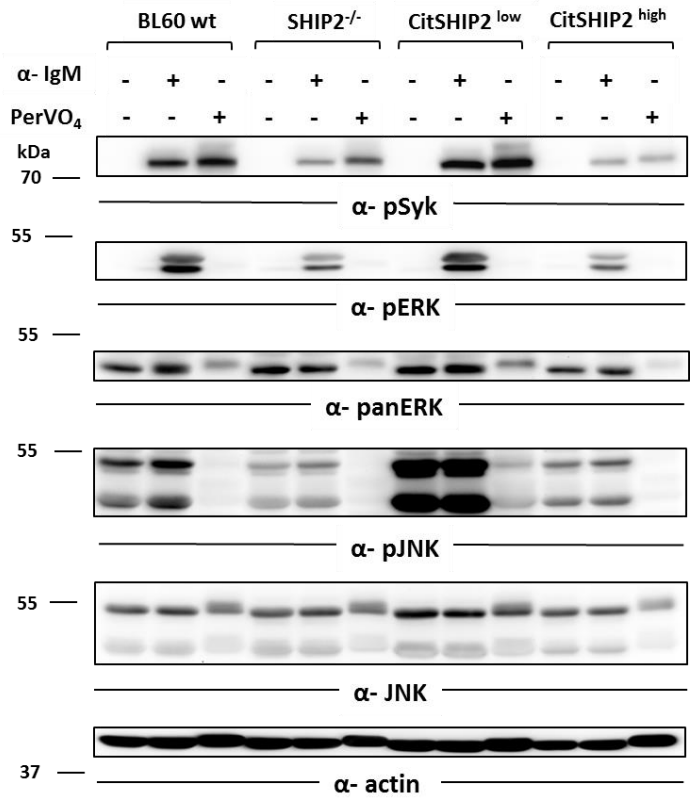


**Figure 42**: **JNK signaling is increased upon BCR stimulation in BL60 cells**. *For legend see next page.*

**Figure 42 (*previous page*): JNK signaling is increased upon BCR stimulation in BL60 cells.**
BL60 wt, SHIP2-deficient (SHIP2$^{-/-}$), CitSHIP2$^{low}$ - and CitSHIP2$^{high}$ - expressing cells were left untreated or were incubated with 5 µg/ml F(ab')$_2$ α-IgM or Pervanadate ($PerVO_4$) for 10 min prior to cell lysis. Lysates were subjected to Western Blot analysis and blots were decorated with phospho-specific antibodies for BCR effector proteins SyK (upper panel), ERK (second panel) and JNK (fourth panel). α-actin and antibodies detecting total levels of ER and JNK protein were used for loading control (lower panel and third as well as fifth panel, respectively). Standard protein molecular masses are indicated in kDa.

### 3.3.6 Tonic BCR signaling regulates SHIP2-dependent JNK activation in BL60 cells

Although I could show that BCR engagement can induce low levels of JNK activation, it remained unclear whether the effect of SHIP2 on JNK phosphorylation in resting cells was related to tonic BCR signaling. To address this, I generated cell lines that inducibly downregulate the BCR and hence abrogate tonic BCR signals. For this, I silenced gene expression of CD79A, which is needed for BCR surface expression, by using short hairpin RNA (shRNA) targeting CD79A. BL60 wt, SHIP2-deficient, CitSHIP2$^{low}$- and CitSHIP2$^{high}$-expressing cells were lentivirally transduced with a doxycycline-inducible shCD79A expression plasmid (LT3-GECIR shCD79a-1) and a control shRNA (shCtrl, LT3-GECIR shGL2) in a collaboration with Dr. Doebele, Department of Medicine II, Hematology & Oncology, University Hospital Frankfurt. Since both shRNA expression plasmids are also carrying a mCherry expression cassette, transduced cells could be analyzed for successful integration by flow cytometry. After transduction, approximately 60% of cells were positive for mCherry expression (data not shown). However, CitSHIP2$^{low}$-expressing cells were no longer positive for Citrine expression, therefore they were excluded from further analyses.

First, I aimed to check the function of the shRNAs. To this end, I seeded cell lines at a similar density in fresh medium and treated cells with 250 ng/ml doxycycline (Dox) for 48 h or left them untreated. To check for induction of shRNAs, cells were analyzed by flow cytometry by staining with APC-conjugated α-human IgM antibody (Figure 43 a). Upon induction with doxycycline (+ Dox), all cell lines carrying the shCD79A expression plasmid showed a reduction of IgM-BCR expression compared to untreated (- Dox) cells. Induction of control shRNA did not alter IgM-BCR expression levels (data not shown). To test whether JNK phosphorylation levels were altered upon knockdown of CD79A, I prepared lysates of + Dox and - Dox cells and performed Western Blot analysis testing for JNK phosphorylation (Figure 43 b). Upon treatment with doxycycline, phosphorylation of JNK was reduced in BL60 wt and CitSHIP2$^{high}$-expressing cells by 18% and 36%, respectively, when compared to their untreated counterparts. JNK phosphorylation was also decreased in SHIP2-deficient cells, however only by 6%. In summary, these results indicate that SHIP2-dependent JNK activation is influenced by tonic BCR signaling in BL60 cells.

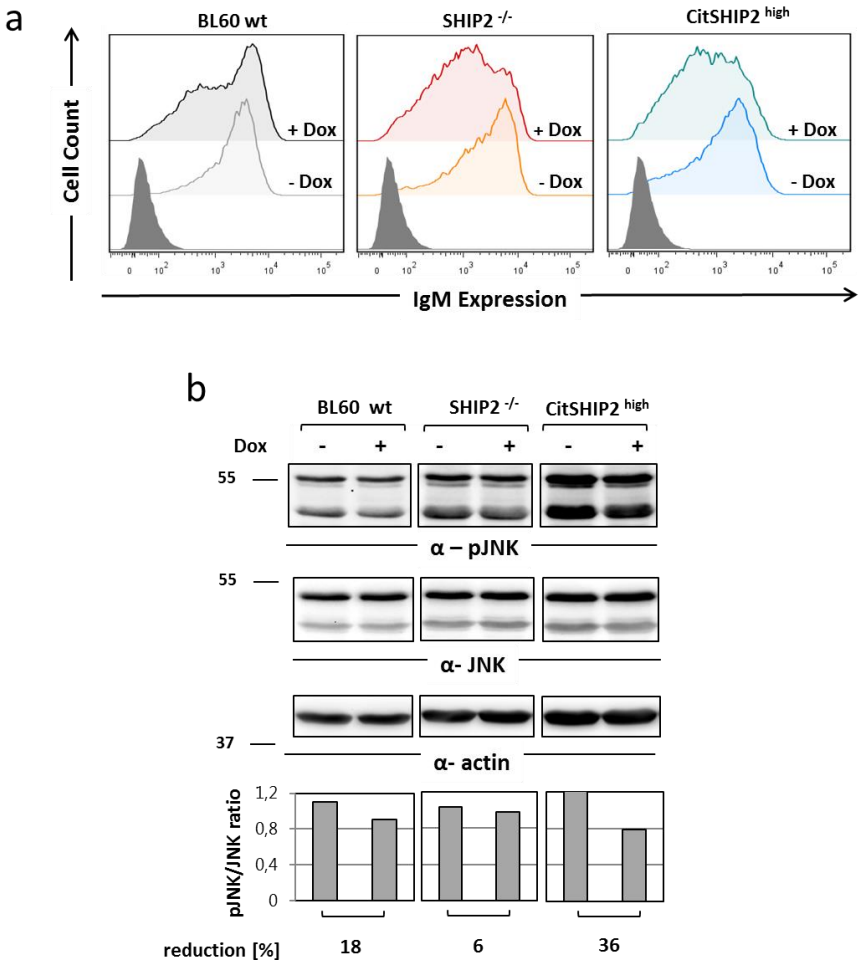


**Figure 43: SHIP2-dependent JNK activation is influenced by tonic BCR signaling in BL60 cells.**
BL60 wild-type (wt), SHIP2-deficient (*SHIP2*$^{-/-}$) and CitSHIP2$^{high}$-expressing cells were transduced with doxycycline-inducible plasmids encoding for shCD79A. (a) Cells were stained with APC-conjugated α-human IgM antibody and analyzed for IgM surface expression by flow cytometry when treated with (+) or without (-) 250 ng/ml doxycycline (Dox) for 48 h. (b) Following Dox treatment, wells were lysed and subjected to Western Blot analysis for JNK phosphorylation status using phospho-specific α-JNK antibody (upper panel). Re-probing with α-JNK (second panel) and α-actin (third panel) antibodies was used for loading control. Standard protein molecular masses are indicated in kDa. Ratios of signal intensities of α-pJNK to that of α-JNK were calculated and depicted as a bar diagram and reduction of signal intensities of untreated to treated cells was calculated (lower panel).

### 3.3.6 Establishing an inducible shCD79A system in Daudi cells

Similar to the approach described for the BL60 cell lines, I next assessed whether the identified SHIP2-dependent signaling processes are part of the tonic BCR signaling network in Daudi cells. For this purpose, Daudi wt, SHIP2-deficient and CitSHIP2$^{low}$-expressing cells were lentivirally transduced with the same shRNA expression plasmids as described above and tested for their functionality 48h after doxycycline induction. For testing, I used Daudi SHIP2-deficient and CitSHIP2$^{low}$-expressing cells both transduced either with constructs encoding for shCD79A or shCtrl and compared CD79A

expression levels by Western Blot analysis (Figure 44 a). In shCD79A transduced cell lines, doxycycline treatment led to reduced expression levels of CD79A compared to untreated cells, whereas shCtrl transduced cell lines were not affected by doxycycline. Transduced plasmids also carry a GFP-encoding cassette to check for sufficient induction by doxycycline. Re-probing of the membrane with α-GFP antibody confirmed doxycycline-induced GFP expression. Additionally, I stained all doxycycline-treated samples with APC-conjugated α-human IgM antibody and analyzed IgM surface expression levels by flow cytometry (Figure 44 b). Only in shCD79A transduced cells, doxycycline treatment decreased IgM-BCR expression levels, proving the validity of the experimental setup for further analyses.

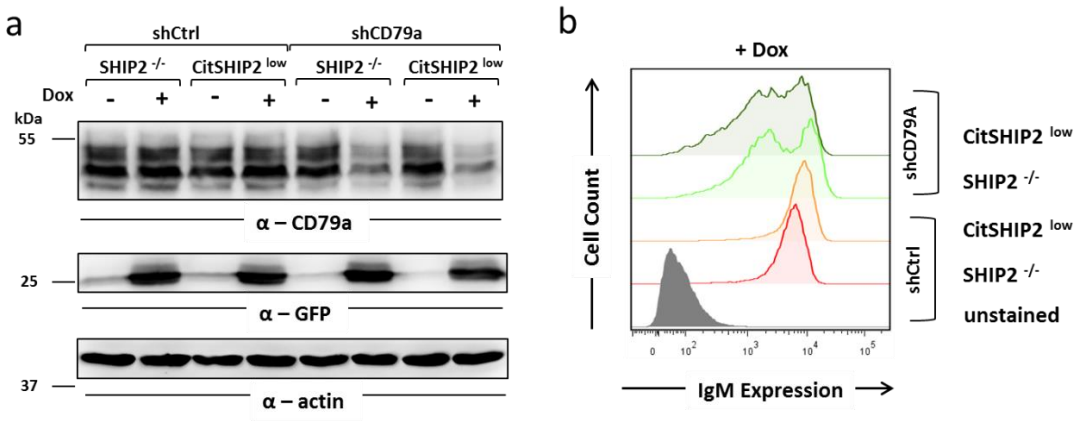


**Figure 44: shCD79A specifically decreases CD79A and IgM expression in Daudi cells.**
Daudi SHIP2-deficient (*SHIP2*$^{-/-}$) and CitSHIP2$^{low}$-expressing cells were transduced with constructs encoding doxycycline-inducible shCD79A or control (shCtrl) shRNAs and were induced with (+) 250 ng/ml doxycycline (Dox) for 48 h or left untreated (-). (a) Cells were then lysed and subjected to Western Blot analysis followed by probing for total protein expression of CD79A and GFP using α-CD79A (upper panel) and α-GFP antibodies (second panel), respectively. α-actin was used for loading control (lower panel). Standard protein molecular masses are indicated in kDa. (b) Following Dox-treatment, cells were stained with APC-conjugated α-human IgM antibody and analyzed for IgM surface expression by flow cytometry.

Next, I aimed to identify the optimal induction time to analyze shCD79A cells. Since shCD79A induction in Daudi cells had been proven to be toxic over the course of 10 days (Corso et al. 2016), I aimed for a sufficient reduction in IgM-BCR expression without affecting the viability of cells. I treated Daudi wt, SHIP2-deficient and CitSHIP2$^{low}$-expressing cells with 250 ng/ml doxycycline for 48 h or 72 h and analyzed IgM surface expression levels as described previously (Figure 45 a). Although all cell lines already showed reduction of IgM expression after 48h, IgM expression was further reduced after 72 h. Thus, untreated cells and cells treated with Dox for 72 h were lysed and subjected to Western Blot analysis. By probing with α-CD79a antibody, I could verify a decline of CD79A expression in Dox-treated cells (Figure 45 b), which correlated with GFP expression, thereby indicating the activity of the shRNA. Because knockdown CD79A is supposed to decrease tonic and

thereby PI3K signaling of the BCR, I additionally analyzed phosphorylation of PI3K subunit p85. Treatment with Dox enhanced p85 phosphorylation in all cell lines. (Figure 45 c). However, phosphorylation of AKT downstream of p85 was found to be reduced upon CD79A knockdown (Figure 44 d). In summary, CD79A knockdown was sufficiently induced after 72h and was able to decrease tonic PI3K signaling on the level of AKT phosphorylation.

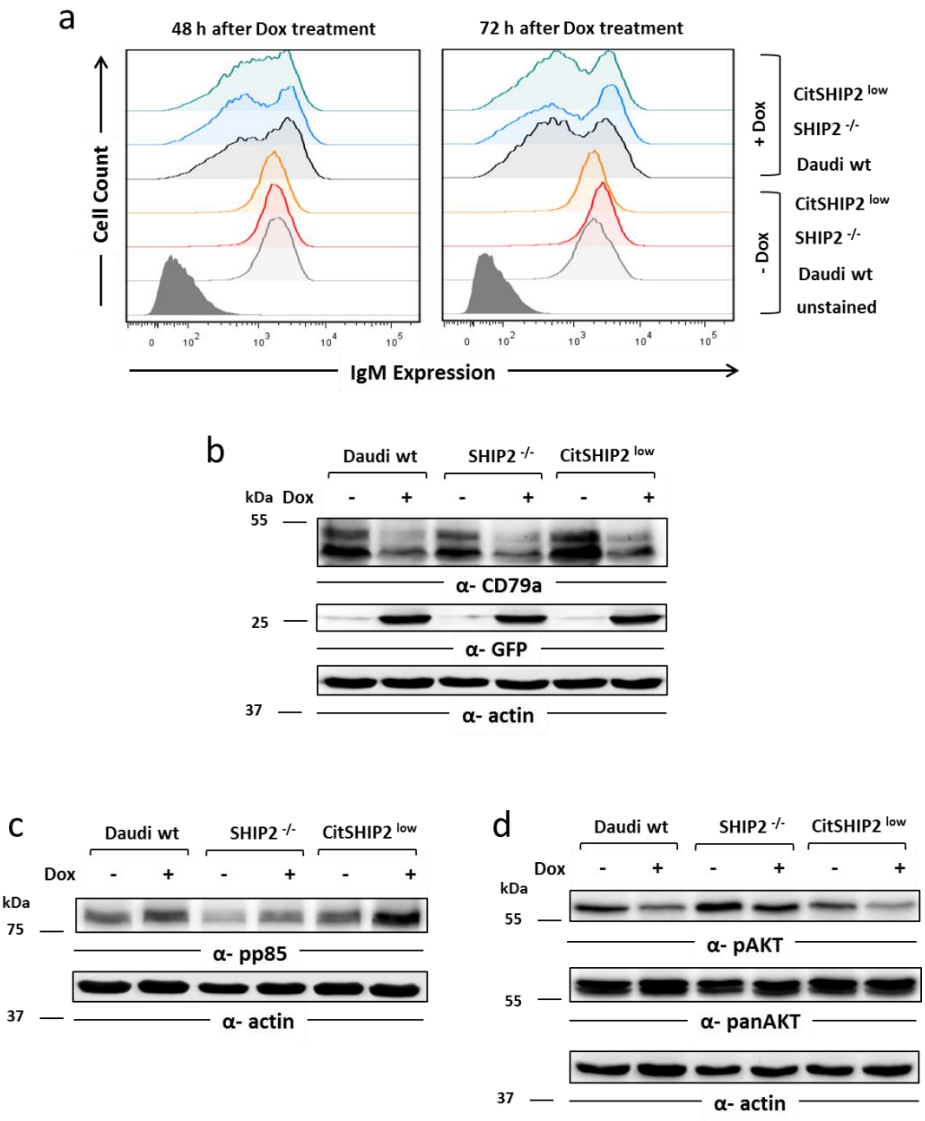


**Figure 45: shCD79A knockdown decreases IgM expression and AKT signaling in Daudi cells.**
Daudi wild-type (wt), SHIP2-deficient (*SHIP2*$^{-/-}$) and CitSHIP2$^{low}$-expressing cells were transduced with constructs encoding doxycycline-inducible shCD79A or control (shCtrl) shRNA and were induced with (+) 250 ng/ml doxycycline (Dox) for 48 h or 72 h or left untreated (-). (a) Cells were stained with APC-conjugated α-human IgM to test for IgM surface expression by flow cytometry. (b-d) 72 h after Dox induction, cells were lysed and subjected to Western Blot analysis. (b) Analysis for CD79A expression and Dox induction by probing with α-CD79A (upper panel) and α-GFP (second panel), respectively. Re-probing with α-actin (lower panel) for loading control. To test for PI3K-AKT pathway activation, blots were decorated with phospho-specific (c) α-p85 and (d) α-AKT antibodies (c & d, upper panels). Re-probing with α-panAKT (d, second panel) and α-actin antibodies (c & d, lower panels) for loading control. Standard protein molecular masses are indicated in kDa.

### 3.3.7 Tonic BCR signaling via SHIP2 activates JNK signaling in Daudi cells

Next, I aimed to analyze the effect of CD79A knockdown in the context of SHIP2-dependent regulation of tonic BCR signaling pathways. I used Daudi-derived cells for this analysis due to aberrant BCR expression levels in BL60-derived cells as described in 3.3.1. For this purpose, I also included the SHIP2 inhibitor AS1949490 in the experiment. Daudi cells transduced with constructs encoding shCD79A were induced with Dox for 72 h, harvested and treated with 5µM AS1949490 for 30 min in RPMI only or left untreated. Cells were subsequently lysed and subjected to Western Blot analysis.

In order to check for sufficient induction of shRNAs, I started by probing membranes with α-GFP antibody (Figure 46 a). GFP expression was sufficiently induced upon doxycycline treatment to comparable levels in all cell lines. To test for activation of the PI3K pathway, I decorated membranes with α-pAKT and α-pFOXO1 antibodies, respectively (Figure 46 b & c). Expectedly, knockdown of CD79A decreased AKT and FOXO1 phosphorylation in all Daudi cell lines. Treatment with the SHIP2 inhibitor elevated AKT and FOXO1 phosphorylation levels in Daudi wt and CitSHIP2$^{low}$-expressing cells independent of CD79A knockdown, whereas in SHIP2-deficient cells, phosphorylation of AKT and FOXO1 was not affected by the SHIP2 inhibitor.

Based on my findings described in section 3.3.4, I now tested the activation of MAPK JNK and ERK in this experimental setup. Upon CD79A knockdown, ERK phosphorylation was only minimally affected in Daudi wt cells but no differences were observed in Daudi SHIP2-deficient and CitSHIP2$^{low}$-expressing cells (Figure 46 d). Moreover, I probed blots with phospho-specific α-JNK antibody (Figure 46 e). In all CD79A knockdown samples, JNK phosphorylation was decreased compared to untreated samples, indicating that phosphorylation of JNK is dependent on tonic BCR signaling. For Daudi wt and CitSHIP2$^{low}$-expressing cells, the reduction in JNK phosphorylation was more severe, namely 17% and 21%, respectively, compared to untreated cells. In contrast, SHIP2-deficient cells only displayed a reduction in phosphorylation of 11% upon CD79A knockdown. In summary, these data show that the SHIP2-dependent regulation of the JNK pathway is part of the tonic BCR signaling network.

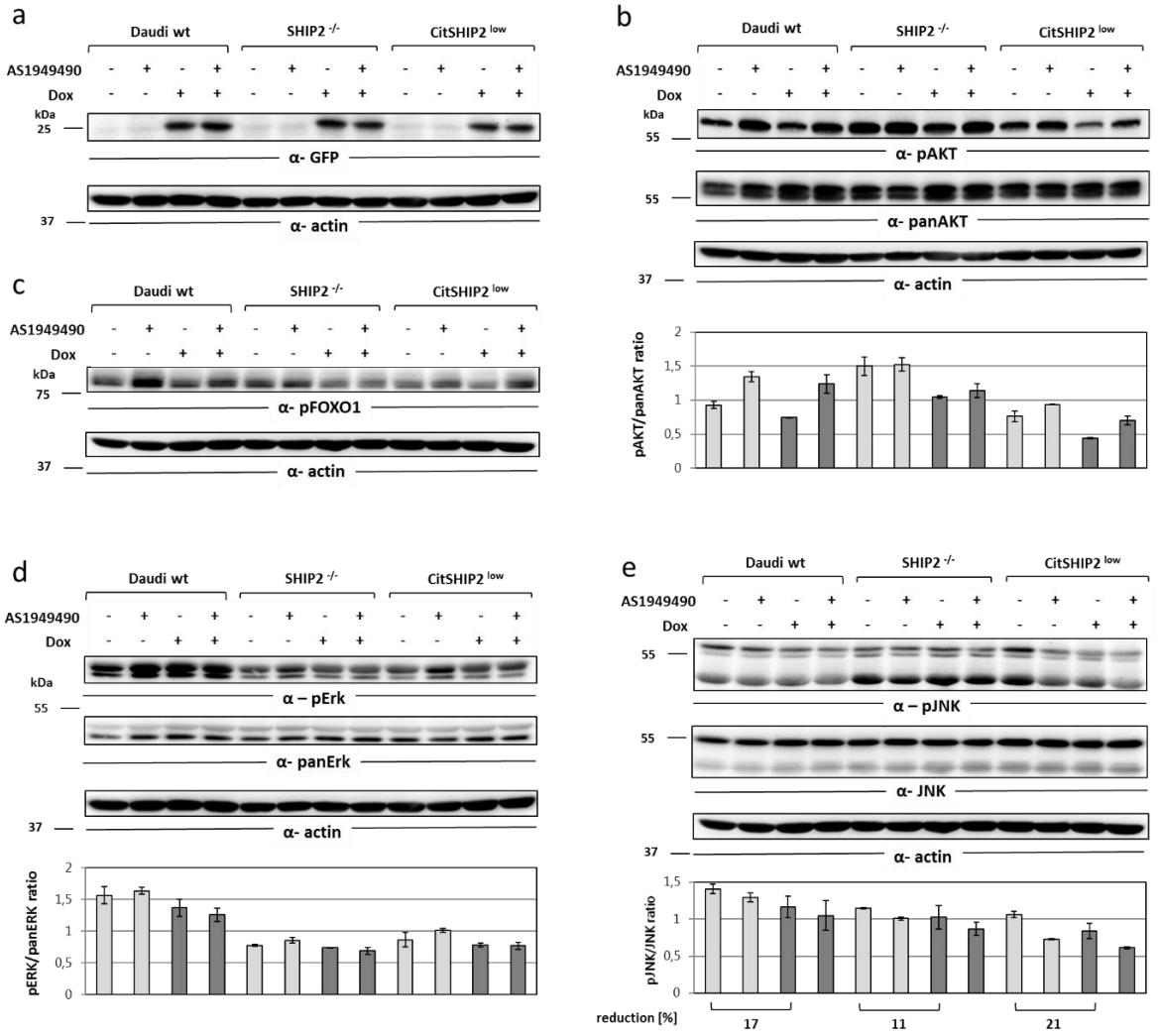


**Figure 46**: **SHIP2-dependent JNK activation is influenced by tonic BCR signaling in Daudi cells.**
Daudi wild-type (wt), SHIP2-deficient (*SHIP2*$^{-/-}$) and CitSHIP2$^{low}$-expressing cells were transduced with plasmids encoding for doxycycline-inducible shCD79A or control (shCtrl) shRNA and were induced with (+, dark grey) 250 ng/ml doxycycline (Dox) for 72 h or left untreated (-, light grey). Before lysis, cells were either treated with 5 µM AS1949490 (+) for 30 min or left untreated (-). Lysates were subjected to Western Blot analysis. (a) Dox-induced GFP expression was detected with α-GFP antibody (upper lane) and equal loading was tested with α-actin (lower panel). (b) Phosphorylation of AKT was analyzed using phospho-specific α-AKT antibody (upper panel), α-panAKT (second panel) and α-actin (third panel) for loading control. Ratios of signal intensities of α-pAKT to that of α-panAKT were calculated and depicted as a bar diagram (lower panel). (c) Probing membranes with phospho-specific α-FOXO1 antibody (upper panel) and re-probing with α-actin (lower panel). (d) Analysis of ERK signaling using phospho-specific α-ERK antibody (upper panel), α-panERK (second panel) and α-actin (third panel). Ratios of signal intensities of α-pERK to that of α-panERK were calculated and depicted in a bar diagram (lower panel). (e) JNK signaling upon CD79A knockdown was analyzed by probing with phospho-specific α-JNK antibody (upper panel), α-JNK (second panel) and α-actin antibodies (third panel). Ratios of signal intensities of α-pJNK to that of α-JNK were calculated and depicted as a bar diagram and reduction of signal intensities of untreated to treated cells was calculated (lower panel). Quantification data are means + SD of two independent experiments. Standard protein molecular masses are indicated in kDa

# 4 Discussion

Tonic signaling via the BCR and subsequent activation of the PI3K pathway is believed to be of central importance for the survival and proliferation of BL cells (Schmitz et al. 2012), but the underlying molecular details remain unclear to date. Based on a proteogenomic screen in different BL cell lines, I have characterized the function of Nck1, BIG2 and SHIP2 in BL-specific tonic BCR signaling. My data imply that beyond the PI3K pathway, the activity of the MAPK JNK is regulated by Nck1, SHIP2 and BIG2 upon tonic BCR signaling. Hence, my study sheds some light on the molecular aspects of BL-specific tonic BCR signaling and emphasizes the JNK pathway to be a promising target for novel therapeutic approaches for BL.

## 4.1 Redundant and non-redundant functions of Nck proteins in BL signaling

Upon BCR stimulation, the adaptor protein Nck is recruited to the phosphorylated non-ITAM tyrosine (Y204) in Igα via its SH2 domain in addition to bind to proline-rich regions of the adaptor BCAP via its SH3 domains in DT40 chicken B cells (Castello et al. 2013). Tyrosine phosphorylation of BCAP by Syk and Btk allows binding of the PI3K subunit p85 (Okada et al. 2000), thereby linking activation of the BCR to PI3K activation and localization. Here, I provide evidence that Nck1 and Nck2 also regulate PI3K activation in tonic BCR signaling of BL cells and additionally identified Nck1 to promote JNK and p38 MAPK signaling.

### 4.1.1 Nck1 and Nck2 regulate PI3K-AKT activation in tonic BCR signaling

Evidence for the impact of Nck1/2 on tonic BCR signaling via the PI3K pathway, which has been reported to be crucial for survival of BL cells (Schmitz et al., 2014), comes from DG75 cell lines lacking expression of either or both Nck proteins that I generated during this thesis. According to my analyses, Nck1 deficiency leads to lower phosphorylation levels of the PI3K effectors AKT and FOXO1 under tonic signaling conditions. In comparison, loss of Nck2 expression only led to a mild decrease in AKT and FOXO1 phosphorylation. Although, according to these results, Nck1 appears to be the dominant isoform involved in tonic PI3K-AKT activation, Nck2 expression further increases the efficiency of AKT activation. In line with these findings, Nck-dependent AKT activation was also observed in mouse B cells (Castello et al. 2013). Although not particularly addressed in the study, the phosphorylation of AKT was reduced in absence of Nck1 and Nck2 already in resting cells hence supporting the positive role of Nck1 and Nck2 for PI3K-AKT signaling in the context of tonic BCR signaling identified in this thesis.

Noteworthy, the functional reconstitution of Nck1- and Nck1-2-deficient DG75 cell lines was only partly successful, which is in line with lower levels of the pivotal Nck-PI3K adaptor BCAP. In the context of activated BCR signaling, BCAP deletion leads to an almost complete block in BCR-mediated AKT phosphorylation (Aiba et al. 2007; Okada et al. 2000), whereas the impact of BCAP expression for tonic BCR signaling has not been tested. However, the reduction of AKT phosphorylation in both Nck1- and Nck1-2 deficient DG75 cell lines might be potentiated by lower BCAP expression in these cell lines and the cause of insufficient functional reconstitution. Nevertheless, the fact that I could observe some reconstitution allows for the conclusion that Nck1 in co-operation with Nck2 regulates the PI3K pathway in the tonic BCR signaling network of DG75 cells.

While my study is the first to show a role of Nck proteins in the activation of the PI3K pathway in tonic BCR signaling, studies are available assessing the role of Nck proteins in activated receptor signaling (Lu et al. 2015; Castello et al. 2013). Castello and colleagues found reduced BCR-induced $Ca^{2+}$ mobilization in Nck-deficient mouse B cells and DT40 cells (Castello et al. 2013). While in DT40 cells Nck2 is the only expressed Nck protein, loss of Nck2 did not further attenuate the $Ca^{2+}$ signal in Nck1-deficient mouse B cells. Similar to mouse B cells, I found a marked reduction of BCR-induced $Ca^{2+}$ mobilization in Nck1-deficienct DG75 cells and no effect of Nck2 in these experiments. These data are further corroborated be the fact that the PI3K-inhibitor Wortmannin significantly decreased BCR-induced $Ca^{2+}$ mobilization in Nck1-expressing but not Nck1-deficient cells. These results indicate that in human B cells, Nck1 is signaling upstream of BCR-dependent PI3K activation (Castello et al. 2013). However, in contrast to the reports and to my analyses of tonic BCR signaling, I could not identify an impact of Nck1 on the PI3K effectors AKT and FOXO1 following BCR stimulation. Because my focus was on the investigation of tonic BCR signaling I did not further asses the Nck function in activated BCR signaling, but the data indicate, that for an efficient activation of AKT and FOXO1 not only Nck1 but also Nck2 is important. This is supported by findings in naïve mouse B cells (Castello et al. 2013), showing that although already decreased in Nck1 KO mouse B cells, AKT and FOXO1 phosphorylation was more attenuated in B cells derived from Nck1-2 KO mice. In summary, I could show that Nck proteins are relevant for efficient PI3K signaling in the tonic BCR signaling network of BL cells.

### 4.1.2 Nck1 is required for efficient p38 activation in tonic BCR signaling

Beyond the PI3K pathway, activation of different MAPK is a hallmark of BCR signaling. I could show that in resting BL cell lines the MAPKs ERK, p38 and JNK are phosphorylated indicating their activation. While I found no impact of Nck proteins on the efficiency of ERK activation, p38 MAPK phosphorylation was reduced in the absence of Nck1 but not Nck2. This effect seems to be specific for tonic BCR signaling since p38 phosphorylation was not altered by Nck1 deficiency after BCR engagement. This is in agreement with studies in Jurkat T cells (Ngoenkam et al. 2014) and in mouse B cell lymphoma cells (Mizuno et al. 2002), which reported Nck proteins did not alter p38 signaling after TCR and BCR receptor stimulation, respectively. A potential candidate linking Nck1 to p38 activation could be the Nck-interacting kinase (NIK, also known as MAP4K4) which was shown to activate p38 signaling during mouse gastrulation (Zohn et al. 2006). Indeed, NIK was found to be tonically phosphorylated in our phospho-proteomic approaches but the exact molecular mechanism how Nck1 regulates the p38 pathway in tonic BCR signaling remains to be studied.

### 4.1.3 Nck1-dependent JNK activation in tonic and activated BL signaling

JNK is another MAPK I found to be regulated by Nck proteins in tonic BCR signaling. Nck1- and Nck1-2-deficient DG75 cells displayed lower levels of JNK phosphorylation, which could be partially restored by expression of Nck1 or both Nck isoforms, respectively. Again, Nck1 was identified as the primary isoform involved in this process but Nck2 expression further augments JNK activation. The role of Nck proteins in JNK activation does not appear to be restricted to tonic BCR signaling since the BCR-induced activation of JNK was compromised in the absence of Nck1, too.

From the literature, two possible mechanisms of how Nck1 helps to activate JNK are conceivable. First, a loss of BCAP recruitment in absence of Nck1 might cause insufficient JNK phosphorylation. Studies of BCAP-deficient DT40 chicken B cells revealed that following BCR engagement BCAP is required for efficient JNK activation (Okada et al. 2000). Since BCAP expression was also reduced in Nck1- and Nck1-2-deficient DG75 cells and their sub-clones, this might explain - similar to AKT - the only partial restoration of JNK phosphorylation after reconstitution of my cell lines. Okada and colleagues proposed that loss of BCAP reduced PI3K activation and caused decreased JNK signaling via the PH-domain containing guanine-exchange factor Vav. Hence, Nck1 via recruitment of BCAP and subsequent activation of the PI3K-Vav signaling axis could orchestrate JNK activation in the tonic BCR signaling network of BL cells.

A second possible way for Nck to control JNK activation might be mediated by its interaction with SLP65. The BCR-induced association of SLP65 and Nck has been shown to activate JNK signaling in the mouse B cell lymphoma cell line WEHI-231 (Mizuno et al. 2002). However, WEHI-231 cells show characteristics of immature B cells including growth arrest and apoptosis upon BCR stimulation (Benhamou et al. 1990), which was not observed germinal-center derived BL DG75 cells (data not shown). Differences in the net-result of BCR signaling might also be reflected by different regulatory mechanisms in signaling pathways. Thus, whether the SLP65/Nck1, the BCAP/Nck1 interaction, or both are required for efficient JNK activation in BL cells needs further investigation. In conclusion, I could identify an impact of Nck proteins on different signaling pathways in the tonic BCR signaling network of BL cells. How this Nck-dependent signaling might contribute to the survival and proliferation of BL cells will be discussed in the next section.

### 4.1.4 Nck proteins affect survival and proliferation of DG75 BL cells

The fate of a cell to live or die depends on activation and inhibition of different signaling pathways triggered by extrinsic pro-survival signals or intrinsic and extrinsic stress-signals. Proliferation and apoptosis therefore represent the net-result of integration of different signaling pathways. With regard to the role of Nck in tonic BCR signaling, these pathways include - but might not limited to - the PI3K-AKT, p38, and JNK pathways. In the following chapter, I will discuss these pathways with respect to proliferation and apoptosis.

I could show that DG75 cells lacking expression of Nck1, Nck2, or both isoforms have an attenuated proliferation in comparison to DG75 wt cells. However, reconstituted cells were not able to compensate for growth differences, indicating clonal effects altering proliferation. This is in part also reflected by the analysis of signaling pathways since re-expression of Nck proteins was only partially able to reconstitute the phenotypes observed for PI3K-AKT, p38, and JNK signaling. Lower levels of PI3K-AKT signaling are likely causing decreased cell cycle activity in Nck-deficient cells. In mammalian cells, AKT can phosphorylate GSK3β at S9 resulting in inhibition of its kinase activity (Cross et al. 1995; Fang et al. 2000). Following, the cell-cycle promoting protein Cyclin D1 is released from GSK3β-dependent negative regulation (Diehl et al. 1998). In line with its described suppression of cell proliferation in other cells, GSK3β functions as a metabolic senor that restricts cell mass accumulation in GC B cells (Jellusova et al. 2017; Cui et al. 1998). Interestingly, PI3K and AKT were identified to act as upstream regulators of JNK and Cyclin D1 in human bronchial epithelial cells, and signaling via the PI3K/AKT/JNK/cyclin D axis promoted cell growth (Ding et al. 2009).

In addition, reconstitution of the AKT and JNK phosphorylation in Nck1- and Nck1-2-deficient cells was challenging, indicating a possible causal dependency of AKT and JNK activity. Notably, JNK has been described to control PI3K and AKT in other cells (Chen et al. 2016), and thus it remains to be analyzed how the interdependency between these pathways is organized in tonic BCR signaling. Functionally, increased signaling via JNK and p38 is associated with increased survival and cell growth in BL cells (Gururajan et al. 2005; Horie et al. 2007). Lower signaling intensity of AKT, JNK and p38 thus might contribute to proliferative defects in Nck-deficient cells.

Decreased AKT signaling identified in Nck-deficient cells may also limit the repression of pro-apoptotic effector proteins such as FOXO, Bad and Caspase-9 (Cardone et al. 1998; Downward 2004), leading to an increase of pro-apoptotic signaling. This corresponds to Nck2-deficient cells which showed a higher number of apoptotic cells compared to DG75 wt and Citrine-Nck2-expressing cells. In contrast, Nck1-deficient cells displayed lower numbers of apoptotic cells, which cannot be explained based on this dataset. However, it is conceivable that serum-limiting conditions (1% FCS), which were necessary for induction of apoptosis, might be the cause for this phenotype. In hepatocytes, Nck1 was identified to negatively regulate PI3K-AKT signaling in response insulin and growth factors PDGF and EGF (Li et al. 2014). In the absence of growth-factors provided by the serum, Nck1 may inhibit PI3K activation leading to decreased survival of Nck1-expressing cells. While this is purely speculative, this may provide an explanation for the proliferative advantage of Nck1-deficient cells observed in serum-limiting apoptosis assays.

In summary, Nck-deficient cells showed proliferative defects possibly mediated via decreased activation of AKT and decreased activation of JNK and p38 signaling pathways in Nck1-deficient cells. The absence of complete reconstitution within these signaling pathways is presumably also the cause for insufficient functional reconstitution in proliferation assays. Despite these difficulties, I identified Nck1 as a novel regulator for effector proteins AKT, JNK and p38 in the context of tonic BCR signaling.

## 4.2 BIG2 is mediating survival signaling in Daudi BL cells

In my thesis, I provide evidence for the importance of the Brefeldin-A-inhibited guanine exchange factor 2 (BIG2), encoded by the *ARFGEF2* gene, for the survival of BL cells. Phospho-proteome analysis revealed BIG2 to be phosphorylated in tonic BCR signaling and moreover was identified to be crucial for survival of BL cells (Corso et al. 2016). While there have been no further reports investigating the role of BIG2 in B cells, in other cells BIG2 has been reported to be involved in vesicle trafficking between the Golgi and the recycling endosomes and was described to play a role in actin cytoskeleton organization by regulating FilaminA phosphorylation (Shin et al. 2004; Zhang et al. 2012). Here, I show that BIG2 may control survival in Daudi BL cells by promoting high levels of c-MYC expression.

### 4.2.1 Loss of BIG2 leads to augmented apoptosis of Daudi cells

To characterize the role of BIG2 in the context of BCR signaling, I generated a BIG2-deficient cell line on the background of Daudi BL cells. While activated BCR signaling i.e. the BCR-induced $Ca^{2+}$ mobilization was not affected by BIG2, BIG2-deficient cells showed a drastic decrease in proliferation compared to Daudi wt cells, which could not be mitigated upon expression of Citrine-tagged-BIG2. This lack of complete reconstitution implies that BIG2-deficient cells might have adapted during their generation to cope with the loss of BIG2. However, it was still apparent that loss of BIG2 hindered proliferation, similarly as seen for BL cell lines Daudi, DG75 and BL41 upon shRNA-mediated “knockdown” of BIG2 (Corso et al. 2016).

Besides the proliferation defect, apoptosis was increased in BIG2-deficient Daudi cells compared to Daudi wt cells in serum-deprived medium. The same effect was observed in DG75 and Daudi cells upon shRNA-mediated “knockdown” of BIG2 (Corso et al. 2016), indicating that BIG2-expression is crucial for survival of BL cells by limiting spontaneous apoptosis. Interestingly, the apoptosis rate of BIG2-deficient cells was only restored by reconstitution with moderate expression levels that resemble the endogenous situation. In contrast, stronger BIG2 expression revealed an apoptosis rate similar to BIG2-deficient cells, showing that the amount of BIG2 in BL cells appear to be critical and overexpression might potentially cause secondary effects interfering with the survival of BL cells. These analyses show that despite the obvious clonal specificities caused by the BIG2 deficiency, the generated cell lines provide a basis for the further analysis of BIG2 in the tonic BCR signaling network of BL cells.

### 4.2.2 BIG2 increases survival of BL cells by decreasing c-MYC protein levels

Continuous expression of the proto-oncogene c-MYC is a prerequisite for BL lymphomagenesis and is essential for BL proliferation and survival (Sampson et al. 2007; Gomez-Curet et al. 2006). This was demonstrated by multiple studies using pharmacological inhibitors (Yin et al. 2003), the c-MYC inducible cell line P493-6 (Pajic et al. 2000) and mouse models for MYC-induced lymphomagenesis (Harris et al. 1988; Park et al. 2005).

Similar to a report stating that c-MYC mRNA expression was decreased upon knockdown of BIG1 and BIG2 in HeLa cells (Li et al. 2016), I identified decreased c-MYC protein levels in BIG2-deficient Daudi cells. c-MYC expression could be reconstituted by the re-expression of BIG2, further emphasizing the BIG2 specificity of this effect. Since c-MYC is known to regulate cell growth by increasing metabolic activity essential for BL proliferation and survival (Spender & Inman 2014; Gomez-Curet et al. 2006), a decrease in c-MYC expression is likely to explain the defects in proliferation observed in BIG2-deficient Daudi cells.

A model how BIG2 could modulate c-MYC expression was proposed by Li and colleagues. BIG2, via its N-terminal AKAP (A-kinase anchoring protein) domain, can assemble cAMP-dependent Protein kinase A (PKA) (Li et al. 2003). Moreover, BIG2 forms a complex with BIG1 that can bind β-catenin, which is phosphorylated by PKA. Phosphorylated β-catenin can translocate into the nucleus to induce subsequent transcription of T cell factor/ lymphoid enhancer binding factor (TCF/LEF) genes (Li et al., 2016), which are known to drive expression of c-MYC and cyclin D1 (He et al. 1998; Shtutman et al. 1999). However, in BL cells *c-MYC* is under the control of Ig enhancer elements while the normal *c-MYC* allele is considered to be silent (ar-Rushdi et al. 1983; Spender & Inman 2014). Thus, it is unlikely that the proposed pathway is regulating c-MYC expression in BL cells.

A possible candidate mediating the BIG2-dependent c-MYC expression is the MAPK JNK. JNK phosphorylation was decreased in BIG2-deficient cells and could be reconstituted with Citrine-tagged BIG2. JNK is known to enhance c-MYC expression in repose to growth factor receptor activation (Iavarone et al. 2003) and was found to regulate proliferation and c-MYC expression in lymphoma B cell lines (Gururajan et al. 2005). In the aforementioned study, authors proposed that *c-MYC*, despite its translocation, might still be regulated by the MAPK pathway. Therefore, JNK signaling could potentially link BIG2 and c-MYC expression levels.

Another candidate potentially linking BIG2 and c-MYC expression is the associate of MYC-1 (AMY-1). AMY-1 is a c-MYC-binding protein known enhance c-MYC transcription and activity (Taira et al. 1998).

Additionally, AMY-1 co-precipitates with BIG1 and BIG2 and binds to AKAPs (Ishizaki et al. 2006), several of which were found to be phosphorylated in resting BL cells (Corso et al. 2016). Hence, loss of BIG2 may therefore result in decreased c-MYC levels in BL cells by loss if its association to AMY-1. However, we don't have further hints for an involvement of AMY-1 in tonic BCR signaling and therefore the question whether BIG2 regulates c-MYC levels in BL cells via JNK, AMY-1, or by a different pathway remains to be determined.

### 4.2.3 The GEF activity of BIG2 might contribute to survival signaling

Additionally, BIG2 was reported to interact with Filamin A, an actin-crosslinking protein (Hartwig & Stossel 1981), in the Golgi and along the plasma membrane. Phosphorylation of Filamin A induces the recruitment of BIG2 from the Golgi to the cell membrane in melanoma and mouse neuroblastoma cells (Sheen 2014; Zhang et al. 2012; Zhang et al. 2013) and interaction with Filamin A is crucial for BIG2-dependent activation of ADP-ribosylation factor (ARF) 1 at the cell membrane (Zhang et al. 2013). On a functional level, ARF1 knockdown decreased cyclin D1 levels and inhibited cell proliferation due to less efficient ARF1-dependent activation of the PI3K pathway in ovarian cancer cells (Gu et al. 2017). Similarly, a CRISPR dropout screen identified ARF1 to be crucial for survival of BL cell lines in addition to shRNA data showing Filamin A to be essential for DG75 BL cell survival (unpublished data, kindly provided by Dr. Oellerich). These data indicate the GEF-activity of BIG2 for ARF1 activation could also be relevant for BIG2-dependent survival signaling in BL.

### 4.2.4 Altered PI3K signaling may enable survival of BIG2-deficient cells

In contrast to studies using for a shRNA-based "knockdown" models of either BIG2 in HeLa cells or ARF1 in an ovarian carcinoma cell line (Gu et al., 2017; Li et al., 2016), I found AKT and FOXO1 to be stronger phosphorylated in the absence of BIG2. Hence, it might be possible that during the generation of BIG2-deficient cells AKT signaling enabled the survival of BIG2-deficient Daudi cells. However, since the effect could be reconstituted, I propose that activation of the AKT signaling is likely a specific response of the BL signaling network upon loss of BIG2.

On another note, I identified the Growth factor receptor bound protein 2 (Grb2) to be slightly enriched in BIG2-deficient Daudi cells, which was previously reported by others upon BIG2-knockdown in HeLa cells (Shen et al. 2012). Grb2 is an adaptor protein, which is involved in many different signaling pathways including MAPK pathways in Epidermal growth factor (EGF) and BCR

signaling. Recently, Grb2 was reported to directly associate with the Igα subunit of the BCR via the non-ITAM Y204 following BCR activation (Vanshylla et al. 2018) and BIG2 was identified in high throughput interactome analysis to interact with CD79B (Huttlin et al. 2017) thereby providing a possible link of BIG2 and Grb2 to the BCR signaling complex. In addition, Grb2-deficient mouse B cells were reported to display strongly reduced AKT activation (Ackermann et al. 2011) and Grb2 is suggested to bind to modulators of PI3K-AKT signaling including BCAP and CD19 (Neumann et al. 2009). Therefore, it was proposed by others that Grb2 association to these proteins might be important for activation of the PI3K-AKT pathway (Ackermann et al. 2011). In response to EGF signaling, Grb2 was described to recruit ARF1, which becomes activated by a GEF leading to activation of the PI3K-AKT pathway (Haines et al. 2014). Increased Grb2 expression might therefore enable increased activation of AKT signaling as seen in BIG2-deficienct cells. However, a mechanism how BIG2 regulates Grb2 expression levels remains unclear for now. In conclusion, I propose that increased AKT signaling - Grb2-dependent or not - enables BIG2-deficient Daudi cells to survive despite their detrimental deletion of BIG2.

Taken together, I could show that BIG2 is relevant for survival of Daudi BL cells by regulation of c-MYC expression levels. c-MYC expression could be mediated by a MAPK JNK, as reported in other B cell lymphoma lines. The activation of AKT signaling might contribute to survival of Daudi BIG2-deficient cells, eventually by a Grb2-dependent mechanism. However, further experiments will be necessary to identify causal effects of the identified correlations to decipher the BIG2-dependent signaling network in BL in more detail.

### 4.3 Impact of SHIP2 on BL survival and signaling

The 5'-inositol phosphatase SHIP2 was previously found to be phosphorylated at S132 during tonic BCR signaling when compared to CD79A "knockdown" DG75 cells (Corso et al. 2016). This finding together with the likely involvement in PI3K signaling due to its enzymatic activity tempted me to analyze the role of SHIP2 in the BCR-dependent survival of BL cells. While the role of the sister protein SHIP1 in BCR signaling has been well described (Okada et al. 1998; Manno et al. 2016; Pauls & Marshall 2017), little is known about the function of SHIP2 in B cells. In this study, I could confirm the essential role of SHIP2 by showing that deletion of SHIP2 as well as inhibition of its phosphatase function limits proliferation of BL cell lines and induces apoptosis. While loss of SHIP2 or SHIP2 inhibition in BL cell lines promoted signaling of PI3K-AKT pathway, signaling of the MAPK JNK was attenuated in activated and tonic BCR signaling.

### 4.3.1 SHIP2 is relevant for survival of BL cells

Evidence for the essential role of SHIP2 in the BCR-dependent BL survival arises from proliferation and apoptosis assays that revealed an anti-apoptotic role of SHIP2 in Daudi and BL60 cells. Numbers of living BL cells were decreased upon knockout of SHIP2 as well as upon inhibition of its phosphatase function using the small molecule inhibitor AS1949490. Notably, in normal culture conditions, SHIP2-deficient BL60 cells showed no defect in proliferation, which is possibly caused by the identified clonal upregulation of SHIP1. These clonal differences were mitigated by the use of the SHIP2 inhibitor AS1949490 which prevented proliferation in all SHIP2-expressing cells. Similar correlations were shown in other cell types using AS1949490 (Saurus et al. 2017; Agollah et al. 2014), a pan-SHIP inhibitor in SHIP1-deficient cells (Fuhler et al. 2012), or SHIP2 depletion (Ghosh et al. 2018). SHIP2 overexpression was also described to inhibit cell proliferation and to induce apoptosis in other cells (Gorgani-Firuzjaee et al. 2015; Ye et al. 2016), further emphasizing the pro-survival function of SHIP2 and indicating the importance of SHIP2 expression levels.

The SHIP2 inhibitor AS1949490 also decreased numbers of SHIP2-deficient Daudi cells, whereas SHIP2-deficient BL60 cells were able to proliferate despite inhibitor treatment. Drug sensitivity and resistance are highly sensitive to the number of cell divisions during the course of a response assay (Hafner et al. 2016). During my experimental work, I observed Daudi cells to proliferate at a slower rate than BL60 cells (undocumented observation). Although proliferation assays were performed with the same inhibitor concentration, SHIP2-deficient Daudi cells were therefore exposed to a higher inhibitor to cell concentration than SHIP2-deficient BL60 cells over the course of the experiment. While this dose-dependent effect must be considered, it also implies an off-target activity of the inhibitor. Although AS1949490 was reported to be over twenty times more potent against SHIP2 than SHIP1 (Suwa et al. 2009; Thomas et al. 2016), additional SHIP1 inhibition cannot be excluded as a cause for the reduced proliferation rate in SHIP2-deficient cells.

Apoptosis assays confirmed the pro-survival function of SHIP2, since SHIP2-deficient Daudi and BL60 cells were more prone to apoptosis under serum-limiting conditions. The data obtained from experiments with the BL60 cell lines bear the obstacle that here the surface BCR expression is reduced in SHIP2-deficient and CitSHIP2$^{high}$-expressing cells but not those cells that were reconstituted with SHIP2 expression levels more resembling the endogenous situation (CitSHIP2$^{low}$). These differences in surface IgM expression levels might be responsible for the insufficient functional reconstitution, because the cells gain less pro-survival tonic BCR signals than BCR$^{high}$-expressing cells (Yasuda et al. 2017). Still, the pro-apoptotic effect of SHIP2 appears to be valid and not just caused by low BCR expression, because the SHIP2 inhibitor AS1949490 was able to induce

apoptosis in BL60 wt cells, whereas SHIP2-deficient cells were not affected. Due to time limitations, I could not obtain further experimental data that would allow to determine whether the augmented apoptosis observed in CitSHIP2$^{high}$-expressing cells was due low BCR expression levels or caused by SHIP2 overexpression, as reported for other cells (Gorgani-Firuzjaee et al. 2015; Ye et al. 2016). In summary these analyses provide evidence that SHIP2 is an important factor for the survival of BL cells and imply that the expression level of SHIP2 is a crucial parameter for its pro-survival function.

### 4.3.2 Despite the pro-survival effect of SHIP2, AKT signaling is augmented in SHIP2-deficient cells

For many B cell neoplasms, including BL, the PI3K-AKT pathway has been described to be essential (Xu et al. 2013; Schmitz et al. 2012; Evangelisti et al. 2018; Tabe et al. 2014; Batlevi & Younes 2017). Consequently, 5'-inositol phosphatases SHIP1 and SHIP2 had been described to act as negative regulators and hence as tumor suppressors by hydrolyzing the PI3K product PI(3,4,5)$P_3$ (Miletic et al. 2010). However, the produced PI(3,4)$P_2$ was reported to correlate with AKT phosphorylation at S473 in B cells and was found to be important for overall AKT activity thus suggesting a potential function of SHIP1 and SHIP2 as proto-oncogenes (Fuhler et al. 2012; Li & Marshall 2015; Ma et al. 2008).

This could explain why I found increased AKT and FOXO1 activities in SHIP2-deficient and AS1949490-treated BL cells. Similar results have been reported previously in other cells upon shRNA-based SHIP2 "knockdown" or treatment with AS1949490 (Agollah et al. 2014). Despite the reduced BCR surface expression in the SHIP2-deficient BL60 cells discussed above, I found the inhibitory effect of SHIP2 in both Daudi and BL60 cells further demonstrating the specific role of SHIP2 in this pathway. Similar to the proliferation and apoptosis assays discussed above, only the SHIP2-deficient cells reconstituted with SHIP2 expression levels similar to the endogenous SHIP2 expression and not BL60 CitSHIP2$^{high}$-expressing were able to restore the AKT phosphorylation to the level of wt BL60 cells. SHIP2-deficient Daudi cells showed increased levels of AKT phosphorylation upon treatment with AS1949490, further confirming an off-target activity of the inhibitor, previously discussed in chapter 4.3.1. The negative regulatory function of SHIP2 on AKT activity is not restricted to tonic BCR signaling since I found prolonged BCR-induced phosphorylation of the PI3K effectors AKT and its target FOXO1 in the absence of SHIP2, which is in agreement with studies of receptor tyrosine kinase signaling (Liu et al. 2015; Wang et al. 2004). The inhibitory role in activated BCR signaling is further demonstrated by my results that the BCR-induced $Ca^{2+}$ mobilization is decreased in the presence of SHIP2 as previously described for SHIP1 in DT40 chicken

B cells (Okada et al. 1998; Manno et al. 2016). Since AS1949490 treatment enhanced $Ca^{2+}$ mobilization in SHIP2-expressing but not in SHIP2-deficient Daudi cells, I conclude that this effect is likely to be dependent on the phosphatase activity of SHIP2.

Although PI3K activation is classically described to activate AKT signaling, AKT activation inversely correlated with phosphorylation of the PI3K subunit p85 in Daudi cells under tonic BCR signaling conditions. AS1949490 treatment or SHIP2 deletion slightly decreased phosphorylation of the PI3K subunit p85. Additionally, p85 phosphorylation was stronger after induced "knockdown" of CD79A knockdown. While an impact of Doxycycline treatment in these experiments cannot be excluded because it has been reported to be associated with activation of the PI3K-AKT pathway in other cells (Chang et al. 2014), AKT phosphorylation was decreased in CD79A knockdown cells, which is in agreement with observations by others (Schmitz et al. 2012; Corso et al. 2016; Yasuda et al. 2017). These data indicate that SHIP2 attenuates AKT activity by acting downstream of PI3K activation, possibly by providing $PI(3,4)P_2$. SHIP2 product $PI(3,4)P_2$ was shown to have a relatively similar specificity for AKT as $PI(3,4,5)P_3$ (Manna et al. 2007). However, PDK1, which facilitates AKT phosphorylation at T308, prefers binding to $PI(3,4,5)P_3$ (Alessi et al. 1997; Xie et al. 2013) and increased $PI(3,4,5)P_3$ levels in the absence of SHIP2 could augment the PDK-dependent AKT phosphorylation.

Additionally, the tandem PH-containing proteins (TAPP)1 and TAPP2 have been shown to specifically bind to the SHIP2 product $PI(3,4,)P_2$ and are proposed to activate a negative feedback loop terminating BCR-dependent PI3K-AKT signaling (Manna et al. 2007; Landego et al. 2012; Xie et al. 2013). Hence, the less efficient production of $PI(3,4,)P_2$ in the absence of SHIP2 could compromise this inhibitory loop and thus prolong PI3K-AKT signaling. In summary, my results confirm the expected inhibitory role of SHIP2 in activated and tonic BCR signaling of BL cells. This is in apparent contrast to the pro-survival function of SHIP2 revealed by the proliferation/apoptosis assays discussed above, but could imply that SHIP2 functions beyond the regulation of AKT activity may be more important for providing tonic BCR-dependent survival signals to BL cells.

### 4.3.3 JNK phosphorylation is regulated by tonic BCR signaling in a SHIP2-dependent manner

JNK phosphorylation and activation is classically associated with induction of apoptosis by expression of pro-apoptotic genes and activation of the caspase cascade (reviewed in Dhanasekaran & Reddy 2008). However, JNK inhibitor studies showed that JNK has a unique pro-survival role in

murine and human B cell lymphomas (Gururajan et al. 2005), which is further supported by shRNA screens indicating the relevance of JNK proteins for survival of BL cells (unpublished data, kindly provided by Dr. Oellerich). In this study, I could show that SHIP2 is a positive regulator of JNK activity in the tonic BCR signaling network presumably contributing to survival of BL cells. The relevance of SHIP2 expression for JNK phosphorylation in the context of tonic BCR-signaling was identified in immunoblot analysis and confirmed by intracellular staining of SHIP2-deficient BL60- and Daudi-derived cell lines. Additionally, decreased activation of JNK signaling in Daudi SHIP2-deficient cells was also confirmed by phospho-proteomics. Here, samples derived from Daudi wt cells displayed a stronger phosphorylation of MAP3K2 in comparison to samples from SHIP2-deficient cells. MAP3K2 subsequently activates MAP2K7 which in turn can activate JNK phosphorylation and signaling (Cheng et al. 2000).

Since to my knowledge there are no studies linking SHIP2 and JNK to tonic BCR signaling, I also analyzed the SHIP2-dependent JNK activation upon engagement of the BCR for comparison. BCR engagement has been reported to induce JNK phosphorylation in DT40 chicken B cells (Okada et al. 2000) and mouse splenic B cells (O'Neill et al. 2009). In mouse B cells, JNK phosphorylation was associated with trafficking of internalized BCR complexes (O'Neill et al. 2009) or regulation of BCR-mediated proliferation (Han et al. 2003), further indicating the important function of JNK activation in B cells.

Following BCR engagement, JNK phosphorylation was impaired in SHIP2-deficient Daudi and BL60 cells but not in their respective parental or CitSHIP2$^{low}$-expressing cells. This indicates a positive correlation of SHIP2 expression, JNK activation and the intensity of BCR signaling. Notably, in SHIP2-deficient BL60 and CitSHIP2$^{high}$-expressing cells, phosphorylation of JNK, as well as Syk and ERK was impaired upon BCR engagement. This might imply a more general defect in JNK activation possibly caused by lower BCR surface expression levels. Nevertheless, BCR engagement increased JNK phosphorylation in a SHIP2-dependent manner.

Since the phosphatase function of SHIP2 was also shown to be crucial for cytoskeletal re-organization during lamellipodia formation and migration of cells (Erneux et al., 2011; Ghosh et al., 2018; Kato et al., 2012; Prasad, Topping, & Decker, 2001; Venkatareddy et al., 2011), JNK regulation by SHIP2 could be independent of tonic BCR signaling. However, my CD79A "knockdown" experiments prove that the SHIP2 function is related to tonic BCR signals. Because CD79A is necessary for BCR surface expression (Venkitaraman et al., 1991), "knockdown" of CD79A results in decreased tonic BCR signaling and thus serves as a negative control.

While ERK phosphorylation was not significantly changed upon CD79A “knockdown”, JNK levels were decreased in all tested Daudi-derived cell lines, however to a lower degree in SHIP2-deficient cells. A similar effect was observed in SHIP2-deficient BL60 cells, thereby suggesting that SHIP2 is mediating tonic BCR signaling to regulate JNK phosphorylation. The observation that CD79A “knockdown” further decreased JNK phosphorylation even in SHIP2-deficient cells also implies that SHIP2 is an important but not exclusive mediator of JNK activation.

While I could show that SHIP2-dependent JNK activation is indeed regulated by tonic BCR-signaling, the mechanism how SHIP2 is mediating this process is less clear. Inhibition of the catalytic activity of SHIP2 by AS1949490 resulted in decreased levels of JNK phosphorylation in Daudi but not in BL60 cells. While these differences could simply be cell line dependent, it remains unclear whether the phosphatase activity of SHIP2 is required for efficient JNK activation or whether SHIP2 adapter functions mediate this process. Support for the latter was published in 2008, when SHIP2 was identified to positively regulate JNK signaling via the JNK-interacting protein 1 (JIP1) independent of its phosphatase activity (Xie et al. 2008). However, immunoblot analysis of BL60 and Daudi cell lysates showed no specific signal for JIP1 (data not shown), indicating that JIP1 is not expressed. This observation is in line with data from the human protein atlas database, in which Daudi cells are listed negative for JIP1 RNA expression (Thul et al. 2017). Furthermore, a connection of SHIP2 and JNK activation had previously been described in breast cancer stem cells but, similar to my findings, JIP1 was not detected in SHIP2-immunoprecipitates (Fu et al., 2014). Thus, the mechanism how SHIP2 is regulating JNK phosphorylation independent of JIP1 awaits further investigation. In following experiments, generation and expression of catalytically inactive SHIP2 mutants or SHIP2 mutants defective for certain binding sites of interacting proteins may help to elucidate the underlying mechanism of SHIP2-dependent JNK activation.

A promising candidate mediating SHIP2-dependent JNK activation that is dependent on the inositol 5’ phosphatase activity might be the B cell adaptor protein of 32 kDa (Bam32, also referred to as DAPP1). Bam32 is phosphorylated by Src-family kinases and recruited to the BCR in a PI3K-dependent manner and is able to activate JNK signaling independent of PLCγ2 (Han et al. 2003). Interestingly, Bam32 binds with high affinity to $PI(3,4)P_2$ and its recruitment is therefore enhanced by phosphatases SHIP1 and SHIP2 (Allam & Marshall 2005). Since the phosphatase function of SHIP2 was relevant in Daudi cells, Bam32 could be a possible mediator of SHIP2-dependent JNK activation.

A schematic depiction of a possible mechanism for SHIP2-dependent JNK activation in Daudi cells is summarized in Figure 46. Upon tonic BCR signaling, the PI3K is active and produces $PI(3,4,5)P_3$, which is dephosphorylated by SHIP1 and SHIP2 to $PI(3,4)P_2$. This creates an equilibrium of PIPs resulting in constitutive phosphorylation of JNK and survival of BL cells (Figure 46 a). In SHIP2-deficient BL cells, the equilibrium of PIPs shifts to higher levels of $PI(3,4,5)P_3$ and lower levels of $PI(3,4)P_2$ (Figure 46 b). Lower $PI(3,4)P_2$ levels correlate with reduced JNK phosphorylation, possibly mediated by reduced membrane recruitment of the $PI(3,4)P_2$-binding adaptor protein Bam32. Inefficient JNK signaling is likely contributing to apoptosis in SHIP2-deficient cells.

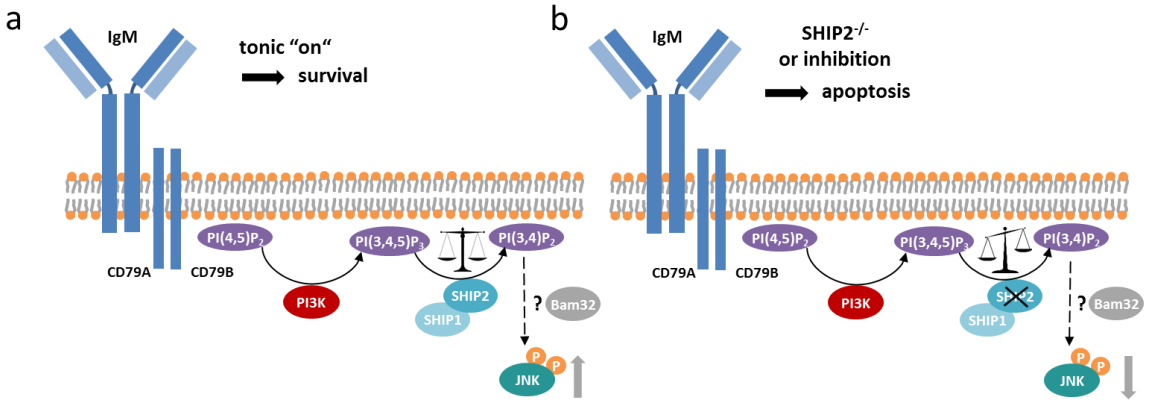


**Figure 47: Model for SHIP2-dependent JNK activation upon tonic BCR signaling.**
(a) Tonic BCR signaling in BL cells is mediated by activation of PI3K, which phosphorylates membrane bound $PI(4,5)P_2$ at the 3' position generating $PI(3,4,5)P_3$. Inositol 5' phosphatases SHIP1 and SHIP2 can decrease the pool of $PI(3,4,5)P_3$ by generating $PI(3,4)P_2$. JNK is constitutively phosphorylated in BL cells, possibly involving the $PI(3,4)P_2$-binding protein Bam32. (b) Upon loss of SHIP2 or SHIP2 inhibition, $PI(3,4,5)P_3$ dephosphorylation to $PI(3,4)P_2$ is limited to SHIP1 activity. JNK phosphorylation decreases in the absence of SHIP2 possibly caused by lower levels of $PI(3,4)P_2$ mediating membrane recruitment of Bam32. Impaired JNK activation may lead to apoptosis in SHIP2-deficient cells. Grey arrows indicate phosphorylation levels of JNK in response to BCR signaling.

In summary, loss of SHIP2 increased AKT signaling but led to decreased levels of JNK phosphorylation and contributed to apoptosis in BL cell lines Daudi and BL60. In addition, I could show that JNK activation was dependent on tonic BCR signals and that signaling - although not exclusively - was regulated by SHIP2, thereby possibly identifying a new pathway that is regulated by tonic BCR signaling.

## 4.4 BCR-dependent JNK signaling in B cells

During my work on this thesis, the JNK pathway was recurrently regulated by the analyzed BL effector proteins. Previous studies had described JNK signaling to be necessary for proliferation of primary B cells and B cell neoplasms including BL, DLBCL of both subtypes, follicular lymphoma and multiple myeloma (Gururajan et al. 2005; Schmid et al. 2015; Knies et al. 2015; Hideshima et al. 2003). Here, I could show that JNK signaling is regulated by tonic signals of the BCR and thereby may be a novel, putatively druggable pathway for the treatment of BL. The JNK pathway is one of the major signaling hubs of the MAPK signaling pathways. JNK signaling can be activated by a plethora of mechanisms ranging from G-protein couples receptors, to growth factors, cytokines or cellular stress (Lopez-Ilasaca 1998; Cano et al. 1994; Westwick et al. 1994; Hibi et al. 1993). Here, I would like to briefly summarize how JNK signaling can be activated by the BCR.

In B cells, activation of JNK signaling so far only described upon BCR engagement. A central protein in the activation of JNK is the adaptor SLP65. SLP65 is constitutively associated with small GEF Vav (Wienands et al. 1998), which is activated upon tyrosine phosphorylation by tyrosine kinases like Syk (Deckert et al. 1996). Following, Vav can activate several Rho-family GTPases such as RhoA and Rac1 (Saci & Carpenter 2005; Brezski & Monroe 2007). Besides Vav, SLP65 also recruits PLCγ2, and activation of both PLCγ2 and Rac1 is necessary for subsequent JNK activation (Ishiai et al. 1999). In addition, SLP65 also associates to Nck, and this complex was previously shown to activate JNK activation in B cells (Mizuno et al. 2002). Upstream of SLP65, Syk triggers activation of both the PLCγ2- and Vav-dependent Rac1 pathways (Ishiai et al. 1999; Teramoto et al. 1997), while SHP1 is a negative regulator of JNK signaling (Mizuno et al. 2002). Downstream of Rac1, MAP3Ks including ASK1 and MAP3K2 are activated which can in turn activate MAPK2s such as MAP2K7 which subsequently phosphorylate JNK MAPKs (reviewed in Dhanasekaran & Reddy 2008). When phosphorylated, JNK can translocate into the nucleus where it can activate its target transcription factors including c-Jun, c-MYC or Elk-1 (reviewed in Zeke et al. 2016).

In addition, signaling via the PI3K-AKT pathway is also involved in BCR-dependent JNK activation, however, the mode for activation is less clear. Loss of the Nck1-interacting protein BCAP, which is phosphorylated by Syk and Btk, reduced PI3K activation and authors proposed a pathway involving recruitment of Vav by its PH-domain to mediate JNK signaling (Okada et al. 2000). Moreover, the adaptor protein Bam32 is recruited to the BCR in a PI3K-dependent manner and is able to activate JNK signaling independent of PLCγ2 (Han et al. 2003). Interestingly, Bam32 binds with high affinity to $PI(3,4)P_2$ and its recruitment is therefore enhanced by phosphatases SHIP1 and SHIP2 (Allam & Marshall 2005).

More recently, another pathway for BCR-dependent JNK activation has been identified that involves ezrin, a member of the ezrin/radixin/moesin (ERM) family of proteins, which cross-link the plasma membrane to the actin cytoskeleton and are important for the assembly of BCR microclusters (Treanor et al. 2011). Ezrin, which localizes in a pre-formed complex with Syk in unstimulated cells, is phosphorylated by Syk upon IgM stimulation (Parameswaran et al. 2013). In turn, Syk-specific ezrin phosphorylation induces association of MAP2K7 and JNK followed by subsequent JNK activation.

Although studies so far only focused antigen-dependent instead of tonic BCR-dependent JNK phosphorylation, activation of the JNK cascade is complex and can be accomplished by different signaling networks. Despite this complexity, all pathways described so far are dependent on Syk activation following BCR engagement. Thus, Syk might also be a promising candidate to act as an upstream regulator for newly identified mediators of BL-specific tonic JNK signaling including SHIP2, Nck1 and BIG2. Generated cell lines could be treated with a SYK inhibitor and tested for JNK phosphorylation in the presence or absence of SHIP2, Nck1 and BIG2. Further studies determining interacting proteins necessary for JNK activation will help to gain a deeper insight into the survival-relevant role of JNK activation in the context of tonic BL-specific BCR signaling.

## 4.5 CRISPR/Cas9-based gene editing – challenges and what to consider

While having been able to characterize some aspects of BL-specific tonic BCR signaling, the experimental approach of CRISPR/Cas9-mediated gene targeting bears the risk to miss some functional aspects. This is likely due to the fact that the cells were given time to adapt for the missing signaling effector, i.e. by changing expression levels of certain proteins. In the previous chapters, I have already described some effects like the downregulation of BCAP in Nck1-deficient cells, the upregulation of SHIP1 or different BCR-expression levels in SHIP2-deficient BL60 cells. Due to these clonal effects, I cannot exclude that additional signaling pathways might be mediated by analyzed BL-effector proteins that were not identified with the CRISPR/Cas9 gene targeting approach.

To address this, different strategies targeting the transcript or protein instead of the gene itself might help to reveal further signaling pathways. Common technologies used for these applications include the use of small-molecule inhibitors - if available - or dominant negative mutant proteins (Sheppard 1994; Arkin et al. 2014). In addition, inducible RNA interference (RNAi) systems mediate a post-transcriptionally, specific and transient loss of protein expression and are extensively used for reverse genetics approaches (Boettcher & McManus 2015). Moreover, CRISPR interference

(CRISPRi) or transcription activator-like effector (TALE) transcriptional repressors prevent the transcription of the gene of interest in the nucleus (Cong et al. 2012; Qi et al. 2013; Gilbert et al. 2013). Here, similar to RNAi, the expression of the gene of function is reduced but not completely abrogated. Therefore, these methods sometimes do not mirror the complete loss of function induced by genetic approaches and also display their fair share of off-target activity (Boettcher & McManus 2015). To achieve a post-transcriptional loss of protein function, systems enabling directed ubiquitylation and subsequent proteasomal degradation may be used. Auxin-inducible degron systems were initially established in plants but previously also used in human cells rapidly targeting nuclear and cytoplasmic proteins as well as proteins assembled in protein complexes (Holland et al. 2012; Natsume et al. 2016). The reported rapid depletion of target proteins by proteasomal degradation could therefore be beneficial to study survival-relevant proteins in BL.

In summary, although the CRISPR/Cas9-genome editing approach came with some challenges, I nevertheless was able to characterize BL-specific effector proteins involved in the pro-survival tonic BCR signaling. However, for further studies the aforementioned strategies should be considered to avoid putative clonal artefacts, which might allow to identify potential effector functions beyond the ones described in this thesis.

# 5 Summary and Conclusion

The results of my PhD project reveal molecular details of how tonic BCR signaling contributes to the survival of BL cells. Previously, tonic BL-specific signaling via the BCR was mainly associated with the PI3K-AKT pathway contributing to survival and proliferation of BL cells. However, the underlying molecular details remained unclear. Based on a proteogenomic screen in different BL cell lines, I have characterized the function of Nck1, BIG2 and SHIP2 in BL-specific tonic BCR signaling using CRISPR/Cas9 gene editing of BL cell lines. My data demonstrate that the BL-specific BCR-effector proteins Nck1, SHIP2 and BIG2 regulate the activity of the MAPK JNK in tonic BCR signaling conditions. In agreement with previous inhibitor studies, constitutive JNK activation in BL cell lines could be linked to overall survival and was confirmed to be mediated by tonic BCR signals. In summary, my study sheds some light on the molecular aspects of BL-specific tonic BCR signaling and emphasizes that beyond PI3K signaling the JNK pathway may be a promising target for novel approaches in the treatment of BL.

# 6 Bibliography

Ackermann, J.A. et al., 2011. Grb2 regulates B-cell maturation, B-cell memory responses and inhibits B-cell Ca2+ signalling. *The EMBO journal*, 30(8), pp.1621–33.

Agollah, G.D. et al., 2014. Evidence for SH2 Domain-Containing 5'-Inositol Phosphatase-2 (SHIP2) Contributing to a Lymphatic Dysfunction J. H. Fritz, ed. *PLoS ONE*, 9(11), p.e112548.

Aiba, Y. et al., 2007. Regulation of B-cell development by BCAP and CD19 through their binding to phosphoinositide 3-kinase. *Blood*, 111(3), pp.1497–1503.

Alberts, B. et al., 2002. *Molecular Biology of the Cell - The Generation of Antibody Diversity*, Garland Science.

Alessi, D.R. et al., 1997. 3-Phosphoinositide-dependent protein kinase-1 (PDK1): structural and functional homology with the Drosophila DSTPK61 kinase. *Current biology : CB*, 7(10), pp.776–89.

Alizadeh, A.A. et al., 2000. Distinct types of diffuse large B-cell lymphoma identified by gene expression profiling. *Nature*, 403(6769), pp.503–511.

Allam, A. & Marshall, A.J., 2005. Role of the adaptor proteins Bam32, TAPP1 and TAPP2 in lymphocyte activation. *Immunology Letters*, 97(1), pp.7–17.

Allday, M.J., 2009. How does Epstein-Barr virus (EBV) complement the activation of Myc in the pathogenesis of Burkitt's lymphoma? *Seminars in cancer biology*, 19(6), pp.366–76.

ar-Rushdi, A. et al., 1983. Differential expression of the translocated and the untranslocated c-myc oncogene in Burkitt lymphoma. *Science (New York, N.Y.)*, 222(4622), pp.390–3.

Arkin, M.R., Tang, Y. & Wells, J.A., 2014. Small-molecule inhibitors of protein-protein interactions: progressing toward the reality. *Chemistry & biology*, 21(9), pp.1102–14.

Aronheim, A. et al., 1994. Membrane targeting of the nucleotide exchange factor Sos is sufficient for activating the Ras signaling pathway. *Cell*, 78(6), pp.949–61.

Baba, Y. & Kurosaki, T., 2015. Role of Calcium Signaling in B Cell Activation and Biology. In Springer, Cham, pp. 143–174.

Backers, K. et al., 2003. The termination of PI3K signalling by SHIP1 and SHIP2 inositol 5-phosphatases. *Advances in Enzyme Regulation*, 43(1), pp.15–28.

Baliakas, P. et al., 2015. Splenic marginal-zone lymphoma: ontogeny and genetics. *Leukemia & Lymphoma*, 56(2), pp.301–310.

Basso, K. & Dalla-Favera, R., 2015. Germinal centres and B cell lymphomagenesis. *Nature Reviews Immunology*, 15(3), pp.172–184.

Batlevi, C.L. & Younes, A., 2017. Revival of PI3K inhibitors in non-Hodgkin's lymphoma. *Annals of Oncology*, 28(9), pp.2047–2049.

Ben-Bassat, H. et al., 1977. Establishment in continuous culture of a new type of lymphocyte from a "Burkitt like" malignant lymphoma (line D.G.-75). *International journal of cancer*, 19(1), pp.27–33.

Benhamou, L.E., Cazenave, P. & Sarthou, P., 1990. Anti-immunoglobulins induce death by apoptosis in WEHI-231 B lymphoma cells. *European Journal of Immunology*, 20(6), pp.1405–1407.

Bhatia, K.G. et al., 1992. The pattern of p53 mutations in Burkitt's lymphoma differs from that of solid tumors. *Cancer research*, 52(15), pp.4273–6.

Bhaya, D., Davison, M. & Barrangou, R., 2011. CRISPR-Cas Systems in Bacteria and Archaea: Versatile Small RNAs for Adaptive Defense and Regulation. *Annual Review of Genetics*, 45(1), pp.273–297.

Boettcher, M. & McManus, M.T., 2015. Choosing the Right Tool for the Job: RNAi, TALEN, or CRISPR. *Molecular cell*, 58(4), pp.575–85.

Bornkamm, G.W., von Knebel-Doeberitz, M. & Lenoir, G.M., 1984. No evidence for differences in the Epstein-Barr virus genome carried in Burkitt lymphoma cells and nonmalignant lymphoblastoid cells from the same patients. *Proceedings of the National Academy of Sciences of the United States of America*, 81(15), pp.4930–4.

Brezski, R.J. & Monroe, J.G., 2007. B cell antigen receptor-induced Rac1 activation and Rac1-dependent spreading are impaired in transitional immature B cells due to levels of membrane cholesterol. *Journal of immunology (Baltimore, Md. : 1950)*, 179(7), pp.4464–72.

Buchner, M. & Müschen, M., 2014. Targeting the B-cell receptor signaling pathway in B lymphoid malignancies. *Current opinion in hematology*, 21(4), pp.341–9.

Burkitt, D., 1958. A sarcoma involving the jaws in African children. *The British journal of surgery*, 46(197), pp.218–23.

Buvall, L. et al., 2013. Proteasomal degradation of Nck1 but not Nck2 regulates RhoA activation and actin dynamics. *Nature communications*, 4, p.2863.

Cano, E., Hazzalin, C.A. & Mahadevan, L.C., 1994. Anisomycin-activated protein kinases p45 and p55 but not mitogen-activated protein kinases ERK-1 and -2 are implicated in the induction of c-fos and c-jun. *Molecular and cellular biology*, 14(11), pp.7352–62.

Cardone, M.H. et al., 1998. Regulation of cell death protease caspase-9 by phosphorylation. *Science (New York, N.Y.)*, 282(5392), pp.1318–21.

Castello, A. et al., 2013. Nck-mediated recruitment of BCAP to the BCR regulates the PI(3)K-Akt pathway in B cells. *Nature immunology*, 14(9), pp.966–75.

Chang, M.-Y. et al., 2014. Doxycycline enhances survival and self-renewal of human pluripotent stem cells. *Stem cell reports*, 3(2), pp.353–64.

Chen, M. et al., 1998. Identification of Nck Family Genes, Chromosomal Localization, Expression, and Signaling Specificity. *Journal of Biological Chemistry*, 273(39), pp.25171–25178.

Chen, Q. et al., 2016. JNK/PI3K/Akt signaling pathway is involved in myocardial ischemia/reperfusion injury in diabetic rats: effects of salvianolic acid A intervention. *American journal of translational research*, 8(6), pp.2534–48.

Cheng, J. et al., 2000. Synergistic interaction of MEK kinase 2, c-Jun N-terminal kinase (JNK) kinase 2, and JNK1 results in efficient and specific JNK1 activation. *Molecular and cellular biology*, 20(7), pp.2334–42.

Chu, C.C. et al., 2010. Many chronic lymphocytic leukemia antibodies recognize apoptotic cells with exposed nonmuscle myosin heavy chain IIA: implications for patient outcome and cell of origin. *Blood*, 115(19), pp.3907–15.

Collins, M.K.L. et al., 1996. Expression systems. PCT/GB96/02061. WO 97/08330.

Cong, L. et al., 2012. Comprehensive interrogation of natural TALE DNA-binding modules and transcriptional repressor domains. *Nature Communications*, 3(1), p.968.

Cooper, M.D., 2015. The early history of B cells. *Nature Reviews Immunology*, 15(3), pp.191–197.

Cooper, M.D., Peterson, R.D.A. & Good, R.A., 1965. Delineation of the thymic and bursal lymphoid systems in the chicken. *Nature*, 205(4967), pp.143–146.

Cornall, R.J. et al., 1998. Polygenic autoimmune traits: Lyn, CD22, and SHP-1 are limiting elements of a biochemical pathway regulating BCR signaling and selection. *Immunity*, 8(4), pp.497–508.

Corso, J. et al., 2016. Elucidation of tonic and activated B-cell receptor signaling in Burkitt's lymphoma provides insights into regulation of cell survival. *Proceedings of the National Academy of Sciences*, 113(20), pp.5688–5693.

Coughlin, J.J. et al., 2005. RasGRP1 and RasGRP3 regulate B cell proliferation by facilitating B cell receptor-Ras signaling. *Journal of immunology (Baltimore, Md. : 1950)*, 175(11), pp.7179–84.

Coughlin, S. et al., 2015. An extracatalytic function of CD45 in B cells is mediated by CD22. *Proceedings of the National Academy of Sciences of the United States of America*, 112(47), pp.E6515-24.

Craig, V.J. et al., 2010. Gastric MALT lymphoma B cells express polyreactive, somatically mutated immunoglobulins. *Blood*, 115(3), pp.581–591.

Cross, D.A.E. et al., 1995. Inhibition of glycogen synthase kinase-3 by insulin mediated by protein kinase B. *Nature*, 378(6559), pp.785–789.

Cui, H., Meng, Y. & Bulleit, R.F., 1998. Inhibition of glycogen synthase kinase 3beta activity regulates proliferation of cultured cerebellar granule cells. *Brain research. Developmental brain research*, 111(2), pp.177–88.

Dave, S.S. et al., 2006. Molecular Diagnosis of Burkitt's Lymphoma. *New England Journal of Medicine*, 354(23), pp.2431–2442.

Davis, R.E. et al., 2010. Chronic active B-cell-receptor signalling in diffuse large B-cell lymphoma. *Nature*, 463(7277), pp.88–92.

Deckert, M. et al., 1996. Functional and physical interactions of Syk family kinases with the Vav proto-oncogene product. *Immunity*, 5(6), pp.591–604.

Deveau, H., Garneau, J.E. & Moineau, S., 2010. CRISPR/Cas System and Its Role in Phage-Bacteria Interactions. *Annual Review of Microbiology*, 64(1), pp.475–493.

Dhanasekaran, D.N. & Reddy, E.P., 2008. JNK signaling in apoptosis. *Oncogene*, 27(48), pp.6245–51.

Diehl, J.A. et al., 1998. Glycogen synthase kinase-3beta regulates cyclin D1 proteolysis and subcellular localization. *Genes & development*, 12(22), pp.3499–511.

Ding, J. et al., 2009. PI3K/Akt/JNK/c-Jun signaling pathway is a mediator for arsenite-induced cyclin D1 expression and cell growth in human bronchial epithelial cells. *Current cancer drug targets*, 9(4), pp.500–9.

Dominguez-Sola, D. et al., 2012. The proto-oncogene MYC is required for selection in the germinal center and cyclic reentry. *Nature Immunology*, 13(11), pp.1083–1091.

Downward, J., 2004. PI 3-kinase, Akt and cell survival. *Seminars in Cell & Developmental Biology*, 15(2), pp.177–182.

Dunn-Walters, D.K., Isaacson, P.G. & Spencer, J., 1995. Analysis of mutations in immunoglobulin heavy chain variable region genes of microdissected marginal zone (MGZ) B cells suggests that the MGZ of human spleen is a reservoir of memory B cells. *The Journal of experimental medicine*, 182(2), pp.559–66.

Engelke, M. et al., 2007. Ca(2+) signaling in antigen receptor-activated B lymphocytes. *Immunological reviews*, 218, pp.235–46.

Engels, N., Wollscheid, B. & Wienands, J., 2001. Association of SLP-65/BLNK with the B cell antigen receptor through a non-ITAM tyrosine of Ig-alpha. *European journal of immunology*, 31(7), pp.2126–34.

Erneux, C. et al., 2011. SHIP2 multiple functions: a balance between a negative control of PtdIns(3,4,5)$P_3$ level, a positive control of PtdIns(3,4)$P_2$ production, and intrinsic docking properties. *Journal of cellular biochemistry*, 112(9), pp.2203–9.

Evangelisti, C. et al., 2018. Phosphatidylinositol 3-kinase inhibition potentiates glucocorticoid response in B-cell acute lymphoblastic leukemia. *Journal of Cellular Physiology*, 233(3), pp.1796–1811.

Falasca, M. et al., 1998. Activation of phospholipase C gamma by PI 3-kinase-induced PH domain-mediated membrane targeting. *The EMBO journal*, 17(2), pp.414–22.

Fang, J. et al., 2015. Downregulation of tNASP inhibits proliferation through regulating cell cycle-related proteins and inactive ERK/MAPK signal pathway in renal cell carcinoma cells. *Tumor Biology*, 36(7), pp.5209–5214.

Fang, X. et al., 2000. Phosphorylation and inactivation of glycogen synthase kinase 3 by protein kinase A. *Proceedings of the National Academy of Sciences of the United States of America*, 97(22), pp.11960–5.

Fowler, N. & Davis, E., 2013. Targeting B-cell receptor signaling: changing the paradigm. *Hematology / the Education Program of the American Society of Hematology. American Society of Hematology. Education Program*, 2013(1), pp.553–60.

Frech, M. et al., 1997. High affinity binding of inositol phosphates and phosphoinositides to the pleckstrin homology domain of RAC/protein kinase B and their influence on kinase activity. *The Journal of biological chemistry*, 272(13), pp.8474–81.

Fu, C.-H. et al., 2014. A novel oncogenic role of inositol phosphatase SHIP2 in ER-negative breast cancer stem cells: involvement of JNK/vimentin activation. *Stem cells (Dayton, Ohio)*, 32(8), pp.2048–60.

Fuhler, G.M. et al., 2012. Therapeutic potential of SH2 domain-containing inositol-5'-phosphatase 1 (SHIP1) and SHIP2 inhibition in cancer. *Molecular medicine (Cambridge, Mass.)*, 18(1), pp.65–75.

Fütterer, K. et al., 1998. Structural basis for syk tyrosine kinase ubiquity in signal transduction pathways revealed by the crystal structure of its regulatory SH2 domains bound to a dually phosphorylated ITAM peptide. *Journal of Molecular Biology*, 281(3), pp.523–537.

Gabay, C. et al., 1999. Somatic mutations and intraclonal variations in the rearranged Vkappa genes of B-non-Hodgkin's lymphoma cell lines. *European journal of haematology*, 63(3), pp.180–91.

Gaidano, G. et al., 1991. p53 mutations in human lymphoid malignancies: association with Burkitt lymphoma and chronic lymphocytic leukemia. *Proceedings of the National Academy of Sciences of the United States of America*, 88(12), pp.5413–7.

Garneau, J.E. et al., 2010. The CRISPR/Cas bacterial immune system cleaves bacteriophage and plasmid DNA. *Nature*, 468(7320), pp.67–71.

Ghosh, S. et al., 2018. Inhibition of SHIP2 activity inhibits cell migration and could prevent metastasis in breast cancer cells. *Journal of Cell Science*, p.jcs.216408.

Gilbert, L.A. et al., 2013. CRISPR-Mediated Modular RNA-Guided Regulation of Transcription in Eukaryotes. *Cell*, 154(2), pp.442–451.

Glick, B., Chang, T.S. & Jaap, R.G., 1956. The Bursa of Fabricius and Antibody Production. *Poultry Science*, 35(1), pp.224–225.

Gomez-Curet, I. et al., 2006. c-Myc inhibition negatively impacts lymphoma growth. *Journal of Pediatric Surgery*, 41(1), pp.207–211.

Gorgani-Firuzjaee, S., Adeli, K. & Meshkani, R., 2015. Inhibition of SH2-domain-containing inositol 5-phosphatase (SHIP2) ameliorates palmitate induced-apoptosis through regulating Akt/FOXO1 pathway and ROS production in HepG2 cells. *Biochemical and biophysical research communications*, 464(2), pp.441–6.

Gu, G. et al., 2017. Overexpression of ARF1 is associated with cell proliferation and migration through PI3K signal pathway in ovarian cancer. *Oncology Reports*, 37(3), pp.1511–1520.

Gururajan, M. et al., 2005. c-Jun N-terminal kinase (JNK) is required for survival and proliferation of B-lymphoma cells. *Blood*, 106(4), pp.1382–1391.

Hafner, M. et al., 2016. Growth rate inhibition metrics correct for confounders in measuring sensitivity to cancer drugs. *Nature methods*, 13(6), pp.521–7.

Haines, E., Saucier, C. & Claing, A., 2014. The adaptor proteins p66Shc and Grb2 regulate the activation of the GTPases ARF1 and ARF6 in invasive breast cancer cells. *The Journal of biological chemistry*, 289(9), pp.5687–703.

Han, A. et al., 2003. Bam32 links the B cell receptor to ERK and JNK and mediates B cell proliferation but not survival. *Immunity*, 19(4), pp.621–32.

Harris, A.W. et al., 1988. The E mu-myc transgenic mouse. A model for high-incidence spontaneous lymphoma and leukemia of early B cells. *The Journal of experimental medicine*, 167(2), pp.353–71.

Hartwig, J.H. & Stossel, T.P., 1981. Structure of macrophage actin-binding protein molecules in solution and interacting with actin filaments. *Journal of molecular biology*, 145(3), pp.563–81.

Hashimoto, A. et al., 1998. Involvement of guanosine triphosphatases and phospholipase C-gamma2 in extracellular signal-regulated kinase, c-Jun NH2-terminal kinase, and p38 mitogen-activated protein kinase activation by the B cell antigen receptor. *The Journal of experimental medicine*, 188(7), pp.1287–95.

Hashimoto, S. et al., 1999. Identification of the SH2 domain binding protein of Bruton's tyrosine kinase as BLNK--functional significance of Btk-SH2 domain in B-cell antigen receptor-coupled calcium signaling. *Blood*, 94(7), pp.2357–64.

Hayday, A.C. et al., 1984. Activation of a translocated human c-myc gene by an enhancer in the immunoglobulin heavy-chain locus. *Nature*, 307(5949), pp.334–340.

Hayden, M.S., West, A.P. & Ghosh, S., 2006. NF-kappaB and the immune response. *Oncogene*, 25(51), pp.6758–80.

He, T.C. et al., 1998. Identification of c-MYC as a target of the APC pathway. *Science (New York, N.Y.)*, 281(5382), pp.1509–12.

Henry Dunand, C.J. & Wilson, P.C., 2015. Restricted, canonical, stereotyped and convergent immunoglobulin responses. *Philosophical transactions of the Royal Society of London. Series B, Biological sciences*, 370(1676).

Hibi, M. et al., 1993. Identification of an oncoprotein- and UV-responsive protein kinase that binds and potentiates the c-Jun activation domain. *Genes & development*, 7(11), pp.2135–48.

Holland, A.J. et al., 2012. Inducible, reversible system for the rapid and complete degradation of proteins in mammalian cells. *Proceedings of the National Academy of Sciences of the United States of America*, 109(49), pp.E3350-7.

Horie, K. et al., 2007. The role of p38 mitogen-activated protein kinase in regulating interleukin-10 gene expression in Burkitt's lymphoma cell lines. *Microbiology and immunology*, 51(1), pp.149–61.

Horvath, P. & Barrangou, R., 2010. CRISPR/Cas, the Immune System of Bacteria and Archaea. *Science*, 327(5962), pp.167–170.

Hozumi, N. & Tonegawa, S., 1976. Evidence for somatic rearrangement of immunoglobulin genes coding for variable and constant regions. *Proceedings of the National Academy of Sciences of the United States of America*, 73(10), pp.3628–32.

Humphrey, M.B., Lanier, L.L. & Nakamura, M.C., 2005. Role of ITAM-containing adapter proteins and their receptors in the immune system and bone. *Immunological Reviews*, 208(1), pp.50–65.

Huttlin, E.L. et al., 2017. Architecture of the human interactome defines protein communities and disease networks. *Nature*, 545(7655), pp.505–509.

Iacobucci, I. et al., 2012. Cytogenetic and molecular predictors of outcome in acute lymphocytic leukemia: recent developments. *Current hematologic malignancy reports*, 7(2), pp.133–43.

Iavarone, C. et al., 2003. The platelet-derived growth factor controls c-myc expression through a JNK- and AP-1-dependent signaling pathway. *The Journal of biological chemistry*, 278(50), pp.50024–30.

Isaacson, P.G. & Spencer, J., 1987. Malignant lymphoma of mucosa-associated lymphoid tissue. *Histopathology*, 11(5), pp.445–62.

Ishiai, M. et al., 1999. BLNK Required for Coupling Syk to PLCγ2 and Rac1-JNK in B Cells. *Immunity*, 10(1), pp.117–125.

Ishizaki, R. et al., 2006. AMY-1 (associate of Myc-1) localization to the trans-Golgi network through interacting with BIG2, a guanine-nucleotide exchange factor for ADP-ribosylation factors. *Genes to cells : devoted to molecular & cellular mechanisms*, 11(8), pp.949–59.

Jabbour, E. & Kantarjian, H., 2016. Chemoimmunotherapy as a new standard of care for Burkitt leukaemia/lymphoma. *Lancet (London, England)*, 387(10036), pp.2360–1.

Jacobson, C. & LaCasce, A., 2014. How I treat Burkitt lymphoma in adults. *Blood*, 124(19), pp.2913–20.

Jellusova, J. et al., 2017. Gsk3 is a metabolic checkpoint regulator in B cells. *Nature immunology*, 18(3), pp.303–312.

Jinek, M. et al., 2012. A Programmable Dual-RNA-Guided DNA Endonuclease in Adaptive Bacterial Immunity. *Science*, 337(6096), pp.816–821.

Kar, P., Nelson, C. & Parekh, A.B., 2012. CRAC Channels Drive Digital Activation and Provide Analog Control and Synergy to Ca2+-Dependent Gene Regulation. *Current Biology*, 22(3), pp.242–247.

Kato, K. et al., 2012. The inositol 5-phosphatase SHIP2 is an effector of RhoA and is involved in cell polarity and migration. *Molecular biology of the cell*, 23(13), pp.2593–604.

Kebache, S. et al., 2002. Modulation of protein translation by Nck-1. *Proceedings of the National Academy of Sciences of the United States of America*, 99(8), pp.5406–11.

Khiem, D. et al., 2008. A p38 MAPK-MEF2C pathway regulates B-cell proliferation. *Proceedings of the National Academy of Sciences*, 105(44), pp.17067–17072.

Klee, C.B., Crouch, T.H. & Krinks, M.H., 1979. Calcineurin: a calcium- and calmodulin-binding protein of the nervous system. *Proceedings of the National Academy of Sciences of the United States of America*, 76(12), pp.6270–3.

Klein, E. et al., 1968. Surface IgM-kappa specificity on a Burkitt lymphoma cell in vivo and in derived culture lines. *Cancer research*, 28(7), pp.1300–10.

Klumb, C.E., 2012. A step towards the cure of Burkitt's lymphoma in developing countries. *Revista brasileira de hematologia e hemoterapia*, 34(5), pp.332–3.

Kraus, M. et al., 2004. Survival of Resting Mature B Lymphocytes Depends on BCR Signaling via the Igα/β Heterodimer. *Cell*, 117(6), pp.787–800.

Kreck, B. et al., 2013. Base-pair resolution DNA methylome of the EBV-positive Endemic Burkitt lymphoma cell line DAUDI determined by SOLiD bisulfite-sequencing. *Leukemia*, 27(8), pp.1751–3.

Küppers, R., 2005. Mechanisms of B-cell lymphoma pathogenesis. *Nature Reviews Cancer*, 5(4), pp.251–262.

Kyriakis, J.M. & Avruch, J., 2001. Mammalian Mitogen-Activated Protein Kinase Signal Transduction Pathways Activated by Stress and Inflammation. *Physiological Reviews*, 81(2), pp.807–869.

Lam, K.P., Kühn, R. & Rajewsky, K., 1997. In vivo ablation of surface immunoglobulin on mature B cells by inducible gene targeting results in rapid cell death. *Cell*, 90(6), pp.1073–83.

Landego, I. et al., 2012. Interaction of TAPP adapter proteins with phosphatidylinositol (3,4)-bisphosphate regulates B-cell activation and autoantibody production. *European Journal of Immunology*, 42(10), pp.2760–2770.

Lenz, G. et al., 2008. Oncogenic CARD11 Mutations in Human Diffuse Large B Cell Lymphoma. *Science*, 319(5870), pp.1676–1679.

Leslie, N.R. et al., 2012. Distinct inactivation of PI3K signalling by PTEN and 5-phosphatases. *Advances in Biological Regulation*, 52(1), pp.205–213.

Li, C.-C. et al., 2016. Enhancement of β-catenin activity by BIG1 plus BIG2 via Arf activation and cAMP signals. *Proceedings of the National Academy of Sciences of the United States of America*, 113(21), pp.5946–51.

Li, H. et al., 2003. Protein kinase A-anchoring (AKAP) domains in brefeldin A-inhibited guanine nucleotide-exchange protein 2 (BIG2). *Proceedings of the National Academy of Sciences of the United States of America*, 100(4), pp.1627–32.

Li, H., Dusseault, J. & Larose, L., 2014. Nck1 depletion induces activation of the PI3K/Akt pathway by attenuating PTP1B protein expression. *Cell communication and signaling : CCS*, 12, p.71.

Li, H. & Marshall, A.J., 2015. Phosphatidylinositol (3,4) bisphosphate-specific phosphatases and effector proteins: A distinct branch of PI3K signaling. *Cellular Signalling*, 27(9), pp.1789–1798.

Liu, Q. et al., 2015. SHIP2 on pI3K/Akt pathway in palmitic acid stimulated islet β cell. *International journal of clinical and experimental medicine*, 8(3), pp.3210–8.

Lopez-Ilasaca, M., 1998. Signaling from G-protein-coupled receptors to mitogen-activated protein (MAP)-kinase cascades. *Biochemical pharmacology*, 56(3), pp.269–77.

Love, C. et al., 2012. The genetic landscape of mutations in Burkitt lymphoma. *Nature genetics*, 44(12), pp.1321–5.

Lu, K.-H. et al., 2015. Nck adaptor proteins modulate differentiation and effector function of T cells. *J. Leukoc. Biol*, 98, pp.301–311.

Ma, K. et al., 2008. PI(3,4,5)P3 and PI(3,4)P2 levels correlate with PKB/akt phosphorylation at Thr308 and Ser473, respectively; PI(3,4)P2 levels determine PKB activity. *Cellular Signalling*, 20(4), pp.684–694.

Mann, M., 2006. Functional and quantitative proteomics using SILAC. *Nature reviews. Molecular cell biology*, 7(12), pp.952–8.

Manna, D. et al., 2007. Mechanistic basis of differential cellular responses of phosphatidylinositol 3,4-bisphosphate- and phosphatidylinositol 3,4,5-trisphosphate-binding pleckstrin homology domains. *The Journal of biological chemistry*, 282(44), pp.32093–105.

Manno, B. et al., 2016. The Dok-3/Grb2 adaptor module promotes inducible association of the lipid phosphatase SHIP with the BCR in a coreceptor-independent manner. *European Journal of Immunology*, 46(11), pp.2520–2530.

Marinkovic, D. et al., 2004. Reversible lymphomagenesis in conditionally c-MYC expressing mice. *International Journal of Cancer*, 110(3), pp.336–342.

Miletic, A. V. et al., 2010. Coordinate suppression of B cell lymphoma by PTEN and SHIP phosphatases. *The Journal of Experimental Medicine*, 207(11), pp.2407–2420.

Minden, M.D. et al., 2012. Chronic lymphocytic leukaemia is driven by antigen-independent cell-autonomous signalling. *Nature*, 489(7415), pp.309–312.

Mizuno, K. et al., 2002. Src homology region 2 domain-containing phosphatase 1 positively regulates B cell receptor-induced apoptosis by modulating association of B cell linker protein with Nck and activation of c-Jun NH2-terminal kinase. *Journal of immunology (Baltimore, Md. : 1950)*, 169(2), pp.778–86.

Mohr, S. et al., 2017. Hoxa9 and Meis1 Cooperatively Induce Addiction to Syk Signaling by Suppressing miR-146a in Acute Myeloid Leukemia. *Cancer cell*, 31(4), p.549–562.e11.

Molyneux, E.M. et al., 2012. Burkitt's lymphoma. *Lancet*, 379(9822), pp.1234–44.

Monroe, J.G., 2006. ITAM-mediated tonic signalling through pre-BCR and BCR complexes. *Nature reviews. Immunology*, 6(4), pp.283–94.

Morita, S., Kojima, T. & Kitamura, T., 2000. Plat-E: an efficient and stable system for transient packaging of retroviruses. *Gene Therapy*, 7(12), pp.1063–1066.

Morton, L.M. et al., 2006. Lymphoma incidence patterns by WHO subtype in the United States, 1992-2001. *Blood*, 107(1), pp.265–76.

Mullis, K. et al., 1986. Specific enzymatic amplification of DNA in vitro: the polymerase chain reaction. *Cold Spring Harbor symposia on quantitative biology*, 51 Pt 1, pp.263–73.

Natsume, T. et al., 2016. Rapid Protein Depletion in Human Cells by Auxin-Inducible Degron Tagging with Short Homology Donors. *Cell reports*, 15(1), pp.210–218.

Neumann, K. et al., 2009. The B-lymphoid Grb2 interaction code. *Immunological Reviews*, 232(1), pp.135–149.

Ngo, V.N. et al., 2011. Oncogenically active MYD88 mutations in human lymphoma. *Nature*, 470(7332), pp.115–119.

Ngoenkam, J. et al., 2014. Non-overlapping functions of Nck1 and Nck2 adaptor proteins in T cell activation. *Cell communication and signaling : CCS*, 12, p.21.

Nitschke, L., 2005. The role of CD22 and other inhibitory co-receptors in B-cell activation. *Current Opinion in Immunology*, 17(3), pp.290–297.

Oeckinghaus, A. & Ghosh, S., 2009. The NF-kappaB family of transcription factors and its regulation. *Cold Spring Harbor perspectives in biology*, 1(4), p.a000034.

Oellerich, T. et al., 2011. The B-cell antigen receptor signals through a preformed transducer module of SLP65 and CIN85. *The EMBO Journal*, 30(17), pp.3620–3634.

Oh-hora, M. et al., 2003. Requirement for Ras Guanine Nucleotide Releasing Protein 3 in Coupling Phospholipase C-γ2 to Ras in B Cell Receptor Signaling. *The Journal of Experimental Medicine*, 198(12), pp.1841–1851.

Oh-hora, M. & Rao, A., 2009. The calcium/NFAT pathway: role in development and function of regulatory T cells. *Microbes and infection*, 11(5), pp.612–9.

Okada, H. et al., 1998. Role of the inositol phosphatase SHIP in B cell receptor-induced Ca2+ oscillatory response. *Journal of immunology (Baltimore, Md. : 1950)*, 161(10), pp.5129–32.

Okada, T. et al., 2000. BCAP: The Tyrosine Kinase Substrate that Connects B Cell Receptor to Phosphoinositide 3-Kinase Activation. *Immunity*, 13(6), pp.817–827.

Pajic, A. et al., 2000. Cell cycle activation by c-myc in a Burkitt lymphoma model cell line. *International Journal of Cancer*, 87(6), pp.787–793.

Pao, L.I., Famiglietti, S.J. & Cambier, J.C., 1998. Asymmetrical phosphorylation and function of immunoreceptor tyrosine-based activation motif tyrosines in B cell antigen receptor signal transduction. *Journal of immunology (Baltimore, Md. : 1950)*, 160(7), pp.3305–14.

Parameswaran, N. et al., 2013. Spatial coupling of JNK activation to the B cell antigen receptor by tyrosine-phosphorylated ezrin. *Journal of immunology (Baltimore, Md. : 1950)*, 190(5), pp.2017–26.

Park, S.S. et al., 2005. Insertion of *Myc* into *Igh* Accelerates Peritoneal Plasmacytomas in Mice. *Cancer Research*, 65(17), pp.7644–7652.

Patsoukis, N. et al., 2013. PD-1 increases PTEN phosphatase activity while decreasing PTEN protein stability by inhibiting casein kinase 2. *Molecular and cellular biology*, 33(16), pp.3091–8.

Pauls, S.D. & Marshall, A.J., 2017. Regulation of immune cell signaling by SHIP1: A phosphatase, scaffold protein, and potential therapeutic target. *European Journal of Immunology*, 47(6), pp.932–945.

Pelanda, R. & Torres, R.M., 2012. Central B-cell tolerance: where selection begins. *Cold Spring Harbor perspectives in biology*, 4(4), p.a007146.

Pensiero, M. et al., 1999. Retroviral vectors produced by producer cell lines resistant to lysis by human serum.

Perry, E. et al., 2004. TMF/ARA160 is a BC-box-containing protein that mediates the degradation of Stat3. *Oncogene*, 23(55), pp.8908–8919.

Pettersen, H.S. et al., 2015. AID expression in B-cell lymphomas causes accumulation of genomic uracil and a distinct AID mutational signature. *DNA Repair*, 25, pp.60–71.

Pierce, S.K. & Liu, W., 2010. The tipping points in the initiation of B cell signalling: how small changes make big differences. *Nature Reviews Immunology*, 10(11), pp.767–777.

Prasad, N., Topping, R.S. & Decker, S.J., 2001. SH2-containing inositol 5'-phosphatase SHIP2 associates with the p130(Cas) adapter protein and regulates cellular adhesion and spreading. *Molecular and cellular biology*, 21(4), pp.1416–28.

Qi, L.S. et al., 2013. Repurposing CRISPR as an RNA-guided platform for sequence-specific control of gene expression. *Cell*, 152(5), pp.1173–83.

Ran, F.A. et al., 2013. Genome engineering using the CRISPR-Cas9 system. *Nature protocols*, 8(11), pp.2281–308.

Reth, M., 1989. Antigen receptor tail clue. *Nature*, 338(6214), pp.383–384.

Reth, M. et al., 1991. The B-cell antigen receptor complex. *Immunology Today*, 12(6), pp.196–201.

Richter, J. et al., 2012. Recurrent mutation of the ID3 gene in Burkitt lymphoma identified by integrated genome, exome and transcriptome sequencing. *Nature genetics*, 44(12), pp.1316–20.

Rickert, R.C., 2013. New insights into pre-BCR and BCR signalling with relevance to B cell malignancies. *Nature reviews. Immunology*, 13(8), pp.578–91.

Rolli, V. et al., 2002. Amplification of B cell antigen receptor signaling by a Syk/ITAM positive feedback loop. *Molecular cell*, 10(5), pp.1057–69.

Röllig, C., Knop, S. & Bornhäuser, M., 2015. Multiple myeloma. *The Lancet*, 385(9983), pp.2197–2208.

Rossi, D. & Gaidano, G., 2010. Biological and clinical significance of stereotyped B-cell receptors in chronic lymphocytic leukemia. *Haematologica*, 95(12), pp.1992–5.

Rowland, S.L. et al., 2010. Ras activation of Erk restores impaired tonic BCR signaling and rescues immature B cell differentiation. *The Journal of experimental medicine*, 207(3), pp.607–21.

Russell, W.C. et al., 1977. Characteristics of a Human Cell Line Transformed by DNA from Human Adenovirus Type 5. *Journal of General Virology*, 36(1), pp.59–72.

Saci, A. & Carpenter, C.L., 2005. RhoA GTPase Regulates B Cell Receptor Signaling. *Molecular Cell*, 17(2), pp.205–214.

Salim, K. et al., 1996. Distinct specificity in the recognition of phosphoinositides by the pleckstrin homology domains of dynamin and Bruton's tyrosine kinase. *The EMBO journal*, 15(22), pp.6241–6250.

Sambrook, J. & Russell, D.W., 2001. *Molecular Cloning : A Laboratory Manual*

Sampson, V.B. et al., 2007. MicroRNA let-7a down-regulates MYC and reverts MYC-induced growth in Burkitt lymphoma cells. *Cancer research*, 67(20), pp.9762–70.

Sander, S. et al., 2012. Synergy between PI3K signaling and MYC in Burkitt lymphomagenesis. *Cancer cell*, 22(2), pp.167–79.

Sarbassov, D.D. et al., 2005. Phosphorylation and Regulation of Akt/PKB by the Rictor-mTOR Complex. *Science*, 307(5712), pp.1098–1101.

Saurus, P. et al., 2017. Inhibition of SHIP2 in CD2AP-deficient podocytes ameliorates reactive oxygen species generation but aggravates apoptosis. *Scientific Reports*, 7(1), p.10731.

Schamel, W.W. & Reth, M., 2000. Monomeric and oligomeric complexes of the B cell antigen receptor. *Immunity*, 13(1), pp.5–14.

Schmidt, T., Schmid-Burgk, J.L. & Hornung, V., 2015. Synthesis of an arrayed sgRNA library targeting the human genome. *Scientific reports*, 5, p.14987.

Schmitz, R. et al., 2012. Burkitt lymphoma pathogenesis and therapeutic targets from structural and functional genomics. *Nature*, 490(7418), pp.116–20.

Schmitz, R. et al., 2014. Oncogenic mechanisms in Burkitt lymphoma. *Cold Spring Harbor perspectives in medicine*, 4(2), p.a014282.

Schmitz, R., Baumann, G. & Gram, H., 1996. Catalytic Specificity of Phosphotyrosine Kinases Blk, Lyn, c-Src and Syk as Assessed by Phage Display. *Journal of Molecular Biology*, 260(5), pp.664–677.

Scudiero, D.A. et al., 1988. Evaluation of a soluble tetrazolium/formazan assay for cell growth and drug sensitivity in culture using human and other tumor cell lines. *Cancer research*, 48(17), pp.4827–33.

Seifert, M. et al., 2012. Cellular origin and pathophysiology of chronic lymphocytic leukemia. *The Journal of Experimental Medicine*, 209(12), pp.2183–2198.

Sheen, V.L., 2014. Filamin A and Big2: a shared endocytic pathway. *Bioarchitecture*, 4(2), pp.53–7.

Shen, X. et al., 2012. Brefeldin A-inhibited ADP-ribosylation factor activator BIG2 regulates cell migration via integrin β1 cycling and actin remodeling. *Proceedings of the National Academy of Sciences of the United States of America*, 109(36), pp.14464–9.

Sheppard, D., 1994. Dominant negative mutants: tools for the study of protein function in vitro and in vivo. *American Journal of Respiratory Cell and Molecular Biology*, 11(1), pp.1–6.

Shin, H.-W. et al., 2004. BIG2, A Guanine Nucleotide Exchange Factor for ADP-Ribosylation Factors: Its Localization to Recycling Endosomes and Implication in the Endosome Integrity. *Molecular Biology of the Cell*, 15(12), pp.5283–5294.

Shtutman, M. et al., 1999. The cyclin D1 gene is a target of the -catenin/LEF-1 pathway. *Proceedings of the National Academy of Sciences*, 96(10), pp.5522–5527.

De Silva, N.S. & Klein, U., 2015. Dynamics of B cells in germinal centres. *Nature reviews. Immunology*, 15(3), pp.137–48.

Spender, L.C. & Inman, G.J., 2014. Developments in Burkitt's lymphoma: novel cooperations in oncogenic MYC signaling. *Cancer management and research*, 6, pp.27–38.

Spender, L.C. & Inman, G.J., 2012. Phosphoinositide 3-kinase/AKT/mTORC1/2 signaling determines sensitivity of Burkitt's lymphoma cells to BH3 mimetics. *Molecular cancer research : MCR*, 10(3), pp.347–59.

Srinivasan, L. et al., 2009. PI3 Kinase Signals BCR-Dependent Mature B Cell Survival. *Cell*, 139(3), pp.573–586.

Staudt, L.M., 2012. Chronic Active B-Cell Receptor Signaling in Lymphoma. *Blood*, 120(21).

Stewart, S.A. et al., 2003. Lentivirus-delivered stable gene silencing by RNAi in primary cells. *RNA (New York, N.Y.)*, 9(4), pp.493–501.

Suwa, A. et al., 2009. Discovery and functional characterization of a novel small molecule inhibitor of the intracellular phosphatase, SHIP2. *British Journal of Pharmacology*, 158(3), pp.879–887.

Tabe, Y. et al., 2014. Class IA Phosphatidylinositol 3-Kinase Inhibition Inhibits Cell Growth and Proliferation in Mantle Cell Lymphoma. *Acta Haematologica*, 131(1), pp.59–69.

Taira, T. et al., 1998. AMY-1, a novel C-MYC binding protein that stimulates transcription activity of C-MYC. *Genes to cells : devoted to molecular & cellular mechanisms*, 3(8), pp.549–65.

Taylor, C.W. & Tovey, S.C., 2010. IP(3) receptors: toward understanding their activation. *Cold Spring Harbor perspectives in biology*, 2(12), p.a004010.

Taylor, V. et al., 2000. 5' Phospholipid Phosphatase SHIP-2 Causes Protein Kinase B Inactivation and Cell Cycle Arrest in Glioblastoma Cells. *Molecular and Cellular Biology*, 20(18), pp.6860–6871.

Teramoto, H. et al., 1997. Tyrosine phosphorylation of the vav proto-oncogene product links FcepsilonRI to the Rac1-JNK pathway. *The Journal of biological chemistry*, 272(16), pp.10751–5.

Thomas, M.P., Erneux, C. & Potter, B.V.L., 2016. SHIP2: Structure, Function and Inhibition. *ChemBioChem*, 18(3), pp.233–247.

Thul, P.J. et al., 2017. A subcellular map of the human proteome. *Science*, 356(6340), p.eaal3321.

Towbin, H., Staehelin, T. & Gordon, J., 1989. Immunoblotting in the clinical laboratory. *Journal of clinical chemistry and clinical biochemistry. Zeitschrift fur klinische Chemie und klinische Biochemie*, 27(8), pp.495–501.

Treanor, B., 2012. B-cell receptor: from resting state to activate. *Immunology*, 136(1), pp.21–7.

Treanor, B. et al., 2011. Dynamic cortical actin remodeling by ERM proteins controls BCR microcluster organization and integrity. *The Journal of Experimental Medicine*, 208(5), pp.1055–1068.

Treanor, B. et al., 2010. The membrane skeleton controls diffusion dynamics and signaling through the B cell receptor. *Immunity*, 32(2), pp.187–99.

Unanue, E.R., 1984. Antigen-Presenting Function of the Macrophage. *Annual Review of Immunology*, 2(1), pp.395–428.

Vanhaesebroeck, B. & Alessi, D.R., 2000. The PI3K-PDK1 connection: more than just a road to PKB. *The Biochemical journal*, 346 Pt 3(Pt 3), pp.561–76.

Vanshylla, K. et al., 2018. Grb2 and GRAP connect the B cell antigen receptor to Erk MAP kinase activation in human B cells. *Scientific Reports*, 8(1), p.4244.

Vaqué, J.P. et al., 2014. B-cell lymphoma mutations: improving diagnostics and enabling targeted therapies. *Haematologica*, 99(2), pp.222–31.

Vazquez, F. et al., 2000. Phosphorylation of the PTEN tail regulates protein stability and function. *Molecular and cellular biology*, 20(14), pp.5010–8.

Venkatareddy, M. et al., 2011. Nephrin regulates lamellipodia formation by assembling a protein complex that includes Ship2, filamin and lamellipodin. *PloS one*, 6(12), p.e28710.

Venkitaraman, A.R. et al., 1991. The B-cell antigen receptor of the five immunoglobulin classes. *Nature*, 352(6338), pp.777–781.

Vermes, I. et al., 1995. A novel assay for apoptosis. Flow cytometric detection of phosphatidylserine expression on early apoptotic cells using fluorescein labelled Annexin V. *Journal of immunological methods*, 184(1), pp.39–51.

Victora, G.D. et al., 2012. Identification of human germinal center light and dark zone cells and their relationship to human B-cell lymphomas. *Blood*, 120(11), pp.2240–2248.

Wang, Y. et al., 2004. SHIP2 is recruited to the cell membrane upon macrophage colony-stimulating factor (M-CSF) stimulation and regulates M-CSF-induced signaling. *Journal of immunology (Baltimore, Md. : 1950)*, 173(11), pp.6820–30.

Weber, K. & Osborn, M., 1969. The reliability of molecular weight determinations by dodecyl sulfate-polyacrylamide gel electrophoresis. *The Journal of biological chemistry*, 244(16), pp.4406–12.

Weill, J.-C., Weller, S. & Reynaud, C.-A., 2009. Human Marginal Zone B Cells. *Annual Review of Immunology*, 27(1), pp.267–285.

Westwick, J.K. et al., 1994. Tumor necrosis factor alpha stimulates AP-1 activity through prolonged activation of the c-Jun kinase. *The Journal of biological chemistry*, 269(42), pp.26396–401.

Wienands, J. et al., 1998. SLP-65: a new signaling component in B lymphocytes which requires expression of the antigen receptor for phosphorylation. *The Journal of experimental medicine*, 188(4), pp.791–5.

Wienands, J., Larbolette, O. & Reth, M., 1996. Evidence for a preformed transducer complex organized by the B cell antigen receptor. *Proceedings of the National Academy of Sciences of the United States of America*, 93(15), p.7865.

Wiman, K.G. et al., 1991. Mutant p53 detected in a majority of Burkitt lymphoma cell lines by monoclonal antibody PAb240. *Oncogene*, 6(9), pp.1633–9.

Xie, J. et al., 2008. The docking properties of SHIP2 influence both JIP1 tyrosine phosphorylation and JNK activity. *Cellular Signalling*, 20(8), pp.1432–1441.

Xie, J., Erneux, C. & Pirson, I., 2013. How does SHIP1/2 balance PtdIns(3,4)P 2 and does it signal independently of its phosphatase activity? *BioEssays*, 35(8), pp.733–743.

Xu, Z.-Z. et al., 2013. Activation of the PI3K/AKT/mTOR pathway in diffuse large B cell lymphoma: clinical significance and inhibitory effect of rituximab. *Annals of Hematology*, 92(10), pp.1351–1358.

Yang, J. et al., 2014. High SHIP2 expression indicates poor survival in colorectal cancer. *Disease markers*, 2014, p.218968.

Yang, J. & Reth, M., 2010a. Oligomeric organization of the B-cell antigen receptor on resting cells. *Nature*, 467(7314), pp.465–469.

Yang, J. & Reth, M., 2010b. The dissociation activation model of B cell antigen receptor triggering. *FEBS Letters*, 584(24), pp.4872–4877.

Yankee, T.M. et al., 1999. Inhibition of signaling through the B cell antigen receptor by the protooncogene product, c-Cbl, requires Syk tyrosine 317 and the c-Cbl phosphotyrosine-binding domain. *Journal of immunology (Baltimore, Md. : 1950)*, 163(11), pp.5827–35.

Yasuda, S. et al., 2017. A model integrating tonic and antigen-triggered BCR signals to predict the survival of primary B cells. *Scientific Reports*, 7(1), p.14888.

Yasuda, T. et al., 2011. ERKs Induce Expression of the Transcriptional Repressor Blimp-1 and Subsequent Plasma Cell Differentiation. *Science Signaling*, 4(169), pp.ra25-ra25.

Ye, Y. et al., 2016. Suppression of SHIP2 contributes to tumorigenesis and proliferation of gastric cancer cells via activation of Akt. *Journal of gastroenterology*, 51(3), pp.230–40.

Yin, X. et al., 2003. Low molecular weight inhibitors of Myc–Max interaction and function. *Oncogene*, 22(40), pp.6151–6159.

Zeke, A. et al., 2016. JNK Signaling: Regulation and Functions Based on Complex Protein-Protein Partnerships. *Microbiology and molecular biology reviews : MMBR*, 80(3), pp.793–835.

Zhang, G. & Neubert, T.A., 2009. Use of Stable Isotope Labeling by Amino Acids in Cell Culture (SILAC) for Phosphotyrosine Protein Identification and Quantitation. In *Methods in molecular biology (Clifton, N.J.)*. pp. 79–92.

Zhang, J. et al., 2012. Brefeldin A-inhibited guanine exchange factor 2 regulates filamin A phosphorylation and neuronal migration. *The Journal of neuroscience : the official journal of the Society for Neuroscience*, 32(36), pp.12619–29.

Zhang, J. et al., 2013. Filamin A regulates neuronal migration through brefeldin A-inhibited guanine exchange factor 2-dependent Arf1 activation. *The Journal of neuroscience : the official journal of the Society for Neuroscience*, 33(40), pp.15735–46.

Zhou, G., Bao, Z.Q. & Dixon, J.E., 1995. Components of a new human protein kinase signal transduction pathway. *The Journal of biological chemistry*, 270(21), pp.12665–9.

Zohn, I.E. et al., 2006. p38 and a p38-Interacting Protein Are Critical for Downregulation of E-Cadherin during Mouse Gastrulation. *Cell*, 125(5), pp.957–969.

Zufferey, R. et al., 1997. Multiply attenuated lentiviral vector achieves efficient gene delivery in vivo. *Nature Biotechnology*, 15(9), pp.871–875.